MINIMALLY INVASIVE POSTERIOR SEGMENT THERAPEUTICS

MINIMALLY INVASIVE COPOLYMERS FOR POSTERIOR SEGMENT OCULAR THERAPEUTICS

By, SCOTT FITZPATRICK, B.Eng.

A Thesis Submitted to the School of Graduate Studies in Partial Fulfillment of the Requirements for the Degree Doctor of Philosophy in the School of Biomedical Engineering

DOCTOR OF PHILOSOPHY (2012) McMaster University
School of Biomedical Engineering Hamilton, Ontario

TITLE: MINIMALLY INVASIVE COPOLYMERS FOR THE TREATMENT OF POSTERIOR SEGMENT OCULAR COMPLICATIONS

AUTHOR: Scott D Fitzpatrick, B.Eng. (McMaster University)

SUPERVISOR: Dr. Heather Sheardown

NUMBER OF PAGES: xxi, 228

ABSTRACT

Efficient delivery of therapeutic cell and pharmaceutical suspensions to the posterior segment of the eye remains an elusive goal. Delivery is made difficult by blood ocular barriers that separate the eye from systemic circulation, the compartmentalized structure of the eye that limits diffusion across the globe, and effective clearance mechanisms that result in short drug residence times. The work presented in this thesis focuses on the design, synthesis, evolution and refinement of novel biomaterial scaffolds ultimately intended to facilitate the minimally invasive delivery of therapeutic payloads into the posterior segment of the eye. The first generation materials presented in this work (Chapter 2) consist of linear chains of temperature-sensitive amine-terminated poly(N-isopropylacrylamide) (PNIPAAm) grafted onto the backbone of type I collagen. Second generation materials (Chapter 3) saw the inclusion of the lubricious polysaccharide, hyaluronic acid (HA), and replacement of the bulky collagen backbone, which was observed to impede scaffold gelation, with small cell adhesive RGD peptide sequences. The introduction of degradability was the emphasis of third generation copolymers (Chapter 4) and was achieved through copolymerization with dimethyl-γ-butyrolactone acrylate (DBA). The DBA lactone side group was found to undergo a hydrolysis dependent ring opening, which raises copolymer LCST above physiologic temperature, triggering the gelled scaffold to solubilize and be excreted from the body via renal filtration without the liberation of any degradation by-products. Degradation was found to occur slowly, which is favourable for long-term release scaffolds intended to decrease the frequency of injections required to maintain therapeutically relevant concentrations

within the vitreous. Finally, the design of a fourth generation material is discussed (Chapter 5), in which optical transparency is achieved through copolymerization of third generation materials with polyethylene glycol (PEG) monomers of varying molecular weight. Synthesis, design and characterization of the various copolymers is described herein.

ACKNOWLEDGEMENTS

Lindsay and I would like to express our extreme gratitude to Heather Sheardown for her mentorship and supervision over the last decade. Heather has been instrumental in helping us progress through the many stages of University. Perhaps it was the flexible hours, which permitted afternoon soccer matches or lengthy sleep-ins, or maybe it was the excellent people Heather often attracted to her group (aka team Larry), but Lindsay and I discovered our enthusiasm for research as undergraduate students spending our summers carrying out experiments in Heather's lab. This passion for research drove us to pursue graduate studies in Biomedical Engineering, where Heather has continued to supervise me throughout the years with unwavering support and patience (sorry about the excessive noise at ARVO, but we both know that was Ben's fault). And while Lindsay moved on from McMaster to do research at UofT, she continues to seek Heather's advice on matters concerning school, work and life in general. Heather has been an incredible mentor and friend for both of us and we will be forever grateful.

Next I would like to thank my two main collaborators, Jafar and Ben. Though we have vastly differing personalities, I think it was these differences that allowed us to work so well together as a team. Jafar, I can't thank you enough for bringing your expertise in chemistry and polymer synthesis to the Sheardown group. You provided me with the capacity to perform all the elaborate experiments I had envisioned and you taught me proper polymerization, purification and characterization techniques. Ben, your wealth of biological knowledge has been tremendously valuable for our work and your extraordinary command of the English language has provided a constant source of entertainment.

Though I supervised Fran for her fourth year thesis project, it quickly became apparent that she was my boss. Through intimidation tactics and positive re-enforcement, Fran has helped keep me on task, made sure I was always aware of upcoming events and well fed. I would like to thank Ajit for the many hours of brainstorming sessions we would hold trying to troubleshoot the various aspects of our projects. Your guidance and insight really helped in the early years of my project. I always enjoyed our deep philosophical conversations and would like to wish you the best of luck with your studies in medical school. As with most students in the Sheardown lab, I owe a great deal of thanks to Lina Liu (aka Wonderwoman). In addition, I would like to thank all of the members of the Sheardown group. This was an exceptional group of students and so many of you have played a huge role in my graduate experience. Thanks also to the Jones, Hoare and Brash groups for your friendship and letting me use your equipment. Thanks Dr. Brash for starting the Chemical Engineering and Biosciences undergraduate program and the School of Biomedical Engineering graduate degree just in time for me to be one of the first 'guinea pigs' in both programs. Thanks also to the new directors of BME, Dr. Noseworthy and Judy West-Mays as well as the administrators, both past and present, David Ryan, Laura Kobayashi and Natalie Illingworth, for answering thousands of my questions (Lynn Falkiner too).

I would like to offer my sincere gratitude to my committee members, Dr. Carlos Filipe and Dr. Michael Brook for providing their critical perspective on my project. Committee meetings were often quite entertaining and even though the typical feedback was that I needed to narrow my focus, our meetings often evolved into brainstorming sessions where we would postulate the fascinating projects or products we might be able to spin-off.

Finally, I'd like to thank all of my friends and family. You didn't always understand why a PhD takes so long to finish, but most of you got the hint to stop asking: "when are you going to finish?" I'd like to thank my parents, who continue to amaze me by running half-marathons, skiing and snowboarding, travelling the world and remaining young at heart despite recently turning the ripe old age of 60. Next I want to thank Kyle, John, Maya, Mike and Erin; you have been incredibly generous over the years and have been great roommates and awesome teammates (Leuty Taplin Best of the Beaches). Speaking of generous, Wayne and Norma, I could not ask for better parents-in-law; you are truly two of the nicest people I have ever met. I would also like to acknowledge my Papa, Nana, Nony, Vic, Ed and Wyatt. Finally, I am extremely happy to thank my wife, Lindsay. Without you, I wouldn't be here. Literally, I'd still be stuck in undergrad! But in all seriousness, Lindsay, you are my inspiration, my entertainment, and my best friend. Thanks for everything.

Table of Contents

LIST OF FIGURES

LIST OF TABLES

LIST OF REACTION SCHEMES

LIST OF ABBREVIATIONS AND SYMBOLS

^{1}H NMR	Proton nuclear magnetic resonance spectroscopy
AA	Acrylic Acid
AAA	Alpha-amino adipic acid
ADH	Adipic acid dihydrazide
AESH	Cysteamine hydrochloride
AIBN	N,N'-Azobisisobutyronitrile
AMD	Age-related macular degeneration
ANOVA	One-factor analysis of variance
ASP	Aspartic acid
BPO	Benzoyl peroxide
BRB	Blood-retinal barrier
CMC	Critical micelle concentration
CMV	Cytomegalovirus
CNTF	Ciliary neurotrophic factor
DBA	Dimethyl-γ-butyrolactone acrylate
DDS	Dexamethasone drug delivery system
DEAAm	Poly(N,N-diethylacrylamide)
DME	Diabetic macular edema
DMF	Dimethylformamide
DMSO	Dimethyl sulfoxide
DR	Diabetic retinopathy
DSC	Differential scanning calorimetry
ECM	Extracellular matrix
ECT	Encapsulated cell technology
EDC	1-Ethyl-(3-3-dimethylaminopropyl) carbodimiide
EGF	Epidermal growth Factor
ELP	Elastin-like polypeptides
EO	Electroosmotic
EO	Ethylene oxide
EPR	Enhanced permeability and retention effect
ERG	Electroretinography
ESEM	Environmental scanning electron microscopy
EthD-1	Ethidium homodimer
EVA	Ethylene vinyl acetate
FAME	Fluocinolone acetonide in diabetic macular edema
FBR	Foreign body reaction
FBS	Fetal bovine serum
FDA	Food and Drug Administration

FT-IR	Fourier transform infrared spectroscopy
Glu	Glutamic acid
GP	Glycerophosphate
GPC	Gel permeation chromatography
η	Intrinsic viscosity
H&E	Hematoxylin and eosin
HA	Hyaluronic acid
HAMC	Hyaluronan and methylcellulose
HEMA	2-Hydroxyethyl methacrylate
HOBT	1-Hydroxybenzotriazole hydrate
HPLC	High performance liquid chromatography
HPMC	Hydroxypropylmethylcellulose
ICAM-1	Intercellular adhesion molecule-1
IGF-1	Insulin-like growth factor-1
IL-6	Interleukin-6
IOP	Intraocular pressure
IPN	Interpenetrating networks
iPS	Induced pluripotent stem cells
IVTA	Intravitreal triamcinolone
LCST	Lower critical solution temperature
MAPLA	Methacrylate-polylactide
MC	Methylcellulose
m_d	Dry mass
m_{df}	Final copolymer dry mass
m_{di}	Initial copolymer dry mass
MEHQ	4-Methoxyphenol
MEMS	Micro-electromechanical
m_w	Wet mass
MWCO	Molecular weight cutoff
NAS	N-acryloxysuccinimide
NF-κB	Nuclear factor kappa B
NHS	N-hydroxysuccinimide
NIPAAm	N-isopropylacrylamide
NP-1	Neuropilin-1
NPDR	Non-proliferative diabetic retinopathy
NVD	New vessel disc
NVE	New vessel elsewhere
OLM	Outer limiting membrane
ONL	Outer nuclear layer
PAF	Platelet-activating factor

PBS	Phosphate buffered saline solution
PCL	Poly(caprolactone)
PCol	PNIPAAm-grafted-collagen synthesized via EDC / NHS chemistry
PDGF	Platelet-derived growth factor
PDMS	Polydimethylsiloxane
PDR	Proliferative diabetic retinopathy
PEDF	Pigment epithelium derived factor
PEG	Polyethylene glycol
PEO	Polyethylene oxide
PKC	Protein kinase C
PLA	Polylactide
PLGA	Poly(lactic-co-glycolic acid)
PNIPAAm	poly(N-isopropylacrylamide)
PNN	poly(NIPAAm-NAS)
PNN-HA	poly(NIPAAm-NAS-HA)
PNN-HA.RGDS	poly(NIPAAm-NAS-HA.RGDS)
PNN-RGDS	poly(NIPAAm-NAS-RGDS)
pNNAD	poly(NIPAAm-NAS-AA-DBA
POEGMA	Poly(oligo(ethylene glycol) methacrylate)
PPO	Polypropylene oxide
PRP	Panretinal photocoagulation
PS	Polystyrene
PVA	Polyvinyl alcohol
RDGS	Arginine - glycine - aspartic acid - serine
RGD	Arginine - glycine - aspartic acid
ROP	Retinopathy of prematurity
ROS	Reactive oxygen species
RPE	Retinal pigmented epithelium
RVO	Retinal vein occlusion
SEM	Scanning electron microscopy
siRNA	Small interfering RNA
TA	Triamcinolone acetonide
TCPS	Tissue culture treated polystyrene
TGF-β	Transforming growth factor beta
Tgs	Glass transition temperature
THF	Tetrahydrofuran
TKi	Tyrosine kinase inhibitors
UV	Ultraviolet
UV PCol	PNIPAAm-grafted-collagen synthesized via UV photocrosslinking
VEGF	Vascular endothelial growth factor

DECLARATION OF ACADEMIC ACHIEVEMENT

In accordance with the guidelines for the preparation of a doctoral thesis set forth by the McMaster University School of Graduate Studies, this work has been prepared as a sandwich thesis. The research conducted in this thesis was performed in collaboration with several students, specifically manuscripts two and three in which first authorship was shared between Mohammad A. Jafar Mazumder (Jafar) and Scott Fitzpatrick. The following statements are intended to outline the contributions of each author to the selected works in the sandwich-style thesis.

Chapter 1: The literature review consists of two merged documents that were prepared separately for publication as review papers. The first review, *Temperature Responsive Materials for Drug Delivery*, was accepted (20/03/2012) for publication as a Special Report in ***Expert Review of Medical Devices***. The second review paper, *Novel Strategies for Posterior Segment Ocular Drug Delivery*, was prepared to review the current state of diabetic retinopathy and the challenges of posterior segment ocular drug delivery and has not yet been submitted for publication. Both review articles were written primarily by Scott. Jafar and Ajit Thakur contributed through manuscript planning and editing of the final submitted version of the ***Expert Reviews*** paper. Lindsay Fitzpatrick compiled a list of natural and synthetic thermoresponsive copolymers with their LCST values, Table 1-1, prepared Figure 1-1 and Figure 1-2 and helped with editing of the final draft of the ***Expert Reviews*** paper.

Chapter 2: In this manuscript, Scott was responsible for the synthesis, design, write-up and the majority of materials characterization, including GPC, FT-IR, NMR (not shown), turbidity testing, gelling time characterization, cell culture studies, confocal microscopy and ESEM imaging. Jafar helped with the FT-IR studies to confirm successful grafting of PNIPAAm chains onto the collagen backbone. Frances Lasowski assisted Scott in obtaining confocal microscopy images to demonstrate improved scaffold entrapment with collagen-containing gels. Lindsay Fitzpatrick aided Scott with statistical analysis, aided in troubleshooting and designed the PNIPAAm-grafted-collagen cartoon in Figure 2-1.

Chapter 3: This manuscript was a collaborative work and first authorship was shared between Jafar and Scott. Contributions to this work were as follows. Scott was responsible for copolymer design (with Jafar), LCST characterization via UV spectrophotometry, DSC, assessing water content, performing cell culture studies, examining copolymer morphology using SEM and paper write-up. Jafar was responsible for copolymer design (with Scott), material synthesis, characterization of copolymer composition via FT-IR and NMR, determination of molecular weight, DSC and some help with the write-up. Ben performed the *in vivo* testing, including sub-cutaneous injections, histological staining and imaging and some help with paper write-up.

Chapter 4: This manuscript was a collaborative work and first authorship was shared between Scott and Jafar. Contributions to this work were as follows. Scott was

responsible for copolymer design (with Jafar), polymer synthesis, LCST characterization via UV spectrophotometry, DSC, water content, cell culture studies, copolymer morphology using SEM, degradation in simulated physiological conditions, drug release, determination of intact copolymer molecular weight, verification of composition via NMR and paper write-up. Jafar was responsible for copolymer design (with Scott), initial polymer synthesis, characterization of copolymer composition via FT-IR and NMR, determination of molecular weight, accelerated degradation studies, DSC and some help with the write-up. Ben performed the *in vivo* testing, including sub-cutaneous injections, histological staining and imaging and some help with the paper write-up.

Chapter 5: This ongoing work is a collaborative project and contributions are as follows. Scott was responsible for initial copolymer design (with Jafar), polymer synthesis, LCST characterization via UV spectrophotometry, copolymer morphology analysis using SEM, drug release studies and write-up. Jafar was responsible for copolymer design (with Scott), initial polymer synthesis, characterization of copolymer composition via FT-IR and NMR, determination of molecular weight, accelerated degradation studies and DSC. Future work to be performed is as follows. Scott will be responsible for degradation studies, cell culture studies, mechanical testing, drug release studies, and water content analysis. Ben will perform *in vivo* testing, including sub-cutaneous injections and relevant histological analysis and intraocular cell and drug injections.

CHAPTER 1: LITERATURE REVIEW

Temperature-Sensitive Polymers for Drug Delivery and Novel Strategies for Delivery of Pharmaceuticals to the Posterior Segment of the Eye

Authors: Scott D Fitzpatrick, Lindsay E. Fitzpatrick, Mohammad A. Jafar Mazumder, Ajit Thakur, and Heather Sheardown.

Publication Information:

The literature review consists of two merged review papers that have been prepared for publication. The first review paper in the literature review, Chapter 1, section 1.2, "*Temperature Responsive Materials for Drug Delivery*", was accepted (20/03/12) for publication as a Special Report in the journal ***Expert Review of Medical Devices***. The second review paper, "*Novel Strategies for Posterior Segment Ocular Drug Delivery*", was prepared as a review of the current state of diabetic retinopathy and novel posterior segment drug delivery strategies. This review article encompasses Chapter 1, sections 1.3 and 1.4, and has been adapted to suit the scope of the thesis. This review paper has not been submitted for publication to date.

Objectives:

The objectives of the special report submitted to ***Expert Reviews*** were to briefly discuss several of the key temperature-sensitive materials, both natural and synthetic, that are important in the field of drug delivery and to speculate on the 5-year direction of the field. The objectives of the second review paper were to highlight the challenges of delivering pharmaceuticals to the back of the eye, to review several pertinent intravitreal drug delivery scaffolds, and to emphasize the need for improved delivery modalities for treatment of posterior segment conditions.

Author Contributions:

Both review articles were written primarily by Scott. Jafar and Ajit contributed through manuscript planning and editing of the final submitted version of the ***Expert Reviews*** paper. Lindsay Fitzpatrick compiled a list of natural and synthetic thermoresponsive copolymers with their LCST values, Table 1-1, prepared Figure 1-1 and Figure 1-2 and helped with editing of the final draft of the ***Expert Reviews*** paper.

1.1 INTRODUCTION

Retinal diseases, such as age-related macular degeneration (AMD) and diabetic retinopathy (DR) have a devastating effect on the health and well being of patients. DR is one of the leading causes of preventable blindness in working aged adults and impacts both developing and developed countries [1, 2]. It is estimated that by 2010, the prevalence of diabetes had risen to 285 million people worldwide and by 2030 this number is expected to increase to 438 million [3]. It is believed that roughly one third of diabetics show signs of DR and a third of these suffer from vision-threatening retinopathy [2]. Almost all patients with type 1 diabetes will develop DR within 15 years and 50 to 80% of type 2 diabetics develop DR within 20 years of their initial diagnosis [4]. More than 12,000 people lose their vision as a result of DR every year in the US [5] and the number of people at risk is expected to double in the next 25 years with the aging population [6]. AMD is the leading cause of irreversible blindness in people over 50 years old in the developed world [7]. It is estimated that over 8 million Americans currently suffer from AMD, and this number is anticipated to increase by more than 50% by 2020 [7]. In recent years, posterior segment diseases have seen exciting advances in the development of new pharmaceuticals, improvements in the understanding of the underlying biochemical pathways implicated in disease progression and in cell-based therapeutics, particularly with developments in stem cell technologies. However, effective delivery of pharmaceutical and cell-suspensions into the posterior segment of the eye remains one of the most significant unmet needs of visual health care. Posterior segment delivery is made difficult by the isolated nature of the eye, with barriers such as the blood

retinal barrier (BRB) separating the back of the eye from systemic circulation. Additionally, there are numerous barriers within the compartmentalized eye itself, which limit the diffusion of drugs within the globe. Topical drug administration is an extremely inefficient approach to deliver pharmaceuticals to the back of the eye. Typically, less than 5% of topically applied drugs successfully enter the aqueous humour, and negligible amounts reach the posterior segment [8]. Furthermore, only 1 – 2% of systemically applied drugs cross the restrictive blood ocular barriers to reach the posterior segment [9]. Intravitreal injections offer an effective means of introducing therapeutically relevant concentrations of pharmaceutical directly into the posterior segment of the eye while minimizing systemic exposure. However, due to efficient clearance mechanisms within the eye, frequent injections are required to maintain therapeutic concentrations of drug within the vitreous. Frequent injections are associated with an increased risk of complication and patient discomfort and compliance issues. Therefore, in this work, we present a series of novel biomaterial scaffolds designed to undergo a rapid phase transition, from liquid to gel, following injection into the body, allowing the introduction of a solid drug depot into the vitreous via minimally invasive techniques. Ideally, the solid drug-releasing scaffold will release low levels of pharmaceutical for sustained periods of time, maintaining therapeutic concentrations within the vitreous while minimizing systemic exposure and increasing the time between injections. Furthermore, through the incorporation of cell adhesive bioactives, we created a series of *in situ* gelling biomaterial scaffolds designed to introduce suspensions of anchorage dependant retinal

pigment epithelial (RPE) cells into the delicate subretinal space and provide a synthetic adhesion substrate for the transplanted cells.

1.2 BACKGROUND: TEMPERATURE RESPONSIVE MATERIALS FOR DRUG DELIVERY

Stimuli responsive materials have gained considerable attention for their potential to create targeted, tunable and personalized therapeutics that respond directly to the physiologic environment. With recent advances in medical polymer technology, it is becoming increasingly possible to tailor drug-releasing scaffolds to produce on-demand delivery of therapeutic payloads locally in response to physiological requirements [10]. Stimuli responsive polymers, also termed intelligent, smart, environmentally responsive and sensitive polymers, are a class of materials that undergo significant, rapid physicochemical changes in response to small changes in environmental conditions. There are a number of different classes of responsive polymers, which respond to a distinct set of stimuli, including light, pH, temperature, ultrasound, magnetism, electric field, enzymes, antibodies, or the presence of specific molecules, such as glucose [11]. Additionally, the specific response varies depending on the system. Polymers may undergo changes in hydrophobic / hydrophilic balance, solubility, hydration, conformation, shape, degradation, or micellization in response to the presence, or absence, of an external stimulus [11]. It is therefore possible to employ these materials to generate drug delivery scaffolds that respond with predictable, controllable, pre-defined response profiles to impart a large degree of control and tunability over drug dosing. The ability to produce targeted on-demand drug release has implications in a number of

different clinical applications, including hormone replacement therapy, chemotherapy, rhythmic heart disorders, diabetes, birth control and posterior segment ocular drug delivery. Of the various stimuli responsive materials, temperature-sensitive polymers are the most widely studied and this special report, while not exhaustive, will focus on several of these materials that have particular importance in drug delivery applications. A list of natural and synthetic thermoresponsive homopolymers and copolymers that are relevant to drug delivery is provided in Table 1.

1.2.1 Thermo-Responsive Polymers and their Applicability for Controlled Release Drug Delivery

Thermoresponsive polymers utilize subtle changes in temperature to trigger macroscopic changes in material properties. Polymers that possess a lower critical solution temperature (LCST) typically undergo a sol-gel phase transition when heated above their LCST, whereas polymers that become soluble upon heating are said to possess an upper critical solution temperature (UCST) [12]. Both systems can be exploited for drug delivery purposes. LCST copolymers can simply be mixed with drug as a liquid suspension at room temperature and delivered via minimally invasively injection techniques directly to hard-to-access target tissues within the body. Heating to physiologic temperature drives a sol-gel phase transition, which entraps infused drug within a solid depot, and can provide sustained-release of therapeutic concentrations of drug directly at the site of interest [13]. Drug-releasing polymer systems possessing a UCST may employ temperature-induced swelling or scaffold destabilization to rapidly release drug at a target site [14]. Localized heating (tumor tissues) or the application of an

externally applied stimulus (ultrasound, infrared laser, etc.) may be utilized to induce the local destabilization of a UCST drug releasing copolymer scaffold to produce targeted release [15, 16].

Thermoresponsive drug delivery scaffolds offer numerous advantages, such as eliminating the need for invasive surgical implantation and the ability to bypass physiological barriers allowing delivery to hard to access locations within the body [17]. Furthermore, drug encapsulation within a scaffold may protect the therapeutic agent from enzymatic or environmental degradation. The release rate can be tailored to locally produce persistent levels of therapeutically relevant concentrations of drug, thus overcoming the ineffectiveness of simple injections, which are associated with an initial spike that may lead to toxic levels initially followed by a rapid decrease to levels that possess little to no therapeutic benefit, Figure 1 [17].

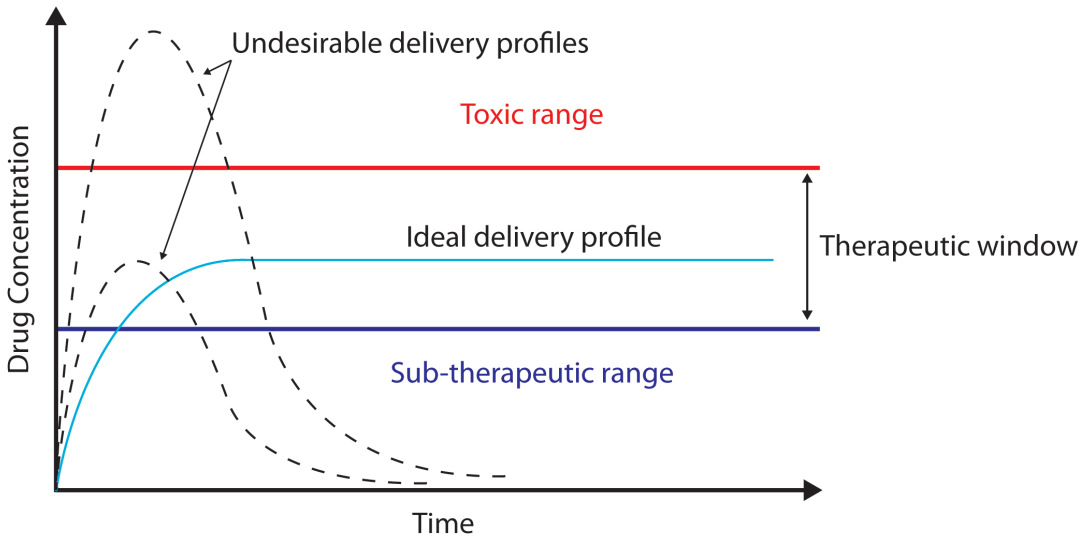

Figure 1-1: Representation of the ideal delivery profile in which drug concentration is maintained within the therapeutic window, below the toxic threshold, but high enough to exert a therapeutic effect.

1.2.1.1 Synthetic Thermoresponsive Materials

1.2.1.1.1 Poly(N-isopropylacrylamide) (PNIPAAm)

Polymer hydrogels that display reversible volume changes have gained considerable interest since Tanaka observed the tendency of polyacrylamide gels to undergo phase separation in response to temperature or fluid composition [18]. Poly(N-isopropylacrylamide) (PNIPAAm) is one of the most widely studied temperature-sensitive polymers; it exhibits a rapid sol-gel transition when heated above its LCST, approximately 32^{o}C, allowing injection at room temperature and scaffold formation at body temperature [13]. One of the major limitations of PNIPAAm is that it is non-degradable. Degradable drug delivery materials afford elimination of the scaffold following exhaustion of the drug reservoir without the requirement for secondary surgical removal. Therefore, there has been an increased emphasis in recent years on introducing degradability into NIPAAm-based copolymers. Ultimately, it is desirable to preserve the thermal phase transition properties of NIPAAm, while promoting the eventual degradation and clearance from the body following exhaustion of the therapeutic effect. In 1999, Neradovic et al. synthesized NIPAAm-based polymers with 2-hydroxyethyl methacrylate – monolactate (HEMA-monolactate) [19]. As the hydrolytically labile lactate ester side groups were cleaved, the hydrophilicity of the copolymer increased, raising the LCST. If the LCST is raised above body temperature, the thermoreversible NIPAAm-based copolymers revert back into a hydrated liquid state, allowing uptake into systemic circulation and clearance from the body, provided the molecular weight is below the renal filtration limit of 30 – 50 kDa [20]. Yoshida et al. designed NIPAAm-based

copolymers that were crosslinked with degradable poly(amino acids) [21], which showed a similar clearance mechanism. Guan et al. synthesized a series of protein-reactive NIPAAm-based copolymers possessing relatively high tensile strength that hydrolyze to produce soluble, non-toxic degradation products through copolymerization with HEMA-polylactide (HEMA-PLA), N-acryloxysuccinimide (NAS) and acrylic acid (AA) [22]. Ma et al. further improved mechanical properties through incorporation of methacrylate-polylactide (MAPLA) and HEMA [23]. Cui et al. developed a series of slow-degrading NIPAAm-based copolymers through copolymerization with dimethyl-γ-butyrolactone acrylate (DBA). These copolymers undergo a hydrolysis-dependent opening of the DBA lactone ring structure, capable of increasing LCST above body temperature without producing any degradation products [24, 25]. The Sheardown group prepared bioactive NIPAAm / DBA copolymers through copolymerization with NAS [26] for posterior segment ophthalmic cell and drug delivery purposes. For a list of thermoresponsive homopolymers and copolymers of PNIPAAm, see Liu, 2008 [27]. There are many other examples of N-substituted thermoresponsive polyacrylamides that may be suitable for drug delivery, such as poly(N,N-diethylacrylamide (DEAAm) [28, 29] and poly(N-vinyl caprolactam) (PVCL) [30]. For a comprehensive list, see Asayev, 2010 [31]. Similar to PNIPAAm, linear polymers of DEAAm and PVCL have LCST values of 32^{o}C [28] and 31^{o}C [27] respectively.

1.2.1.1.2 Polyethylene Oxide (PEO) Based Thermoresponsive Copolymers

Triblock copolymers possessing an A-B-A configuration of poly(ethylene oxide)-poly(propylene oxide)-poly(ethylene oxide) (PEO-PPO-PEO), referred to as Pluronics or

Poloxamers, are another family of thermogelling synthetic materials that have been extensively studied for their potential use as drug carriers [32]. Through manipulation of concentration, composition and molecular weight, these copolymers can be tuned to undergo reversible gelation at physiological temperature and pH [32]. The combination of hydrophilic ethylene oxide and hydrophobic propylene oxide units creates an amphiphilic copolymer that can self-associate into micelles under aqueous conditions when above a critical micelle concentration (CMC), Figure 2. The CMC is highly temperature dependent, as below a critical micelle temperature, both ethylene oxide and propylene oxide blocks are relatively soluble in water [32]. As the temperature of the system increases, the PPO chains become less soluble, resulting in micelle formation. Pluronic micelles typically possess a diameter ranging from 10 to 100 nm and consist of a hydrophobic, PPO-rich core and a hydrated, hydrophilic PEO-rich shell [33]. The PPO core is capable of incorporating up to 30 wt % of water insoluble drugs, while the PEO corona maintains the micelles in a dispersed state and improves drug stability by shielding the reserves from undesirable interaction with cells and proteins [33]. However, these hydrogels tend to possess poor mechanical strength, limited stability, and high permeability, thereby limiting their effectiveness as sustained-release systems [33, 34]. Cohn et al. have utilized a number of strategies to improve the mechanical integrity of PEO / PPO copolymers. Such strategies include the introduction of *in situ* crosslinking end-groups, such as carbon-carbon double bonds [35], methacrylate groups [36] and triethoxysilane groups [36] and covalently linking PEO and PPO using carbonyl chloride and diacyl chloride coupling agents [37]. In recent years, there has been extensive

investigation into the synthesis of copolymers of polyethylene glycol (PEG) with degradable polyesters such as polylactide (PLA), poly(lactide-co-glycolide) (PLGA) and poly(caprolactone) (PCL) to generate thermoresponsive copolymers with improved rigidity that degrade *in vivo*, allowing their ultimate clearance from the body [37-39]. PEG-containing copolymers that have attracted significant interest include PLGA-PEG-PLGA, PEG-PLA-PEG, PCL-PEG-PCL, and poly(oligo(ethylene glycol) methacrylate) (POEGMA) to name a few [10].

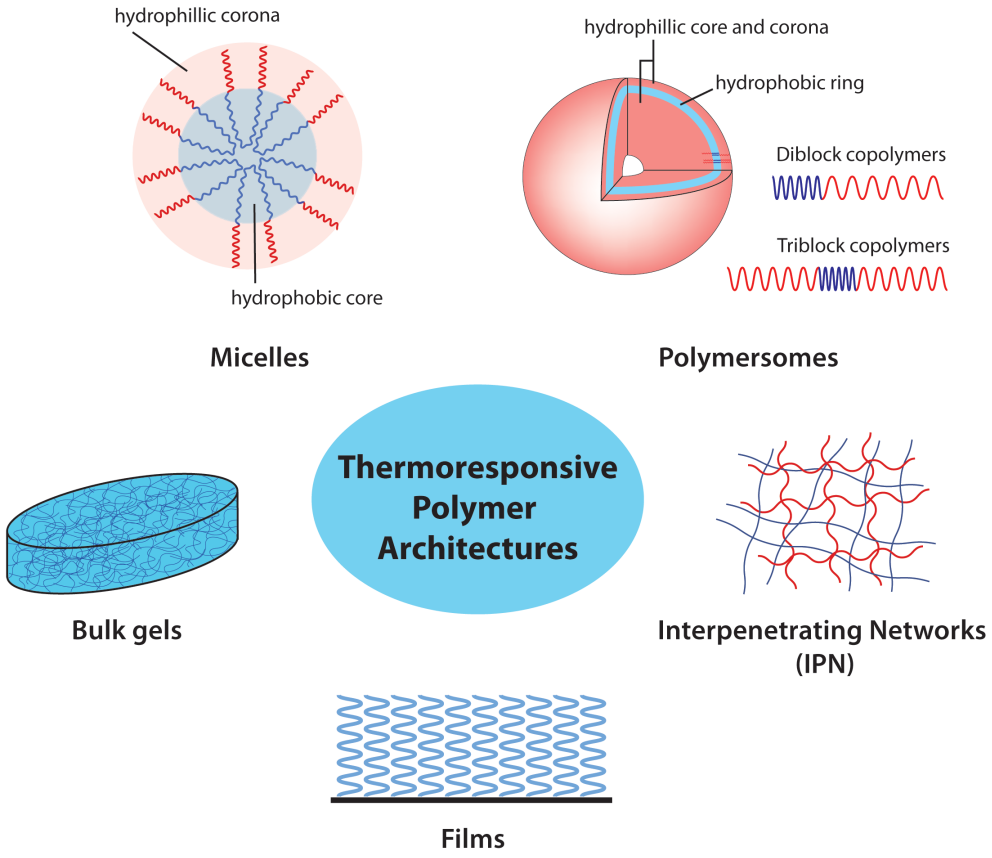

Figure 1-2: Illustration of some of the architectures that can be obtained using thermoresponsive copolymers for drug delivery applications. The architectures include bulk gels, micelles possessing a hydrophobic core and hydrophilic corona, polymersome that have a hydrophobic layer sandwiched between a hydrophilic core and corona, IPNs and polymer films.

1.2.1.1.3 Polyphosphazenes

Polyphosphazenes are a thermoresponsive family of hybrid organic-inorganic polymers. These polymers contain an inorganic backbone consisting of alternating nitrogen and phosphorous atoms connected by alternating single and double bonds [40]. Attached to every phosphorous group are two organic groups that impart a high degree of versatility for modification and manipulation of properties and functionality, which can be utilized to impart thermoresponsive properties [13]. Numerous approaches have been explored to develop hydrolytically susceptible copolymers that have highly controllable degradation kinetics, capable of breaking down in periods that range from hours to years [40-43]. Polyphosphazenes have demonstrated good compatibility with numerous cell lines in culture [44, 45] and *in vivo* [46]. Furthermore, the degradation byproducts, namely ammonia, phosphate and alcohol, are well tolerated and the copolymers can be designed to possess fast *in situ* gelation with tunable release kinetics, making polyphosphazenes attractive candidates for drug delivery [40, 47]. For an in depth review of polyphosphazenes, see Kumbar 2006 [40].

1.2.1.2 Natural Thermoresponsive Materials

1.2.1.2.1 Elastin-Like Polypeptides

Elastin-like polypeptides (ELPs) are synthetic elastin-inspired polymers with a pentapeptide amino acid repeat structure, Val-Pro-Gly-Xaa-Gly, where the Xaa guest residue can be any natural amino acid except proline [48, 49]. Below the phase transition temperature (T_t), ELPs exist as a clear homogeneous aqueous solution. When heated above their transition temperature, the solution becomes turbid through ELP coacervation

into droplets [50]. The ELP droplet size and distribution can be manipulated through concentration and temperature [50], while the transition temperature can be adjusted by varying the concentration, molecular weight, salt content and ELP composition (ie – through modifying the Xaa guest residue, using variable amino acid sequences or by functionalization with other proteins or polymers) [50]. ELPs are interesting candidates for drug delivery as they possess tunable characteristics, are well tolerated *in vivo*, and degrade into simple amino acid residues [51]. Additionally, the molecular weight and composition of ELPs can be precisely controlled through genetic engineering approaches to form narrowly dispersed polymers, which allows an increased level of control over drug release performance [52]. Furthermore, ELPs can be expressed in high quantities from Escherichia Coli and can be easily purified as a result of their thermo-gelling behavior [53]. The Chilkoti group has extensively studied ELPs for their ability to target tumor tissues [54-57]. In one strategy, the group passively targeted tumor tissues by employing drug-conjugated ELPs with a T_t that was well above physiologic temperature. The small, soluble, ELPs took advantage of the enhanced permeability of tumor vasculature to accumulate within tumor tissues following systemic delivery [56]. In another approach, ELP-drug conjugates were designed to thermally target tumor tissues. The peptides were engineered to possess a T_t between 37 and 42^{o}C and an externally applied stimuli induced localized hyperthermia causing the ELP-drug conjugates to aggregate and adhere to the vessel walls [57]. Mild hyperthermia was also used to drive the localized assembly of micelles that possessed a tumor-targeting ligand on the hydrophilic corona, leading to enhanced cellular uptake [55]. In another strategy, ELPs

with a sub-physiologic T_t were injected directly into tumorous tissues to produce a sustained-release drug depot directly within the tumor tissues for extended treatment [54].

1.2.1.2.2 Chitosan

Chitosan is a polysaccharide that is derived from chitin [13]. While on its own chitosan is not thermoresponsive, it becomes so when mixed with glycerophosphate (GP) [13]. At elevated temperatures, GP forms strong hydrogen bonds with chitosan, which leads to gel formation [13]. However, chitosan/GP mixtures tend to possess slow gelation rates. Therefore, for applications requiring more rapid gelation, the derivative chitosan chloride can be used to expedite the gelling process [58]. Chitosan scaffolds also suffer from relatively rapid release of loaded protein and drugs possessing low molecular weight; complete release is often achieved within several hours [13, 59]. There are also concerns about the suitability of chitosan/GP hydrogels for *in vivo* application as they have been shown to induce a relatively significant inflammatory response [60].

1.2.1.2.3 Cellulose Derivatives

Several cellulose derivatives, such as methylcellulose (MC) and hydroxypropylmethylcellulose (HPMC) display LCST behavior that can be exploited for drug delivery and tissue engineering applications [61]. MC and HPMC display LCST values between 40 – 50^{o}C and 75 – 90^{o}C respectively [62]. However these values can be substantially lowered using both physical and chemical methods, such as the addition of NaCl or a reduction in the hydroxypropyl content [62, 63]. At low temperatures, the macromolecules exist in a fully hydrated state with little polymer-polymer interaction

aside from physical entanglement [61]. Upon heating, intermolecular hydrophobic interactions between the methoxy groups result in gradual dehydration and gel formation [62]. Recently, a physical blend of hyaluronan and MC (HAMC) demonstrated rapid thermo-reversible *in situ* gelation, degradability, good *in vivo* tolerance and potential for minimally invasive intrathecal drug delivery for spinal cord injuries [64, 65]. Formulations of HAMC have also demonstrated favorable results as injectable cell scaffolds for retinal therapeutics [66].

1.2.1.2.4 Xyloglucan

In its native form, the xyloglucan polysaccharide does not form a gel [67]. However, Miyazaki et al. developed a thermally reversible xyloglucan hydrogel through partial degradation of xyloglucan from the seeds of *Tamarindus indica* [68]. When more than 35% of the galactose residues have been removed, xyloglucan exhibits temperature responsive behavior under dilute aqueous conditions and possesses a relatively high storage modulus [32, 34]. Xyloglucan gels have been examined as drug delivery scaffolds for oral [69], ocular [70], rectal [68], percutaneous [71] and intraperitoneal [72] applications.

1.2.2 Polymer Architecture

A crucial parameter to consider when designing *in situ* forming drug delivery scaffolds is the type of polymeric architecture that will be most suitable for the intended application. *In situ* forming hydrogels can form numerous scaffold architectures, such as interpenetrating networks (IPN), micelles, polymersomes, films and other variations,

Figure 2. There are two main types of gels: physical gels and crosslinked gels. Physical gels are formed through the physical entanglement of polymer chains or micelle ordering, whereas crosslinked gels are covalently bound [17]. Covalently linked thermoresponsive networks undergo a change in their degree of swelling in response to temperature, while physically linked gels undergo a sol-gel phase transition [17]. Covalently linked networks can either be formed *in situ* or prior to implantation. *In situ* crosslinking minimizes invasiveness of instillation, but requires the use of crosslinking chemistry that is safe *in vivo*.

IPNs consist of two or more polymer networks that are bound through physical entanglement such that the networks can only be separated through bond breakage. IPNs offer a powerful tool for drug delivery as each polymer in the network can introduce specific properties, such as temperature-sensitivity, and new properties can arise from the interaction of the various polymers within the network. Furthermore, it is relatively easy to manipulate properties by varying the polymer ratio within the IPN and modifying the polymers within the network. Liu et al. have designed transparent silicone/PNIPAAm IPN materials which show temperature transitions that are useful for drug loading and which show particular promise for the delivery of hydrophobic drugs (Liu and Sheardown, J Controlled Rel submitted). Semi-interpenetrating copolymer networks (semi-IPNs) contain at least one crosslinked polymer network, either linear or branched [73]. Kim et al. prepared thermoresponsive semi-IPNs based on chitosan and poly(acryl amide) (PAAm) in which the hybrid synthetic and natural copolymers displayed high swelling ratios that were dependent on temperature, pH, ion concentration and electric

field [73]. Nanoparticle IPNs consisting of poly (acrylic acid) (PAA) and PAAm display UCST behavior and rapidly swell in response to heating above a critical temperature [74]. Chen et al. prepared semi-IPN nanogels based on hydroxypropylcellulse (HPC), which possesses an LCST around 41^{o}C, and PAA, which, as mentioned, possesses UCST behavior [75]. By varying the chemical composition and the degree of crosslinking, the phase transition properties of these HPC-PAA nanogel semi-IPNs could be shifted from UCST to LCST. IPNs and semi-IPNs of thermoresponsive copolymers offer a high degree of flexibility and can be tailored to provide variable release profiles to suit a broad range of applications.

As discussed, amphiphilic block copolymers can spontaneously assemble into micelles with a hydrophilic corona and a hydrophobic core. Therefore, micelles may be particularly useful for cancer therapeutics, as many chemotherapeutics are small hydrophobic compounds with a poor therapeutic index [53]. Micelle drug carriers can increase drug accumulation in tumor tissues while minimizing off-target effects through the enhanced permeability and retention (EPR) effect, which allows extravasation of the small drug carriers through the leaky tumor vasculature, as mentioned previously [53]. Quan et al. designed an elegant thermoresponsive micelle carrier for tumor-triggered drug release [76]. Upon encountering the subtle physiological changes in tumor physiology (pH 6.8, T > 37 ^{o}C), PEGylated RGD peptides were de-protected allowing internalization by RGD-receptor overexpressing tumor cells and destabilization of drug-loaded micelles for localized treatment. Wei et al. synthesized a series of NIPAAm-containing thermoresponsive shell crosslinked micelles [77]. They found that the crosslinked shell

slowed drug release at temperatures below the LCST (25^{o}C), but the rate accelerated dramatically above the LCST (37^{o}C) as pNIPAAm gelation led to a deformation of the micelle structure.

Polymersome*s*, also known as polymer vesicles, are similar to micelles in that they are self-assembling amphiphilic block copolymers, however they arrange to form a hydrophobic ring sandwiched between a hydrophilic core and corona [17]. The polymersome structure allows interior encapsulation of both hydrophilic and hydrophobic drugs while the hydrophilic shell protects the entrapped drug from undesirable interactions and can help the drug delivery system to evade the immune system. The hydrophilic corona can act as a rate controlling membrane to modulate the release of drug from the hydrophobic ring, which in turn can serve to impede release from the hydrophilic core [78]. Li et al. synthesized thermoresponsive, self-assembling polymersomes consisting of diblock copolymers of poly(N-(3-aminopropyl)methacrylamide hydrochloride) (PAMPA) and PNIPAAm [79]. In aqueous conditions, the amphiphilic block copolymers existed as unimers at room temperature and transitioned to form vesicles when heated above their LCST, which could be adjusted between 30 – 40^{o}C by varying composition. The vesicle shells were then crosslinked by polyelectrolyte complexation. Qin et al. prepared thermoresponsive, doxorubicin-containing PEG-PNIPAAm-based polymersomes that self-associated upon heating above their LCST and could be destabilized, or ruptured, upon local cooling with either ice or penetrating cryoprobes [80]. These experiments demonstrate how temperature-sensitivity can be utilized to create localized drug release following minimally invasive delivery. For

an in depth review of stimuli-responsive polymersomes in targeted drug delivery, see Meng 2009 [81].

Thermoresponsive *films* can also be used as coatings on medical implants to create a stimuli-responsive material capable of modulating the microenvironment surrounding the implant. For example, a rate-controlling thermoresponsive film may increase its release rate in response to slightly elevated increases in temperature due to localized inflammation.

Using thermoresponsive materials, there are numerous design architectures that can be generated, and researchers must decide which type is suitable for their intended application. For an in depth review on temperature responsive polymer architecture, see Ward 2011 [17] and Stuart 2010 [78].

1.2.3 Expert Commentary

When designing drug delivery vehicles, an important design question to consider is whether to use natural or synthetic materials. Both choices possess inherent advantages and disadvantages. While natural materials offer great potential for inherent biocompatibility, synthetic materials offer greater flexibility for manipulation and tuning of system performance. With natural materials, we are limited in our ability to modulate material properties, unless we resort to the use of synthetic modification techniques. Furthermore, natural materials often possess indefinite composition, poor mechanical strength, variable and uncontrollable degradation kinetics, microbial contamination and compatibility issues [40]. Whereas synthetic polymers allow a high degree of control over important design constraints, such as mechanical properties, degradation rates, pore size,

morphology, scaffold shape and size, drug release kinetics and bio-mimetic behavior [40]. It is the opinion of the authors that, moving forward, synthetic polymers inspired by and potentially augmented by natural materials will provide valuable tools for the design of novel drug releasing scaffolds. Patenaude et al. synthesized novel hybrids of natural and synthetic materials based on PNIPAAm and various carbohydrate polymers [82]. These studies demonstrated a high degree of control over copolymer properties, such as swelling, degradation, phase transition, and mechanical properties, effectively combining the desired performance features of both natural (degradation and biological interactions) and synthetic (compositional diversity and thermal sensitivity) materials. Table 2 lists some of the advantages and disadvantages of natural and synthetic materials for medical application.

The current state of temperature-sensitive drug delivery copolymers offers minimally invasive implantation of sustained-release scaffolds to hard-to-access regions within the body through simple injection and *in situ* gelation. Furthermore, through utilization of the subtle temperature increase in tumor tissues, it is possible to tailor scaffolds to undergo a sol-phase transition upon encountering a tumor, thus targeting the subtle physiological differences and providing localized dosing. Several strategies, such as localized ultrasound application, can induce subtle temperature increases that lead to directed accumulation of drug carriers that possess gelling temperatures slightly above physiologic temperature and penetrating cryoprobes can induce localized cooling to destabilize drug carriers. Thus, temperature-sensitive drug delivery scaffolds are particularly interesting for cancer therapeutics and applications where minimally invasive

procedures are crucial, such as spinal cord [65] and ocular cell and drug delivery purposes [83]. However, temperature-responsive copolymers alone are limited in their ability to respond to the abundance of subtle differences that characterize specific diseased states. Therefore, when used in conjunction with additional stimuli responsive materials, the degree of control vastly increases, as dual, or multi-responsive materials can respond with controllable properties to a number of different physiological states.

There are two classifications of stimuli-responsive materials that can be used to further functionalize temperature-sensitive drug delivery scaffolds: materials that respond to internal stimuli present in the *in vivo* environment and those that respond to externally applied stimuli. Light, magnetism, electrical impulses and ultrasound are examples of stimuli that can be externally applied to manipulate and regulate the performance of implanted scaffolds [84]. Ionic strength, pH, enzymes, antigen-antibody interactions, or the presence of specific chemicals are examples of internal stimuli that may drive a behavioral change in an implanted scaffold [85]. Internal stimuli have the ability to act as a negative feedback loop and generate a direct response to the surrounding physiologic environment. In contrast, externally regulated stimuli responsive materials require active manipulation from an outside source to generate a change in performance properties. While internal stimuli may provide better on-demand release profiles and tighter regulation of the pathological state, materials requiring external stimuli afford physicians a greater degree of control over the dosing parameters, which is particularly important should complications arise. For an in depth review on recent advances and future

perspectives of various stimuli-responsive materials, see Roy (2010) [85], McCoy (2010) [86] and Bawa (2009) [84].

1.2.3.1 Thermoresponsive and Externally Regulated Stimuli Responsive Systems

There are many examples of dual thermo- and externally regulated copolymer systems. Temperature and light responsive materials were prepared from photochromic derivatives of ELP, in which one azobenzene moiety was incorporated for ever 30 amino acid residues [87]. Irradiation at 350 nm induced a trans – cis isomerization, which increased the hydrophilicity of the material and shifted the phase transition temperature from 32 – 42^{o}C. Irradiation with a longer wavelength was found to reform 50% of the hydrophobic trans isomer, thus driving phase separation. Such a system could be used to generate a pulsed-release profile for on-demand release. Zrinyi synthesized thermo- and magnetoresponsive polymer beads by incorporating magnetic nanoparticles into crosslinked PNIPAAm and PVA hydrogels [88]. In uniform magnetic fields, the gel beads arranged into linear, chainlike structures. However, in non-uniform fields, the gels formed random aggregates. This study demonstrates the ability to externally manipulate scaffold architecture with externally applied magnetism. This concept could be extended to manipulate gates in a channeled drug release scaffold, thus creating on-off capabilities and a pulsatile release profile. Kim et al. prepared thermo- and electroresponsive IPNs from PVA and PNIPAAm [89]. Electroresponsive materials tend to swell, shrink, or bend in response to an applied electric field and are typically comprised of polyelectrolyte hydrogels [90]. Deformation of the polyelectrolyte occurs as charged ions are guided towards the cathode or anode side of the gel [90]. Ultrasound is a non-invasive stimuli

that has been shown to influence drug release properties within the body by accelerating degradation in degradable polymers and enhancing the permeation of drug in both eroding and non-eroding scaffolds [90]. Ultrasound can be used to disrupt micelle architecture through acoustic destabilization, thus inducing release of the therapeutic payload [90, 91]. It can also be used to induce localized heating and aggregation of thermoresponsive drug scaffolds.

1.2.3.2 Thermoresponsive and Internally Regulated Stimuli Responsive Systems

Thermoresponsive copolymers have also been combined with a number of materials that respond to internal stimuli. pH responsive systems have received considerable attention owing to the significant variation of pH within the different locations of the body. In the GI tract, the stomach has an acidic pH between 1 and 3, whereas the duodenum ranges from 4.8 – 8.2 [12]. Cancer tissue has a slightly acidic extracellur pH between 6.5 – 7.2, whereas normal tissues and blood possess a pH around 7.4 [12]. Furthermore, intracellular variations in pH can be exploited for targeted delivery; the early endosome, late endosome and lysosome have pH values of 6.0 – 6.5, 5.0 – 6.0, and 4.5 – 5.0 [12]. pH responsive polymers contain weak acids or weak bases, such as carboxylic acids or amines, and thus undergo changes in their ionization state in response to changes in pH [12]. Changes in the ionization state can lead to conformational changes, such as micelle formation or disruption, or changes in swelling properties of crosslinked gels [11]. Ionizable polymers possessing a pKa that closely matches the pH of the target tissues can utilize the conformational pH-induced changes to release drug at a specific location. There are many examples of thermo- and pH-

responsive polymers systems. Peppas et al. described the synthesis and characterization of temperature and pH-responsive hydrogels of methacrylic acid and PNIPAAm [92] and Leung et al. synthesized microgels with a thermoresponsive core and ph-sensitive shell [93]. These studies demonstrate the potential to target tissues based on their pH and are particularly interesting for cancer therapeutics as tumor tissues possess an elevated temperature and a slightly acidic pH. In addition to pH, antigen-responsive materials are capable of undergoing significant property changes in response to highly specific stimuli recognition. Lu et al. reported the synthesis of thermo- and antigen-responsive hydrogels from the combination of a polymerizable antibody Fab' fragment, which was prepared from an anti-fluorescein monoclonal antibody, with NIPAAm and N,N'-methylenebis(acrylamide) (MBAAm) [94]. The resulting hydrogels underwent significant reversible volume changes in response to both temperature and the presence of antigens. Glucose-responsive copolymers are of considerable interest for their ability to detect glucose levels and deliver insulin as required [90]. Glucose-responsive polymers typically function either through enzymatic oxidation of glucose via glucose oxidase (GOx), through glucose binding with concanavalin A (ConA), or through reversible bond formation with boronic acids [90]. Thermo-and glucose responsive copolymers have been synthesized from comb-type graft copolymers of poly(N-isopropylacrylamide-co-3-acrylamidophenylboronic acid) [95], and through covalently linking GOx to copolymers of NIPAAm, MAA and octadecylacrylate (ODA) and subsequently immobilizing to the surface of liposomes [96]. Such scaffolds could introduce sustained release scaffolds that detect blood sugar levels and accordingly modify their insulin-release profile, thus

decreasing the frequency of insulin injections and allowing tighter regulation of blood sugar levels.

While temperature-sensitive materials have tremendous potential for targeted drug delivery, combination with dual and multi-responsive polymer systems has the potential to unleash and help realize the true capabilities of these drug release scaffolds to create personalized and on-demand release profiles.

1.2.4 Five-Year Outlook

It is becoming increasingly possible to synthesize drug delivery scaffolds consisting of multiple stimuli-responsive materials that can locally release a multitude of different pharmaceuticals on-demand in response to internal physiological feedback and externally applied signals. Such control will allow drastically improved manipulation of the microenvironment of diseased tissues and improve the regulation of systemic conditions. As our understanding of the physiological signature of different diseases increases, so too will our ability to design drug releasing scaffolds that produce a predictable and controllable response to disease specific stimuli. As mentioned, temperature-sensitive systems alone are limited in their ability to respond to the surplus of stimuli that characterize a specific disease. Therefore, the true power of thermoresponsive drug releasing scaffolds will be realized when they are combined with additional stimuli-responsive materials. Such dual and multi-responsive drug delivery scaffolds are beginning to emerge in the literature as temperature-sensitive polymers are combined with materials capable of external regulation through stimuli such as light [97], magnetism [98] and ultrasound [99]. However, a new generation of stimuli responsive

materials is emerging, wherein the identification of differentiating environmental factors characterizing various conditions is allowing the use of intricate internal stimuli to manipulate polymer properties to create a pre-defined response to disease-specific environmental cues, thus providing on-demand, personalized treatment. A thermoresponsive, glucose-sensitive copolymer that forms an insulin-loaded scaffold upon injection into the body with release that is dictated by blood sugar levels would mimic the body's natural regulation mechanism and help provide tighter regulation of blood sugar levels for diabetic patients. The generation of such nature-mimicking scaffolds will be driven by the improved understanding of biochemical pathways implicated in various diseases. Better characterization of the chemical signature of various diseases expands the engineer's toolbox for designing novel scaffolds capable of providing personalized treatment. Thus, future generations of drug delivery scaffolds will require a multi-disciplinary approach to harness the true potential of stimuli-responsive materials.

1.2.5 Key Issues

- Temperature-sensitive drug delivery scaffolds allow minimally invasive instillation of sustained release scaffolds for localized or systemic treatment.
- Encapsulation within a scaffold protects pharmaceuticals from undesirable interactions and enzymatic or environmental degradation. Furthermore, the scaffolds can be designed to generate sustained drug release, maintaining concentrations within the therapeutic window and avoiding complications frequently associated with simple injections.

- There are numerous temperature responsive polymers and architectures to choose from when designing drug delivery scaffolds. Several design choices include whether to use degradable versus non-degradable scaffolds, natural versus synthetic materials and which architecture (simple hydrogel aggregates, interpenetrating networks, micelles, polymersomes, films etc) is best suited for the intended application.
- Synthetic materials offer a high degree of flexibility, allowing manipulation of mechanical properties, degradation rates, pore size, morphology, scaffold shape and size and drug release kinetics, whereas natural materials often possess uncontrollable degradation kinetics, microbial contamination and compatibility issues. Ultimately, combinations of natural and synthetic materials may overcome the limitations while capitalizing on the strengths of both types of materials.
- Temperature-sensitive drug delivery scaffolds are particularly well suited for delivery of chemotherapeutics. Scaffolds designed with a gelling temperature slightly above physiologic value utilize the subtle temperature increase in tumor tissues to drive scaffold formation and accumulation in tumor vasculature and surrounding tissues.
- *In situ* gelling temperature-sensitive drug delivery scaffolds have tremendous potential for hard-to-access complications requiring minimally invasive techniques, such as ocular and spinal cord therapeutics.
- Combining temperature-sensitive polymers with additional stimuli responsive materials imparts the ability to respond to numerous external and internal stimuli,

such as light, magnetism, electrical impulses, ultrasound (external) and ionic strength, pH, enzymes, antigen-antibody interactions, or specific chemicals (internal). Such dual and multi-responsive drug delivery scaffolds afford a significant level of control over dosing characteristics and treatment personalization.

- The continued identification of differentiating environmental factors characterizing specific diseases will allow the development of increasingly intricate scaffolds capable of responding to disease-specific cues to provide negative feedback that attempts to mimic the body's natural regulation mechanisms.

Table 1-1: A list of natural and synthetic thermoresponsive homopolymers and copolymers with their corresponding thermal phase transition temperatures.

Name	Abbreviation	LCST/ UCST (°C)	Ref.
Synthetic Homopolymers			
Poly(N-vinylcaprolactam)	PVCL	31	[100]
Poly(N-isopropylacrylamide)	PNIPAAm	32	[101]
Poly(N-n-propylacrylamide)	PNPAm	25	[102]
Poly(N,N-ethylmethylacrylamide)	PEMA	70	[102]
Poly(N-ethylacrylamide)	PEA	82	[103]
Poly(N,N-diethylacrylamide)	PDEAAm	~28 - 32	[28]
Poly(ethoxypropylacrylamide)	PEPA	~32	[104]
Poly(N,N-bis(2-methoxyethyl) acrylamide)	PBMEAm	49	[105]
Poly(N-(3-methoxypropyl)acrylamide)	PMPAm	>60	[105]
Poly(vinyl methyl ether)	PVME	34	[106]
Poly(2-dimethylamino)ethyl methacrylate)	PDMA	50	[107]
Poly(proprylene oxide)	PPO	10–20	[108]
Poly(2-ethyl-2-oxazoline)	PEOZ	~62	[109]
Poly(2-isopropyl-2-oxazoline)	PIPOZ	~36	[110]
Polyphosphazenes		~25 - 99	[82, 90]
Synthetic Multi-Block Copolymers			
Poly(ethylene oxide)-poly(propylene oxide)-poly(ethylene oxide) [Pluronics®]	PEO-PPO-PEO	10 - 100	[111]
*L42**	*PEO_4-PPO_{22}-PEO_4*	*37*	[111]
*L62**	*PEO_6-PPO_{34}-PEO_6*	*32*	[111]
*L63**	*PEO_9-PPO_{32}-PEO_9*	*34*	[111]
Polyester/PEG block copolymers			
Poly(lactic acid-co- glycolic acid)-polyethylene glycol- poly(lactic acid-co- glycolic acid)	*PLGA-PEG-PLGA*	*~37*	[112]
Poly(ethylene glycol)–b-poly(D,L-lactic acid-co-glycolic acid)–b-poly(ethylene glycol)	*PEG-PLA-PEG*	*~37*	[113]
Poly(oligo(ethylene glycol) methacrylate)	POEGMA	26 - 90	[114]
sPoly(ethylene glycol)-b- poly(2-(2-methoxy ethoxy) ethyl methacrylate-co-oligo(ethylene glycol) methacrylate)	*sPEG-b-P(MEO2MA-co-$OEGMA_{475}$)*	*35 - 41*	[115]
Poly(2-(2-methoxyethoxy)ethyl methacrylate-co-oligo(ethylene glycol) methacrylate)	*P(MEO2MA-co- OEGMA) 5-8% OEGMA units per chain*	*32 - 37*	[114]
Poly(ε-caprolactone)-poly(ethylene glycol)-poly(ε-caprolactone)	PCL-PEG-PCL	~15 - 50	[116]
	PCL_{1000}-PEG_{1000}-PCL_{1000} (15 – 35 wt%)	*~ 18 - 25*	[116]

Name	Abbreviation	LCST/ UCST (°C)	Ref.
	PCL_{1000}-PEG_{1500}-PCL_{1000} (15 – 35 wt%)	*~ 39 - 46*	[116]
	PCL_{1500}-PEG_{1500}-PCL_{1500} (15 – 35 wt%)	*~ 37 - 45*	[116]
	PCL_{1950}-PEG_{1750}-PCL_{1950} (20 wt %)	*~ 42*	[117]
	PCL_{2110}-PEG_{2000}-PCL_{2110} (20 wt%)	*~ 44*	[117]
Natural polymers and derivatives			
Chitosan-glycerophosphate	Chitosan-GP	~37	[59, 60]
Methylcellulose	MC	50	[106]
Hydroxypropylcellulose	HPC	42	[101]
Ethyl(hydroxyethyl)cellulose	EHEC	65	[106]
Xyloglucan (*with 44% removal of galactose)*		22 – 27	[68]
Elastin-like Polypeptides	ELP	0 – 100	[118]
	ELP[$V_5A_2G_3$-90]	*49*	[50]
	ELP[$V_5A_2G_3$-150]	*40*	[57]
	ELP [$V_5A_2G_3$-160]	*55*	[57]
	poly(VPGVG)	*27*	[119]

* Pluronic Nomenclature: The first letter in the copolymer name indicates the physical state of starting polymer is a liquid (L). The last number indicates the weight content of PEO block (in terms of weight percent), while the remaining numbers give an indication of the molecular weight of the PPO block (taken from [111]).

** Table adapted from Liu et al [120].

Table 1-2: A list of some of the advantages and disadvantages of using naturally derived and synthetic materials in medical applications.

	Natural Materials	Synthetic Materials
Advantages	• Inherent biocompatibility • Safe degradation byproducts • Defined cellular and biological interactions • Natural materials are well suited for 'nature mimicking' strategies popular in tissue engineering • Can provide a close approximation of native extracellular matrix	• Synthetic flexibility and compositional diversity • High degree of control over performance parameters, such as MW, mechanical properties, elasticity, stimulus-response, release profile, degradation kinetics, etc. • Easily sterilized
Disadvantages	• Limited number of natural polymers, therefore restricted range of attainable properties • Batch to batch variability with indefinite composition • Poor mechanical strength • Can illicit an immune response • Biological contamination • Sterilization can be difficult	• Carbon-carbon backbone is not inherently degradable, thus degradation strategies are often required, which can induce inflammation and cytotoxicity • Often engineered in attempt to 'mimic' biological tissues, however, unable to recreate 'true' extracellular microenvironment • Can illicit a foreign body reaction

1.3 BACKGROUND: POSTERIOR SEGMENT OCULAR DRUG DELIVERY

Delivery of pharmaceuticals into the eye is a particularly daunting task, but emerging concepts in ocular drug delivery systems utilizing engineered materials and devices stand to revolutionize the treatment of posterior eye diseases. Delivery of drugs to the eye is complicated by its relatively isolated nature as well as by its numerous physical barriers. The eye is divided into anterior and posterior regions. The anterior chamber consists of the cornea, aqueous humour, ciliary body and the lens, while the posterior segment contains the vitreous body, choroid and the retina. Additionally, the eye contains a number of efficient drainage routes that rapidly clear pharmaceuticals that successfully enter the ocular environment, Figure 1-3.

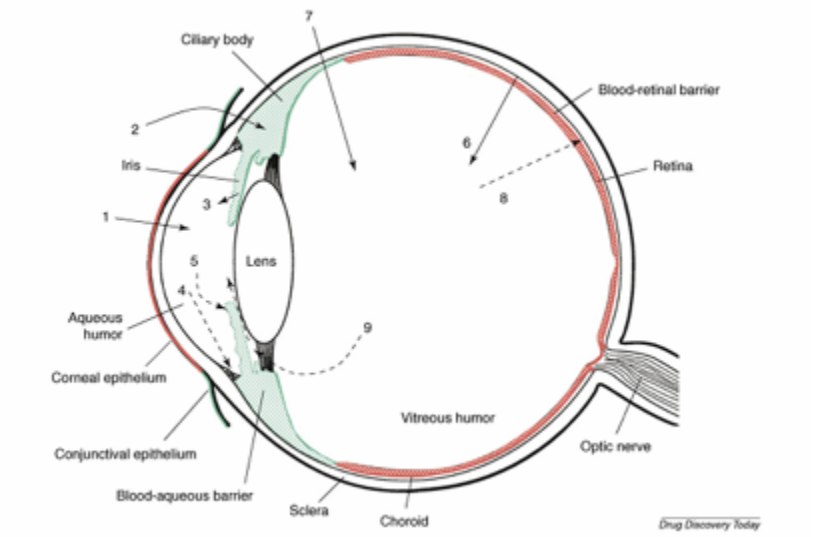

Figure 1-3: The eye contains many different potential routes of entry (solid arrows) and clearance (dashed arrows) that dictate the kinetics of ophthalmic drug delivery. These delivery and clearance routes must be well understood when designing devices to deliver drugs to the eye. The efficient clearance routes typically result in short half-lives of free-drug within the posterior segment. Therefore, polymeric scaffolds that slowly release small amounts of drug over a prolonged period of time represent an attractive means to treat posterior segment disorders. Reproduced with permission from Advanced Drug Delivery Reviews [121].

Figure 1-3 illustrates the number of routes that drugs can enter and be eliminated from the eye. Topical application results in delivery into the anterior chamber of the eye either through the trans-corneal route (arrow 1, Figure 1-3), or through the non-corneal route, in which drug diffuses across the conjunctiva and sclera into the uvea (arrow 2). Drugs may also enter the anterior chamber via the systemic circulation by crossing the blood aqueous barrier (arrow 3). Within the aqueous, the half life of a typical drug is about an hour [121]. Elimination from the anterior chamber occurs through constant turnover of the aqueous to the trabecular meshwork and Schlemm's canal (arrow 4), or by re-absorption into systemic circulation through venous flow of the anterior uvea (arrow 5). Drugs can enter the posterior segment from the systemic circulation by crossing the blood retinal barrier (BRB) (arrow 6) or by direct injection into the posterior segment. Some topically applied drugs that follow the non-corneal route into the uvea (particularly large molecular weight hydrophilic drugs that do not readily penetrate the cornea) may enter the posterior segment (arrow 2). However, this is a highly inefficient means of delivery for posterior segment conditions. From the posterior segment, drugs are eliminated either through the posterior (arrow 8) or anterior (arrow 9) routes. The anterior route is accessible to all compounds and involves diffusion to the posterior chamber and elimination via uveal blood flow and aqueous turnover. Removal via the posterior route requires permeation across the BRB, which favours small molecular weight, lipophilic compounds. Therefore, the posterior route is less effective at removing large molecular weight, hydrophilic drugs. These pharmacokinetic properties of the eye can be exploited to manipulate and tailor drugs and their delivery systems in

order to prolong the retention time of pharmaceuticals within the posterior segment of the eye and increase the time between treatments.

Due to the number of barriers and clearance routes within the segmented eye, delivery of pharmaceuticals via topical eye drops is extremely inefficient and typically results in less than 5% uptake into the anterior chamber and negligible amounts in the posterior segment [8]. The majority of topically applied drugs are absorbed into the bloodstream through the conjunctival and nasal blood vessels [8]. Therefore, topical eye drop application is limited primarily to the treatment of anterior segment eye diseases [122-125]. Systemic drug administration is also limited in its ability to successfully deliver drugs to the posterior segment, as only 1 – 2% of a systemically delivered dose crosses the restrictive blood-ocular barriers (blood aqueous barrier and BRB) [9]. Therefore, large systemic doses are necessary to achieve therapeutic levels within the eye [126]. However, the use of large systemic doses is accompanied by increased risk of undesirable side effects, and makes inefficient use of expensive pharmaceuticals. Consequently, this is not an attractive means of delivering drugs to the posterior eye. Periocular delivery routes, in which drugs are applied to the tissues surrounding the eye, including the peribulbar, posterior juxtascleral, subtenon, retrobulbar and subconjunctival space, represent another potential avenue for delivering drugs to the posterior segment (Figure 1-4) [9]. Although periocular delivery is considered relatively safe, as it does not require perforation of the eye wall, the requirement for externally applied drugs to cross the restrictive physical barriers to gain access to the posterior segment makes it inefficient [8]. Direct injection into the vitreous cavity however, is a highly efficient method to

achieve high concentrations of drug within the vitreous body and retinal tissues [126]. Unfortunately, due to the relatively short half life of drugs within the vitreous, repeated injections are needed (often every 4 – 6 weeks) in order to maintain a therapeutic concentration [127]. Frequent intravitreal injections are associated with significant risks, such as vitreous haemorrhage, endophthalmitis, cataract formation, retinal detachment and patient discomfort [126, 128]. However, as intravitreal injections are capable of leading to therapeutic levels within the vitreous segment while minimizing systemic exposure, this route is attractive for posterior segment drug delivery purposes. Novel drug delivery approaches that safely utilize the intravitreal route for prolonging residence time of pharmaceuticals within the vitreal chamber represent an exciting potential for future treatment of posterior segment eye diseases.

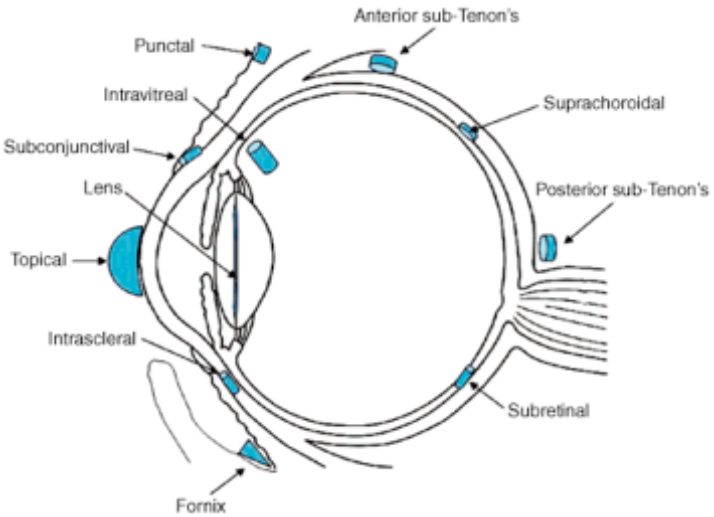

Figure 1-4: Drugs can be delivered to numerous locations surrounding or within the eye as injections, drops or as slow-release scaffolds. Direct introduction into the vitreal cavity is the most efficient means to obtain high concentrations of drug within the posterior segment while minimizing off-target effects. Reproduced with permission from the Nature Publishing Group [129].

1.3.1 Various Sustained Release Ocular Drug Delivery Modalities

There are a number of implantable drug delivering platforms designed to produce sustained release of pharmaceuticals within the posterior segment of the eye to treat conditions such as AMD, DR, DME, dry eye, cytomegalovirus, inflammation, infections or glaucoma [8]. Novel delivery modalities currently being explored for long-term ocular drug release include injectable micro and nanoparticles, iontophoresis, cell encapsulation strategies, *in situ* gelling systems, and numerous implantable solid scaffolds or devices with varying geometries and degradation kinetics, providing unique release profiles [126]. While the majority of implantable drug delivery devices were designed for a specific ocular condition, it is likely that many of these delivery systems can be appropriately adapted for delivery of various pharmaceuticals to treat a number of different posterior segment conditions. For in-depth reviews of the various strategies for posterior segment drug delivery, please see, Choonara (2009) [126], Del Amo (2008) [8], Lee (2009) [130], Novack (2009) [129] and Thrimawithana (2011) [131].

1.3.2 Implantable Scaffolds

Implantable scaffolds capable of achieving sustained release profiles within the intravitreal chamber have gained considerable interest in recent years as promising methods of treating posterior segment eye diseases [126]. When designing an implantable ocular drug delivery platform, one of the most important features is deciding whether the system will be degradable or non-degradable. Both systems can be employed for ocular delivery and are associated with certain advantages and disadvantages. Non-degrading devices offer improved control over sustained release profiles, but degradable

systems do not require secondary surgical intervention for removal [126]. Control over release kinetics is made difficult in degrading scaffolds as the release profile changes with device degradation. Numerous factors, such as pH, temperature and host response influence the rate of polymer degradation, and *in vivo* conditions are not as well-defined or predictable as laboratory testing [126]. As delivery devices degrade, changes in surface area can have a profound influence on the release kinetics, therefore it is desirable to utilize geometries that will not be significantly altered as the material degrades [126]. It is important to design devices that do not erode more rapidly than the drug releases as this could result in a large secondary burst phase as remaining drug is expelled from the degraded scaffold.

1.3.3 Microparticles and Nanoparticles

Controlled release can be obtained by encapsulating a drug within a suspension of microparticles (1 – 1000 μm) or nanoparticles (1 – 1000 nm) [8]. Typically, microparticles and nanoparticles are formulated using degradable polymers such as PLA and PLGA [126]. Microparticles and nanoparticles can be injected directly into the vitreal cavity, providing sustained release for weeks or months [132, 133]. However, a potential drawback of microparticles and nanoparticles is their tendency to cause vitreal clouding [133]. This is typically not a significant problem for microparticles as they have a tendency to sink to the bottom of the vitreal cavity out of the pathway of incoming light, however nanoparticles often remain suspended within the vitreous and are more likely to cause clouding of the central vision. Periocular microsphere formulations have been examined in animal models for trans-scleral delivery in attempts to bypass the need to

perforate the eye wall [134]. As discussed, the trans-scleral delivery route is less efficient when compared with intravitreal delivery as there is an increased number of barriers that the drug must cross to reach the target tissues [130]. However, subconjunctival application of anti-TGF-β2 (transforming growth factor β2) using PLGA microspheres has been shown to prevent post-surgical fibrosis for 42 days following trabeculectomy [135]. Studies such as this have demonstrated the potential for long-term drug release through relatively non-invasive trans-scleral application via microparticle suspensions. Microspheres have also been examined for intravitreal administration by a number of groups and have been fairly well tolerated [136, 137]. Previous studies by Shive and Anderson have demonstrated that microspheres having a diameter greater than 5 – 10 μm, may not be phagocytosed by macrophages and foreign body giant cells, leading to the formation of a foreign body response at the surface of the spheres [138]. However, microspheres smaller than 5 μm may undergo phagocytosis, leading to rapid degradation and subsequently, an increased rate of release, leading to a shorter duration of treatment [138]. Therefore, the selection of microsphere size must be a trade-off between duration of action and host response. Giordano et al. examined the degradation of PLGA microspheres (diameter: 54 and 105 μm) and the tissue response following intravitreal injection into rabbit eyes [136]. A mild, localized, non-progressive foreign body response was reported and the major cells implicated in response to microsphere injection were proposed to be glial cells and fibroblasts. No changes were observed in the choroid or the retina and no abnormalities were revealed through electroretinography (ERG). Furthermore, no clinical inflammatory signs were observed 4 days postoperatively.

While there have been some promising studies with microparticles, their small size has the potential to lead to poor control over drug release and localization. Furthermore, should complications arise, removal of the microparticles would be very challenging.

Many different nanoparticulate systems including nanospheres, liposomes and micelles are being examined in pre-clinical studies. Nanoparticulates from a single intravitreal injection were shown to persist within RPE cells following phagocytosis for up to four months, demonstrating their potential use in sustained delivery [139]. Similarly, early studies showed the localization of albumin nanoparticles within the ciliary body and vitreous for 2 weeks following intravitreal injection, demonstrating the potential for controlled drug release from a scaffold having safe degradation products [140]. However, a longer release profile is needed for this system to become an effective delivery vehicle. Micelles are generated with amphiphilic surfactants or diblock copolymers and have been examined for the treatment of choroidal neovascularization using photodynamic therapy [141-143]. Liposomes are lipid-based vesicles that can range from 25 – 10,000 nm in diameter [8]. Different preparation methods of liposomes result in various sizes, stability and release profiles. Hydrophobic drugs can be loaded into the lipid walls whereas hydrophilic agents can be uptaken by the aqueous interior of liposomes. Phagocytic cells such as the RPE engulf liposomes, enabling intracellular delivery [8]. Liposomes can also be surface-modified to target specific cells. However, vitreal clouding may occur following intravitreal injections of liposomes [8].

1.3.4 Scleral Plugs and Intrascleral Discs

Several degradable scleral plugs have been developed that transverse the sclera at the pars plana with the drug releasing segment protruding into the vitreous chamber [144, 145]. Numerous scleral plug designs have been examined, typically consisting of PLA, PLGA, or HA [126]. Release profiles from degradable scleral plugs are typically characterized by an initial burst, followed by a diffusional release period and a final burst as the plug degrades [126]. Kunou et al. demonstrated the ability to release therapeutic levels of ganciclovir from PLGA scleral plugs for up to one year [146]. More recently, a non-degrading, scleral plug with a refillable reservoir has been developed [147]. In attempts to develop less invasive means of delivering pharmaceuticals into the posterior segment of the eye, several degradable intrascleral implants have been developed for implantation into the periocular space, thus eliminating the need for perforation of the eye wall [126]. These intrascleral discs, which make use of the sclera's large surface area, accounting for approximately 95% of the eye's total surface area, have shown promise in animal models, but need further examination to determine their safety and effectiveness profiles [148]. Furthermore, the need for drug diffusion across the sclera into the vitreous represents a significant barrier to delivery that will reduce the efficiency of this route.

1.3.5 Iontophoresis

Iontophoresis is a non-invasive technique that enhances the delivery of ionized drugs through physical barriers with the aid of a mild electric current as shown in Figure 1-5 [8]. There are three classifications of ocular iontophoresis: trans-corneal, trans-scleral and corneoscleral. Trans-scleral iontophoresis is the most applicable for delivery of drugs

into the posterior segment. The surface area of the sclera is much larger than the cornea, is well hydrated, has a low cell density and is permeable to large compounds [149].

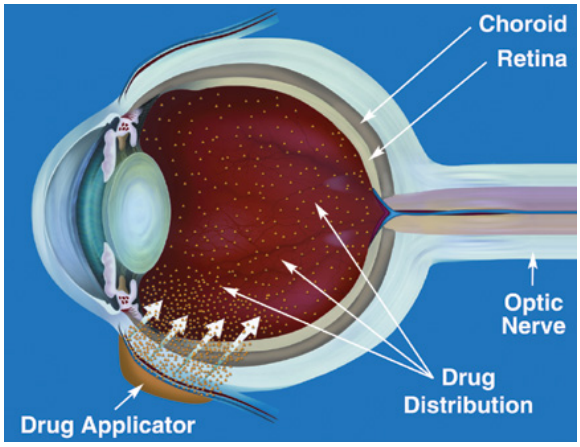

Figure 1-5: Ocular iontophoresis represents a relatively non-invasive method for delivery of charged drugs into the posterior segment of the eye without having to perforate the eye wall. However, delivery is inefficient and the drug action is much shorter than intravitreal drug-releasing devices. Reproduced with permission from Drug Delivery Technology [150].

More recent ocular iontophoresis systems require lower levels of electrical current and are easier to use than previous generations [8]. While ocular iontophoresis is a minimally invasive route of administration, the duration of drug activity is significantly reduced compared with prolonged release systems [8] making it potentially less attractive than more invasive forms of treatment.

1.3.6 Cell Encapsulation

Encapsulated cell technology (ECT) attempts to entrap genetically modified cells within a semi-permeable enclosed system that allows passage of oxygen and nutrients but prevents the infiltration of immune cells [8]. In theory, this allows delivery of engineered cells that are programmed to continuously generate and release therapeutic proteins

directly at the site of interest, thus providing controlled, continuous, and sustained release directly within the vitreous chamber of the eye. ECTs are sutured in place at the pars plana outside the visual field.

The ECT contains genetically modified cells, which can theoretically be tailored to secrete therapeutic proteins to combat the major manifestations of retinal disease: retinal cell degeneration, inflammation and neovascularization. Neurotech has demonstrated the ability to engineer RPE cells to express ciliary neurotrophic factor (CNTF) to combat retinal cell loss, and a VEGF antagonist, rhuFab V2, a ranibizumab-like compound to treat neovascularization [126]. ECT technology however, is a controversial field, as it is not known whether genetically modified cells produce other compounds in a disproportionate quantity to natural RPE cells. Long-term safety and efficacy of ECTs need to be further examined. Furthermore, it is not clear how Neurotech has overcome issues of cell death at the centre of the device as has been seen in other cell-based systems and can arise from poor oxygen and nutrient transport [152]. Neurotech Inc. has recently completed Phase II clinical trials with their lead product NT-501, a semi-permeable, hollow-fibre membrane surrounding modified RPE cells designed to express CNTF for the treatment of dry AMD [153] and for the treatment of early and late stage RP [154, 155]. NT-501 demonstrated the ability to stabilize vision loss with 96.3% of ECT treated patients losing less than 3 lines of vision after 12 months compared with 75% in the sham group [156]. There appears to be a correlation between vision stabilization and retinal thickening, which is proposed to arise from secretion of CNTF via engineered RPEs, which provides protection for the photoreceptor cells, preserving

their health. Concerns regarding the viability of transplanted cells were addressed by explanting 23 devices 12 – 18 months post-implantation and demonstrating that all implants contained viable cells capable of producing CNTF [156]. However, the ECT implants were not able to produce any improvements in visual acuity, possibly due to pre-existing photoreceptor damage that CNTF secretion was not able to reverse.

1.3.7 *In Situ* Gelling and Stimuli Responsive Systems

Stimuli-responsive polymers can be used in topical eye drops to slightly enhance drug retention times, increase drug uptake into the aqueous chamber and reduce required dosing frequency in comparison with conventional formulations [157]. The use of intelligent materials that undergo a stimuli-induced phase transition from liquid to gel represents an interesting approach to deliver drug-containing scaffolds to the posterior segment of the eye through minimally invasive techniques. Polymer-drug suspensions can be mixed together and injected directly into the vitreous chamber or applied periocularly. Changes in stimuli (i.e. temperature, light, pH) induce a phase transition from liquid to semi-solid gel that entraps infused drug allowing prolonged release from an *in situ*-formed drug depot [8]. In the Sheardown lab, we are interested in the potential use of thermally gelling biomaterials, such as PNIPAAm, for minimally invasive posterior segment drug delivery. In Figure 1-6, which is intended to illustrate the concept of *in situ* gelling ocular drug delivery, a liquid suspension of drug (Coomasie Blue in this case)-infused PNIPAAm is injected into a pre-heated aqueous environment, which represents the eye. Upon contacting the heated aqueous medium, the polymer forms a drug-loaded scaffold as it is heated above its LCST, Figure 1-6a. Ideally, this temperature-driven

scaffold formation allows the minimally invasive introduction of a sustained release scaffold into the vitreous, which can locally release low-levels of drug for extended periods of time, thus decreasing systemic exposure and increasing the time between injections (left and middle vials, Figure 1-6b) [34, 158]. Upon exhaustion of the majority of the drug reservoir, the scaffold will commence degradation, allowing the copolymer to be cleared from the eye and body (vial on the right, Figure 1-6b).

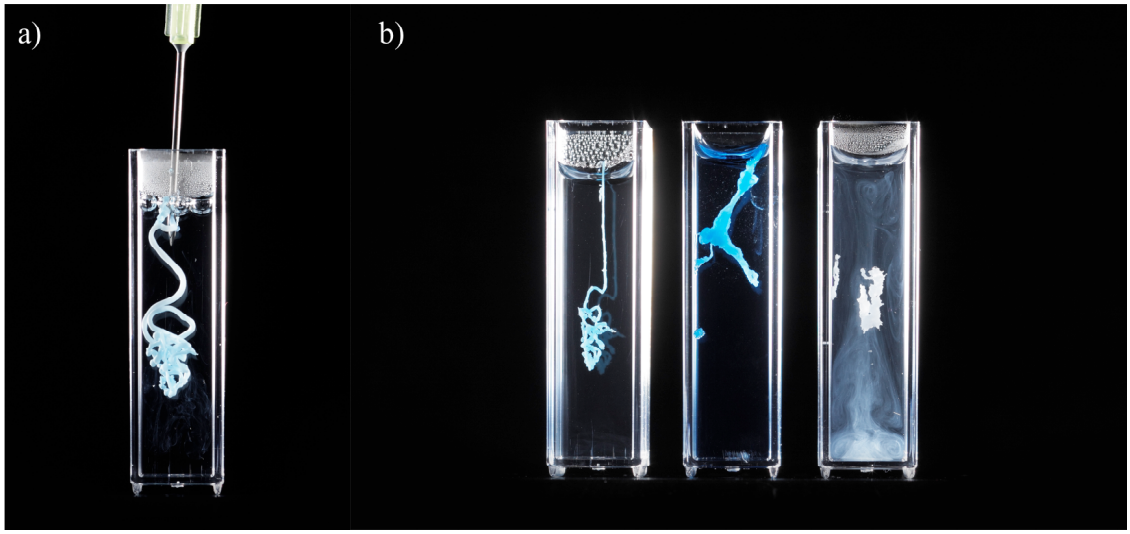

Figure 1-6: A drug-infused thermoresponsive polymer solution (PNIPAAm-based) is injected into a heated aqueous medium, which represents the vitreous body (a). The polymer undergoes a temperature-induced phase transition, from liquid to gel, thus entrapping the infused drug and forming a solid scaffold capable of providing sustained release (left and middle vials in b). Following exhaustion of the majority of the drug reservoir, the scaffold degrades and is cleared from the eye and the body via renal filtration, eliminating the need for surgical removal (vial on the right in b). Images reproduced with permission from Ron Scheffler (photographer).

1.3.8 Alternative Stimuli Responsive Systems

In addition to temperature-responsive materials, a vast number of stimuli responsive materials exist and many are being examined for their potential use in drug delivery applications. As discussed, materials can also undergo numerous stimuli-induced

transformations in response to various stimuli, such as pH, light, magnetism, electricity, changes in ionic strength and mechanical stress [84, 158]. In addition to thermoresponsive cell and drug delivery scaffolds, the Sheardown lab is developing polymeric scaffolds capable of producing externally controllable release profiles through light-induced changes in copolymer network crosslinks [159-161]. Through stimuli-induced dimerization and de-dimerization of light-sensitive polymer side chains, we can reversibly control the crosslinking and un-crosslinking of our scaffolds. In the dimerized / crosslinked state, the pore size of the polymer scaffold shrinks, hindering the release of entrapped drug, slowing its release. De-dimerization leads to an un-crosslinked network, decreasing resistance and allowing drug to be released more rapidly. The degree of crosslinking can be controlled by adjusting the amount of time the scaffold is exposed to its stimulus, allowing externally controlled, tunable release kinetics of an implanted scaffold.

1.3.9 Micro-Electromechanical Devices

Micro-electromechanical (MEMS) drug delivering systems may soon be incorporated into mainstream ocular drug delivery. When made with a small enough form-factor, such MEMS devices may be capable of resting on the external eye and delivering drugs through a canula or microneedle array into the subconjunctival space, or directly into the chambers of the eye [126]. Recently, the Prausnitz group demonstrated the ability to deliver drugs and particles into the scleral tissues in a minimally invasive fashion using hollow microneedles [162]. Drug release profiles from MEMS devices are not governed by diffusion, and can therefore be tightly controlled and adjusted remotely,

allowing external regulation [126]. Furthermore, re-fillable drug reservoirs connected to a syringe port allow administration of subsequent doses without the need for surgical intervention. However, the manufacture of sophisticated MEMS devices for intraocular therapy is extremely difficult and expensive. Further research is needed in this area before clinically relevant devices become commonplace.

Recent work in the Sheardown and Selvaganapathy labs has focussed on the development of inexpensive, soft, flexible MEMS devices for ocular drug delivery, Figure 1-7 [163]. The development of a remotely controllable electroosmotic (EO) micropump capable of delivering small amounts of drug in a controlled, tunable fashion using inexpensive materials and fabrication techniques will enhance the flexibility of these systems. The design architecture of this novel hybrid MEMS device will theoretically eliminate the need for expensive clean room fabrication and will allow direct control over drug release rates, which will be achieved by communicating with the device through medically-designated radio frequencies. The use of hollow glass microcapillaries instead of conventional microneedles greatly reduces the cost of manufacture and allows accurate positioning and fabrication within the soft, flexible body of the EO micropump which is designed to sit on top of the eye and conform to its contours, which would not be possible with the rigid, flat base required for conventional microneedles. An easily accessible port connected to the reservoir will permit re-filling of the drug reservoir, allowing long-term therapy with minimally invasive intervention. Preliminary results demonstrate that continuous and constant delivery through porcine sclera is possible and that it is possible to target specific layers of the retina.

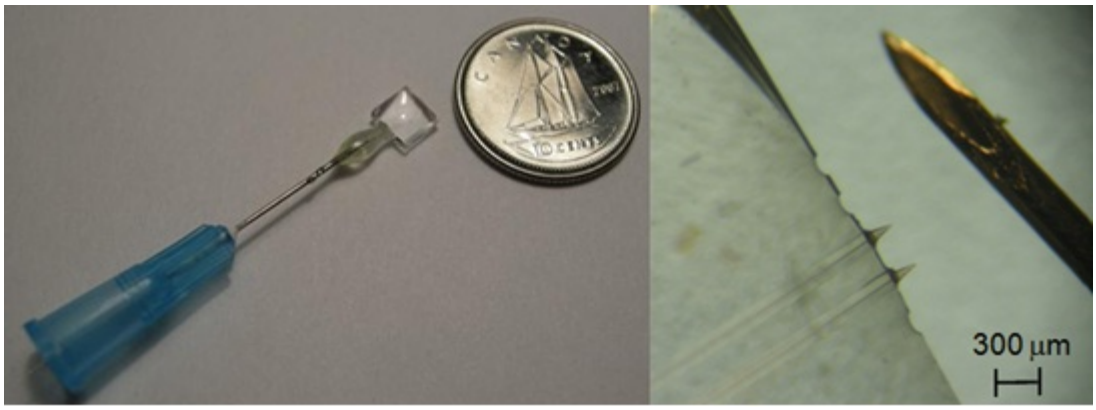

Figure 1-7: A prototype of the soft, flexible, inexpensive PDMS-based MEMS device being developed in the Sheardown and Selvaganapathy labs for non-invasive, pain-free delivery of pharmaceuticals to the posterior segment of the eye is shown next to a Canadian dime. On the right, the fabricated microneedles are pictured next to a 30-gauge stainless steel needle, a commonly used size for intravitreal injections. The microneedles are 300 μm long with 148 μm outer diameter and 10 μm tips. (Unpublished image from Mahadevan and Sheardown).

1.3.10 Future Directions

With the advent of intravitreally implantable drug-releasing scaffolds, there has been considerable improvement in the ability to deliver pharmaceuticals into the posterior segment of the eye for prolonged periods of time. Future approaches will likely investigate new polymer formulations and novel pharmacotherapies. There does however remain a significant need to improve methods for extended delivery of drugs to the back of the eye, particularly in the treatment of chronic diseases of the young such as DR. Future devices will aim to offer less invasive delivery, greater control over release profiles, slower degradation rates, and longer release kinetics. Figure 1-8 illustrates several of the various strategies for intravitreally implantable devices capable of providing sustained delivery to the back of the eye. It is likely that many of these strategies will be modified to include novel polymer formulations and new

pharmaceuticals in an increasing effort to combat the many ailments affecting the posterior segment of the eye. Stimuli responsive materials are likely to play an important role in the design of next-generation ophthalmic drug delivery devices. Perhaps combinations of stimuli-responsive materials capable of responding to several externally applied stimuli will be employed to provide tailored release kinetics of multiple drugs. It is the opinion of the authors that degradable devices with slow degradation rates and prolonged release profiles, capable of being delivered intravitreally with minimally invasive techniques, preferably administered in an office setting, will likely become the preferred delivery modality for posterior segment ocular complications.

1.4 Pharmacotherapies

VEGF inhibitors and corticosteroids are two of the most important families of drugs for posterior segment eye conditions. Anti-VEGF agents are particularly useful for their ability to limit the progression of ocular neovascularization, which is prevalent in both AMD and DR [164]. The anti-inflammatory properties of corticosteroids make them powerful agents to treat patients suffering from macular edema.

1.4.1 VEGF Inhibitors

While numerous factors appear to be involved in the pathogenesis of neovascular eye diseases, VEGF has been widely implicated for its role in the formation of new vessels. [128, 164]. When injected intravitreally into healthy primate eyes, VEGF induces a proliferative diabetic retinopathy (PDR)-like state, including microaneurysm formation, intraretinal haemorrhages, venous beading, capillary closure, and increased

permeability of retinal vasculature [165, 166]. VEGF has also been shown to contribute to the breakdown of the blood-retinal barrier in the early stages of diabetes [167]. Anti-VEGF therapies have demonstrated considerable success in the treatment of age-related macular degeneration (AMD), which has motivated the study of anti-VEGF therapies for other exudative ocular diseases, such as DR, DME, RVO and retinopathy of prematurity (ROP) [164]. VEGF is a pro-angiogenic, vasopermeable, endothelial-specific factor that binds with tyrosine kinase activity to membrane bound receptors [128]. It is produced in the retina via the retinal pigmented epithelial (RPE) cells and all the major retinal neurons [128]. $VEGF_{165}$ is the most abundant of the VEGF isoforms, has the highest biological potency [168], and appears to play the greatest role in the pathogenesis of neovascularization in ocular diseases [169]. Intraocular neovascularization in diabetic retinopathy is stimulated by retinal ischemia and can result in vitreous haemorrhage, neovascular glaucoma, retinal detachment and vision loss [128].

Currently there are three commercial anti-VEGF agents available: pegaptanib sodium (Macugen), bevacizumab (Avastin) and ranibizumab (Lucentis) [128]. Pegaptanib and ranibizumab have been approved by the Food and Drug Administration (FDA) for the treatment of AMD [128] and clinical trials are underway to assess the use of anti-VEGF agents for treatment of DR [128, 170]. Bevacizumab has received FDA approval for intravenous use in cancer therapy and has been used off-label to treat ocular neovascularization [128, 171].

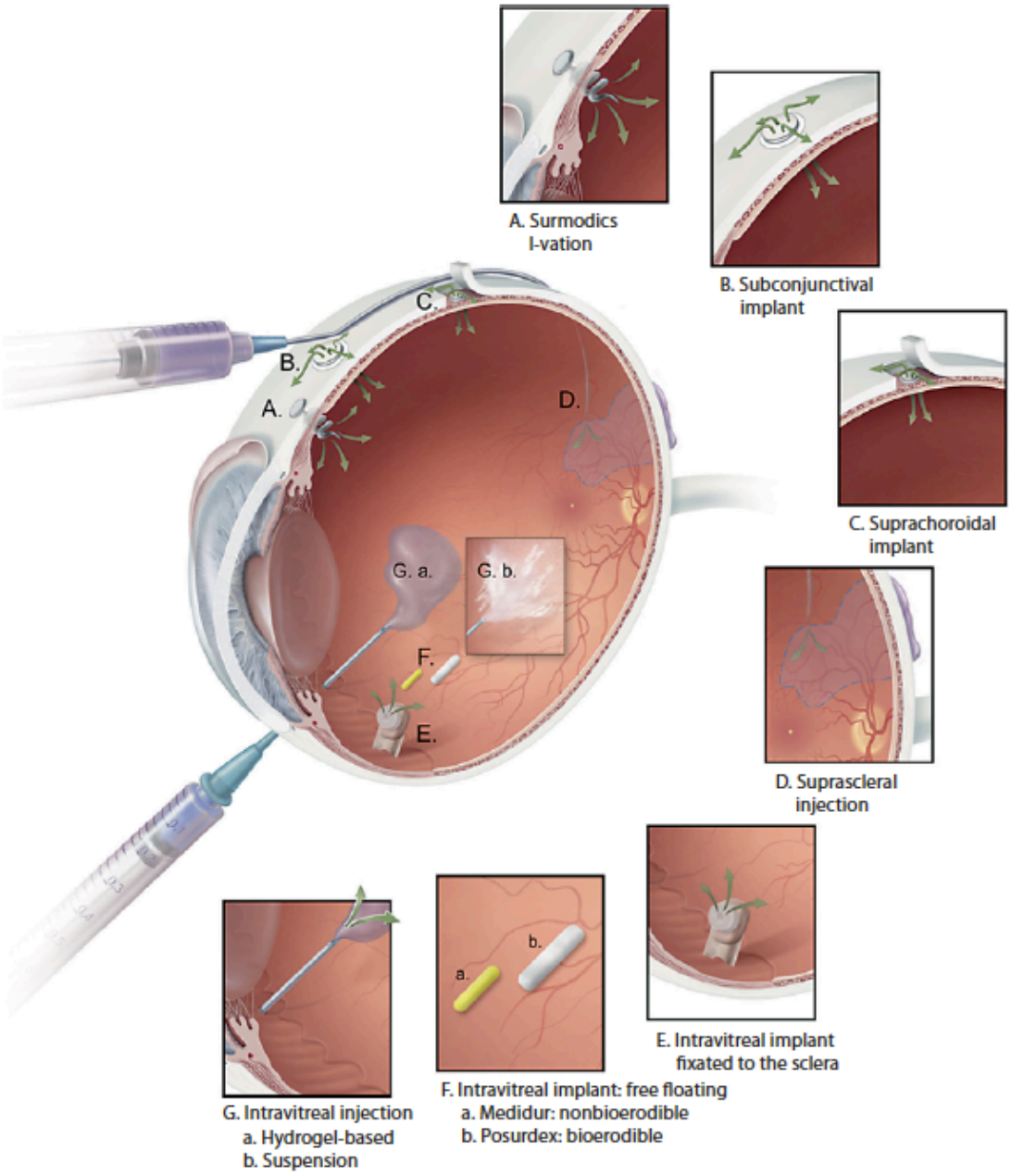

Figure 1-8: A summary of the various intravitreal drug delivery modalities and their locations within the eye. Reproduced with permissios from S. Karger AG, Basel [130].

1.4.1.1 Pegaptanib (Macugen)

In 2004, Pegaptanib became the first VEGF inhibitor to receive FDA approval for the treatment of AMD [172]. Pegaptanib is a nuclease resistant peglyated RNA aptamer

that specifically targets highly potent $VEGF_{165}$ [173]. Unlike other anti-VEGF agents that target all active VEGF isoforms and directly inhibit VEGF from binding with its receptor (VEGFR), pegaptanib selectively binds $VEGF_{165}$ and larger isoforms and indirectly modulates VEGF-induced neovascularization through interaction with the heparin-binding domain [173, 174]. The heparin binding domain serves to enhance VEGF signalling by binding with coreceptor neuropilin-1 (NP-1) [174]. Therefore, pegaptanib does not directly block the interaction between VEGF and its receptor, instead it limits the amplification of VEGFR signalling, decreasing the ability of VEGF to enhance vascular permeability and stimulate endothelial division [128]. A recent case study demonstrated regression of ocular neovascularization following intravitreal injection of pegaptanib (0.3 mg) and there was no evidence of new vessel formation after 15 months [175]. A phase II clinical trial demonstrated that intravitreal pegaptanib injections in patients with DME resulted in the regression of neovascularization in 62% (8/13) of patients six weeks after their last treatment, whereas patients receiving sham injections showed no signs of regression (0/3) [176]. However, neovascularization returned in 38% (3/8) of patients following their last injections, demonstrating the need for frequent, recurring injections, which can be painful, inconvenient and increases the risk of injection-related complications [176].

1.4.1.2 Bevacizumab (Avastin)

Bevacizumab is a full-length humanized recombinant antibody that non-selectively targets all VEGF isoforms and received FDA approval in 2004 for the treatment of colon cancer [128]. As mentioned, bevacizumab and ranibizumab directly

interact with the receptor-binding domain of VEGF to inhibit its interaction with VEGFR. [174]. Bevacizumab has demonstrated success in small observational case studies in which off-label injections of the drug were used to treat neovascular AMD, macular edema and iris neovascularization [177, 178]. Small pilot studies have examined the use of bevacizumab to treat PDR, with a reported 100% (44/44) of treated eyes demonstrating regression of vascular leakage to some extent within one week of intravitreal injection [179]. Complete resolution of new vessel formation at the optic disc (NVD) and elsewhere on the retina (new vessel elsewhere, NVE) was reported in 73% and 59% of treated eyes, respectively [179]. However, recurrence of neovascularization occurred as early as two weeks following injection, once again demonstrating the need for frequent re-administration. Interestingly, neovascularization was also observed to subside in several untreated eyes, which raises concerns of potential off-target effects [179].

1.4.1.3 Ranibizumab (Lucentis)

Approved by the FDA in June 2006 for the treatment of neovascular AMD, Ranibizumab is a recombinant humanized antibody fragment derived from the full length monoclonal antibody, Bevacizumab, that targets all isoforms of VEGF [180]. It is a chimeric compound consisting of a nonbinding human sequence and an epitope derived from mice that binds VEGF with high affinity [180]. The small recombinant fragment was developed in attempts to promote diffusion through the retina following intravitreal injection, allowing treatment of subretinal neovascularization in AMD [181]. Ranibizumab has demonstrated the ability to reduce VEGF-induced proliferation of retinal endothelial cells [182] and its efficacy has been demonstrated in two pilot studies

for DME [183, 184]. The effectiveness of ranibizumab in the treatment of PDR remains to be established. The small Ranibizumab antibody fragment was designed to lack the constant Fc region and therefore does not bind complement C1q or FCγ receptors, in order to prevent any complement-mediated responses directed against the compound [180].

1.4.1.4 Comparison Between Pegaptanib, Bevacizumab and Ranibizumab

In a direct comparison of pegaptanib, bevacizumab and ranibizumab, Klettner and Roider examined the VEGF-sequestering and neutralizing efficiencies of the three VEGF-inhibitors *in vitro* [174]. Interestingly, they found pegaptanib had no neutralizing effect *in vitro*, which may help to explain why pegaptanib has somewhat fallen out of favour in the treatment of AMD [185]. As suggested by the authors, this finding may also have been related to the experimental design and the fact that pegaptanib interacts with VEGF through the heparin binding domain [174]. It was found however, that at clinical doses, ranibizumab and bevacizumab neutralized VEGF equally, whereas when diluted, ranibizumab demonstrated higher potency [174]. Although ranibizumab has been demonstrated to be highly effective and has received FDA approval for the treatment of neovascular AMD, bevacizumab is often used off-label as it is approximately one-fortieth the price of ranibizumab [174]. Furthermore, early clinical evidence has suggested bevacizumab may be just as effective in the treatment of neovascularization as ranibizumab [1].

1.4.1.5 Alternative Anti-VEGF Strategies

A number of anti-VEGF strategies are currently in the development phase. VEGF-trap (Aflibercept, Regeneron Pharmaceuticals) is a fusion protein that acts as a receptor decoy and inhibits all forms of VEGF with a high binding affinity [186]. It consists of segments of the extracellular domains of VEGF receptors 1 (VEGFR-1) and 2 (VEGFR-2) fused together with the constant Fc domain of human IgG [187]. Small molecule tyrosine kinase inhibitors (TKi) such as Pazopanib (GlaxoSmithKline) have been examined for treatment of VEGF-induced ocular neovascularization [164]. TKi inhibit the tyrosine kinase cascade that is activated by the binding of VEGF with its receptor, preventing downstream effects [180]. Bevasiranib (OPKO Health) is the first small interfering RNA (siRNA) agent developed for AMD and has been examined for the treatment of DME [164, 188]. Bevasiranib is a gene silencing mechanism that causes the catalytic destruction of VEGF messenger RNA [188]. As each of these methods directly targets VEGF, all should yield somewhat similar results; in all cases however, a more sustained delivery method would be favourable to ensure efficacy.

1.4.1.6 Adverse Effects of Intravitreal Anti-VEGF Agents

Although anti-VEGF therapies have demonstrated promising results for the treatment of ocular neovascularization, there are potential complications that may arise from this form of treatment. In addition to being an angiogenic factor, VEGF is known to possess neuroprotective properties; it is important for the survival of photoreceptors, Muller cells and retinal neurons, and is essential for maintaining a healthy retina [128, 189, 190]. Therefore long-term treatment with anti-VEGF agents may result in adverse

events by preventing VEGF from exerting its neuroprotective effects. There is concern that intravitreal injections may result in absorption into systemic circulation, leading to undesired effects. A 12-month case study examining the safety profile of intravitreal bevacizumab injections found adverse systemic effects in 1.5% of patients (18 / 1173) [191]. Complications of bevacizumab injections included hypertension (7 / 1173), cerebrovascular accidents (6 / 1173) and myocardial infarcts (5 / 1173) [191]. Five patient deaths were attributed to these complications [191]. These results suggest a need for delivery of the smallest efficacious dose over a prolonged period of time directly to the site of interest. In addition to systemic risks of anti-VEGF therapy, there is also a significant risk associated with intravitreal injections, including cataracts, endophthalmitis, retinal detachment, corneal abrasion, haemorrhage and RPE tears [128, 131]. Injection-related risks are not limited to anti-VEGF treatments, but are common to all intravitreal injections. The risks associated with intravitreal injections greatly increase with frequent perforation of the eye wall, which is often required to maintain therapeutic concentrations within the vitreous. As such, there is a significant need for sustained treatment options that prolong drug residence times within the eye and require less frequent intervention.

1.4.2 Corticosteroids

Corticosteroids have been used since the 1950s to treat ocular inflammatory conditions [192, 193]. Recently, intravitreal corticosteroids have been used to treat several ocular diseases, such as AMD, PDR and macular edema [186]. Prior to the use of intravitreal delivery techniques, high systemic doses of corticosteroids were required to

achieve therapeutically relevant concentrations within the posterior segment of the eye [194]. High systemic exposure to corticosteroids can cause a number of adverse side effects, including exacerbation of diabetes, adrenal suppression, cushingoid state and osteoporosis [194]. However, intravitreal administration of corticosteroids has allowed high local concentrations within the posterior segment while minimizing systemic exposure. Corticosteroids, which are widely known and used for their anti-inflammatory properties, combat macular edema through suppression of VEGF expression and stabilization of the blood-retinal barrier [195]. VEGF suppression is believed to occur through repression of proinflammatory genes and transcription factors such as cytokines and nuclear factor-κ B (NF-κB) [5, 196]. Stabilization of the BRB is thought to occur through inhibition of leukostasis as adhesion of leukocytes to the endothelium can disrupt tight junctions, which increases vessel permeability and deteriorates the BRB [194]. Triamcinolone acetonide has been used for many years, generally demonstrating favourable results and has shown promise when used in conjunction with panretinal photocoagulation (PRP) [197, 198]. In the US there are four commercial formulations of intravitreal triamcinolone (IVTA), including Kenalog-40 (Bristol-Myers Squibb), preservative-free triamcinolone acetonide, Triesence (Alcon) and Trivaris (Allergan) [199]. Dexamethasone and fluocinolone acetonide are other corticosteroids currently under investigation for treatment of DME [199]. Table 1 lists the relative potencies of various corticosteroids.

Table 1-3: Relative potency of several candidate corticosteroids for treatment of macular edema [200, 201].

Corticosteroid	Relative Potency
Cortisone	0.8
Cortisol	1
Triamcinolone	5
Fluocinolone	25
Dexamethasone	25

1.4.2.1 Adverse Effects of Corticosteroids

Intravitreal injections of corticosteroids also pose significant risks to the patient. One of the most common risks is an increase in IOP, resulting in secondary open-angle glaucoma [202]. Increases in IOP up to 24 mm Hg have been reported in as many as 40% of patients injected intravitreally with corticosteroids [203]. Another important risk factor is cataract formation, which has been reported to become visually significant in 50% of eyes within one year of injection [204]. Migration of corticosteroid into the anterior chamber may also cause problems such as pseudoendophthalmitis [205]. In January 2010, the FDA issued a warning that corticosteroid formulations containing benzyl alcohol, such as Kenalog, are not suitable for intraocular injection due to potential toxicity issues [206]. It was found that benzyl alcohol was toxic in rabbit eyes when injected at concentrations higher than that found in commercial Kenalog, resulting in the loss of photoreceptors and outer segments [207]. Typical injection-related side effects also pose a risk for intravitreally administered corticosteroids [194]. Recently, a large randomized multicenter clinical trial found that focal / grid photocoagulation was more effective at treating patients with DME and resulted in fewer side effects in comparison

with IVTA [208]. Nevertheless, corticosteroids have demonstrated exciting potential for the treatment of DME and further investigation is warranted. Sustained-release scaffolds that act as a drug reservoir may limit the free steroid exposure within the eye, significantly reducing associated complications and prolonging the duration of drug action [209].

Despite being associated with a relatively high rate of cataract and glaucoma, TA is the most commonly used intravitreal corticosteroid [210]. However, Dr. Kupperman suggests dexamethasone may be better suited for intravitreal administration as it is more potent than TA and may have a lower risk of cataract, glaucoma and retinal toxicity [210]. *In vitro* testing revealed that, compared with TA, dexamethasone possessed decreased toxicity towards lens epithelial cells [211], trabecular meshwork cells [210, 212], and retinal RPE and neurosensory cells [213, 214]. One of the major drawbacks of intravitreal dexamethasone however, is its relatively short half-life within the vitreous (3.5 hours) compared with TA (18 days), which persists for approximately 3 months within the eye [215, 216]. Therefore, sustained release drug delivery modalities that extend the residence time within the eye and increase the duration of activity may make dexamethasone a more desirable therapeutic for posterior segment therapies, specifically macular edema, and lower the incidence of corticosteroid-related complications.

As our understanding of the biochemical pathways implicated in the onset and pathogenesis of posterior segment ocular disorders increases, so too will the number of potential targets available for pharmacological intervention. However, the need for

effective delivery of these agents to the target tissue over prolonged periods of time remains crucial for the ultimate success of these highly specialized pharmaceuticals.

1.5 Conclusions

With many new drugs and potential treatment options, posterior segment ocular complications stand to benefit greatly from novel delivery techniques. Ophthalmic drug delivery is a rapidly expanding field with a unique set of challenges. Sustained delivery of pharmaceuticals to the posterior segment of the eye is one of the most significant unmet needs of visual health care. Although substantial progress has been made in recent years, there are still major obstacles to overcome. An ideal device for ophthalmic drug delivery to the posterior segment must be non-invasive, easy to administer, provide prolonged release decreasing the need for frequent dosing, and must minimize the risk of complications frequently associated with current techniques such as infections, cataracts, hemorrhages, increases in IOP and retinal detachments. For an ocular delivery device to achieve commercial success, it must be accepted by the patients receiving the treatment as well as the physicians that will ultimately administer the technology. Therefore, ease of use and minimal 'scare factor' are important design criteria for novel drug delivery devices. Advances in polymer technology and improved understanding of the biochemical pathways involved in the pathogenesis of posterior segment eye diseases will ultimately yield safe, long-term therapies capable of improving outcomes in these debilitating complications.

References

[1] Singh R, Ramasamy K, Abraham C, Gupta V, Gupta A. Diabetic retinopathy: an update. Indian JOphthalmol 2008;56:178-88.
[2] Cheung N, Mitchell P, Wong TY. Diabetic retinopathy. The Lancet 2010;376:124-36.
[3] International_Diabetes_Federation. Diabetes Atlas. 2009.
[4] Klein R, Klein BE, Moss SE, Davis MD, DeMets DL. The Wisconsin epidemiologic study of diabetic retinopathy. III. Prevalence and risk of diabetic retinopathy when age at diagnosis is 30 or more years. ArchOphthalmol 1984;102:527-32.
[5] Ali TK, El Remessy AB. Diabetic retinopathy: current management and experimental therapeutic targets. Pharmacotherapy 2009;29:182-92.
[6] Wild S, Roglic G, Green A, Sicree R, King H. Global prevalence of diabetes: estimates for the year 2000 and projections for 2030. Diabetes Care 2004;27:1047-53.
[7] Jager RD, Mieler WF, Miller JW. Age-related macular degeneration. N Engl J Med 2008;358:2606-17.
[8] Del Amo EM, Urtti A. Current and future ophthalmic drug delivery systems. A shift to the posterior segment. Drug DiscovToday 2008;13:135-43.
[9] Gaudana R, Jwala J, Boddu SH, Mitra AK. Recent perspectives in ocular drug delivery. PharmRes 2009;26:1197-216.
[10] Bikram M, West JL. Thermo-responsive systems for controlled drug delivery. Expert Opinion on Drug Delivery 2008;5:1077-91.
[11] Bajpai AK, Bajpai J, Saini R, Gupta R. Responsive Polymers in Biology and Technology. Polymer Reviews 2011;51:53-97.
[12] Schmaljohann D. Thermo- and pH-responsive polymers in drug delivery. Adv Drug Deliv Rev 2006;58:1655-70.
[13] Li Z, Guan J. Thermosensitive hydrogels for drug delivery. Expert Opinion on Drug Delivery 2011;8:991-1007.
[14] Hoogenboom R, Lambermont-Thijs HML, Jochems MJHC, Hoeppener S, Guerlain C, Fustin C-A, et al. A schizophrenic gradient copolymer: switching and reversing poly(2-oxazoline) micelles based on UCST and subtle solvent changes. Soft Matter 2009;5:3590-2.
[15] Rapoport N. Physical stimuli-responsive polymeric micelles for anti-cancer drug delivery. Progress in Polymer Science 2007;32:962-90.
[16] Hirsch LR, Stafford RJ, Bankson JA, Sershen SR, Rivera B, Price RE, et al. Nanoshell-mediated near-infrared thermal therapy of tumors under magnetic resonance guidance. Proceedings of the National Academy of Sciences of the United States of America 2003;100:13549-54.
[17] Ward MA, Georgiou TK. Thermoresponsive Polymers for Biomedical Applications. Polymers 2011;3:1215-42.
[18] Tanaka T. Collapse of Gels and the Critical Endpoint. Physical Review Letters 1978;40:820-3.
[19] Neradovic D, Hinrichs WLJ, Kettenes-van den Bosch JJ, Hennink WE. Poly(N-isopropylacrylamide) with hydrolyzable lactic acid ester side groups: a new type of thermosensitive polymer. Macromol Rapid Commun 1999;20:577-81.

[20] Ruggiero A, Villa CH, Bander E, Rey DA, Bergkvist M, Batt CA, et al. Paradoxical glomerular filtration of carbon nanotubes. Proceedings of the National Academy of Sciences of the United States of America 2010;107:12369-74.
[21] Yoshida T, Aoyagi T, Kokufuta E, Okano T. Newly designed hydrogel with both sensitive thermoresponse and biodegradability. Journal of Polymer Science Part a-Polymer Chemistry 2003;41:779-87.
[22] Guan J, Hong Y, Ma Z, Wagner WR. Protein-reactive, thermoresponsive copolymers with high flexibility and biodegradability. Biomacromolecules 2008;9:1283-92.
[23] Ma Z, Nelson DM, Hong Y, Wagner WR. Thermally Responsive Injectable Hydrogel Incorporating Methacrylate-Polylactide for Hydrolytic Lability. Biomacromolecules 2010;11:1873-81.
[24] Cui ZW, Lee BH, Vernon BL. New hydrolysis-dependent thermosensitive polymer for an injectable degradable system. Biomacromolecules 2007;8:1280-6.
[25] Cui Z, Lee BH, Pauken C, Vernon BL. Manipulating degradation time in a N-isopropylacrylamide-based co-polymer with hydrolysis-dependent LCST. J Biomater Sci Polym Ed 2010;21:913-26.
[26] Fitzpatrick SD, Mazumder MAJ, Muirhead B, Sheardown H. Development of Injectable, Resorbable, Drug-Releasing Copolymer Scaffolds for Minimally Invasive Sustained Ophthalmic Therapeutics. Accepted (7/3/2012) for publication in *Acta Biomaterialia* 2012.
[27] Liu CB, Gong CY, Huang MJ, Wang JW, Pan YF, Zhang YD, et al. Thermoreversible gel–sol behavior of biodegradable PCL-PEG-PCL triblock copolymer in aqueous solutions. Journal of Biomedical Materials Research Part B: Applied Biomaterials 2008;84B:165-75.
[28] Geever LM, Lyons JG, Higginbotham CL. Photopolymerisation and characterisation of negative temperature sensitive hydrogels based on N,N-diethylacrylamide. Journal of Materials Science 2011;46:509-17.
[29] Patra L, Vidyasagar A, Toomey R. The effect of the Hofmeister series on the deswelling isotherms of poly(N-isopropylacrylamide) and poly(N,N-diethylacrylamide). Soft Matter 2011;7:6061-7.
[30] Beija M, Marty J-D, Destarac M. Thermoresponsive poly(N-vinyl caprolactam)-coated gold nanoparticles: sharp reversible response and easy tunability. Chemical Communications 2011;47:2826-8.
[31] Aseyev V, Muller AHE, Tenhu H, Borisov O, Winnik FM. Advances in Polymer Science. Advances in Polymer Science. Berlin, Heidelberg: Springer Berlin Heidelberg; 2010. p. 29-89.
[32] Klouda L, Mikos AG. Thermoresponsive hydrogels in biomedical applications. European Journal of Pharmaceutics and Biopharmaceutics 2008;68:34-45.
[33] Batrakova EV, Kabanov AV. Pluronic block copolymers: evolution of drug delivery concept from inert nanocarriers to biological response modifiers. Journal of controlled release : official journal of the Controlled Release Society 2008;130:98-106.
[34] Wells LA, Lasowski F, Fitzpatrick SD, Sheardown H. Responding to change: thermo- and photo-responsive polymers as unique biomaterials. Crit Rev Biomed Eng 2010;38:487-509.

[35] Sosnik A, Cohn D, Rom, n JS, Abraham GA. Crosslinkable PEO-PPO-PEO-based reverse thermo-responsive gels as potentially injectable materials. Journal of Biomaterials Science, Polymer Edition 2003;14:227-39.
[36] Cohn D, Sosnik A, Garty S. Smart Hydrogels for in Situ Generated Implants,Ä†. Biomacromolecules 2005;6:1168-75.
[37] Sosnik A, Cohn D. Reverse thermo-responsive poly(ethylene oxide) and poly(propylene oxide) multiblock copolymers. Biomaterials 2005;26:349-57.
[38] Cohn D, Lando G, Sosnik A, Garty S, Levi A. PEO–PPO–PEO-based poly(ether ester urethane)s as degradable reverse thermo-responsive multiblock copolymers. Biomaterials 2006;27:1718-27.
[39] Wang Y, Tan Y, Huang X, Xu G. Gelation Behavior of Thermo-Responsive Poly(ethylene oxide) and Poly(propylene oxide) Multiblock Polycarbonates. Journal of Macromolecular Science Part a-Pure and Applied Chemistry 2009;46:397-404.
[40] Kumbar SG, Bhattacharyya S, Nukavarapu SP, Khan YM, Nair LS, Laurencin CT. In vitro and in vivo characterization of biodegradable poly(organophosphazenes) for biomedical applications. Journal of Inorganic and Organometallic Polymers and Materials 2006;16:365-85.
[41] Schacht E, Vandorpe J, Dejardin S, Lemmouchi Y, Seymour L. Biomedical applications of degradable polyphosphazenes. Biotechnol Bioeng 1996;52:102-8.
[42] Laurencin CT, Koh HJ, Neenan TX, Allcock HR, Langer R. Controlled release using a new bioerodible polyphosphazene matrix system. Journal of Biomedical Materials Research 1987;21:1231-46.
[43] Lee KY, Mooney DJ. Hydrogels for tissue engineering. Chem Rev 2001;101:1869-79.
[44] Conconi MT, Lora S, Baiguera S, Boscolo E, Folin M, Scienza R, et al. In vitro culture of rat neuromicrovascular endothelial cells on polymeric scaffolds. Journal of Biomedical Materials Research Part A 2004;71A:669-74.
[45] Bhattacharyya S, Lakshmi S, Bender J, Greish YE, Brown PW, Allcock HR, et al. Preparation of poly bis(carboxylato phenoxy)phosphazene non-woven nanofiber mats by electrospinning. In: Wong JY, Plant AL, Schmidt CE, Shea L, Coury AJ, Chen CS, et al., editors. Architecture and Application of Biomaterials and Biomolecular Materials. Warrendale: Materials Research Society; 2004. p. 157-63.
[46] Langone F, Lora S, Veronese FM, Caliceti P, Parnigotto PP, Valenti F, et al. Peripheral-Nerve Repair Using a Poly(organo)phosphazene Tubular Prosthesis. Biomaterials 1995;16:347-53.
[47] Al-Abd AM, Hong K-Y, Song S-C, Kuh H-J. Pharmacokinetics of doxorubicin after intratumoral injection using a thermosensitive hydrogel in tumor-bearing mice. Journal of Controlled Release 2010;142:101-7.
[48] Chilkoti A, Dreher MR, Meyer DE. Design of thermally responsive, recombinant polypeptide carriers for targeted drug delivery. Advanced Drug Delivery Reviews 2002;54:1093-111.
[49] Ge X, Filipe CDM. Simultaneous phase transition of ELP tagged molecules and free ELP: An efficient and reversible capture system. Biomacromolecules 2006;7:2475-8.

[50] Ge X, Hoare T, Filipe CDM. Protein-Based Aqueous-Multiphasic Systems. Langmuir 2010;26:4087-94.
[51] Bessa PC, Machado R, Nürnberger S, Dopler D, Banerjee A, Cunha AM, et al. Thermoresponsive self-assembled elastin-based nanoparticles for delivery of BMPs. Journal of controlled release : official journal of the Controlled Release Society 2010;142:312-8.
[52] Meyer DE, Chilkoti A. Genetically encoded synthesis of protein-based polymers with precisely specified molecular weight and sequence by recursive directional ligation: Examples from the elastin-like polypeptide system. Biomacromolecules 2002;3:357-67.
[53] McDaniel JR, Callahan DJ, Chilkoti A. Drug delivery to solid tumors by elastin-like polypeptides. Advanced Drug Delivery Reviews 2010;62:1456-67.
[54] Liu W, MacKay JA, Dreher MR, Chen M, McDaniel JR, Simnick AJ, et al. Injectable intratumoral depot of thermally responsive polypeptide-radionuclide conjugates delays tumor progression in a mouse model. Journal of Controlled Release 2010;144:2-9.
[55] Dreher MR, Simnick AJ, Fischer K, Smith RJ, Patel A, Schmidt M, et al. Temperature triggered self-assembly of polypeptides into multivalent spherical micelles. Journal of the American Chemical Society 2008;130:687-94.
[56] MacKay JA, Chen M, McDaniel JR, Liu W, Simnick AJ, Chilkoti A. Self-assembling chimeric polypeptide-doxorubicin conjugate nanoparticles that abolish tumours after a single injection. Nature Materials 2009;8:993-9.
[57] Meyer DE, Shin BC, Kong GA, Dewhirst MW, Chilkoti A. Drug targeting using thermally responsive polymers and local hyperthermia. Journal of Controlled Release 2001;74:213-24.
[58] Chang Y, Xiao L, Du Y. Preparation and properties of a novel thermosensitive N-trimethyl chitosan hydrogel. Polymer Bulletin 2009;63:531-45.
[59] Chenite A, Chaput C, Wang D, Combes C, Buschmann MD, Hoemann CD, et al. Novel injectable neutral solutions of chitosan form biodegradable gels in situ. Biomaterials 2000;21:2155-61.
[60] Molinaro G, Leroux JC, Damas J, Adam A. Biocompatibility of thermosensitive chitosan-based hydrogels: an in vivo experimental approach to injectable biomaterials. Biomaterials 2002;23:2717-22.
[61] Ruel-Gariepy E, Leroux JC. In situ-forming hydrogels--review of temperature-sensitive systems. Eur J Pharm Biopharm 2004;58:409-26.
[62] Van Vlierberghe S, Dubruel P, Schacht E. Biopolymer-based hydrogels as scaffolds for tissue engineering applications. Biomacromolecules 2011;12:1387-408.
[63] Sarkar N. Thermal Gelation Properties of Methyl and Hydroxypropyl Methylcellulose. Journal of Applied Polymer Science 1979;24:1073-87.
[64] Gupta D, Tator CH, Shoichet MS. Fast-gelling injectable blend of hyaluronan and methylcellulose for intrathecal, localized delivery to the injured spinal cord. Biomaterials 2006;27:2370-9.
[65] Kang CE, Poon PC, Tator CH, Shoichet MS. A new paradigm for local and sustained release of therapeutic molecules to the injured spinal cord for neuroprotection and tissue repair. Tissue Eng Part A 2009;15:595-604.

[66] Ballios BG, Cooke MJ, van der Kooy D, Shoichet MS. A hydrogel-based stem cell delivery system to treat retinal degenerative diseases. Biomaterials 2010;31:2555-64.
[67] de Freitas RA, Busato AP, Mitchell DA, Silveira JLM. Degalatosylation of xyloglucan: Effect on aggregation and conformation, as determined by time dependent static light scattering, HPSEC-MALLS and viscosimetry. Carbohydrate Polymers 2011;83:1636-42.
[68] Miyazaki S, Suisha F, Kawasaki N, Shirakawa M, Yamatoya K, Attwood D. Thermally reversible xyloglucan gels as vehicles for rectal drug delivery. Journal of controlled release : official journal of the Controlled Release Society 1998;56:75-83.
[69] Itoh K, Tsuruya R, Shimoyama T, Watanabe H, Miyazaki S, D'Emanuele A, et al. In situ gelling xyloglucan/alginate liquid formulation for oral sustained drug delivery to dysphagic patients. Drug Development and Industrial Pharmacy 2010;36:449-55.
[70] Miyazaki S, Suzuki S, Kawasaki N, Endo K, Takahashi A, Attwood D. In situ gelling xyloglucan formulations for sustained release ocular delivery of pilocarpine hydrochloride. International Journal of Pharmaceutics 2001;229:29-36.
[71] Takahashi A, Suzuki S, Kawasaki N, Kubo W, Miyazaki S, Loebenberg R, et al. Percutaneous absorption of non-steroidal anti-inflammatory drugs from in situ gelling xyloglucan formulations in rats. International Journal of Pharmaceutics 2002;246:179-86.
[72] Suisha F, Kawasaki N, Miyazaki S, Shirakawa M, Yamatoya K, Sasaki M, et al. Xyloglucan gels as sustained release vehicles for the intraperitoneal administration of mitomycin C. International Journal of Pharmaceutics 1998;172:27-32.
[73] Kim SJ, Shin SR, Kim NG, Kim SI. Swelling behavior of semi-interpenetrating polymer network hydrogels based on chitosan and poly(acryl amide). Journal of Macromolecular Science-Pure and Applied Chemistry 2005;A42:1073-83.
[74] Owens DE, III, Jian Y, Fang JE, Slaughter BV, Chen Y-H, Peppas NA. Thermally responsive swelling properties of polyacrylamide/poly(acrylic acid) interpenetrating polymer network nanoparticles. Macromolecules 2007;40:7306-10.
[75] Chen Y, Ding D, Mao Z, He Y, Hu Y, Wu W, et al. Synthesis of Hydroxypropylcellulose-poly(acrylic acid) Particles with Semi-interpenetrating Polymer Network Structure. Biomacromolecules 2008;9:2609-14.
[76] Quan C-Y, Chen J-X, Wang H-Y, Li C, Chang C, Zhang X-Z, et al. Core-shell nanosized assemblies mediated by the alpha-beta cyclodextrin dimer with a tumor-triggered targeting property. ACS nano 2010;4:4211-9.
[77] Wei H, Cheng, Chang C, Chen W-Q, Cheng S-X, Zhang X-Z, et al. Synthesis and Applications of Shell Cross-Linked Thermoresponsive Hybrid Micelles Based on Poly(N-isopropylacrylamide- co-3-(trimethoxysilyl)propyl methacrylate)- b-poly(methyl methacrylate). Langmuir : the ACS journal of surfaces and colloids 2008;24:4564-70.
[78] Stuart MAC, Huck WTS, Genzer J, Müller M, Ober C, Stamm M, et al. Emerging applications of stimuli-responsive polymer materials. Nature Materials 2010;9:101-13.
[79] Li Y, Lokitz BS, McCormick CL. Thermally responsive vesicles and their structural "locking" through polyelectrolyte complex formation. Angewandte Chemie-International Edition 2006;45:5792-5.

[80] Qin S, Geng Y, Discher DE, Yang S. Temperature-controlled assembly and release from polymer vesicles of poly(ethylene oxide)-block-poly(N-isopropylacrylamide). Advanced Materials 2006;18:2905-+.
[81] Meng F, Zhong Z, Feijen J. Stimuli-responsive polymersomes for programmed drug delivery. Biomacromolecules 2009;10:197-209.
[82] Patenaude M, Hoare T. Injectable, Mixed Natural-Synthetic Polymer Hydrogels with Modular Properties. Biomacromolecules 2012;13:369-78.
[83] Fitzpatrick SD, Mazumder MAJ, Lasowski F, Fitzpatrick LE, Sheardown H. PNIPAAm-Grafted-Collagen as an Injectable, In Situ Gelling, Bioactive Cell Delivery Scaffold. Biomacromolecules 2010;11:2261-7.
[84] Bawa P, Pillay V, Choonara YE, du Toit LC. Stimuli-responsive polymers and their applications in drug delivery. Biomedical Materials 2009;4.
[85] Roy D, Cambre JN, Sumerlin BS. Future perspectives and recent advances in stimuli-responsive materials. Progress in Polymer Science 2010;35:278–301.
[86] McCoy CP, Brady C, Cowley JF, McGlinchey SM, McGoldrick N, Kinnear DJ, et al. Triggered drug delivery from biomaterials. Expert Opin Drug Deliv 2010;7:605-16.
[87] Strzegowski LA, Martinez MB, Gowda DC, Urry DW, Tirrell DA. Photomodulation of the Inverse Temperature Transition of a Modified Elastin Poly(pentapeptide). Journal of the American Chemical Society 1994;116:813-4.
[88] Zrinyi M. Intelligent polymer gels controlled by magnetic fields. Colloid and Polymer Science 2000;278:98-103.
[89] Kim SJ, Park SJ, Lee SM, Lee YM, Kim HC, Kim SI. Electroactive characteristics of interpenetrating polymer network hydrogels composed of poly(vinyl alcohol) and poly(N-isopropylacrylamide). Journal of Applied Polymer Science 2003;89:890-4.
[90] Urban M. Handbook of Stimuli-Responsive Materials. Wiley-VCH 2011.
[91] Munshi N, Rapoport N, Pitt WG. Ultrasonic activated drug delivery from Pluronic P-105 micelles. Cancer Lett 1997;118:13-9.
[92] Brazel CS, Peppas NA. Synthesis and Characterization of Thermo- and Chemomechanically Responsive Poly(N-isopropylacrylamide-co-methacrylic acid) Hydrogels. Macromolecules 1995;28:8016-20.
[93] Leung MF, Zhu JM, Harris FW, Li P. Novel synthesis and properties of smart core-shell microgels. Macromolecular Symposia 2005;226:177-85.
[94] Lu ZR, Kopeckova P, Kopecek J. Antigen responsive hydrogels based on polymerizable antibody Fab ' fragment. Macromolecular Bioscience 2003;3:296-300.
[95] Zhang S-B, Chu L-Y, Xu D, Zhang J, Ju X-J, Xie R. Poly(N-isopropylacrylamide)-based comb-type grafted hydrogel with rapid response to blood glucose concentration change at physiological temperature. Polymers for Advanced Technologies 2008;19:937-43.
[96] Jo SM, Lee HY, Kim JC. Glucose-sensitivity of liposomes incorporating conjugates of glucose oxidase and poly(N-isopropylacrylamide-co-methacrylic acid-co-octadecylacrylate). Int J Biol Macromol 2009;45:421-6.
[97] Ramanan VV, Hribar KC, Katz JS, Burdick JA. Nanofiber-nanorod composites exhibiting light-induced reversible lower critical solution temperature transitions. Nanotechnology 2011;22.

[98] Fan T, Li M, Wu X, Li M, Wu Y. Preparation of thermoresponsive and pH-sensitivity polymer magnetic hydrogel nanospheres as anticancer drug carriers. Colloids and Surfaces B-Biointerfaces 2011;88:593-600.
[99] Nelson JL, Roeder BL, Carmen JC, Roloff F, Pitt W. Ultrasonically activated chemotherapeutic drug delivery in a rat model. 2002;62:7280-3.
[100] Laukkanen A, Valtola L, Winnik F. Formation of Colloidally Stable Phase Separated Poly(N-vinylcaprolactam) in Water: A Study by Dynamic Light Scattering, Microcalorimetry, and Pressure Perturbation Calorimetry - Macromolecules (ACS Publications). Macromolecules 2004.
[101] Schild H. Microcalorimetric detection of lower critical solution temperatures in aqueous polymer solutions - The Journal of Physical Chemistry (ACS Publications). Journal of Physical Chemistry 1990.
[102] Cao Y, Zhu X, Luo J. Effects of Substitution Groups on the RAFT Polymerization of N-Alkylacrylamides in the Preparation of Thermosensitive Block Copolymers - Macromolecules (ACS Publications). Macromolecules 2007.
[103] Liu HY, Zhu XX. Lower critical solution temperatures of N-substituted acrylamide copolymers in aqueous solutions. Polymer 1999;40:6985-90.
[104] Uguzdogan E, Camh T, Kabasakal O, Patır S, Öztürk E, Denkbaş E, et al. A new temperature-sensitive polymer: Poly(ethoxypropylacrylamide). European Polymer Journal 2005;41:2142-9.
[105] Yamazaki A, Song J, Winnik F, Brash J. Synthesis and Solution Properties of Fluorescently Labeled Amphiphilic (N-alkylacrylamide) Oligomers Macromolecules 1998;31:109-15.
[106] Persson J, Johansson HO, Galaev I, Mattiasson B, Tjerneld F. Aqueous polymer two-phase systems formed by new thermoseparating polymers. Bioseparation 2000;9:105-16.
[107] Yuk S, Cho S, Lee S. pH/Temperature-Responsive Polymer Composed of Poly((N,N-dimethylamino)ethyl methacrylate-co-ethylacrylamide). Macromolecules 1997;30:6856-9.
[108] Liu S, Armes S. The Facile One-Pot Synthesis of Shell Cross-Linked Micelles in Aqueous Solution at High Solids. Journal of the American Chemical Society 2001;123:9910-1.
[109] Chiu TT, Thill BP, Fairchok WJ. Poly(2-ethyl-2-oxazoline): A New Water- and Organic-Soluble Adhesive. Advances in Chemistry. Washington, DC: American Chemical Society; 1986. p. 425-33.
[110] Uyama H, Kobayashi S. A Novel Thermo-Sensitive Polymer. Poly(2-iso-propyl-2-oxazoline). Chem Lett 1992;21:1643-6.
[111] Fusco S. Perspectives on: PEO-PPO-PEO Triblock Copolymers and their Biomedical Applications. J Bioact Compat Polym 2006;21:149-64.
[112] Gao Y, Sun Y, Ren F, Gao S. PLGA–PEG–PLGA hydrogel for ocular drug delivery of dexamethasone acetate. Drug Development and Industrial Pharmacy 2010;36:1131-8.
[113] Jeong B, Bae YH, Lee DS, Kim SW. Biodegradable block copolymers as injectable drug-delivery systems. Nature 1997;388:860-2.

[114] Lutz J-F, Akdemir O, Hoth A. Point by point comparison of two thermosensitive polymers exhibiting a similar LCST: is the age of poly(NIPAM) over? Journal of the American Chemical Society 2006;128:13046-7.
[115] Badi N, Lutz J-F. PEG-based thermogels: Applicability in physiological media. Journal of Controlled Release 2009;140:224-9.
[116] Gong C, Shi S, Wu L, Gou M, Yin Q, Guo Q, et al. Biodegradable in situ gel-forming controlled drug delivery system based on thermosensitive PCL–PEG–PCL hydrogel. Part 2: Sol–gel–sol transition and drug delivery behavior. Acta Biomater 2009;5:3358-70.
[117] Dayananda K, He C, Lee DS. In situ gelling aqueous solutions of pH- and temperature-sensitive poly(ester amino urethane)s. Polymer 2008;49:4620-5.
[118] Chilkoti A, CHRISTENSEN T, MACKAY J. Stimulus responsive elastin biopolymers: applications in medicine and biotechnology. Current Opinion in Chemical Biology 2006;10:652-7.
[119] Urry D, Luan C, Parker T. Temperature of polypeptide inverse temperature transition depends on mean residue hydrophobicity - Journal of the American Chemical Society (ACS Publications). Journal of the … 1991.
[120] Liu R, Fraylich M, Saunders BR. Thermoresponsive copolymers: from fundamental studies to applications. Colloid Polym Sci 2009;287:627-43.
[121] Urtti A. Challenges and obstacles of ocular pharmacokinetics and drug delivery. Adv Drug Deliv Rev 2006;58:1131-5.
[122] Laties AM, Rapoport S. The blood-ocular barriers under osmotic stress. Studies on the freeze-dried eye. ArchOphthalmol 1976;94:1086-91.
[123] Rapoport SI. Osmotic opening of the blood-brain barrier: principles, mechanism, and therapeutic applications. Cell MolNeurobiol 2000;20:217-30.
[124] Foulds WS, Moseley H, Eadie A, McNaught E. Vitreal, retinal, and pigment epithelial contribution to the posterior blood-ocular barrier. TransOphthalmolSocUK 1980;100:341-2.
[125] Cunha-Vaz JG. The blood-ocular barriers: past, present, and future. DocOphthalmol 1997;93:149-57.
[126] Choonara YE, Pillay V, Danckwerts MP, Carmichael TR, du Toit LC. A review of implantable intravitreal drug delivery technologies for the treatment of posterior segment eye diseases. JPharmSci 2009.
[127] Kang Derwent JJ, Mieler WF. Thermoresponsive hydrogels as a new ocular drug delivery platform to the posterior segment of the eye. TransAmOphthalmolSoc 2008;106:206-13.
[128] Jardeleza MS, Miller JW. Review of anti-VEGF therapy in proliferative diabetic retinopathy. SeminOphthalmol 2009;24:87-92.
[129] Novack GD. Ophthalmic drug delivery: development and regulatory considerations. ClinPharmacolTher 2009;85:539-43.
[130] Lee SS, Robinson MR. Novel drug delivery systems for retinal diseases. A review. Ophthalmic Res 2009;41:124-35.
[131] Thrimawithana TR, Young S, Bunt CR, Green C, Alany RG. Drug delivery to the posterior segment of the eye. Drug Discovery Today 2011;16:270-7.

[132] Moshfeghi AA, Peyman GA. Micro- and nanoparticulates. AdvDrug DelivRev 2005;57:2047-52.
[133] Hsu J. Drug delivery methods for posterior segment disease. CurrOpinOphthalmol 2007;18:235-9.
[134] Saishin Y, Silva RL, Callahan K, Schoch C, Ahlheim M, Lai H, et al. Periocular injection of microspheres containing PKC412 inhibits choroidal neovascularization in a porcine model. Invest OphthalmolVisSci 2003;44:4989-93.
[135] Gomes dos Santos AL, Bochot A, Doyle A, Tsapis N, Siepmann J, Siepmann F, et al. Sustained release of nanosized complexes of polyethylenimine and anti-TGF-beta 2 oligonucleotide improves the outcome of glaucoma surgery. JControl Release 2006;112:369-81.
[136] Giordano GG, Chevezbarrios P, Refojo MF, Garcia CA. Biodegradation and Tissue Reaction to Intravitreous Biodegradable Poly(D,L-Lactic-co-Glycolic) Acid Microspheres. Current Eye Research 1995;14:761-8.
[137] Herrero-Vanrell R, Refojo MF. Biodegradable microspheres for vitreoretinal drug delivery. Advanced Drug Delivery Reviews 2001;52:5-16.
[138] Anderson JM, Shive MS. Biodegradation and biocompatibility of PLA and PLGA microspheres. Advanced Drug Delivery Reviews 1997;28:5-24.
[139] Bourges JL, Gautier SE, Delie F, Bejjani RA, Jeanny JC, Gurny R, et al. Ocular drug delivery targeting the retina and retinal pigment epithelium using polylactide nanoparticles. Invest OphthalmolVisSci 2003;44:3562-9.
[140] Irache JM, Merodio M, Arnedo A, Camapanero MA, Mirshahi M, Espuelas S. Albumin nanoparticles for the intravitreal delivery of anticytomegaloviral drugs. MiniRevMedChem 2005;5:293-305.
[141] Jang WD, Nakagishi Y, Nishiyama N, Kawauchi S, Morimoto Y, Kikuchi M, et al. Polyion complex micelles for photodynamic therapy: incorporation of dendritic photosensitizer excitable at long wavelength relevant to improved tissue-penetrating property. JControl Release 2006;113:73-9.
[142] Usui T, Sugisaki K, Amano S, Jang WD, Nishiyama N, Kataoka K. New drug delivery for corneal neovascularization using polyion complex micelles. Cornea 2005;24:S39-S42.
[143] Ideta R, Tasaka F, Jang WD, Nishiyama N, Zhang GD, Harada A, et al. Nanotechnology-based photodynamic therapy for neovascular disease using a supramolecular nanocarrier loaded with a dendritic photosensitizer. NanoLett 2005;5:2426-31.
[144] Weiner AL SK, Johnson S. Tack for intraocular drug delivery and method for inserting and removing same. USA1995.
[145] Ogura YI, Yoshito. Biodegradable scleral plug. 1998.
[146] Kunou N, Ogura Y, Yasukawa T, Kimura H, Miyamoto H, Honda Y, et al. Long-term sustained release of ganciclovir from biodegradable scleral implant for the treatment of cytomegalovirus retinitis. Journal of Controlled Release 2000;68:263-71.
[147] Varner SED, Jr., Eugene; Shelley, Terry; Barnes, Aaron Christopher; Humayun, Mark. Devices for intraocular drug delivery. 2004.

[148] Shin JP, Park YC, Oh JH, Lee JW, Kim YM, Lim JO, et al. Biodegradable intrascleral implant of triamcinolone acetonide in experimental uveitis. J Ocul Pharmacol Ther 2009;25:201-8.
[149] Pitkanen L, Ranta VP, Moilanen H, Urtti A. Permeability of retinal pigment epithelium: effects of permeant molecular weight and lipophilicity. Invest OphthalmolVisSci 2005;46:641-6.
[150] Hastings MSL, S.K; Miller, D.J; Bernstein, P.S.; Mufson, D. VisulexTM: Advancing Iontophoresis for Effective Noninvasive Back-of-the-Eye Therapeutics. Drug Delivery Technology 2004;4.
[151] Neurotech. Novel Therapies for the Eye. 2010.
[152] Corstorphine L, Sefton MV. Effectiveness factor and diffusion limitations in collagen gel modules containing HepG2 cells. J Tissue Eng Regen Med 2010.
[153] ClinicalTrials.gov-Identifier-NCT00447954. Neurotech Pharmaceuticals. A Study of an Encapsulated Cell Technology (ECT) Implant for Patients With Atrophic Macular Degeneration. ClinicalTrials.gov Identifier: NCT00447954.
[154] ClinicalTrials.gov-Identifier-NCT00447993. Neurotech Pharmaceuticals. A Study of Encapsulated Cell Technology (ECT) Implant for Patients With Late Stage Retinitis Pigmentosa. [ClinicalTrials.gov Identifier: NCT00447993].
[155] ClinicalTrials.gov-Identifier-NCT00447980. Neurotech Pharmaceuticals: A Study of Encapsulated Cell Technology (ECT) Implant for Participants With Early Stage Retinitis Pigmentosa.
[156] Neurotech. Positive Results from Neurotech's NT-501 Phase 2 Dry AMD (Geographic Atrophy) Study Demonstrate Proof of Concept. 2009.
[157] Nanjawade BK, Manvi FV, Manjappa AS. In situ.-forming hydrogels for sustained ophthalmic drug delivery. Journal of Controlled Release 2007;122:119-34.
[158] Fitzpatrick SD, Jafar Mazumder MA, Lasowski F, Fitzpatrick LE, Sheardown H. PNIPAAm-Grafted-Collagen as an Injectable, In Situ Gelling, Bioactive Cell Delivery Scaffold. Biomacromolecules 2010.
[159] Wells LA, Brook MA, Sheardown H. Generic, Anthracene-Based Hydrogel Crosslinkers for Photo-controllable Drug Delivery. Macromolecular Bioscience 2011;11:988-98.
[160] Wells LA, Sheardown H. Photosensitive controlled release with polyethylene glycol-anthracene modified alginate. Eur J Pharm Biopharm 2011;79:304-13.
[161] Wells LA, Furukawa S, Sheardown H. Photoresponsive PEG-anthracene grafted hyaluronan as a controlled-delivery biomaterial. Biomacromolecules 2011;12:923-32.
[162] Jiang J, Moore JS, Edelhauser HF, Prausnitz MR. Intrascleral Drug Delivery to the Eye Using Hollow Microneedles. Pharm Res 2009;26:395-403.
[163] Mahadevan G, Sheardown H, Selvaganapathy P. PDMS embedded microneedles as a controlled release system for the eye. J Biomater Appl 2012.
[164] Ciulla TA, Rosenfeld PJ. Anti-vascular endothelial growth factor therapy for neovascular ocular diseases other than age-related macular degeneration. Current Opinion in Ophthalmology 2009;20:166-74.

[165] Tolentino MJ, McLeod DS, Taomoto M, Otsuji T, Adamis AP, Lutty GA. Pathologic features of vascular endothelial growth factor-induced retinopathy in the nonhuman primate. AmJOphthalmol 2002;133:373-85.
[166] Tolentino MJ, Miller JW, Gragoudas ES, Jakobiec FA, Flynn E, Chatzistefanou K, et al. Intravitreous injections of vascular endothelial growth factor produce retinal ischemia and microangiopathy in an adult primate. Ophthalmology 1996;103:1820-8.
[167] Qaum T, Xu Q, Joussen AM, Clemens MW, Qin W, Miyamoto K, et al. VEGF-initiated blood-retinal barrier breakdown in early diabetes. Invest OphthalmolVisSci 2001;42:2408-13.
[168] Saint-Geniez M, Maharaj AS, Walshe TE, Tucker BA, Sekiyama E, Kurihara T, et al. Endogenous VEGF is required for visual function: evidence for a survival role on muller cells and photoreceptors. PLoSOne 2008;3:e3554.
[169] Ishida S, Usui T, Yamashiro K, Kaji Y, Amano S, Ogura Y, et al. VEGF164-mediated inflammation is required for pathological, but not physiological, ischemia-induced retinal neovascularization. JExpMed 2003;198:483-9.
[170] ClinicalTrials.gov-Identifier-NCT00885794. Microperimetry and Optical Coherence Tomography (OCT) With Lucentis for Diabetic Macular Edema (DME) (MORE).
[171] Hurwitz H, Fehrenbacher L, Novotny W, Cartwright T, Hainsworth J, Heim W, et al. Bevacizumab plus irinotecan, fluorouracil, and leucovorin for metastatic colorectal cancer. NEnglJMed 2004;350:2335-42.
[172] Fine SL, Martin DF, Kirkpatrick P. Pegaptanib sodium. Nature Reviews Drug Discovery 2005;4:187-8.
[173] Ng EW, Shima DT, Calias P, Cunningham ET, Jr., Guyer DR, Adamis AP. Pegaptanib, a targeted anti-VEGF aptamer for ocular vascular disease. NatRevDrug Discov 2006;5:123-32.
[174] Klettner A, Roider J. Comparison of bevacizumab, ranibizumab, and pegaptanib in vitro: efficiency and possible additional pathways. Invest OphthalmolVisSci 2008;49:4523-7.
[175] Mendrinos E, Donati G, Pournaras CJ. Rapid and persistent regression of severe new vessels on the disc in proliferative diabetic retinopathy after a single intravitreal injection of pegaptanib. Acta Ophthalmol 2009;87:683-4.
[176] Cunningham ET, Jr., Adamis AP, Altaweel M, Aiello LP, Bressler NM, D'Amico DJ, et al. A phase II randomized double-masked trial of pegaptanib, an anti-vascular endothelial growth factor aptamer, for diabetic macular edema. Ophthalmology 2005;112:1747-57.
[177] Rosenfeld PJ, Fung AE, Puliafito CA. Optical coherence tomography findings after an intravitreal injection of bevacizumab (avastin) for macular edema from central retinal vein occlusion. Ophthalmic SurgLasers Imaging 2005;36:336-9.
[178] Avery RL. Regression of retinal and iris neovascularization after intravitreal bevacizumab (Avastin) treatment. Retina 2006;26:352-4.
[179] Avery RL, Pearlman J, Pieramici DJ, Rabena MD, Castellarin AA, Nasir MA, et al. Intravitreal bevacizumab (Avastin) in the treatment of proliferative diabetic retinopathy. Ophthalmology 2006;113:1695-15.

[180] Barakat MR, Kaiser PK. VEGF inhibitors for the treatment of neovascular age-related macular degeneration. Expert Opinion on Investigational Drugs 2009;18:637-46.
[181] Mordenti J, Cuthbertson RA, Ferrara N, Thomsen K, Berleau L, Licko V, et al. Comparisons of the intraocular tissue distribution, pharmacokinetics, and safety of 125I-labeled full-length and Fab antibodies in rhesus monkeys following intravitreal administration. ToxicolPathol 1999;27:536-44.
[182] Deissler H, Lang S, Lang GE. VEGF-induced effects on proliferation, migration and tight junctions are restored by ranibizumab (Lucentis) in microvascular retinal endothelial cells. BrJOphthalmol 2008;92:839-43.
[183] Chun DW, Heier JS, Topping TM, Duker JS, Bankert JM. A pilot study of multiple intravitreal injections of ranibizumab in patients with center-involving clinically significant diabetic macular edema. Ophthalmology 2006;113:1706-12.
[184] Nguyen QD, Tatlipinar S, Shah SM, Haller JA, Quinlan E, Sung J, et al. Vascular endothelial growth factor is a critical stimulus for diabetic macular edema. AmJOphthalmol 2006;142:961-9.
[185] Ranchod TM, Fine SL. Primary treatment of diabetic macular edema. ClinIntervAging 2009;4:101-7.
[186] Lee SS, Hughes PM, Robinson MR. Recent advances in drug delivery systems for treating ocular complications of systemic diseases. Current Opinion in Ophthalmology 2009;20:511-9.
[187] Simo R, Hernandez C. Advances in the medical treatment of diabetic retinopathy. Diabetes Care 2009;32:1556-62.
[188] Singerman L. Combination Therapy Using the Small Interfering RNA Bevasiranib. Retina-the Journal of Retinal and Vitreous Diseases 2009;29:S49-S50.
[189] Jin KL, Mao XO, Greenberg DA. Vascular endothelial growth factor: Direct neuroprotective effect in in vitro ischemia. Proceedings of the National Academy of Sciences of the United States of America 2000;97:10242-7.
[190] Storkebaum E, Lambrechts D, Carmeliet P. VEGF: once regarded as a specific angiogenic factor, now implicated in neuroprotection. Bioessays 2004;26:943-54.
[191] Wu L, Martinez-Castellanos MA, Quiroz-Mercado H, Arevalo JF, Berrocal MH, Farah ME, et al. Twelve-month safety of intravitreal injections of bevacizumab (Avastin): results of the Pan-American Collaborative Retina Study Group (PACORES). Graefes ArchClinExpOphthalmol 2008;246:81-7.
[192] Nachod GR. ACTH and cortisone in ocular disease. J Am Med Womens Assoc 1951;6:453-5.
[193] Woods AC. Clinical and Experimental Observation on the Use of ACTH and Cortisone in Ocular Inflammatory Disease. Trans Am Ophthalmol Soc 1950;48:259-96.
[194] Cunningham MA, Edelman JL, Kaushal S. Intravitreal steroids for macular edema: The past, the present, and the future. Survey of Ophthalmology 2008;53:139-49.
[195] Shah CA. Diabetic retinopathy: A comprehensive review. Indian JMedSci 2008;62:500-19.
[196] Butler JM, Guthrie SM, Koc M, Afzal A, Caballero S, Brooks HL, et al. SDF-1 is both necessary and sufficient to promote proliferative retinopathy. JClinInvest 2005;115:86-93.

[197] Ferris FL, III, Patz A. Macular edema. A complication of diabetic retinopathy. SurvOphthalmol 1984;28 Suppl:452-61.
[198] Miyamoto K, Khosrof S, Bursell SE, Rohan R, Murata T, Clermont AC, et al. Prevention of leukostasis and vascular leakage in streptozotocin-induced diabetic retinopathy via intercellular adhesion molecule-1 inhibition. ProcNatlAcadSciUSA 1999;96:10836-41.
[199] Schwartz SG, Flynn HW, Scott IU. Pharmacotherapy for diabetic retinopathy. Expert Opinion on Pharmacotherapy 2009;10:1123-31.
[200] Alghadyan AA. Diabetic Retinopathy - An Update. Saudi Journal of Ophthalmology 2011;25:99-111.
[201] Kuppermann BD. Differentiating Steroid Delivery Systems for Macular Edema. Johns Hopkins Advanced Studies in Ophthalmology 2010;7:35-41.
[202] Quiram PA, Gonzales CR, Schwartz SD. Severe steroid-induced glaucoma following intravitreal injection of triamcinolone acetonide. AmJOphthalmol 2006;141:580-2.
[203] Smithen LM, Ober MD, Maranan L, Spaide RF. Intravitreal triamcinolone acetonide and intraocular pressure. AmJOphthalmol 2004;138:740-3.
[204] Thompson JT. Cataract formation and other complications of intravitreal triamcinolone for macular edema. AmJOphthalmol 2006;141:629-37.
[205] Schwartz SG, Flynn HW, Jr. Pharmacotherapies for diabetic retinopathy: present and future. ExpDiabetes Res 2007;2007:52487.
[206] FDA US. Kenalog (triamcinolone acetonide) injectable suspension. 2010.
[207] Morrison VL, Koh HJ, Cheng L, Bessho K, Davidson MC, Freeman WR. Intravitreal toxicity of the Kenalog vehicle (benzyl alcohol) in rabbits. Retina-the Journal of Retinal and Vitreous Diseases 2006;26:339-44.
[208] Network DRCR. A randomized trial comparing intravitreal triamcinolone acetonide and focal/grid photocoagulation for diabetic macular edema. Ophthalmology 2008;115:1447-9, 9 e1-10.
[209] Tilton RG, Chang K, Hasan KS, Smith SR, Petrash JM, Misko TP, et al. Prevention of diabetic vascular dysfunction by guanidines. Inhibition of nitric oxide synthase versus advanced glycation end-product formation. Diabetes 1993;42:221-32.
[210] Kuppermann BD. Toxicity Studies on Triamcinolone Acetonide and Dexamethasone. Retina Today 2010:13-4.
[211] Sharma A, Pirouzmanesh A, Patil J, Estrago-Franco MF, Zacharias LC, Pirouzmanesh A, et al. Evaluation of the toxicity of triamcinolone acetonide and dexamethasone sodium phosphate on human lens epithelial cells (HLE B-3). Journal of ocular pharmacology and therapeutics 2011;27:265-71.
[212] Patil AJ, Mansoor A, Sharma A, Kuppermann BD. Effects of dexamethasone on human trabecular meshwork cells in vitro. Association for Research in Vision and Ophthalmology annual meeting. Fort Lauderdale, FL.2009.
[213] Narayanan R, Mungcal JK, Kenney MC, Seigel GM, Kuppermann BD. Toxicity of triamcinolone acetonide on retinal neurosensory and pigment epithelial cells. Investigative Ophthalmology & Visual Science 2006;47:722-8.

[214] Zacharias LC, Luthra S, Dong J, Kuppermann BD. Effect of dexamethasone on mitochondrial func- tion and cell viability in human retinal pigment epithelial and rat neurosensory retinal cells in vitro. Association for Research in Vision and Ophthalmology annual meeting. Fort Lauderdale, FL.2007.
[215] Beer PM, Bakri SJ, Singh RJ, Liu W, Peters Iii GB, Miller M. Intraocular concentration and pharmacokinetics of triamcinolone acetonide after a single intravitreal injection. Ophthalmology 2003;110:681-6.
[216] Morse LS, Modjtahedi S, Smit-McBride Z. Use of Intravitreal Steroids in the Clinic. Retina Today 2010:6-10.

1.6 THESIS SCOPE

Delivery of therapeutic agents into the posterior segment of the eye is one of the most significant unmet clinical needs of visual health care. Delivery to the back of the eye is made difficult by blood ocular barriers that separate the eye from systemic circulation in addition to the physical barriers within the eye that limit diffusion across the globe. We hypothesize that stimuli-responsive copolymers such as poly(N-isopropylacrylamide) (PNIPAAm), which undergo a rapid phase transition, from liquid to gel, are ideal for introducing therapeutic agents into the posterior segment of the eye through minimally invasive techniques. Cell loaded suspensions can be injected directly into the subretinal space, wherein temperature-induced gel formation and subsequent scaffold spreading will allow the formation of an adhesion substrate capable of supporting the growth and differentiation of anchorage-dependent transplanted cells. Furthermore, a polymer / drug suspension can bypass the blood ocular barriers through direct injection as a liquid at room temperature. Upon heating to body temperature, the liquid polymer will transition to a solid drug-infused scaffold capable of releasing low-levels of pharmaceutical for sustained periods of time, thus maintaining therapeutic concentrations within the vitreous while minimizing systemic exposure and decreasing the number of injections a patient receives. Therefore, *in situ* gelling stimuli responsive materials provide a means to overcome the significant obstacles facing delivery of therapeutic agents into the posterior segment of the eye. *In situ* gelling materials can decrease systemic exposure, extend duration of drug activity, decrease the frequency of injections, which will improve patient compliance, and can provide a synthetic adhesion substrate for cell transplantation.

CHAPTER 2: PNIPAAm-*Grafted*-Collagen as an Injectable, *In Situ* Gelling, Bioactive Cell Delivery Scaffold

Authors: Scott D Fitzpatrick, Mohammad A. Jafar Mazumder, Frances Lasowski, Lindsay E. Fitzpatrick, Heather Sheardown.

Publication Information: Published in ***Biomacromolecules***, August 9, 2010. DOI: 10.1021/bm100299j.

Objectives: Design a thermally gelling biomaterial scaffold based on PNIPAAm and collagen that will ultimately facilitate the minimally invasive delivery of anchorage dependent retinal pigment epithelial cells into the delicate subretinal space.

Main Scientific Contributions:

- Proposed a thermoresponsive, bioactive, PNIPAAm-based scaffold for delivery of anchorage-dependent RPE cells into the delicate subretinal space.
- Synthesized and grafted linear chains of amine-terminated PNIPAAm onto the backbone of type I collagen using EDC / NHS chemistry and UV photocrosslinking.
- Demonstrated the enhanced cell adhesive properties of collagen-containing PNIPAAm scaffolds. PNIPAAm-grafted-collagen scaffolds successfully entrapped RPE cells, which remained suspended throughout the bulk matrix following gelation. Cells were largely absent from the bulk phase of PNIPAAm gels lacking collagen.

Author Contributions:

Scott was responsible for the synthesis, design, write-up and the majority of material characterization in this work, including GPC, FT-IR, NMR (not shown), turbidity testing, gelling time characterization, cell culture studies, confocal microscopy and ESEM imaging. Jafar helped with the FT-IR studies to confirm successful grafting of PNIPAAm chains onto the collagen backbone. Frances Lasowski assisted Scott in obtaining confocal microscopy images to demonstrate improved scaffold entrapment with collagen-containing gels. Lindsay Fitzpatrick aided Scott with statistical analysis, aided in troubleshooting and designed the PNIPAAm-grafted-collagen cartoon in Figure 2-1.

PNIPAAm-*Grafted*-Collagen as an Injectable, *In Situ* Gelling, Bioactive Cell Delivery Scaffold

Scott D Fitzpatrick[1], M.A. Jafar Mazumder[2], Frances Lasowski[1], Lindsay E Fitzpatrick[2], Heather Sheardown[1,2*]

[1]School of Biomedical Engineering and [2]Department of Chemical Engineering

McMaster University
1280 Main St. West
Hamilton ON
L8S 4L7

*To whom correspondence should be addressed sheardow@mcmaster.ca

ABSTRACT

Two thermoresponsive, bioactive cell scaffolds were synthesized by decorating the backbone of type I bovine collagen with linear chains of poly(N-isopropylacrylamide) (PNIPAAm), with the ultimate aim of providing facile delivery via injection and support of retinal pigment epithelial (RPE) cells into the back of the eye for the treatment of retinal degenerative diseases. Both scaffolds displayed rapid, sub-physiological phase transition temperatures, and were capable of non-invasively delivering a liquid suspension of cells that gels *in situ* forming a cell-loaded scaffold, theoretically isolating treatment to the injection site. RPE cells demonstrated excellent viability when cultured with the scaffolds and expulsion of cells arising from temperature-induced PNIPAAm chain collapse was overcome by incorporating a room temperature incubation period prior to scaffold phase transition. These results indicate the potential of using PNIPAAm-grafted-collagen as a vehicle for the delivery of therapeutic cells to the subretinal space.

Keywords: Collagen, thermoresponsive, poly(N-isopropylacrylamide), PNIPAAm, retinal pigment epithelial cells, RPE, retina, cell delivery.

2.1 INTRODUCTION

Cell-based therapies have the potential to provide cures for a vast array of diseases and disorders, especially with the rapid advancement in stem cell technology. However, one of the major obstacles standing in the way of clinical success of cell-based therapies is the development of appropriate vehicles to deliver therapeutic cells to target tissues within the body. Typically, cells are delivered as a liquid suspension injected directly into target tissues, or into the systemic circulation [1]. The cells are then expected to migrate to the site of interest, or remain within target tissues depending on the delivery modality. Very little in the way of guidance cues is provided to transplanted cells and the result is typically large-scale cell death, mass leakage of cells from target tissues, loss of control over transplanted cell fate and extremely poor integration into host tissues, often with less than 3% of cells remaining in the intended tissue [1]. Alternatively, cells can be seeded, expanded and differentiated on or within a biomaterial scaffold *ex vivo*, and subsequently implanted at a target location within the body. Delivering cells within a scaffold addresses many of the issues associated with bolus injections by providing a synthetic extracellular matrix for cell adhesion, preventing anoikis and isolating cells to the implantation site. Furthermore, it is possible to load cell scaffolds with growth factors or pharmaceuticals which help control cell phenotype and modulate the microenvironment at the site of implantation [2]. However, implantation of scaffolds is inherently more invasive than bolus cell delivery, which is achieved by simple injection.

Retinal degenerative diseases are a family of diseases that stand to benefit greatly from recent advances in cell technology as researchers have recently demonstrated the

potential to prevent or reverse vision loss using cell therapy. MacLaren et al. demonstrated the possibility of repopulating a damaged or diseased retina with healthy photoreceptors through delivery of neonatal photoreceptor precursor cells; the cells differentiated and integrated with limited success into the outer nuclear layer (ONL) in both intact and degenerating retinas of mature mice [3]. Delivery of retinal pigment epithelial (RPE) cells is another cell-based therapy that has demonstrated tremendous potential and has seen exciting developments since its first inception over twenty years ago [4-7]. RPE transplantation aims to restore the dynamic interaction between light sensitive photoreceptors and metabolically active RPE cells, a relationship that is critical for the maintenance of retinal homeostasis and preservation of sight [8]. Restoration of the subretinal anatomy and extracellular milieu through RPE transplantation can be used to treat not only RPE specific defects, but also a number of photoreceptor defects as well as more complex retinal diseases such as age-related macular degeneration (AMD) [9]. Delivery of therapeutic cells into the subretinal space with an appropriate scaffold may help ease the transition from implantation to integration and improve outcomes with retinal cells [9, 10]. Subretinally transplanted photoreceptors may also benefit from delivery within a temporary scaffold; however, the need to integrate into retinal tissues requires migration out of the scaffold and into the retina. Thus, an appropriate scaffold should be short-lived and promote localized treatment, while providing temporary adhesive cues and ultimately, may serve best as a template for the controlled release of a symphony of growth factors to aid the migration and differentiation of transplanted cells [2]. Alternatively, anchorage-dependant RPE cells, which need not migrate from the

subretinal space, may benefit greatly from delivery within a relatively long-lasting artificial scaffold that provides enhanced cellular attachment. A temporary scaffold would localize transplanted cells to the subretinal space and allow cells to lay down their own extracellular matrix (ECM). This may aid their eventual adhesion to the native subretinal basement membrane, the Bruch's membrane, which may be compromised due to age- or disease-related structural changes [10].

Notwithstanding the above, delivery of therapeutic cells into the complex subretinal space is a particularly challenging task and typical delivery modalities have resulted in poor integration and limited functioning of transplanted cells in the clinical setting [9]. Bolus cell injections are inefficient, resulting in mass efflux of cells into the vitreal cavity and the formation of island-like cell aggregates, while RPE patch grafts require invasive surgical implantation through a small incision made in the retina, which may damage the highly complex neural retinal tissues [8, 9]. It is likely that minimally invasive cell delivery techniques are crucial for the clinical success of retinal cell-based therapy. Therefore it was hypothesized that the development of cell-carrying 'intelligent materials', delivered through relatively non-invasive methods and which can be tailored to provide short and long-term support as required, may serve as ideal delivery vehicles for transplantation and support of therapeutic cells into the subretinal space, and ultimately other tissues.

Intelligent materials undergo a reversible, stimuli-induced phase transition that can be utilized to deliver therapeutic agents non-invasively via syringe as a liquid suspension followed by scaffold formation *in situ* and subsequent entrapment of the

delivered agent [11]. Poly(N-isopropylacrylamide) (PNIPAAm) is a thermoresponsive intelligent material that undergoes a reversible transition from liquid to gel under aqueous conditions when heated above a lower critical solution temperature (LCST) of approximately 32^{o}C [11]. It was envisioned that the rapid phase-transition, characteristic of PNIPAAm, could be utilized to deliver cells as a liquid suspension into the subretinal space followed by *in situ* scaffold formation, in essence combining the favorable delivery technique of bolus injections with the benefits of providing transplanted cells with a synthetic extracellular matrix for support. PNIPAAm has been used in a number of different biomedical applications. For example, Hoffman et al. developed PNIPAAm-protein conjugates to modulate temperature-induced on-off biochemical activity for use in immunoassays and protein isolation [12, 13]. Additionally, the polymer has been examined extensively for use in drug delivery systems [14, 15] and in 'cell sheet engineering' to generate an intact monolayer of functional cells without the use of digestive enzymes [16]. Cells harvested in this fashion have been examined for transplantation as single sheets for skin [17], cornea [18] and RPE [8] repair, or as more complex layered sheets for cardiac [16], kidney [19] and liver [20] tissue regeneration. However, as PNIPAAm contains no cell binding domains in its unmodified form, it does not serve as an appropriate template for transplanted cell adhesion. Therefore, in order to generate an injectable, *in situ* gelling, cell adhesive scaffold, PNIPAAm must be coupled with adhesion molecules or peptide sequences that support anchorage of the transplanted cells. RPE cells adhere to their extracellular matrix, neighboring cells and Bruch's membrane through a number of different adhesion molecules including integrins,

cadherins, syndecans, selectins and immunoglobulin adhesion proteins [9]. Of these adhesion molecules, the integrins are of significant interest as they play an essential role in the adhesive and phagocytic activity of RPE cells, which is crucial for the maintenance of retinal homeostasis and the preservation of sight [9, 18, 19]. The RPE appear to have major membrane receptors for collagen, vitronectin, laminin and fibronectin [17, 19]. Therefore, in order to generate an appropriate substitute for the native Bruch's membrane, in this work, PNIPAAm was coupled with type I collagen, a naturally occurring cell-matrix protein that serves as one of the major binding proteins for RPE cells [9]. The resulting thermoresponsive PNIPAAm-collagen copolymers were examined as cell-carrying biomaterial scaffolds aimed at improving outcomes in retinal-cell therapy for the treatment of retinal degenerative diseases.

2.2 MATERIALS AND METHODS

Unless otherwise stated, all reagents were purchased from Sigma Aldrich (Oakville ON).

2.2.1 Synthesis of Amine-Terminated PNIPAAm

N-isopropylacrylamide (NIPAAm) was purified by recrystallization from a toluene / hexane mixture. Amine-terminated PNIPAAm was synthesized as described in the literature [20]. Briefly, NIPAAm (88.37 mmol) and cysteamine hydrochloride (AESH) (3.68 mmol) were dissolved in dimethylformamide (DMF). Dry nitrogen was bubbled through the reaction mixture for thirty minutes prior to the addition of N,N'-Azobisisobutyronitrile (AIBN) (1.22 mmol), which had previously been re-crystallized from methanol. Polymerization was allowed to proceed for 7 hours at 70^{o}C. The polymerized product was precipitated in an excess of diethyl ether. The product was

extensively dialyzed with cellulose tubing (Spectrum Laboratories), then freeze-dried and stored at -20^{o}C. Both DMF and tetrahydrofuran (THF) gel permeation chromatography (GPC) were used to assess the molecular weight of the polymer, using polyethylene oxide (PEO) and polystyrene (PS) standards respectively.

2.2.2 Synthesis of PNIPAAm-Grafted-Collagen

Linear chains of amine-terminated PNIPAAm were grafted onto the backbone of type I bovine collagen (a kind gift of Allergan, Santa Barbara CA) using 1-Ethyl-(3-3-dimethylaminopropyl) carbodimiide hydrochloride (EDC) and N-hydroxysuccinimide (NHS) chemistry. The cartoon in Figure 2-1 illustrates the proposed structure of the comb-type graft copolymer. EDC / NHS chemistry was used to generate covalent linkages between the carboxylic acid groups of aspartic acid (Asp) and glutamic acid (Glu) residues present in collagen with the amine-functionalized end groups of the synthesized PNIPAAm [21]. Collagen (0.5 ml, 100 mg/ml) was acidified by thoroughly mixing with HCl (75 μl, 1N). Amine-terminated PNIPAAm (600 mg) was dissolved in PBS (10 ml, pH 7.2) and was mixed vigorously with the acidified collagen. EDC and NHS (5 / 5 / 1 molar ratio of EDC / NHS / collagen COOH groups) were added to the mixture and the pH was adjusted to 5.5 with HCl. The reaction was allowed to proceed under gentle mixing at room temperature for 24 hours. The reaction mixture was dialyzed extensively at 4^{o}C to remove any EDC, NHS and excess PNIPAAm. The final copolymer, designated PCol, was freeze-dried and stored at -20^{o}C.

Alternatively, grafting of amine-terminated PNIPAAm onto a collagen backbone was achieved via UV photocrosslinking, with the resulting copolymer designated UV

PCol. Riboflavin was used as a photosensitizer to generate covalent linkages between PNIPAAm and collagen. Collagen (0.5 ml, 100 mg/ml) was acidified by thoroughly mixing with HCl (75 μl, 1N). PNIPAAm (100 mg) was dissolved in PBS (5 ml, pH 7.2) and mixed with collagen. The pH was adjusted to 5.5 with HCl. The riboflavin photosensitizer (1 mg/ml in PBS) was added to the mixture at a volume ratio of 1 : 20 photoinitiator : collagen solution. The final mixture was placed in a UV oven for 15 minutes, 365 nm, 12.5 W/cm^2. The resulting copolymer was dialyzed extensively at 4^{o}C, freeze-dried and stored at -20^{o}C.

Grafting of PNIPAAm chains onto the collagen backbone via EDC / NHS chemistry and by UV photocrosslinking was confirmed using Fourier Transform Infrared spectroscopy (FTIR) (Nicolet-6700, Thermo Scientific). Samples were prepared in a 12 to 1 PNIPAAm to collagen mass ratio and un-bound chains of PNIPAAm were removed from PCol and UV PCol by extensive dialysis using tubing with MWCO of 50,000. IR spectra were then collected for collagen, amine-terminated PNIPAAm, and purified PCol and UV PCol.

2.2.3 Phase Transition Characterization

Phase transition properties of amine-terminated PNIPAAm, collagen, PCol and UV PCol were analyzed using differential scanning calorimetry (DSC) (TA Instruments, 2910) with hermetic pans. Samples were dissolved (15 mg/ml) in de-ionized water and were stored at 4^{o}C prior to analysis. Thermal scans were performed from 25 to 80^{o}C at a rate of 5^{o}C/min.

A Cary 300 UV/VIS spectrophotometer was used to analyze the change in transmittance associated with the phase transition of PNIPAAm, PCol and UV PCol scaffolds as they transitioned from a relatively clear liquid to a milky white gel. The samples were dissolved in distilled water to a concentration of 1 mg/ml. Samples were placed in 4 ml UV cuvettes and were subjected to a heating rate of 1^{o}C/min from 25 to 45^{o}C. Transmittance measurements were recorded every 30 seconds. To avoid bubble formation during heating, samples were sonicated briefly prior to testing.

The gelling kinetics of PNIPAAm, PCol and UV PCol were assessed as a function of temperature by placing glass vials containing 3 ml suspensions of the various materials (5 mg/ml in PBS) in an oil bath at temperatures ranging from 34 to 45^{o}C. The time required for the samples to reach cloud point was recorded.

2.2.4 Cell Culture

Human retinal pigment epithelial (RPE) cells (CRL-2502) were purchased commercially from ATCC (Manassas, VA) and were cultured under CO_2 (37^{o}C, 5% CO_2, 95% air, 100% humidity). DMEM-F12 culture medium (Gibco) was supplemented with FBS (6.25% final concentration, Gibco), 1X glutamate (1% final concentration, Gibco), penicillin-streptomycin (1% final concentration, Gibco) and sodium bicarbonate (0.8% final concentration, Gibco). Scaffolds were pre-treated with a solution of PBS and penicillin-streptomycin (3:1 v/v) to remove biological contaminants. All tests were run in triplicate. Cell viability was assessed in 2- and 3-D cultures by staining cultured cells with calcein AM and ethidium homodimer (EthD-1) (Invitrogen) and manually counting the total number of live and dead cells. One-factor analysis of variance (ANOVA) was

used to analyze the effect of scaffold type on RPE viability in 2- and 3-D culture conditions, using $\alpha = 0.05$. Statistical analysis of means was performed using PASW Statistics 18 (SPSS Inc. IL). All error bars on graphs represent standard deviation.

2.2.4.1 Two Dimensional Cell Supernatant Assay

RPE cells were seeded at a density of 10,000 cells per well in a 48-well tissue culture treated polystyrene (TCPS) dish. Cells were incubated for 2 hours to allow seeded cells to adhere to the bottom of the dish. Culture media was replaced with fresh media containing either amine-terminated PNIPAAm, PCol or UV PCol (20 mg/ml). Culture dishes were then returned to the incubator, allowing the PNIPAAm-based scaffolds to gel in the supernatants of the pre-adhered cells. Media was changed after 48 hours and viability was assessed after 96 hours.

2.2.4.2 Three Dimensional Cell Suspension Assay

RPE cells were suspended at a concentration of 100,000 cells per well in suspensions of PCol and UV PCol (20 mg/ml in DMEM-F12). Suspensions were added to a 48-well TCPS plate, then placed in a 37^{o}C CO_2 incubator, where the scaffolds gelled, entrapping the cells within the 3-D biomaterial matrix. Culture media was changed every 2 to 3 days and cell viability was assessed at day 4, 7 and 14.

2.2.5 Cellular Entrapment Within the Scaffold

To promote cellular attachment to the collagen backbone and improve entrapment within the scaffolds, a room temperature incubation period was added prior to temperature-induced scaffold gelation. Suspensions of amine-terminated PNIPAAm,

PCol and UV PCol (5 mg/ml in DMEM-F12) were loaded with 500,000 RPE cells pre-stained with calcein AM. Cell-loaded scaffolds were incubated at room temperature for one hour and then placed in a 37°C CO_2 incubator to drive gelation of the mixture. After one hour in the incubator, a temperature-controlled, 37°C Leica DMI 6000 B confocal microscope was used to visualize the distribution of cells within the bulk phase of the scaffolds to assess whether cells remained dispersed within the scaffold or had been expelled with the aqueous phase during temperature-induced condensation of the PNIPAAm chains.

2.2.6 Environmental Scanning Electron Microscopy

High resolution images of the internal pore structure of amine-terminated PNIPAAm, un-modified collagen, PCol and UV PCol were obtained using an Electroscan 2020 environmental scanning electron microscope (ESEM). The samples were swollen (15 mg/ml) in distilled water for 48 hours at 37°C, and then rapidly frozen by submersion in a liquid nitrogen bath to preserve the internal pore structure of the swollen scaffolds. The samples remained in the liquid nitrogen bath for 48 hours, and were subsequently freeze dried for imaging. Additionally, RPE cells were loaded into a PCol suspension (15 mg/ml in DMEM-F12) and imaged using ESEM with the described preparation techniques.

2.3 RESULTS AND DISCUSSION

2.3.1 Synthesis of Amine-Terminated PNIPAAm

Polymerization of NIPAAm in the presence of the chain transfer reagent cysteamine hydrochloride (AESH) yielded an amine-functionalized PNIPAAm with a

rapid, thermoreversible phase transition from liquid to gel in aqueous conditions at 32^{o}C. Amine-terminated PNIPAAm was found to have a molecular weight in the range of 5,000 to 10,000 Da using both DMF and THF GPC with PEO and PS standards, respectively.

2.3.2 Synthesis of PNIPAAm-Grafted-Collagen

Initially, simple blends of PNIPAAm and collagen were investigated as potential delivery vehicles. However, these blends tended to separate as PNIPAAm underwent a temperature-induced phase transition. Therefore it was hypothesized that simple blends would not be sufficient for subretinal cell delivery as separation may lead to efflux of the cell-carrying collagen away from the target tissues and into the vitreal cavity. Thus, it was determined that grafting temperature-sensitive PNIPAAm chains along the cell-adhesive collagen backbone would provide a better cell delivery vehicle for subretinal transplantation. Collagen crosslinking via EDC / NHS chemistry has been shown to yield materials which are non-toxic both *in vitro* and *in vivo* [22]. Therefore, this chemistry was used to facilitate grafting of the amine-terminated PNIPAAm chains to carboxylic acid groups of collagen. Ultraviolet-A (UVA) and riboflavin induction of corneal collagen crosslinks is a method used *in vivo* for the treatment of keratoconnus to increase the biomechanical rigidity and stability of the cornea and offered an alternate means to engraft PNIPAAm chains onto a collagen backbone [23-25]. The presence of approximately 122 carboxylic acid groups per collagen α-chain provides a high number of potential PNIPAAm grafting sites along the collagen backbone [21]. Through EDC / NHS chemistry and photocrosslinking, two cell friendly, presumably comb-type graft copolymers were synthesized that exhibit a sharp phase transition below physiological

temperatures. It is hypothesized that these scaffolds will enable the delivery of a liquid suspension of cells that forms a gel scaffold upon injection into the body that will act as an artificial Bruch's membrane capable of supporting the growth and differentiation of anchorage-dependant RPE cells. The cartoon in Figure 2-1 is an illustration of the presumed comb-type graft architecture achieved by grafting linear chains of PNIPAAm along the length of a collagen backbone.

Unbound PNIPAAm chains were removed from PCol and UV PCol samples through extensive dialysis and samples were analyzed using FTIR. The presence of bound PNIPAAm chains in both samples was confirmed by the occurrence of characteristic PNIPAAm -$CH(CH_3)_2$ asymmetric deformation (vibration) peaks at roughly 1387 and 1367cm^{-1}, Figure 2-2. The presence of these peaks in the purified samples confirms that both EDC / NHS chemistry and UV photocrosslinking were successful in grafting PNIPAAm chains onto the collagen backbone. Further evidence of successful grafting is indicated by the increased intensity of the secondary amide peaks around 1544 cm^{-1} in the spectra.

We are currently working on a number of different techniques to quantify the grafting density of PNIPAAm chains onto the collagen backbone, which will be reported separately along with data on the effect of graft density on the transitions and cellular response.

2.3.3 Phase Transition Characterization

DSC analysis revealed sub-physiological phase transition temperatures for amine-terminated PNIPAAm, PCol and UV PCol, which are essential for *in situ* gelling systems

that are to be delivered non-invasively through a syringe and undergo a temperature-induced phase transition, Table 2-1. Multiple peaks were observed for the PCol and UV PCol scaffolds; presumably, the primary peaks resulted from a PNIPAAm-induced phase transition, whereas secondary peaks arose due to denaturation of the collagen backbone. Denaturation of unmodified collagen was observed at 50^{o}C similar to our previous studies [26]. As expected, typically an increase in the thermal transition of collagen was observed following PNIPAAm grafting, although in some cases clear transitions were not observed and denaturation appeared to take place over a range of temperatures. However, the apparent increase in collagen denaturation temperature suggests that PNIPAAm grafting and the slight collagen crosslinking that is also expected to occur impart stability into the collagen structure, a finding that was previously reported for EDC / NHS and dendrimer crosslinked collagen by Duan et al [26].

2.3.4 Turbidity Analysis

As the PNIPAAm-based scaffolds underwent a phase transition, they transformed from a transparent liquid to a milky white, opaque gel. This cloud point allowed characterization of the scaffold LCST with changes in transmittance using a UV spectrophotometer. PNIPAAm, PCol and UV PCol were dissolved in distilled water to concentrations of 1 mg/ml and transmittance was measured at temperatures ranging from 25 to 45^{o}C with a heating rate of 1^{o}C/min as shown in Figure 2-3.

Phase transition temperatures obtained via UV spectrophotometry corresponded with the DSC analysis. All samples appeared to undergo rapid gelation at their LCST as indicated by the sudden decrease in transmittance. Rapid gelation of the scaffold is

desirable to minimize the leakage of liquid scaffold and transplanted cells from the site of injection, thereby maximizing therapeutic payload while minimizing complications that may arise due to scaffold leakage.

Rapid gelling kinetics of all samples were confirmed by assessing the time required to reach cloud point when vials containing suspensions of the different materials were immersed in an oil bath at various temperatures under gentle agitation, Figure 2-4. Rapid gelling times were observed and were found to decrease as a function of increasing temperature. At physiologic temperature, the cloud point was reached in less than one minute for all samples. However, gelling kinetics were limited by heat transfer from the oil bath to the samples contained within the glass vials as illustrated by the slow, non-homogeneous heating of a representative PNIPAAm solution on a hot plate in Figure 2-4b. When PNIPAAm, PCol and UV PCol were injected directly into aqueous solutions above their LCST, scaffold formation occurred almost instantaneously as demonstrated in Figure 2-4c with the injection of PNIPAAm into a heated water solution.

The rapid scaffold formation displayed by both synthesized biomaterial scaffolds indicated that cell entrapment should occur promptly upon injection into the subretinal space, providing transplanted RPE cells with a synthetic extracellular matrix within which they can adhere. Without an adequate substitute for adhesion, studies have demonstrated that the aged Bruch's membrane may be insufficient for supporting transplanted cell anchorage, differentiation and survival [10]. As a result, transplanted RPE cells that are unable to attach to an appropriate basement membrane will undergo a process of adhesion-dependant apoptosis, or anoikis [9]. Ideally, cells entrapped within the

replacement Bruch's membrane (PCol or UV PCol) will be able to carry out a number of their key functions, such as clearing the subretinal space of debris shed by photoreceptor outer segments, maintenance of the blood-retinal barrier (BRB) and the transport and secretion of various ions, cytokines and growth factors [8]. However, eventual migration from the scaffold and adhesion to the native Bruch's membrane may be required to carry out these functions. By providing a temporary synthetic scaffold, transplanted cells will be afforded time to lay down their own ECM, which should aid the ultimate attachment to the aged Bruch's membrane. The ideal scaffold lifetime will be elucidated in future studies and will be achieved with the use of a cell-adhesive degradable PNIPAAm, which is currently in development and will theoretically be cleared from the subretinal space following emigration of transplanted cells and material degradation.

2.3.5 Two Dimensional Cell Supernatant Assay

Following 96 hours of incubation with either PNIPAAm, PCol or UV PCol suspended in the supernatant, RPE cells were stained with calcein AM and EthD-1 and viability was assessed. Viabilities were found to exceed 90% for all conditions (Figure 2-5) and there were no statistically significant differences among the mean viabilities of the different samples ($p = 0.262$).

2.3.6 Three Dimensional Cell Suspension Testing

RPE cells were entrapped within PCol and UV PCol suspensions at a density of 100,000 cells per well and cultured for 4, 7 and 14 days. TCPS was used as a control. Cells were stained with calcein AM and EthD-1 to assess viability. Results are shown in

Figure 2-6. RPE viability was also high when seeded within the 3-D matrix of the PCol and UV PCol scaffolds. The scaffold type did not significantly affect the mean viability of RPE cells within the scaffolds on day 4, 7 and 14 ($p > 0.18$). However, only a small fraction of the cells originally present in the liquid scaffold remained within the gel following phase transition. The temperature-induced condensation of PNIPAAm chains results in the expulsion of the bulk aqueous phase, which acts as a driving force to expel cells that had not yet adhered to the collagen scaffold.

Successful entrapment and survival of cells within the delivery scaffold is essential for the ultimate success of transplantation as these scaffolds will serve as the replacement substrate for the native Bruch's membrane and must provide temporary support for anchorage-dependent RPE cell attachment while the cells lay down their own ECM. Therefore, it was realized that a change was required to improve the scaffold's ability to successfully entrap transplanted cells and thereby increase the retention of cells when injected into the subretinal space.

2.3.7 Cellular Entrapment Within the Scaffold

In attempts to create an adequate artificial Bruch's membrane, PCol and UV PCol were synthesized with type I collagen. However simply mixing cells together with the PCol and UV PCol scaffolds prior to gelation resulted in insufficient entrapment of RPE cells within the bulk matrix of the scaffolds, presumably due to the fact that the cells did not have time to adhere to the collagen backbone and were expelled from the bulk copolymer as the materials underwent a temperature-induced phase transition. By simply including an incubation period at room temperature prior to gelation, cell retention in the

scaffolds was greatly increased. Incubation with PCol and UV PCol at temperatures below the LCST allowed RPE cells to adhere to the collagen component of the scaffold, preventing their expulsion from the bulk matrix during phase transition. Z-scans in Figure 2-7 show the various cell containing scaffolds at different depths from bottom to top (i – vi). Live cells were stained green with calcein-AM for visualization purposes. These z-scans demonstrate the ability of the PCol and UV PCol scaffolds to entrap cells more efficiently than unmodified PNIPAAm following gelation as cells remain dispersed throughout the cell-adhesive scaffolds, but are absent in the bulk phase of the PNIPAAm gel.

The design architecture of the modified scaffolds prevents mass expulsion of cells from the biomaterial upon scaffold formation and should reduce the number of cells lost due to leakage from the injection site and anoikis. Further changes that may enhance cellular entrapment include modification of the PCol and UV PCol scaffolds to incorporate additional components of the Bruch's membrane, such as fibronectin, laminin and vitronectin, in order to provide a more complete approximation of the healthy Bruch's membrane. Ultimately, it may be desirable to load the scaffolds with growth factors or pharmaceuticals to help create a favorable microenvironment within the subretinal space to aid cell therapy.

2.3.8 Environmental Scanning Electron Microscopy

ESEM images were collected for amine-terminated PNIPAAm, unmodified collagen, PCol and UV PCol to obtain information about the 3-D microenvironment within which transplanted cells will be entrapped. ESEM was originally utilized for the

potential to view scaffolds in a hydrated state, however, the decreased pressure required for imaging rapidly dried the samples, altering their structure. Therefore, samples were swollen for two days at 37^{o}C, rapidly frozen by immersion in liquid nitrogen and lyophilized to generate a dry sample, while preserving the hydrated pore structure, thereby allowing image collection via ESEM, Figure 2-8.

While PNIPAAm and collagen samples displayed relatively homogeneous, ordered structures, PCol and UV PCol appear highly amorphous and somewhat like a crosslinked gel. Furthermore, these materials were quite different in appearance indicating that the chemistry of synthesis and material composition, which were different due to material processing purposes, had a strong influence on final copolymer structure. The UV PCol scaffold appears to be much more fibrillar, likely owing to a higher degree of collagen crosslinking. All scaffolds appear to be adequately porous, which is conducive to the transport of oxygen and nutrients into and out of the scaffold allowing for nourishment of the entrapped cells, particularly over the desired times that will be necessary for the scaffolds to be present. Figure 2-8e) shows RPE cells entrapped within the PCol scaffold; cells appear as the dark spots within the scaffold and are indicated with white arrows. It is interesting to note the degree of variability within the PCol scaffold itself. The variability between PCol images likely stems from the use of different solvents and the presence, or absence, of cells. The PCol scaffold containing no cells was prepared in distilled water, whereas the PCol scaffold containing RPE cells was swollen in DMEM-F12 culture medium. The scaffold's environment appears to have caused changes in regional self-assembly of the copolymer during scaffold formation, resulting

in a relatively amorphous structure in the presence of distilled water and highly organized, interwoven braid-like structures when swelled in cell-containing culture medium.

2.4 CONCLUSIONS

In attempts to develop a non-invasive strategy to deliver therapeutic RPE cells into the highly complex and delicate subretinal space, the backbone of type I bovine collagen was decorated with thermoresponsive PNIPAAm. Collagen was selected as it is an integral adhesion protein associated with the overall health and function of anchorage-dependant RPE cells. The incorporation of PNIPAAm was intended to decrease invasiveness of delivery by driving *in situ* scaffold formation via temperature-induced phase transition. Grafting of amine-terminated PNIPAAm onto the collagen backbone was achieved through either EDC / NHS chemistry (PCol) or excitation of a riboflavin photosensitizer (UV PCol). Polymer grafting was confirmed using FTIR and did not significantly alter the LCST of the scaffolds. While gelling kinetics of PCol and UV PCol scaffolds were hindered slightly by the presence of bulky collagen molecules, rapid gelation was observed upon heating to body temperature. Both scaffolds displayed excellent compatibility with RPE cells and the inclusion of a room temperature incubation period was found to drastically increase cellular retention. The ability to support cellular engraftment of RPE cells *in vitro* indicates that these scaffolds may be suitable as relatively non-invasive delivery vehicles for the transplantation and support of RPE cells into the subretinal space of patients suffering from retinal degenerative diseases such as AMD and retinitis pigmentosa. Future work will examine the biological response to the

scaffolds including subretinal injections of RPE-carrying PCol and UV PCol biomaterials as well as the development of a degradable form of cell-adhesive PNIPAAm that will allow complete clearance from the subretinal tissues.

2.5 TABLES

Table 2-1: Representative phase transition temperatures of the different cell scaffolding components as determined via differential scanning calorimetry using a heating rate of 5^{o}C/min.

Sample	Thermal Phase Transition (^{o}C)	Collagen Denaturation (^{o}C)
PNIPAAm-NH_2	32	---
Collagen	---	50
PCol	32	65 - 72
UV PCol	31	54 - 77

2.6 FIGURES

Figure 2-1: A representative cartoon depicting the presumed structure of the PCol and UV PCol scaffolds in which linear chains of amine-terminated PNIPAAm have been decorated along the backbone of type I bovine collagen, producing a comb-type grafting architecture.

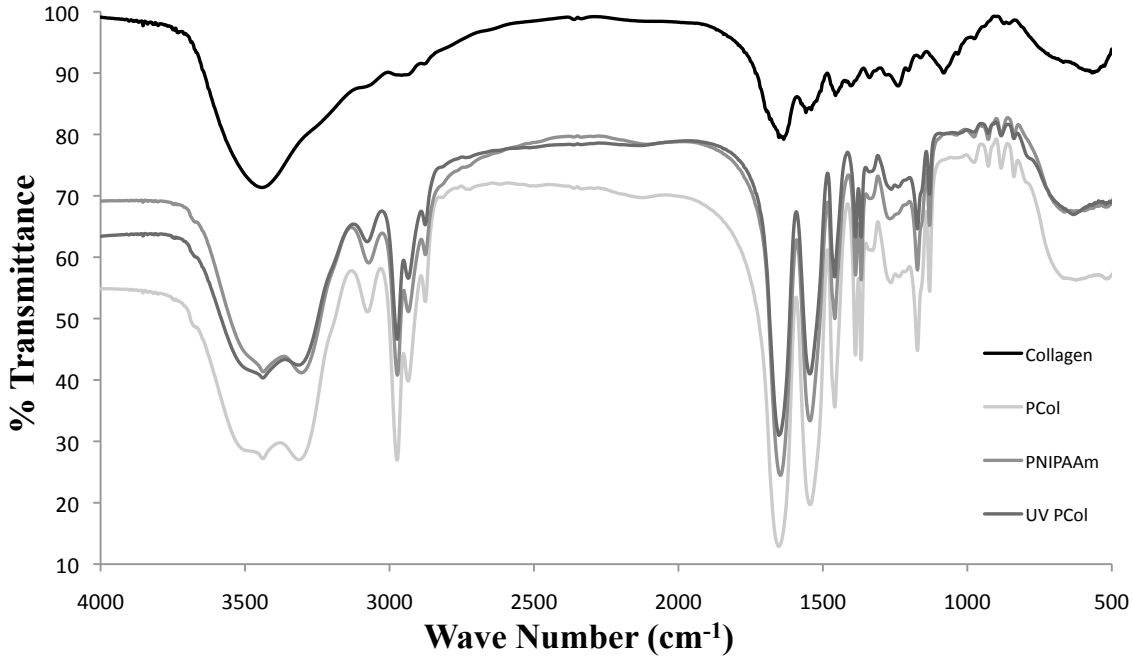

Figure 2-2: FTIR spectra for collagen, amine-terminated PNIPAAm, and purified PCol and UV PCol. Characteristic PNIPAAm peaks are seen in both PCol and UV PCol samples following the removal of un-bound PNIPAAm polymer chains, demonstrating successful grafting has occurred through EDC / NHS chemistry and UV photocrosslinking.

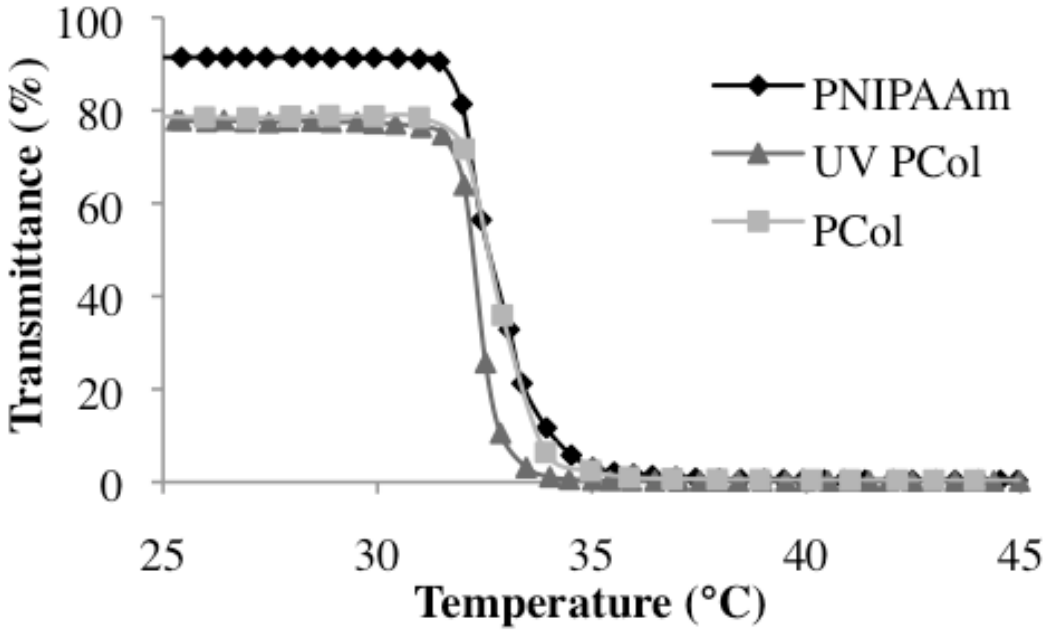

Figure 2-3: Phase transition analysis of the different PNIPAAm-collagen based scaffold as analyzed by UV spectrophotometry. All samples demonstrated a sub-physiological phase transition, which is essential for allowing non-invasive delivery of a liquid suspension of cells that undergo a temperature-induced scaffold formation in situ. Rapid scaffold formation as indicated by the sudden decrease in transmittance will promote isolation of therapy to the target, subretinal tissues.

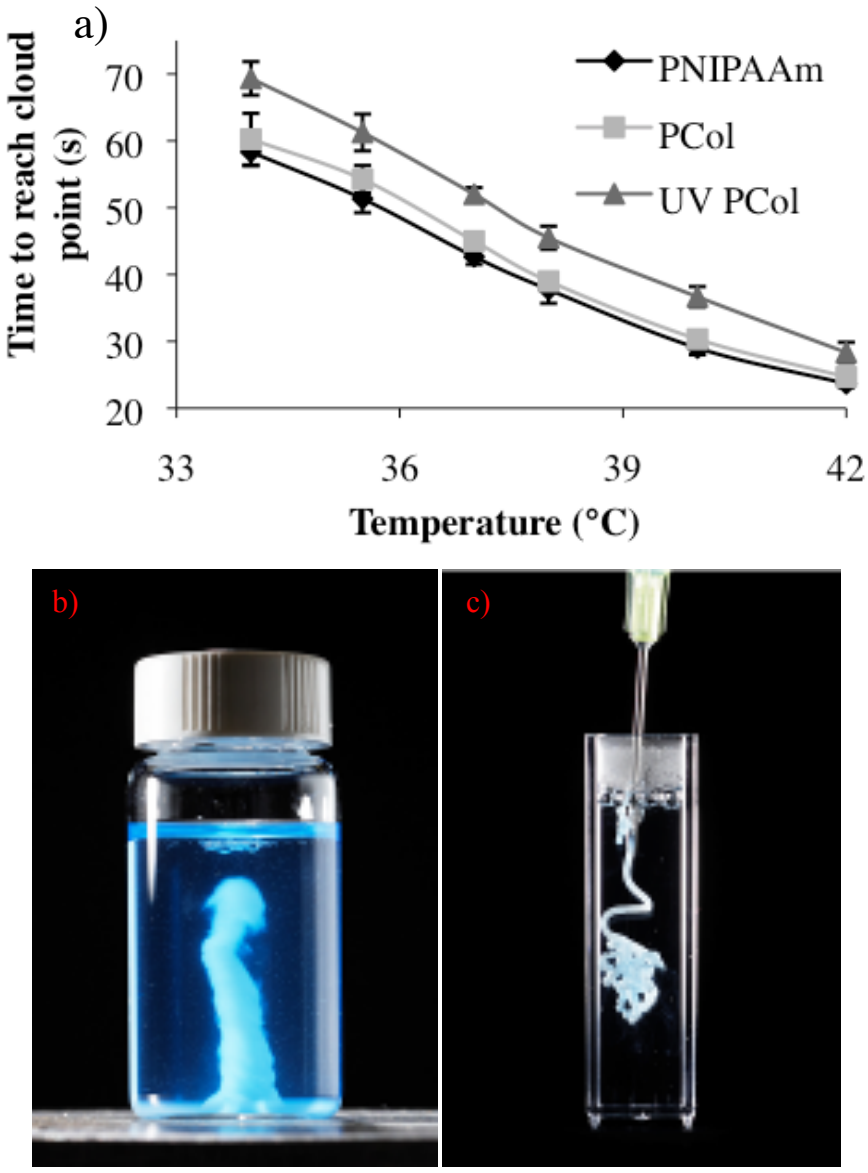

Figure 2-4: Gelling kinetics of amine-terminated PNIPAAm, PCol and UV PCol were assessed by immersing samples in an oil bath at various temperatures and assessing the time required to reach cloud point under gentle agitation (a). Gelling times were limited by heat transfer from the oil bath to the solution within the glass vials as demonstrated by the non-homogeneous scaffold formation occurring at the bottom of the vial of a PNIPAAm solution being heated on a hot plate (b). When injected directly into a heated aqueous environment, scaffold formation occurs almost instantaneously as shown in (c). Error bars represent standard deviation.

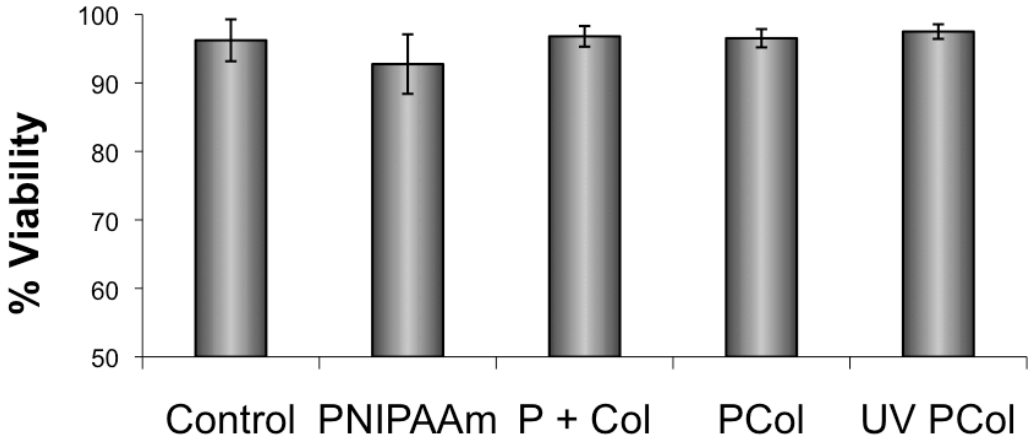

Figure 2-5: Cell viability of RPE cells when seeded for 96 hours in the presence of a) supplemented DMEM-F12 culture medium, b) PNIPAAm, c) PNIPAAm + collagen (P + Col), d) PCol and e) UV PCol. Viabilities were all greater than 90% and there were no were significant differences between mean viabilities (ANOVA, p = 0.262).

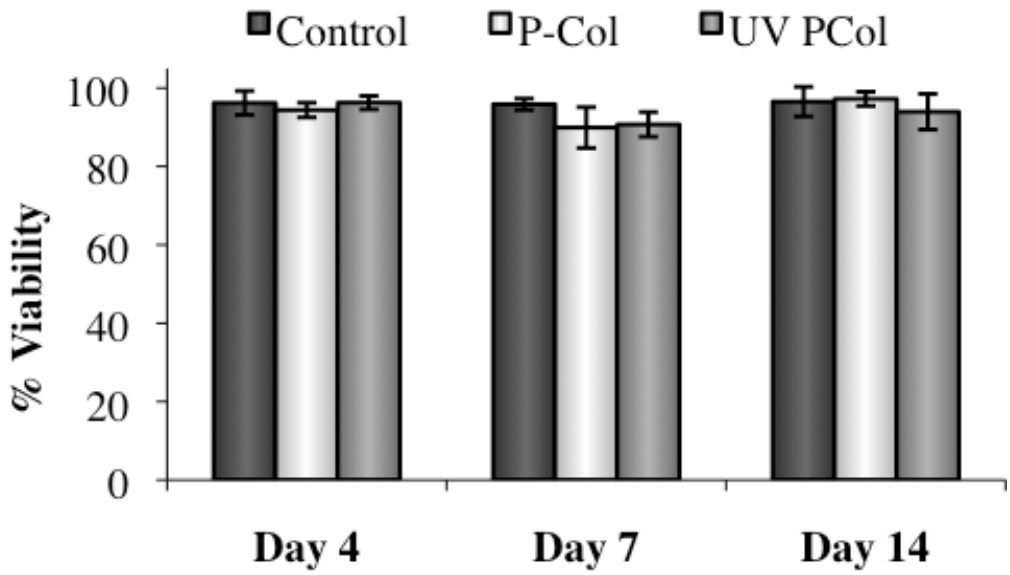

Figure 2-6: RPE cells demonstrated excellent viability when cultured within the bulk matrix of the PCol and UV PCol scaffolds. TCPS was used as a control. The scaffold type did not significantly affect the mean viability on day 4, 7 and 14 ($p > 0.18$). However, while viability remained high, the fraction of cells remaining entrapped within the 3-D architecture was relatively low.

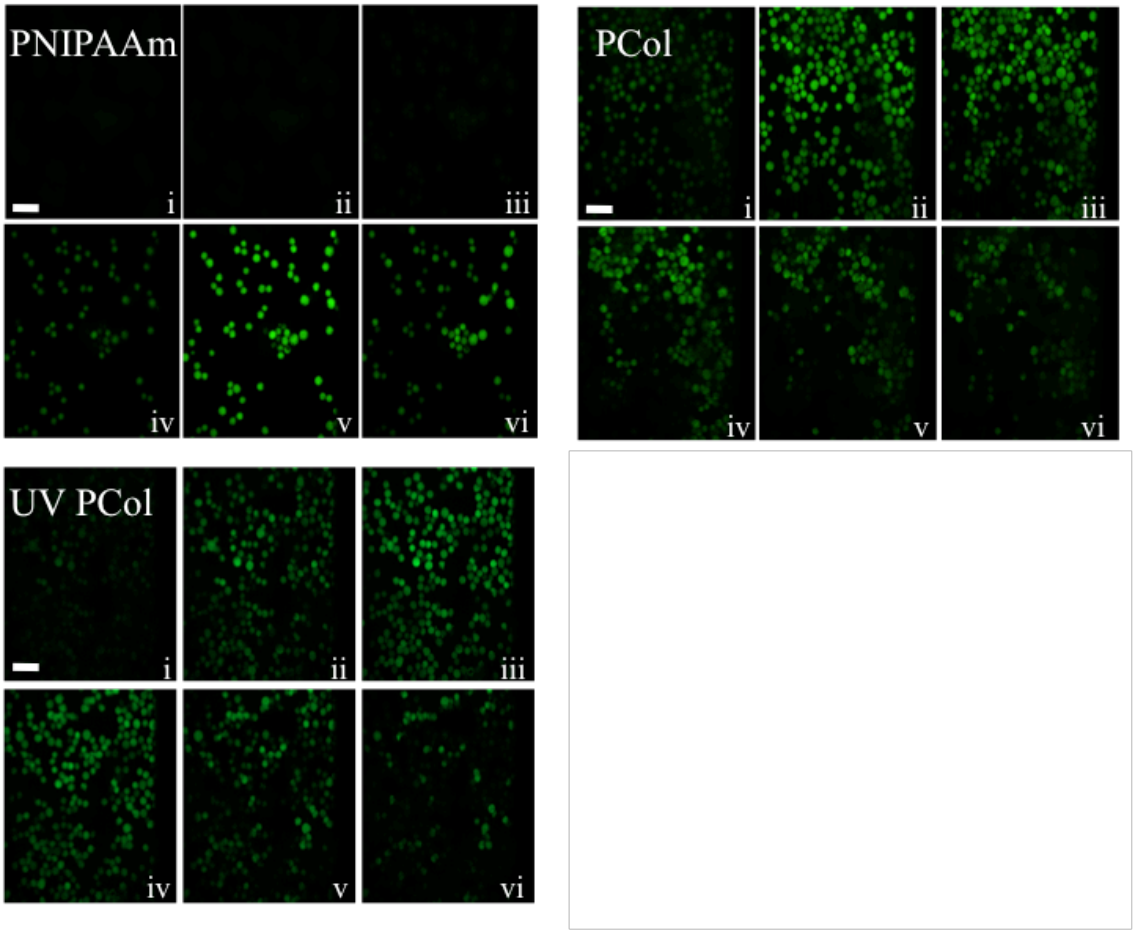

Figure 2-7: Confocal images of calcein AM stained RPE cells that have been incubated with a) Unmodified amine-terminated PNIPAAm, b) PCol and c) UV PCol. Cells were incubated within the various scaffolds for 1 hour prior to being placed in a 37°C CO_2 incubator to drive scaffold formation. Images were collected using a temperature controlled Leica DMI 6000 B confocal microscope. Z-scans show the distribution of cells from bottom to top (i – vi) for the various scaffolds. Scale bar: 80 μm.

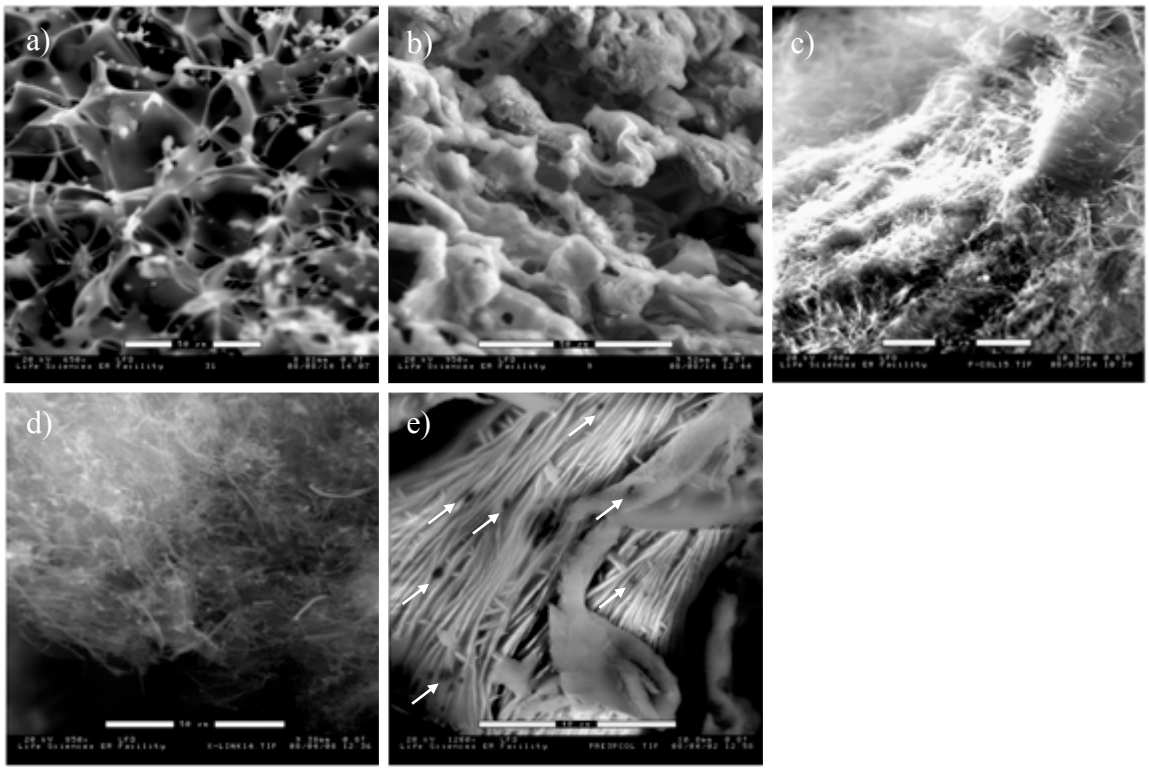

Figure 2-8: Environmental scanning electron microscopy images of a) amine-terminated PNIPAAm; b) un-modified collagen; c) PCol; d) UV PCol; and e) PCol loaded with one million RPE cells. ESEM was used to image the microenvironment of the various scaffolds. Clear differences in microstructure were evident between the two synthesized scaffolds and their starting components. Scale bar: 50 μm (a - d), 40 μm (e).

2.7 ACKNOWLEDGEMENTS

Funding support from NSERC is gratefully acknowledged. Photographs in Figure 2-4 were taken by Ron Scheffler.

2.8 DISCLOSURES

Heather Sheardown is the founder of the 20/20 NSERC Ophthalmic Materials Network, which has ties with and receives funding from the following industrial partners: Alimera Sciences, CIBA Vision Corporation, Custom Contact Lenses, Fovea Pharmaceuticals, iCo Therapeutics, Siltech Corporation, Take Control Cosmedix, Vista Optics Limited and Walsh Medical Devices Incorporated.

2.9 Supporting Information Available

Cell viability images of RPEs cultured in the presence of PNIPAAm, PCol and UV PCol as well as high quality, colour images of Figure 2-4b) and c) are available free of charge via the Internet at http://pubs.acs.org. Live cells were stained green with calcein AM and dead cells were stained red with EthD-1.

References

[1] Mooney DJ, Vandenburgh H. Cell delivery mechanisms for tissue repair. Cell Stem Cell 2008;2:205-13.
[2] Nerem RM. Cell-based therapies: from basic biology to replacement, repair, and regeneration. Biomaterials 2007;28:5074-7.
[3] MacLaren RE, Pearson RA, MacNeil A, Douglas RH, Salt TE, Akimoto M, et al. Retinal repair by transplantation of photoreceptor precursors. Nature 2006;444:203-7.
[4] Gouras P, Lopez R, Kjeldbye H, Sullivan B, Brittis M. Transplantation of retinal epithelium prevents photoreceptor degeneration in the RCS rat. Prog Clin Biol Res 1989;314:659-71.
[5] Lane C, Boulton M, Marshall J. Transplantation of retinal pigment epithelium using a pars plana approach. Eye (Lond) 1989;3 (Pt 1):27-32.
[6] Sheedlo HJ, Li L, Turner JE. Photoreceptor cell rescue in the RCS rat by RPE transplantation: a therapeutic approach in a model of inherited retinal dystrophy. Prog Clin Biol Res 1989;314:645-58.
[7] Gouras P, Flood MT, Kjedbye H, Bilek MK, Eggers H. Transplantation of cultured human retinal epithelium to Bruch's membrane of the owl monkey's eye. Curr Eye Res 1985;4:253-65.
[8] Yaji N, Yamato M, Yang J, Okano T, Hori S. Transplantation of tissue-engineered retinal pigment epithelial cell sheets in a rabbit model. Biomaterials 2009;30:797-803.
[9] da Cruz L, Chen FK, Ahmado A, Greenwood J, Coffey P. RPE transplantation and its role in retinal disease. Prog Retin Eye Res 2007;26:598-635.
[10] Gullapalli VK, Sugino IK, Van Patten Y, Shah S, Zarbin MA. Impaired RPE survival on aged submacular human Bruch's membrane. Exp Eye Res 2005;80:235-48.
[11] Bawa P, Pillay V, Choonara YE, du Toit LC. Stimuli-responsive polymers and their applications in drug delivery. Biomed Mater 2009;4:22001.
[12] Monji N, Hoffman AS. A novel immunoassay system and bioseparation process based on thermal phase separating polymers. Appl Biochem Biotechnol 1987;14:107-20.
[13] Park TG, Hoffman AS. Effect of temperature cycling on the activity and productivity of immobilized beta-galactosidase in a thermally reversible hydrogel bead reactor. Appl Biochem Biotechnol 1988;19:1-9.
[14] Hoare T, Santamaria J, Goya GF, Irusta S, Lin D, Lau S, et al. A magnetically triggered composite membrane for on-demand drug delivery. Nano Lett 2009;9:3651-7.
[15] Kang Derwent JJ, Mieler WF. Thermoresponsive hydrogels as a new ocular drug delivery platform to the posterior segment of the eye. Trans Am Ophthalmol Soc 2008;106:206-13; discussion 13-4.
[16] Shimizu T, Yamato M, Kikuchi A, Okano T. Cell sheet engineering for myocardial tissue reconstruction. Biomaterials 2003;24:2309-16.
[17] Imoto Y, Ohguro N, Yoshida A, Tsujikawa M, Inoue Y, Tano Y. Effects of RGD peptides on cells derived from the human eye. Jpn J Ophthalmol 2003;47:444-53.
[18] McLaughlin BJ, Fan W, Zheng JJ, Cai H, Del Priore LV, Bora NS, et al. Novel role for a complement regulatory protein (CD46) in retinal pigment epithelial adhesion. Invest Ophthalmol Vis Sci 2003;44:3669-74.

[19] Hynes RO. Integrins: bidirectional, allosteric signaling machines. Cell 2002;110:673-87.
[20] Ha DI, Lee SB, Chong MS, Lee YM. Preparation of Thermo-Responsive and Injectable Hydrogels Based on Hyaluronic Acid and Poly(N-isopropylacrylamide) and Their Drug Release Behaviors. Macromolecular Research 2006;14:87-93.
[21] Everaerts F, Torrianni M, Hendriks M, Feijen J. Quantification of carboxyl groups in carbodiimide cross-linked collagen sponges. J Biomed Mater Res A 2007;83:1176-83.
[22] van Wachem PB, Plantinga JA, Wissink MJ, Beernink R, Poot AA, Engbers GH, et al. In vivo biocompatibility of carbodiimide-crosslinked collagen matrices: Effects of crosslink density, heparin immobilization, and bFGF loading. J Biomed Mater Res 2001;55:368-78.
[23] Wollensak G. Crosslinking treatment of progressive keratoconus: new hope. Curr Opin Ophthalmol 2006;17:356-60.
[24] Wollensak G, Spoerl E, Seiler T. Riboflavin/ultraviolet-A-induced collagen crosslinking for the treatment of keratoconus. American Journal of Ophthalmology 2003;135:620-7.
[25] Hafezi F, Mrochen M, Iseli HP, Seiler T. Collagen crosslinking with ultraviolet-A and hypoosmolar riboflavin solution in thin corneas. J Cataract Refract Surg 2009;35:621-4.
[26] Duan X, Sheardown H. Crosslinking of collagen with dendrimers. J Biomed Mater Res A 2005;75:510-8.

CHAPTER 3: Cell-Adhesive Thermo-Gelling PNIPAAm / Hyaluronic Acid Cell Delivery Hydrogels for Potential Application as Minimally-Invasive Retinal Therapeutics

Authors: Mohammad A. Jafar Mazumder*, Scott D Fitzpatrick*, Benjamin Muirhead and Heather Sheardown.

*These authors contributed equally.

Publication Information: Accepted (12/07/2011) for publication in the ***Journal of Biomedical Materials Research: Part A***. Reference ID: JBMR-A-11-0690.R1.

Objectives: Design a temperature-sensitive biomaterial scaffold based on PNIPAAm, hyaluronic acid and cell adhesive RGDS peptides for minimally invasive delivery of pharmaceutical suspensions and / or anchorage dependent cells into the posterior segment of the eye.

Main Scientific Contributions:

- Replaced the bulky collagen backbone from the previously reported PNIPAAm-grafted-collagen scaffolds with small, cell-adhesive RGDS peptides. Elimination of superfluous protein structures should allow delivery of cells within a smaller volume of biomaterial scaffold and decrease overall invasiveness of delivery.
- Incorporated small amounts of hyaluronic acid, a lubricating polysaccharide that has been shown to improve cellular adhesion, proliferation and migration.
- Produced copolymers capable of facile bioconjugation through the incorporation of N-acryloxysuccinimide (NAS), which was utilized for the grafting of RGDS peptides.
- Demonstrated good *in vivo* tolerance following sub-cutaneous implantation between the shoulder blades of SKH1-E mice.

Author Contributions:

This paper was a collaborative work and first authorship was shared between Jafar and Scott. Contributions to this work were as follows. Scott was responsible for copolymer design (with Jafar), LCST characterization via UV spectrophotometry, DSC, assessing water content, performing cell culture studies, examining copolymer morphology using SEM and paper write-up. Jafar was responsible for copolymer design (with Scott), material synthesis, characterization of copolymer composition via FT-IR and NMR, determination of molecular weight, DSC and some help with the write-up. Ben performed the *in vivo* testing, including sub-cutaneous injections, histological staining and imaging and some help with paper write-up.

Cell-Adhesive Thermo-Gelling PNIPAAm / Hyaluronic Acid Cell Delivery Hydrogels for Potential Application as Minimally-Invasive Retinal Therapeutics

M.A. Jafar Mazumder[1]*, Scott D Fitzpatrick[2]*, Ben Muirhead[2], Heather Sheardown[1,2#]

*These authors contributed equally

[1]Department of Chemical Engineering and [2]School of Biomedical Engineering

McMaster University
1280 Main St. West
Hamilton ON, Canada
L8S 4L7

#To whom correspondence should be addressed sheardow@mcmaster.ca

ABSTRACT

Copolymers of N-isopropylacrylamide (NIPAAm) and acrylic acid N-hydroxysuccinimide (NAS) were synthesized via free radical polymerization and conjugated with amine-functionalized hyaluronic acid (HA) and cell adhesive RGDS peptides. These novel copolymers were designed to facilitate non-invasive delivery of a liquid suspension of cells into the delicate subretinal space for treatment of retinal degenerative diseases such as age related macular degeneration (AMD) and diabetic retinopathy. The various synthesized copolymers all displayed sub-physiological phase transition temperatures, thereby allowing temperature-induced scaffold formation and subsequent entrapment of transplanted cells within an adhesive support matrix. Successful grafting of HA and RGDS peptides were confirmed with Fourier Transform Infrared (FTIR) spectroscopy and quantified with ^{1}H Nuclear Magnetic Resonance (NMR) spectroscopy. All copolymers demonstrated excellent compatibility with retinal pigment epithelial (RPE) cells in culture and minimal host response was observed following sub-cutaneous implantation into hairless SKH1-E mice (strain code 447).

Keywords: Thermally responsive, retina, cell delivery, poly(N-isopropylacrylamide), hyaluronic acid.

3.1 INTRODUCTION

Cell based therapies and in particular stem cell technology have undergone numerous exciting advances in recent years that may have profound implications in the development of novel retinal treatments. Takahashi and Yamanaka recently developed a method to genetically re-program differentiated fibroblast cells into a pluripotent, embryonic stem cell-like state through the introduction of four factors; Oct3/4, Sox2, c-Myc, and Klf4 [1]. It is now possible to produce induced pluripotent stem (iPS) cells from adult somatic tissues to generate autologous cell populations of nearly all tissues in the body, including the eye [2]. In 2006, MacLaren et al. demonstrated that it may one day be possible to repopulate damaged or diseased retinas with healthy, functioning photoreceptor cells [3]. West et al. developed a method to improve integration of photoreceptor precursor cells into the outer nuclear layer (ONL) through temporary disruption of the outer limiting membrane (OLM) using a glial toxin, alpha-amino adipic acid (AAA) [4]. In a recent breakthrough, Eiraku et al. demonstrated the ability to generate complex retinal tissue through self-organizing optic-cup morphogenesis in a three dimensional culture setting [5]. However, while photoreceptor cell therapy is an exciting strategy with tremendous therapeutic potential, proper integration and organized wiring with the neural retinal circuitry may represent an extremely difficult process to overcome, especially following retrograde degeneration [6]. Therefore, while it is crucial to continue to investigate photoreceptor regeneration strategies, clinical application remains a distant prospect [7]. It is likely that success in the treatment of retinal degenerative diseases such as age-related macular degeneration (AMD), will stem from

early-stage preventative measures aimed at preserving retinal health through modulation of the subretinal microenvironment [2]. Early-stage delivery of protective cells, such as retinal pigment epithelial (RPE) cells, may provide a means of maintaining retinal homeostasis and preventing the onset of photoreceptor degeneration and loss of vision. The retinal pigment epithelium is a monolayer of metabolically active cells that exists between the photoreceptors and the underlying vasculature, the choriocapillaries [2]. The RPE express several neurotrophic factors such as platelet-derived growth factor (PDGF), pigment-derived epithelial factor (PDEF), vascular endothelial growth factor (VEGF) and epidermal growth factor (EGF), which help maintain photoreceptor health [8]. Furthermore, the RPE is crucial for visual health as it provides nourishment for the photoreceptors, forms the outer component of the blood-retinal barrier (BRB) and clears the subretinal space of debris through phagocytosis of photoreceptor outer segments [9]. In many retinal degenerative diseases, such as AMD, progressive dysfunction of the RPE leads to secondary deterioration of photoreceptor health and visual function [2]. It has long been known that restoration of RPE health through cell therapy may prevent the subsequent loss of photoreceptors; RPE isolation and transplantation was first attempted over 25 years ago [10, 11].

However, delivery of cells into the highly complex, delicate subretinal space represents a significant challenge. In previous studies, cells were delivered into the subretinal space via syringe as a bolus injection [12]. While this method is considered minimally invasive, it is relatively ineffective, as bolus injections tend to offer little in the way of sustained guidance cues or substrates for cellular adhesion [13]. As a result, there

is poor control over transplanted cell fate, uncontrolled leakage from the injection site, aggregation of non-functional cell islands, poor integration into host tissues and cell death [12-14]. Bolus cell injections likely result in failure of the cells to adhere efficiently to the native basement membrane in the subretinal space, the Bruch's membrane, due to age or disease-related structural changes in the collagenous membrane [15]. There have been numerous attempts to increase the capacity of the aged Bruch's membrane to support the growth and differentiation of transplanted cells; however, success has thus far been limited [16, 17]. RPE cells are anchorage-dependent and therefore it is crucial to provide the transplanted cells with an adequate support matrix whether it is the native Bruch's membrane, or a synthetic extracellular matrix analog [12]. In the absence of an appropriate adhesion substrate, such as in the case of an aged Bruch's membrane, RPEs undergo a process of adhesion-dependent apoptosis, or anoikis [12]. Consequently, an alternative delivery approach is to seed and expand cells *ex vivo* on or within a biomaterial scaffold and to implant the construct directly into the subretinal space [2]. While delivering cells within a scaffold addresses many of the shortcomings of bolus injections by providing a substrate for adhesion, isolating cells to the target tissues and offering a scaffold from which guidance molecules may be released for sustained periods, implantation of a solid construct into the delicate subretinal space is inherently more invasive than simple injections. As it is highly likely that the ultimate success of retinal cell therapy will require minimally invasive delivery techniques, in this work, we have synthesized thermoresponsive cell adhesive biomaterial scaffolds that combine the

minimally invasive delivery of bolus injections with the advantages of a solid extracellular support matrix.

Poly (N-isopropylacrylamide) (PNIPAAm), a synthetic polymer that exists as a liquid at room temperature but rapidly gels when heated above a lower critical solution temperature (LCST) around 32°C, forms the major component of the biomaterial scaffold, allowing non-invasive delivery via syringe and subsequent scaffold formation *in situ* following temperature-induced gelation. In our previous work [18], linear chains of amine-terminated PNIPAAm were grafted along the backbone of type I bovine collagen to provide a cell-adhesive, thermo-gelling copolymer to serve as a vehicle for subretinal cell delivery. In this work, cellular adhesive properties were introduced into the scaffolds by replacing the large, bulky collagenous backbone with a small cell adhesion peptide sequence, arginine – glycine – aspartic acid – serine (RGDS), which serves as the major binding sequence of extracellular matrix proteins fibronectin, laminin and collagen, and appears to dictate the adhesion of RPE cells to the Bruch's membrane [19]. In addition, hyaluronic acid (HA), which is a lubricating polysaccharide that has been shown to improve cellular adhesion, proliferation and migration [20], was incorporated into the final copolymers to enhance the ability of the scaffolds to act as cellular substrates. The synthesis and characterization of thermoresponsive, cell adhesive PNIPAAm / HA-based copolymers designed for subretinal transplantation of anchorage-dependent RPE cells is described herein.

3.2 MATERIALS AND METHODS

Acrylic acid N-hydroxysuccinimide (NAS), benzoyl peroxide (97%), adipic acid dihydrazide (≥98%) (ADH), 1-hydroxybenzotriazole hydrate (97%) (HOBT), and 1-ethyl-3-(3-dimethylaminopropyl)-carbodiimide hydrochloride (EDC) were purchased from Sigma- Aldrich (Oakville, ON, Canada), and used as received. Hyaluronic acid (HA) (169 kDa) was purchased from Lifecore Biomedical Co (Chaska, MN, USA) and used as received. N-isopropylacrylamide (NIPAAm) (97%) was purchased from Sigma-Aldrich (Oakville, ON, Canada), and was purified by recrystallization from a toluene / hexane mixture. RGDS (433.4 Da) was purchased from American Peptide (Sunnyvale, CA, USA), and was used as received. 1,4 dioxane, toluene, hexane, tetrahydrofuran (THF), dimethylsulfoxide (DMSO) and anhydrous ethyl ether were purchased from Caledon Laboratories (Caledon, ON), and were used as received. Sodium hydroxide and hydrochloric acid solutions were purchased as concentrates from Anachemia Chemical (Rouses Point, NY, USA), and were prepared by diluting to 1.0 or 0.1 M with deionized water. Deionized water with a resistivity of 18.2 MΩ cm was prepared using a Milli-pore Barnstead water purification system (Graham, NC, USA). Phosphate buffered saline solution (PBS, pH 7.4) was purchased from McMaster University Health Science facilities and used as received. Cellulose dialysis membranes with molecular weight cutoff values of 1- 12 kg/mol were purchased from Spectrum Laboratories Inc (Rancho Dominguez, CA, USA). Human RPE cells (CRL-2502) were purchased commercially from ATCC (Manassas, VA) and were cultured under CO_2 (37°C, 5% CO_2, 95% air, 100% humidity). DMEM-F12 culture medium (Gibco, Carlsbad, CA, USA) was

supplemented with FBS (6.25% final concentration, Gibco), 1 x glutamate (1% final concentration, Gibco), penicillin-streptomycin (1% final concentration, Gibco), and sodium bicarbonate (0.8% final concentration, Gibco). Trypan Blue (0.4%) was purchased from Gibco and used as received.

3.2.1 Synthesis of p(NIPAAm-co-NAS)

p(NIPAAm-*co*-NAS) (PNN) copolymers were synthesized by free radical polymerization. NIPAAm (4.298 g, 37.89 mmol), NAS (0.7181 g, 4.21 mmol) and BPO (0.102 g, 0.42 mmol, 1 mol% relative to monomer) were dissolved in 45 mL 1,4 dioxane to form a 10 wt% monomer solution (90: 10 feed ratio of NIPAAm: NAS). Dry nitrogen was bubbled through the solution for 15 minutes. The reaction vessel was then sealed and heated to 70ºC for 24 hours in a temperature controlled oil bath with continuous stirring to provide uniform mixing. The polymer solution was then cooled to room temperature and isolated by precipitation in anhydrous ethyl ether (1 L). The precipitated polymer was dried in a vacuum oven at 50°C for 48 hours. The copolymer, p(NIPAAm-*co*-NAS) (90:10) (PNN-10), was purified twice by precipitation from THF into anhydrous ethyl ether and then dried to a constant weight in a vacuum oven at 50°C. Copolymer yield for PNN-10 was found to be 86% (4.3 g). PNN-10 was further purified for *in vitro* and *in vivo* studies by extensive dialysis (3.5 kg/mol MW cut-off) against deionized water at 4°C. The dialyzed product was freeze-dried, and stored at -20°C.

Polymerization and purification of a 95:5 NIPAAm: NAS copolymer (PNN-5) was also performed using similar methods as described. Briefly, NIPAAm (4.639 g, 40.96 mmol), NAS (0.3652 g, 2.156 mmol) and BPO (0.1046 g, 0.431 mmol) were

dissolved in 45 mL 1,4 dioxane and polymerization was carried out for 24 hours at 70°C. The copolymer was isolated through precipitation in anhydrous ethyl ether and purified twice from THF. The PNN-5 copolymer was dried to constant weight in a vacuum oven at 50°C and the yield was found to be 91% (4.55 g).

3.2.2 Preparation of Amine-Functionalized Hyaluronic Acid

Amine-functionalized hyaluronic acid was prepared as described previously in the literature [21]. Briefly, HA (169 kDa) (250 mg, 0.625 mmol, based on the repeating unit MW) was dissolved in 47 mL of deionized water. ADH (5.5 g, 31.57 mmol) was added under continuous stirring. EDC (0.6 g, 3.12 mmol) and HOBT (0.478 g, 3.12 mmol) were dissolved in a 2.5 mL solution of DMSO and H_2O (1:1), and then added to the polymer solution under stirring. The pH was adjusted to 4.8 by adding 0.1 M HCl, and the reaction was continued under gentle stirring at room temperature (20°C) for 20 hours in an oil bath. HA-ADH was purified by extensive dialysis (3.5 kg/mol MW cut-off) with deionized water at 4°C. The purified amine-functionalized HA was then lyophilized, and stored at -20°C. The final amine content was determined by ^{1}H Nuclear Magnetic Resonance (NMR), and found to be 24 mol% of the total carboxylic unit for HA.

3.2.3 Preparation of HA grafted PNIPAAm

PNN-10 (0.593 g, 0.502 mmol NAS) was dissolved in 20 mL deionized water. HA-ADH (0.08 g, 0.201 mmol, based on repeating unit MW of HA) was dissolved in 10 mL deionized water, and added to the polymer solution under stirring. The reaction mixture was stirred for 24 hours at room temperature (20ºC). The HA grafted copolymer,

p(NIPAAm-*co*-NAS-HA) (PNN-HA) was dialyzed in deionized water (50 kg/mol MW cut-off). The resulting polymer solution was freeze-dried, and stored at -20°C.

3.2.4 Preparation of RGDS grafted PNIPAAm

PNN-10 (0.7506 g, 0.636 mmol NAS) was dissolved in 10 mL PBS (pH 7.4) in a 20 mL glass vial. RGDS (110 mg, 0.253 mmol) was dissolved in 5 mL PBS (pH 7.4), and added to the polymer solution. The reaction was allowed to proceed for 24 hours at 4ºC. The RGDS-grafted copolymer, p(NIPAAm-*co*-NAS-RGDS) (PNN-RGDS), was extensively dialyzed in deionized water (3.5 kg/mol MW cut-off) at 4ºC. The resulting polymer solution was freeze-dried, and stored at -20°C.

3.2.5 Preparation of HA and RGDS grafted PNIPAAm

PNN-10 (0.75 g, 0.636 mmol NAS) was dissolved in 10 mL PBS (pH 7.4) in a 20 mL glass vial. RGDS (50 mg, 0.115 mmol) and HA-ADH (100.8 mg, 0.254 mmol based on repeating unit MW of HA) were separately dissolved in 5 ml PBS (pH 7.4) and added to the polymer solution. The reaction was allowed to proceed for 24 hours at 4ºC under stirring. The HA and RGDS grafted copolymer p(NIPAAm-*co*-NAS-HA.RGDS) (PNN-HA.RGDS) was extensively dialyzed in deionized water (50 kg/mol MW cut-off) at 4ºC. The resulting polymer solution was freeze-dried, and stored at -20°C.

3.2.6 Material Characterization

The structure of the various PNN-5 and PNN-10 copolymers was characterized by Thermo Fisher Nicolet 6700 FT-IR spectrometer. Copolymer composition was determined by ^{1}H NMR spectroscopy using a Bruker AV 200 spectrometer with DMSO-

d_6 as a solvent. The degree of labeling with HA and RGDS was determined by ^{1}H NMR spectroscopy using a Bruker 600 spectrometer with D_2O as a solvent.

3.2.7 Molecular Weight Determination

A Ubbelohde viscometer (viscometer constant: 0.00314 cSt/s), was used to determine the MW of p(NIPAAm-*co*-NAS) dissolved in methanol at 25.0 ± 0.1 ºC. Prior to measurement, all stock solutions were filtered through a 0.20 μm membrane filter. The intrinsic viscosity [η] was calculated by extrapolation of the Huggins plot (η_{sp}/c versus c) to a concentration of zero. The polymer MW was calculated from the intrinsic viscosity using the relationship $[\eta] = KM^a$ with values for *K* and *a* found in the literature [22].

3.2.8 Characterization of Lower Critical Solution Temperature

The lower critical solution temperatures (LCST) of the hydrogel copolymer solutions were measured by differential scanning calorimetry (DSC, TA Instruments 2910) and UV/vis spectrophotometry (Cary 300). To determine the thermal transition temperature by DSC, samples (15 % w/v in PBS) were heated in hermetic pans from 0 to 70°C at a heating rate of 2°C/min. The temperature at the maximum endothermal peak in the DSC curve was considered as the thermal transition temperature. Transmittance measurements as a function of temperature were assessed to verify LCST values obtained via DSC. Polymer samples were dissolved in PBS (2.5 % w/v) and placed in 4 mL UV cuvettes. The samples were heated from 25 – 45°C at a rate of 1°C/min and transmittance measurements were recorded every 30 seconds.

3.2.9 Copolymer Morphology

High-resolution images of the internal pore structure of the various hydrogels were obtained using a Phillips 515 scanning electron microscope (SEM). Polymer samples were swelled (25 % w/v) in PBS (pH 7.4) at 37°C for 2 days. Excess PBS was then removed and the samples were cryo-preserved by immersion in a liquid nitrogen bath. The copolymers were then lyophilized and the dried samples were mechanically fractured to expose the internal structure. A 10 nm platinum coating was applied using a Precision Etching Coating System (Model 682) to increase sample conductance and allow surface visualization. Images were captured with Mektech URSA 100 Rev. 1.30 imaging software.

3.2.10 Water Content

The water content of the hydrogel was measured gravimetrically. An aqueous copolymer solution (15 % w/v) was placed in a pre-weighed polystyrene petri-dish. The covered dish was then placed into an incubator at 37°C for 6 hours. The supernatant was then removed and the hydrogel pellet was gently dabbed dry with tissue paper to remove residual surface water. The petri-dish was weighed to determine the wet weight of the hydrogel, and then both the wet hydrogel and supernatant were dried to constant weight by heating at 65°C. The water content was calculated using the following equation:

$$Water\ Content = \frac{(m_w - m_d)}{m_d} * 100\%,$$

where m_w is the weight of the wet hydrogel and m_d is the weight of the dry hydrogel.

3.2.11 Cell Culture

To remove biological contaminants, polymer samples were dialyzed extensively in deionized water (3.5 kg/mol MW cut-off), freeze dried and pre-treated with a solution of PBS and penicillin-streptomycin (3:1 v/v). RPE cells were seeded at a density of 10,000 cells per well in a 48 well tissue culture treated polystyrene (TCPS) plate. Cells were incubated in serum supplemented DMEM-F12 culture medium for 2 h to allow adhesion to the culture dish. Cell supernatant was then aspirated and replaced with fresh medium containing 10 mg of PNN-10, PNN-HA, PNN-RGDS or PNN-HA.RGDS. Fresh DMEM-F12 culture medium containing no polymer was used as a control. The samples were placed in the incubator and after 96 hours, the culture medium was aspirated and viability was assessed using a Trypan Blue exclusion assay (0.4 %, Gibco). Live and dead cells were counted using a hemocytometer.

3.2.12 Subcutaneous Injections

Protocols prepared by the McMaster University Animal Research Ethics Board for the care and use of laboratory animals have been observed. Dry polymer samples were sterilized with ethylene oxide (EO) gas, which has been shown to be a minimally reactive and effective method of sterilizing biomaterials [23]. EO sterilization was carried out at the McMaster University histopathology laboratory and was achieved in a 100% ethylene oxide atmosphere at 57°C for 2 hours. Samples were then exposed to sterile air for 15 hours to remove residual EO. The samples were then dissolved in 10 mL aliquots of Fischer Brand medical grade saline to form 15 % w/v solutions. Prior to injection, mice were anaesthetized with isofluorane gas. The polymer samples, syringes and injection

site were pre-cooled to prevent premature gelation of the polymer within the syringe. Polymer suspensions (150 μl) were injected subcutaneously between the shoulder blades of hairless SKH1-E mice (strain code 447). Mice were sacrificed at 3, 7, 20 and 40 days (n = 1, 3, 2 and 2 respectively). The polymer and surrounding tissues were excised, fixed in a 4 % neutral buffered formalin solution for 24 hours, and embedded in paraffin wax. Processed tissue was then sectioned into 4 μm slices using a Leica RM2255 microtome. Sections were stained with hematoxylin and eosin (H&E), and images were collected using an Olympus BX51 optical microscope with QImaging Retiga 2000R camera and Image-Pro Plus (version 7.0) software. The liver and spleen of mice at day 40 were removed, weighed, processed for histological analysis as described above and compared with a control, which received no injection.

3.2.13 Statistical Analysis

A one-factor analysis of variance (ANOVA) was used to analyze scaffold water content and the effect of scaffold presence on RPE viability using $\alpha = 0.05$. A post-hoc analysis was performed on scaffold water content using Tukey's HSD test. Statistical analysis of mean viability and scaffold water content was performed using PASW Statistics 18 (SPSS, Inc., Il). All error bars represent standard deviations.

3.3 RESULTS AND DISCUSSIONS

3.3.1 Synthesis and Characterization of p(NIPAAm-co-NAS) Copolymer

Copolymers with varying ratios of NIPAAm and NAS were prepared by free-radical polymerization. NAS was selected as the reactive co-monomer to provide facile

conjugation with biological molecules, such as cell adhesion peptides, without the need for harsh chemical conditions [24]. Additionally, NAS polymerizes efficiently with a wide range of (meth)acrylate [25] and (meth)acrylamide [26] monomers and is commercially available. In our previous work [18], we examined the potential use of type 1 collagen with linear chains of amine-terminated PNIPAAm grafted along its backbone as a cell delivery scaffold. Collagen was selected as it is one of the major components of the Bruch's membrane and could therefore mimic the natural RPE basement membrane. However, its large size, and limited solubility made it difficult to obtain reproducible polymers. In this work, the bulky collagen backbone has been replaced with small RGDS cell binding peptides, which Tezel et al. suggest may be the most important adhesion sequence that dictates long-term support and survival of RPE cells [19]. The RGD peptide is a bioactive sequence capable of binding surface integrins on RPE cells and has been shown to influence cellular adhesion, migration, proliferation and differentiation [27]. The p(NIPAAm-*co*-NAS) based scaffolds have been conjugated with an RGDS sequence to create thermoresponsive cell delivery vehicles that mimic the native Bruch's membrane. Replacing the bulky collagen molecule with small RGDS peptides eliminates superfluous protein structures, allowing for a more compact polymer scaffold without compromising the potential for cellular adhesion. Less volume would therefore be required for delivery into the limited subretinal space. Furthermore, we hypothesized that the incorporation of hyaluronic acid (HA), or hyaluronan, would improve the performance of the p(NIPAAm-*co*-NAS) copolymers as support matrices for transplanted RPE cells. HA is a naturally occurring hydrophilic lubricating polysaccharide composed

of repeating units of N- acetyl-D-glucosamine and D-glucuronic acid [20]. It is biocompatible, enzymatically degradable and is found in the vitreous humor, synovial fluid, umbilical cord, and the ECM of most tissues [28, 29]. In the eye, HA has demonstrated promising results in the treatment of dry eye [30, 31], has been shown to promote corneal wound healing [32] and is used for visco-supplementation in cataract surgery [33]. The Sheardown group has demonstrated that HA can decrease protein uptake and improve wettability in silicone hydrogel contact lenses [34]. HA has also been shown to have a number of cellular functions, including attachment, migration and proliferation [20]. Thus, amine-functionalized HA was incorporated into the copolymers via coupling with NAS.

There are a number of manuscripts that report the synthesis of poly(NIPAAm-*co*-NAS) copolymers, with a specific interest in protein-reactive systems [24, 35]. Similarly, there are a number of NIPAAm-HA materials in the literature [36, 37]. However, the majority of these materials attach HA to end-functionalized NIPAAm, whereas our system yields distribution of HA throughout, which we believe will be beneficial for providing a synthetic extracellular matrix. Furthermore, our system allows a high degree of flexibility over the molecular weight of HA incorporated and the copolymer content of HA and RGDS. To our knowledge, there are no other reports of NAS chemistry used to functionalize NIPAAm-based copolymers with hyaluronic acid. Several groups have successfully utilized NAS chemistry to graft cell adhesive RGDS peptides onto NIPAAm-based copolymers to create bioactive scaffolds. For instance, Smith et al. demonstrated the ability to generate cell adhesive NIPAAm-based copolymers through

RGD conjugation with protein-reactive NAS groups [38] and later used similar copolymers to facilitate the attachment of bone-morphogenetic protein-responsive C1C12 cells [39]. Li et al. reported the ability to recruit multiple cell lines into artificial corneal implants comprised of copolymers of NIPAAm, NAS, acrylic acid and RGD [40]. Finally, Quan et al. developed an elegant system for tumor-triggered drug release utilizing NAS chemistry to conjugate protected RGD groups onto NIPAAm-based copolymers, which were then coupled with cyclodextrin to create self-assembled, non-covalently coupled micelles (NCCM) [41]. The design employed the subtle physiological changes in the surrounding tumor tissues (pH = 6.8, T > 37˚C) to de-protect the RGD group allowing targeting of tumor cells, which overexpress receptors for RGD, and intracellular destabilization of the NCCM and targeted release [41]. To our knowledge, these are the only examples of copolymers containing NIPAAm, NAS and RGD. We were unable to find evidence of HA-containing RGDS-grafted NIPAAm copolymers in the literature.

FT-IR was used to confirm the final structure of the p(NIPAAm-*co*-NAS) copolymer, Figure 3-1. The FT-IR spectrum shows that the NIPAAm and NAS monomers (Figure 3-1 a, b ↓) have strong characteristic peaks at 1622 and 1408 cm^{-1}, which are attributed to C=C and CH_2= stretching vibration, respectively. However, these two peaks disappear after successful synthesis of the PNN-10 copolymer, Figure 3-1c. The NIPAAm spectrum contains characteristic peaks of C=O and N-H stretching of amide groups I and II around 1652 and 1540 cm^{-1} respectively. Moreover, stretching vibration of the N-H amine group appears around 3309 cm^{-1}, and vibration of the isopropyl group around 1380 cm^{-1} was also observed. The characteristic succinimide

peaks around 1812, 1781 and 1735 cm^{-1} for NAS monomer were observed. The PNN-10 spectra contains succinimide absorption peaks as well as peaks at 3317 and 1660 cm^{-1}, corresponding to the NIPAAm groups mentioned above, confirming the final structure of the PNN-10 copolymer.

The ^{1}H NMR spectra in Figure 3-2 confirms successful copolymerization of PNN-10 and grafting of HA and RGDS onto the copolymer backbone. In the PNN-10 spectrum, characteristic succinimide CH_2 peaks are observed at 2.9 ppm and the CH peak associated with the isopropyl group of NIPAAm is observed at 3.9 ppm. In the PNN-HA spectrum, the HA ring appears broadly in the range of 3 – 4 ppm and a CH_2 peak from the ADH linker is observed at 2.4 ppm. RGDS peaks are observed at 2.5 and 4 ppm in the PNN-RGDS spectrum. Finally, in the PNN-HA.RGDS spectrum, the CH_2 peak of the ADH linker is observed around 2.4 – 2.5 ppm alongside RGDS and a distinct RGDS peak appears at 4 ppm. Additionally, the broad peak associated with the HA ring is observed between 3 – 4 ppm, thus confirming the facile conjugation with biological molecules in the absence of harsh chemical conditions through NAS functionality. The composition of the synthesized copolymers and grafting density of all modified polymers were calculated with ^{1}H NMR. Monomer feed ratios and copolymer compositions are listed in Table 3-1. Copolymer compositions were found to be consistent with the feed ratios.

3.3.2 LCST of the Copolymers

Both DSC and UV spectrophotometry confirmed sub-physiological phase transition temperatures for the various scaffolds, as shown in Table 3-1 and Figure 3-3 respectively. Sub-physiological phase transition temperatures are critical for the

application of cell or drug delivery scaffolds that are designed to utilize body temperature to stimulate *in situ* gel formation. Polymerization with hydrophobic co-monomers such as dimethyl-γ-butyrolactone acrylate (DBA) [42] lowers the LCST, whereas addition of hydrophilic co-monomers such as acrylic acid [24] results in an increase. Therefore copolymerization with NAS in a 95:5 molar feed ratio of NIPAAm: NAS, produced a copolymer with an LCST of 29°C, slightly lower than unmodified PNIPAAm, which is typically reported as 32°C [18]. Increasing the NAS content of the p(NIPAAm-*co*-NAS) copolymer to 10 mol% further decreased the LCST to 27°C, whereas incorporation of either HA or RGDS into PNN-10 increased the LCST to 31°C. Incorporation of both HA and RGDS into PNN-10 further increased the LCST to 32°C.

From the transmittance curves obtained via UV spectrophotometry, rapid gelation kinetics can be observed by the sudden decrease in transmittance when samples are heated above their LCST, Figure 3-3. Rapid gelation is imperative to induce cellular entrapment at the injection site and prevent the efflux of cells away from target tissues and into the vitreous cavity. The presence of small amounts of bulky polysaccharide HA appears to slightly delay gelling kinetics as copolymers lacking HA displayed a sharper decrease in transmittance. The small HA content likely impedes the self-assembly of PNIPAAm and NAS groups to some extent. However, gelation kinetics remain sufficiently rapid for cell delivery purposes as scaffold formation was observed almost instantaneously upon injection into heated aqueous medium and upon subcutaneous injection into mice. Furthermore, it may be possible to incorporate lower molecular weight HA, which will minimize this problem.

3.3.3 Water Content

The water content of the various copolymers was consistent with the LCST findings. Increasing the NAS content from 5 to 10 mol% in the PNN copolymer increased the hydrophobic nature of the material, which decreased the LCST and appears to have slightly decreased the overall water content. The incorporation of HA and RGDS in PNN-HA and PNN-RGDS, which effectively increased copolymer LCST, also yielded copolymers with a higher water content. Finally, PNN-HA.RGDS, which had the highest LCST at 32°C, also had the highest observed water content, Figure 3-4.

3.3.4 Structural Properties of the Hydrogels

High-resolution images of the microstructure of the various polymers were obtained using SEM, as shown in Figure 3-5. From the SEM micrographs, it appears that copolymer morphology and surface roughness correspond closely with water content. As copolymer water content increases, the internal pore morphology appears to become increasingly amorphous and the surface roughness increases. PNN-10, which was the most hydrophobic of the copolymers tested (PNN-5 was not examined) and had the lowest water content, possessed a relatively defined, closed-pore structure. Whereas, PNN-HA.RGDS, which was the most hydrophilic copolymer with the highest water content, had a much more amorphous, interconnected internal pore morphology. The differences in internal pore morphology likely arise during copolymer gelation as the more hydrophobic copolymer tends to collapse more tightly in on itself to minimize interfacial tension at the polymer – aqueous boundary layer. As a result, the hydrophobic copolymer tends to form closed, spherical pockets surrounding aqueous domains trapped

within the hydrogel. As copolymer hydrophilicity increases, interfacial tension decreases, leading to greater interconnectivity between the pores. This behavior explains the relatively smooth exterior shell of PNN-10 and the rough surface possessed by PNN-HA.RGDS (supplementary Figure). Copolymers with an amorphous, interconnected pore network are likely to be conducive to the flow of oxygen and nutrients into and out of the bulk biomaterial scaffold, allowing them to act as viable support matrices for entrapped cells. Therefore, PNN-HA.RGDS, which has a high water content, open-pore network and adhesion peptides to support attachment of anchorage-dependent RPE cells, exhibits desirable characteristics to act as a synthetic cellular support matrix.

3.3.5 In Vitro Cell Viability

A culture of pre-adhered RPE cells was incubated with solutions of supplemented DMEM-F12 medium containing dissolved polymer samples PNN-10, PNN-HA, PNN-RGDS and PNN-HA.RGDS. Culture medium containing no dissolved polymer was used as a control. RPE viability remained very high under all conditions following 96 hours of exposure, Figure 3-6. There were no statistically significant differences among the mean RPE viabilities when cultured in the presence of the various copolymers ($p = 0.103$). These initial studies were intended to provide information about the compatibility of a model RPE cell line with the various copolymers. In future studies, we hope to examine scaffold compatibility with RPE derived from iPS cells. In these studies, we will examine the ability to differentiate iPS cells into RPE cells while cultured within PNN-RGDS and PNN-HA.RGDS scaffolds. Additionally, we will examine characteristics such as RPE

polarity, the ability to phagocytose shed particles from photoreceptor outer segments and the efficiency of cellular entrapment and isolation within the biomaterial scaffold.

3.3.6 Subcutaneous Injections in SKH1-E Mice

Although the intended application of these scaffolds is a minimally invasive delivery vehicle for posterior segment therapeutics, in accordance with the McMaster University Animal Research Ethics Board, we were required to demonstrate material safety prior to intraocular injections. Therefore, our initial *in vivo* studies examine the host response to sub-cutaneous injections of copolymer suspensions between the shoulder blades of nude SKH1-E mice. All samples formed an observable, mechanically robust gel immediately upon injection into the subcutaneous space, Figure 3-7.

In all samples except for PNN-10 (day 3), the gelled material spread out into an apparent thin layer beneath the skin. This scaffold thinning provides favorable conditions for delivery of therapeutic cells into the subretinal space. Initial gel formation may prevent efflux of the cells and scaffold into the vitreous chamber and subsequent material spreading will promote migration within the subretinal space, maximizing coverage of the transplanted cells allowing a single injection to treat a relatively large area [14]. Furthermore, material thinning will minimize visual distortions, which may be caused by protrusion of the gelled scaffold behind the retina. However, the material spreading process made histological analysis of the tissues surrounding the implanted polymer challenging, as it was difficult to locate and identify discrete polymer regions. Therefore, histological sections were obtained by excising tissue from the initial injection site, Figure 3-8.

Mice were sacrificed at day 3, 7, 20 and 40 post-injection (n = 1, 3, 2 and 2 respectively). Histology revealed a relatively minor response to the injected copolymers at day 3. There was an infiltration of immune cells where dermal tissue had been disturbed by the injection. The presence of darkly stained nuclei of leukocytes and fibroblasts indicate a mild inflammatory response consistent with the early stages of the foreign body reaction (FBR). There was no evidence of epidermal necrosis or basophilic debris to indicate acute cytotoxicity in either the dermis or epidermis. At this early stage in the foreign body response, neutrophils predominantly characterize the response (blue arrows). However, there was evidence of progression, with lymphocytes (red arrow) and monocytes (black arrow) infiltrating the implantation site. The infiltration of these leukocytes is often observed perivascularly (blood vessels are denoted with a "V"), indicating chemotaxis from the blood. The control sample shows no evidence of infiltrating cells within the dermis. Fibroblastic cells were labeled with an orange arrow and adipose cells with a green arrow. By day 7, all samples receiving injections appear to have returned to their native state, with no apparent signs of adverse reactivity for the duration of the 40-day experimental period. There was no evidence of fibroplasia or granuloma formation, and there was no histological evidence to suggest infection or hypersensitisation.

Because histological sections of tissues surrounding defined polymer films were difficult to obtain, the liver and spleen were removed and sectioned after 40 days of implant exposure, Figure 3-9. The liver is responsible for metabolising and eliminating foreign materials and contains specialized resident macrophages, termed Kupffer cells, as

well as deposited blood born macrophages. If non-staining copolymers are phagocytosed by these cells, polymer accumulation in the liver will appear as vacuolated cells within the sinusoids of the liver. The spleen is another bioaccumulatory site, which metabolises some metabolites that bypass the liver. Detrimental polymer-induced effects may show up as abnormalities in these tissues.

There was no evidence of necrosis or inflammation of the liver from any of these samples. The anatomy captured in all 4 samples, Figure 3-9 (B-E), show no marked differences from the control mouse, which received no injection. Furthermore, there was no evidence of accumulated phagocytic cells containing polymer that had escaped the site of injection. The masses of the livers (non-desiccated) when removed from the mice were (A) = 1.48 g, (B) = 1.44 g, (C) = 1.51 g, (D) = 1.50 g and (E) = 1.39 g. There was no evidence of liver hypertrophy, neoplastic proliferation, or necrosis. In the spleen, both the red and white pulp were free of visible vacuolated cells from the mononuclear phagocyte system. Furthermore, there was no evidence of splenomegaly or necrosis in any of the samples. None of the examined organs demonstrated any morphological abnormalities, and were indistinguishable from the control sample. The masses of the spleens (non-desiccated) when removed from the mice were (F) = 85 mg, (G) = 90 mg, (H) =78 mg, (I) = 84 mg and (J) = 88 mg.

Histological analysis of tissue at the injection site as well as the liver and spleen were not indicative of any adverse host reaction to the presence of the various p(NIPAAm-*co*-NAS) based copolymers and warrant further studies in an intraocular setting.

3.4 CONCLUSION

Copolymers of NIPAAm and NAS were synthesized via free radical polymerization and conjugated with amine-functionalized hyaluronic acid and cell adhesive RGDS peptides. These novel copolymers were designed to provide non-invasive delivery of therapeutic cells into the hard-to-access subretinal space for the treatment of retinal degenerative diseases, such as AMD and diabetic retinopathy. A sub-physiological phase transition was conserved by incorporating a 90 mol% NIPAAm content into the copolymers. An LCST that is below body temperature allows the delivery of a liquid suspension of cells at room temperature that undergoes a rapid, thermally-induced phase transition as the polymer is heated, forming a cell-infused scaffold *in situ*. Ultimately, this strategy is designed to increase the efficiency of subretinal cell delivery, while decreasing invasiveness of the procedure and providing anchorage-dependant RPE cells with a scaffold to act as an adhesion substrate. It may also be possible to load the liquid polymer / cell suspension with pharmaceuticals, growth factors or guidance molecules, creating a hybrid drug releasing cell scaffold capable of manipulating the conditions within the injection microenvironment. For example, corticosteroids may be co-administered to shore-up complications of macular edema [43], or anti-VEGF agents could be employed to combat ocular neovascularization [44]. These scaffolds demonstrated excellent compatibility with RPE cells *in vitro* and histological analysis following subcutaneous injection between the shoulder blades of SKH1-E mice revealed a mild inflammatory response at day 3 that subsided by day 7. Future studies will examine copolymer drug release profiles, the ability to differentiate and sustain RPE

cells from iPS cells, histological analysis of ocular tissues following injection of the scaffold into the vitreous and subretinal space and the development of a degradable PNIPAAm backbone that ultimately allows the complete clearance of the synthetic scaffold from the body.

3.5 REACTION SCHEMES

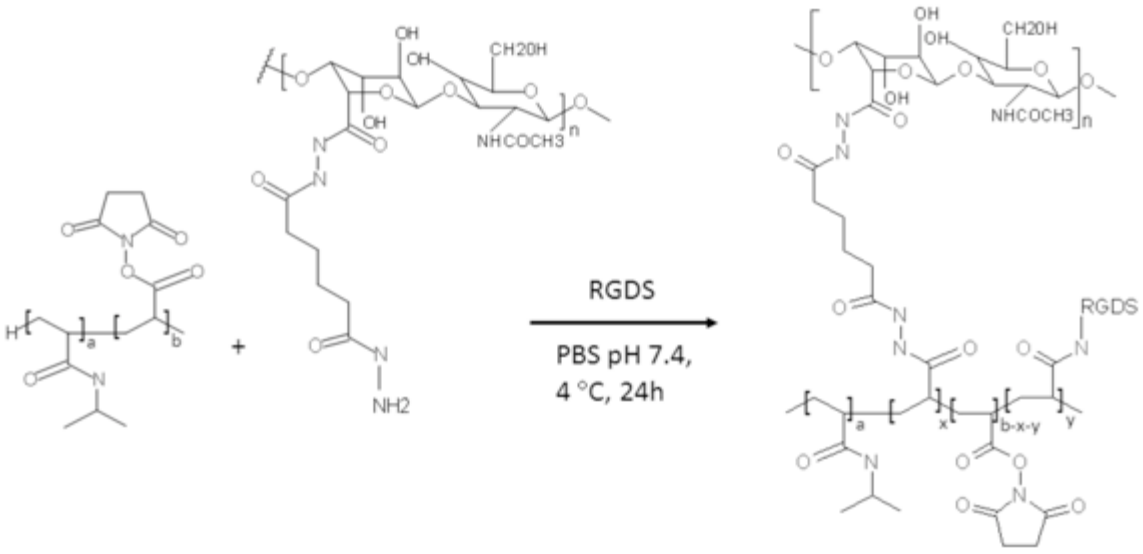

Scheme 3-1: Reaction scheme detailing the grafting of amine-functionalized hyaluronic acid and cell-adhesive RGDS peptide sequences along the p(NIPAAm-co-NAS) copolymer backbone.

3.6 TABLES

Table 3-1: Polymer feed ratios, final copolymer composition, molecular weight determined via Ubbelohde viscometer and phase transition temperatures determined with DSC.

Polymer (feed ratio)	Composition[a]	MW (kg/mol)[b]	LCST[c]
p(NIPAAm-*co*-NAS) (95:5)	94:5 (± 1)	43	29
p(NIPAAM-*co*-NAS) (90:10)	90: 10 (± 2)	30	27
p(NIPAAM-*co*-NAS-HA)	90: 6: 4		31
p(NIPAAM-*co*-NAS-RGDS)	90:6: 4		31
p(NIPAAM-*co*-NAS-HA.RGDS)	90: 4: 4: 2		32

a) Copolymer composition in mol% determined by ^{1}H NMR, b) M_w obtained from viscometry data, c) LCST obtained from Differential Scanning Calorimetry.

3.7 FIGURES

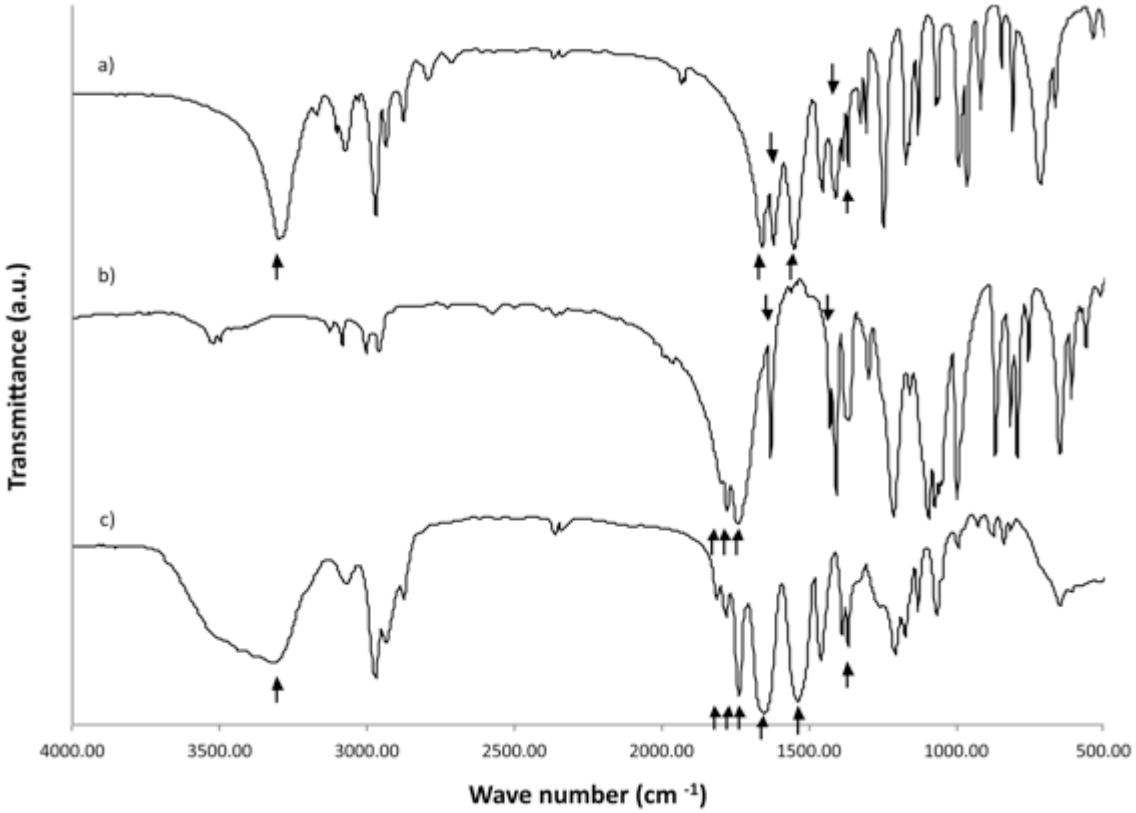

Figure 3-1: FT-IR Spectra of a) NIPAAm, b) NAS, and c) PNN-10 copolymer. FT-IR was used to confirm the successful copolymerization of poly(NIPAAm-co-NAS).

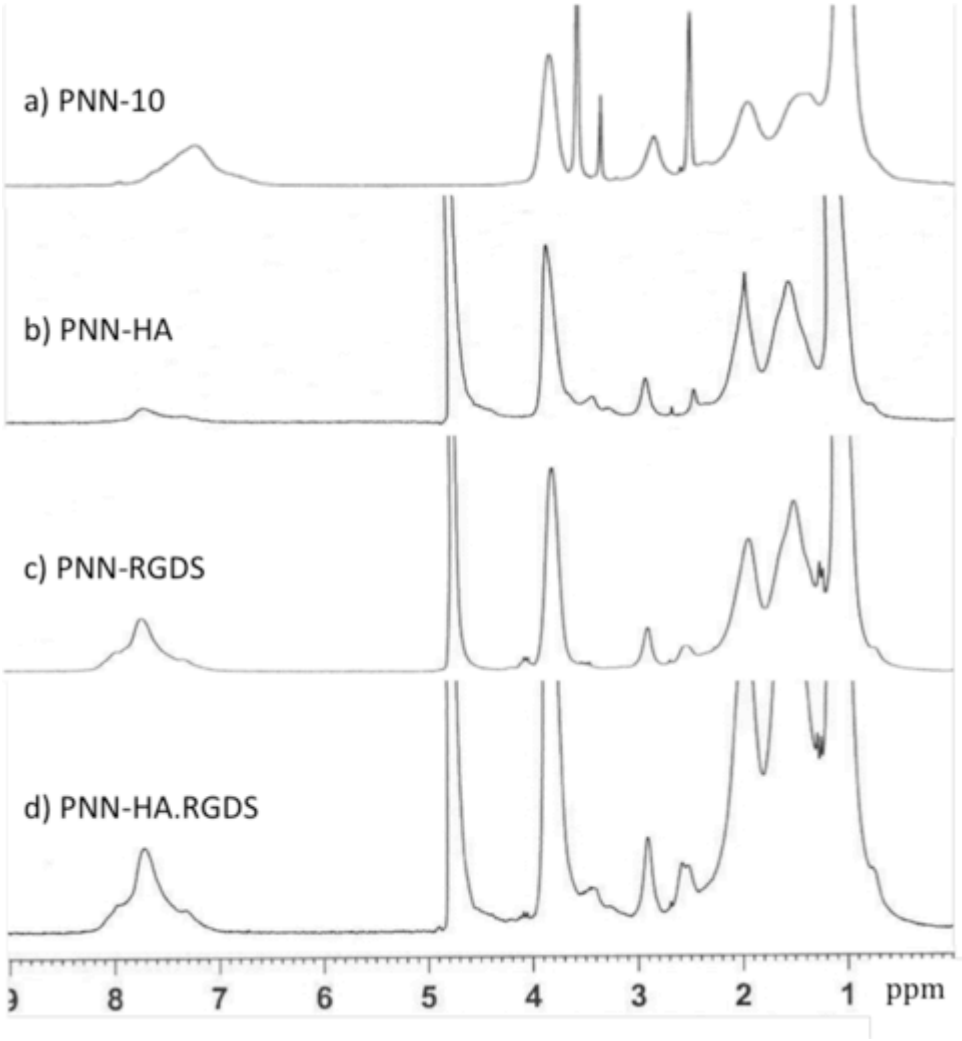

Figure 3-2: ^{1}H NMR Spectra of a) PNN-10, b) PNN-HA, c) PNN-RGDS and d) PNN-HA.RGDS. ^{1}H NMR was used to confirm the successful grafting of HA and RGDS onto the PNN-10 copolymer backbone and to quantify grafting efficiency.

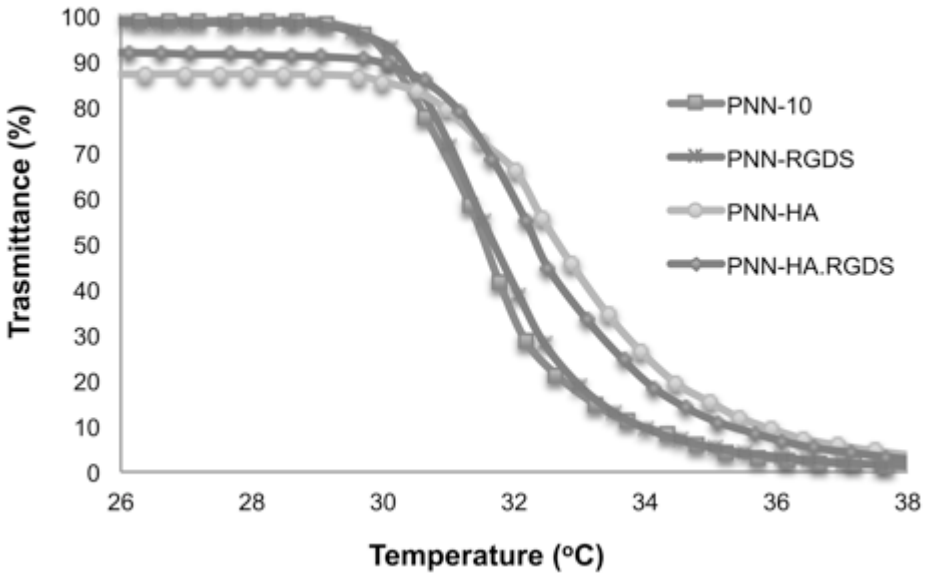

Figure 3-3: UV spectrophotometry was used to confirm LCST values obtained via DSC. Rapid gelling kinetics are observed by the sudden decrease in transmittance as the cloud point is reached.

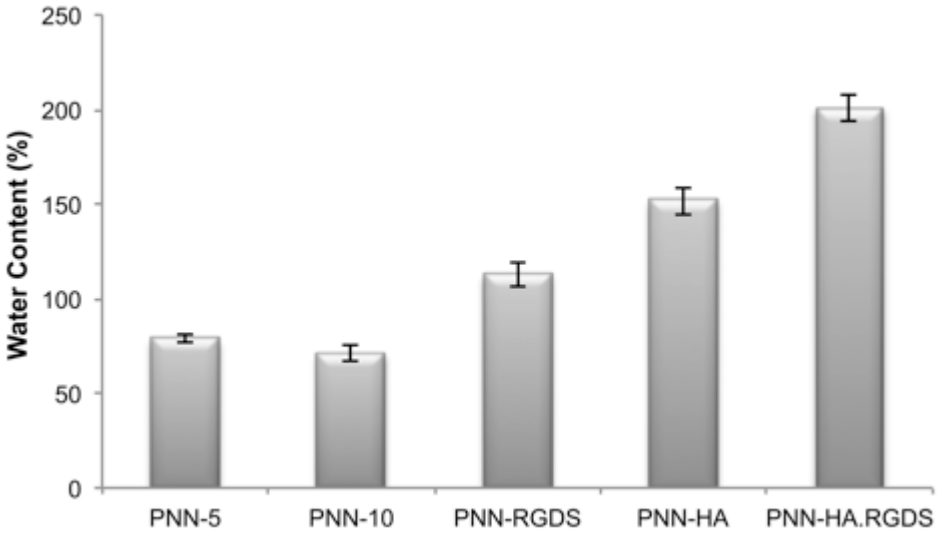

Figure 3-4: Water content of the various copolymers. Incorporation of HA and RGDS increased copolymer water content, whereas hydrophobic NAS resulted in a decrease. The difference among mean water content for each sample was statistically significant ($p < 0.001$) except between PNN-5 and PNN-10 ($p = 0.499$).

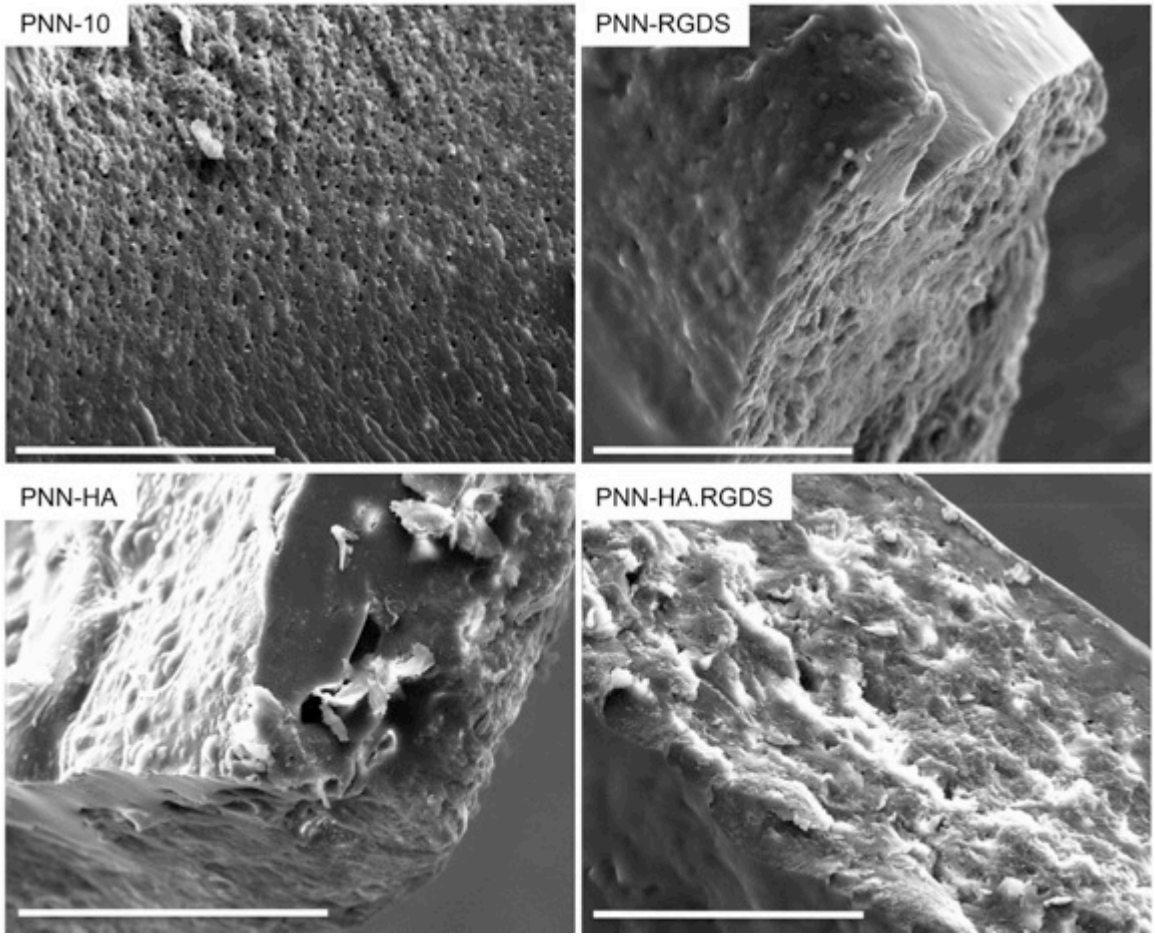

Figure 3-5: SEM images of the internal pore structure of the various copolymers. Dried polymers were mechanically fractured to expose the internal structure. The internal copolymer pore structure appears to become increasingly amorphous as a function of increasing water content. Scale bar = 100 μm.

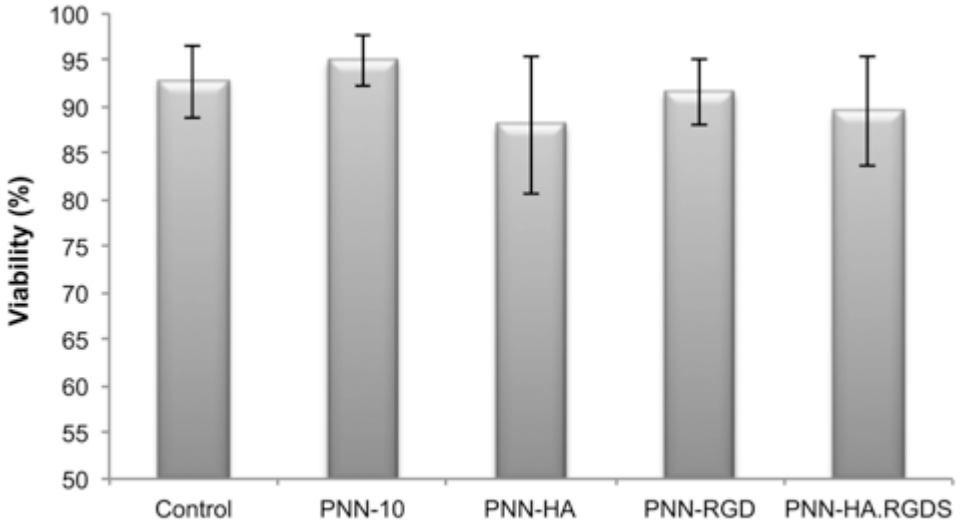

Figure 3-6: Retinal pigment epithelial cells demonstrated excellent compatibility with the various copolymers in culture. RPE cells seeded on a tissue culture treated polystyrene plate served as a control. Viability remained high in all conditions and there was no statistically significant difference among the means ($p = 0.103$).

Figure 3-7: SKH1-E mouse immediately following injection of PNN-10 into the subcutaneous space between the shoulder blades. The copolymer rapidly gelled into a mechanically robust lump following injection, indicated with the dashed line.

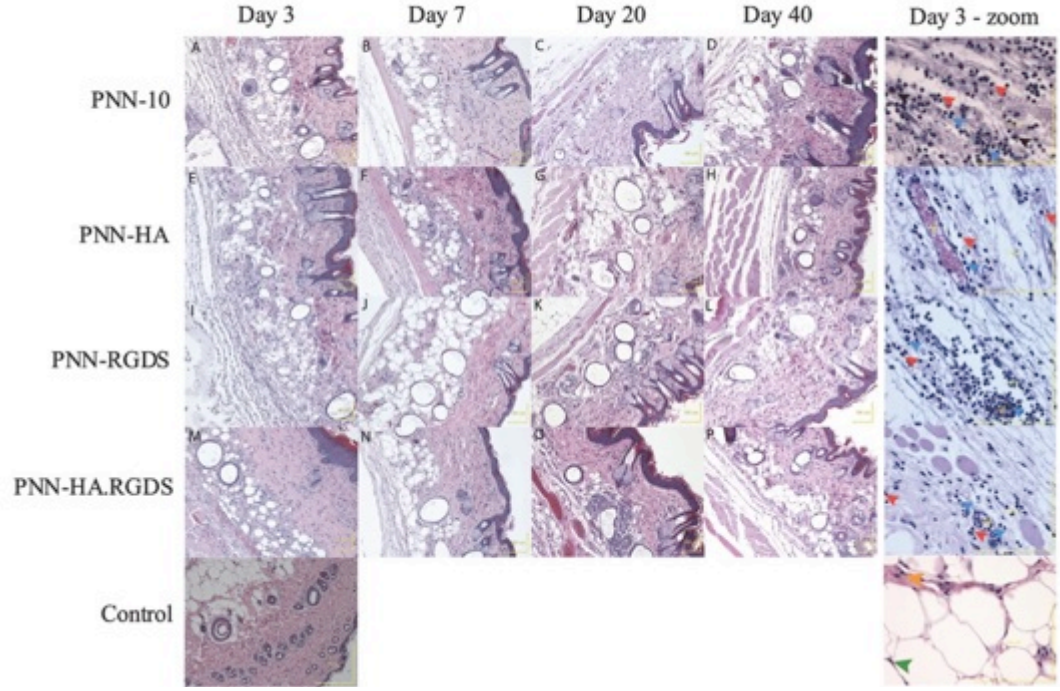

Figure 3-8: Histological sections of tissue at the injection site of PNN-10 (A – D), PNN-HA (E – H), PNN-RGDS (I – L), and PNN-HA.RGDS (M – P). From left to right, tissues were explanted on day 3, 7, 20 and 40 days post-implantation. Neutrophils, lymphocytes, monocytes, fibroblastic cells and adipose cells are labeled with blue, red, black, orange and green arrows respectively in the magnified images from day 3 samples (R – V). Scale bar = 100 μm.

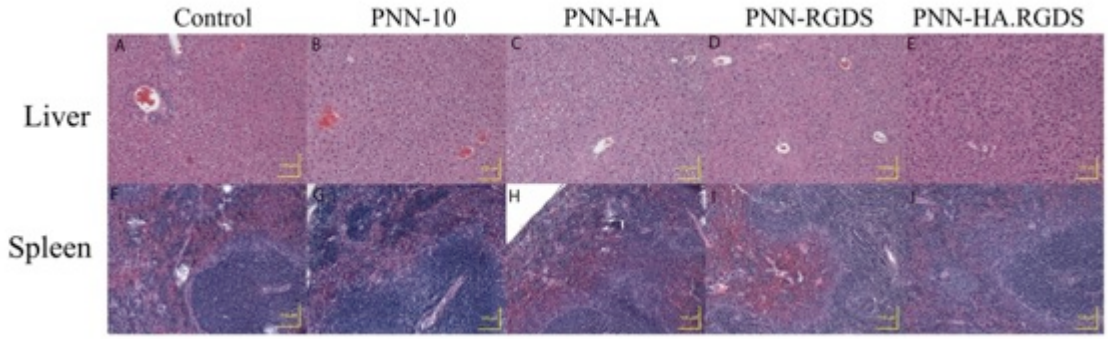

Figure 3-9: The top column shows H&E stained liver sections obtained from mice after 40 days of exposure to control (a), PNN-10 (b), PNN-HA (c), PNN-RGDS (d) and PNN-HA.RGDS (e). The second column (f – j) contains spleen sections in the same conformation. Scale bar =100 μm.

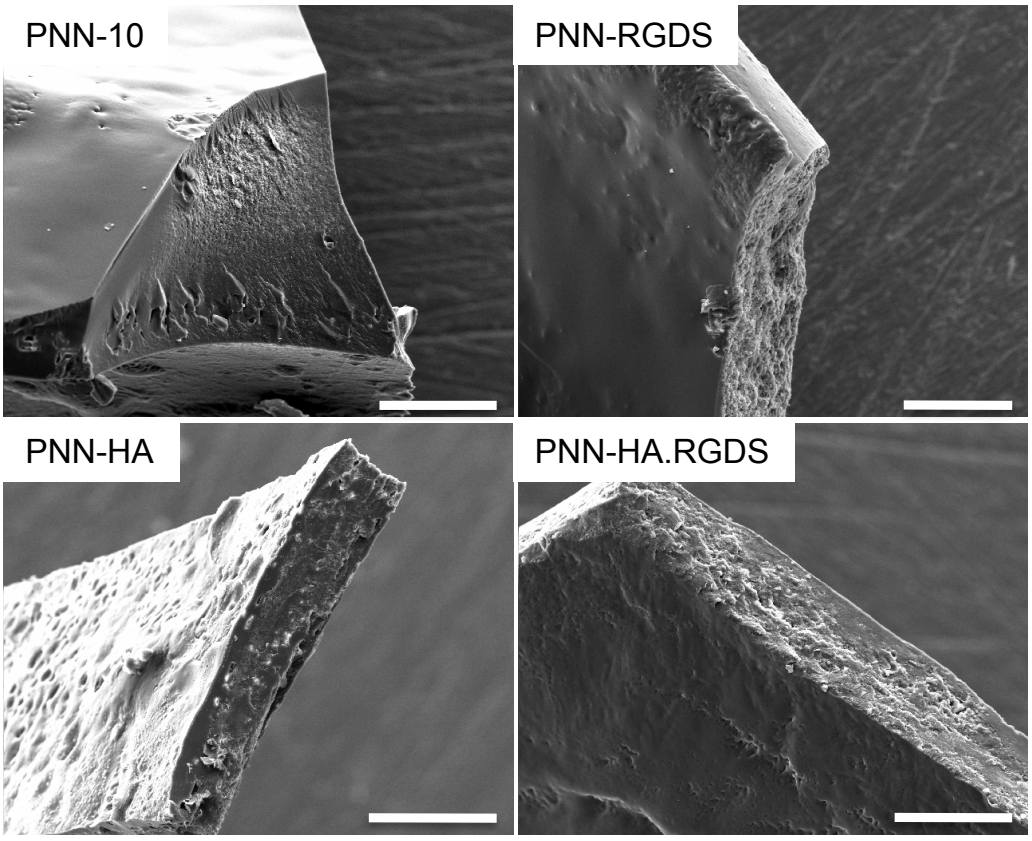

Supplementary Figure 3-1: SEM micrographs of the various copolymer external surface roughness and internal pore structure. These micrographs demonstrate the effect of copolymer water content on surface roughness and internal pore morphology. As copolymer water content increases, the surface at the copolymer / aqueous interface increases in roughness and the internal pore network becomes increasingly interconnected and amorphous. Scale bar = 200 μm.

3.8 ACKNOWLEDGEMENTS

Funding support from NSERC and the 20/20 NSERC Ophthalmic Materials Network is gratefully acknowledged.

3.9 DISCLOSURES

Heather Sheardown is the founder of the 20/20 NSERC Ophthalmic Materials Network, which has ties with and receives funding from the following industrial partners: Alimera Sciences, CIBA Vision Corporation, Custom Contact Lenses, Fovea Pharmaceuticals, iCo Therapeutics, Siltech Corporation, Take Control Cosmedix, Vista Optics Limited and Walsh Medical Devices Incorporated.

References

[1] Takahashi K, Yamanaka S. Induction of pluripotent stem cells from mouse embryonic and adult fibroblast cultures by defined factors. Cell 2006;126:663-76.
[2] Marchetti V, Krohne TU, Friedlander DF, Friedlander M. Stemming vision loss with stem cells. J Clin Invest 2010;120:3012-21.
[3] MacLaren RE, Pearson RA, MacNeil A, Douglas RH, Salt TE, Akimoto M, et al. Retinal repair by transplantation of photoreceptor precursors. Nature 2006;444:203-7.
[4] West EL, Pearson RA, Tschernutter M, Sowden JC, MacLaren RE, Ali RR. Pharmacological disruption of the outer limiting membrane leads to increased retinal integration of transplanted photoreceptor precursors. Exp Eye Res 2008;86:601-11.
[5] Eiraku M, Takata N, Ishibashi H, Kawada M, Sakakura E, Okuda S, et al. Self-organizing optic-cup morphogenesis in three-dimensional culture. Nature 2011;472:51-6.
[6] Marc RE, Jones BW, Watt CB, Strettoi E. Neural remodeling in retinal degeneration. Prog Retin Eye Res 2003;22:607-55.
[7] West EL, Pearson RA, MacLaren RE, Sowden JC, Ali RR. Cell transplantation strategies for retinal repair. Prog Brain Res 2009;175:3-21.
[8] Ming M, Li X, Fan X, Yang D, Li L, Chen S, et al. Retinal pigment epithelial cells secrete neurotrophic factors and synthesize dopamine: possible contribution to therapeutic effects of RPE cell transplantation in Parkinson's disease. J Transl Med 2009;7:53.
[9] Zayit-Soudry S, Moroz I, Loewenstein A. Retinal Pigment Epithelial Detachment. Survey of Ophthalmology 2007;52:227-43.
[10] Gouras P, Flood MT, Kjedbye H, Bilek MK, Eggers H. Transplantation of cultured human retinal epithelium to Bruch's membrane of the owl monkey's eye. Curr Eye Res 1985;4:253-65.
[11] Lane C, Boulton M, Marshall J. Transplantation of retinal pigment epithelium using a pars plana approach. Eye (Lond) 1989;3 (Pt 1):27-32.
[12] da Cruz L, Chen FK, Ahmado A, Greenwood J, Coffey P. RPE transplantation and its role in retinal disease. Prog Retin Eye Res 2007;26:598-635.
[13] Mooney DJ, Vandenburgh H. Cell delivery mechanisms for tissue repair. Cell Stem Cell 2008;2:205-13.
[14] Ballios BG, Cooke MJ, van der Kooy D, Shoichet MS. A hydrogel-based stem cell delivery system to treat retinal degenerative diseases. Biomaterials 2009;31:2555-64.
[15] Gullapalli VK, Sugino IK, Van Patten Y, Shah S, Zarbin MA. Impaired RPE survival on aged submacular human Bruch's membrane. Exp Eye Res 2005;80:235-48.
[16] Tezel TH, Del Priore LV, Kaplan HJ. Reengineering of aged Bruch's membrane to enhance retinal pigment epithelium repopulation. Investigative Ophthalmology & Visual Science 2004;45:3337-48.
[17] Del Priore LV, Geng L, Tezel TH, Kaplan HJ. Extracellular matrix ligands promote RPE attachment to inner Bruch's membrane. Current Eye Research 2002;25:79-89.
[18] Fitzpatrick SD, Mazumder MAJ, Lasowski F, Fitzpatrick LE, Sheardown H. PNIPAAm-Grafted-Collagen as an Injectable, In Situ Gelling, Bioactive Cell Delivery Scaffold. Biomacromolecules 2010;11:2261-7.

[19] Tezel TH, DelPriore LV. Reattachment to a substrate prevents apoptosis of human retinal pigment epithelium. Graefes Archive for Clinical and Experimental Ophthalmology 1997;235:41-7.
[20] Khademhosseini A, Eng G, Yeh J, Fukuda J, Blumling J, Langer R, et al. Micromolding of photocrosslinkable hyaluronic acid for cell encapsulation and entrapment. Journal of Biomedical Materials Research Part A 2006;79A:522-32.
[21] Kim J, Park Y, Tae G, Lee KB, Hwang CM, Hwang SJ, et al. Characterization of low-molecular-weight hyaluronic acid-based hydrogel and differential stem cell responses in the hydrogel microenvironments. Journal of Biomedical Materials Research Part A 2009;88A:967-75.
[22] Zeng F, Tong Z, Sato T. Molecular chain properties of poly(N-isopropyl acrylamide). Science in China Series B-Chemistry 1999;42:290-7.
[23] Holy CE, Cheng C, Davies JE, Shoichet MS. Optimizing the sterilization of PLGA scaffolds for use in tissue engineering. Biomaterials 2001;22:25-31.
[24] Guan J, Hong Y, Ma Z, Wagner WR. Protein-reactive, thermoresponsive copolymers with high flexibility and biodegradability. Biomacromolecules 2008;9:1283-92.
[25] Oliviero G, Bergese P, Canavese G, Chiari M, Colombi P, Cretich M, et al. A biofunctional polymeric coating for microcantilever molecular recognition. Anal Chim Acta 2008;630:161-7.
[26] Xu J, Tao L, Boyer C, Lowe AB, Davis TP. Facile Access to Polymeric Vesicular Nanostructures: Remarkable ω-End group Effects in Cholesterol and Pyrene Functional (Co)Polymers. Macromolecules 2011;44:299-312.
[27] Thomson HA, Treharne AJ, Backholer LS, Cuda F, Grossel MC, Lotery AJ. Biodegradable poly(alpha-hydroxy ester) blended microspheres as suitable carriers for retinal pigment epithelium cell transplantation. Journal of Biomedical Materials Research Part A 2010;95A:1233-43.
[28] Laurent TC, Fraser JRE. Hyaluronan. Faseb Journal 1992;6:2397-404.
[29] Gutowska A, Jeong B, Jasionowski M. Injectable gels for tissue engineering. Anatomical Record 2001;263:342-9.
[30] Limberg MB, McCaa C, Kissling GE, Kaufman HE. Topical Application of Hyaluronic-Acid and Chondroitin Sulfate in the Treatment of Dry Eyes. American Journal of Ophthalmology 1987;103:194-7.
[31] Aragona P, Papa V, Micali A, Santocono M, Milazzo G. Long term treatment with sodium hyaluronate-containing artificial tears reduces ocular surface damage in patients with dry eye. British Journal of Ophthalmology 2002;86:181-4.
[32] Nishida T, Nakamura M, Mishima H, Otori T. Hyaluronan Stimulates Corneal Epithelial Migration. Experimental Eye Research 1991;53:753-8.
[33] Goa KL, Benfield P. Hyaluronic Acid - A Review of its Pharmacology and Use as a Surgical Aid in Ophthalmology, and its Therapeutic Potential in Joint Disease and Wound-Healing. Drugs 1994;47:536-66.
[34] Van Beek M, Jones L, Sheardown H. Hyaluronic acid containing hydrogels for the reduction of protein adsorption. Biomaterials 2008;29:780-9.

[35] Uludag H, Norrie B, Kousinioris N, Gao TJ. Engineering temperature-sensitive poly(N-isopropylacrylamide) polymers as carriers of therapeutic proteins. Biotechnol Bioeng 2001;73:510-21.
[36] Ohya S, Sonoda H, Nakayama Y, Matsuda T. The potential of poly(N-isopropylacrylamide) (PNIPAM)-grafted hyaluronan and PNIPAM-grafted gelatin in the control of post-surgical tissue adhesions. Biomaterials 2005;26:655-9.
[37] Tan H, Ramirez CM, Miljkovic N, Li H, Rubin JP, Marra KG. Thermosensitive injectable hyaluronic acid hydrogel for adipose tissue engineering. Biomaterials 2009;30:6844-53.
[38] Smith E, Bai J, Oxenford C, Yang J, Somayaji R, Uludag H. Conjugation of arginine-glycine-aspartic acid peptides to thermoreversible N-isopropylacrylamide polymers Journal of Polymer Science Part A: Polymer Chemistry 2003;41:3989-4000.
[39] Smith E, Yang J, McGann L, Sebald W, Uludag H. RGD-grafted thermoreversible polymers to facilitate attachment of BMP-2 responsive C2C12 cells. Biomaterials 2005;26:7329-38.
[40] Li F, Griffith M, Li Z, Tanodekaew S, Sheardown H, Hakim M, et al. Recruitment of multiple cell lines by collagen-synthetic copolymer matrices in corneal regeneration. Biomaterials 2005;26:3093-104.
[41] Quan C-Y, Chen J-X, Wang H-Y, Li C, Chang C, Zhang X-Z, et al. Core-shell nanosized assemblies mediated by the alpha-beta cyclodextrin dimer with a tumor-triggered targeting property. ACS nano 2010;4:4211-9.
[42] Cui ZW, Lee BH, Vernon BL. New hydrolysis-dependent thermosensitive polymer for an injectable degradable system. Biomacromolecules 2007;8:1280-6.
[43] Edelman JL, Lutz D, Castro MR. Corticosteroids inhibit VEGF-induced vascular leakage in a rabbit model of blood-retinal and blood-aqueous barrier breakdown. Experimental Eye Research 2005;80:249-58.
[44] Jardeleza MS, Miller JW. Review of anti-VEGF therapy in proliferative diabetic retinopathy. SeminOphthalmol 2009;24:87-92.

CHAPTER 4: Development of Injectable, Resorbable Drug-Releasing Copolymer Scaffolds for Minimally Invasive Sustained Ophthalmic Therapeutics

Authors: Scott D Fitzpatrick*, Mohammad A. Jafar Mazumder*, Benjamin Muirhead and Heather Sheardown.
*These authors contributed equally.

Publication Information: Accepted (07/02/2012) for publication in ***Acta Biomaterialia***. Reference ID: AB-11-1798R1.

Objectives: Design of a degradable thermoresponsive PNIPAAm-based scaffold capable of delivering pharmaceuticals into the posterior segment of the eye via minimally invasive injection techniques followed by scaffold clearance upon exhaustion of the therapeutic payload.

Main Scientific Contributions:

- Developed synthetically flexible, resorbable, thermoresponsive NIPAAm-based copolymers ultimately designed to provide minimally invasive delivery of pharmaceuticals to the posterior segment of the eye.
- Introduced degradability into the NIPAAm-based scaffold through the incorporation of acryloyloxy dimethyl-γ-butyrolactone (DBA).
- Produced copolymers capable of facile bioconjugation through the incorporation of NAS.
- The slow degradation kinetics were designed to mimic non-degrading scaffolds and be favorable for sustained drug release, decreasing the frequency of intervention required to maintain therapeutic concentrations within the vitreous.
- Demonstrated good *in vivo* tolerance following subcutaneous injection into the left flank of C3H and SKH1-E mice

Author Contributions:

This paper was a collaborative work and first authorship was shared between Scott and Jafar. Contributions to this work were as follows. Scott was responsible for copolymer design (with Jafar), polymer synthesis, LCST characterization via UV spectrophotometry, DSC, water content, cell culture studies, copolymer morphology using SEM, degradation in simulated physiological conditions, drug release, determination of intact copolymer molecular weight, verification of composition via NMR and paper write-up. Jafar was responsible for copolymer design (with Scott), initial polymer synthesis, characterization of copolymer composition via FT-IR and NMR, determination of molecular weight, accelerated degradation studies, DSC and some help with the write-up. Ben performed the *in vivo* testing, including sub-cutaneous injections, histological staining and imaging and some help with the paper write-up.

Development of Injectable, Resorbable Drug-Releasing Copolymer Scaffolds for Minimally Invasive Sustained Ophthalmic Therapeutics

Scott D Fitzpatrick[a], M.A. Jafar Mazumder[b]*, Benjamin Muirhead[a], Heather Sheardown[a,b#]*

** These authors contributed equally*

[a]School of Biomedical Engineering and [b]Department of Chemical Engineering

McMaster University
1280 Main Street West
Hamilton ON, Canada
L8S 4L7

#To whom correspondence should be addressed sheardow@mcmaster.ca,
Phone: 1-(905) 525-9140 (24794)
Fax: 1-(905) 521-1350

ABSTRACT

Copolymers based on N-isopropylacrylamide (NIPAAm), acrylic acid N-hydroxysuccinimide (NAS) and varying concentrations of acrylic acid (AA) and acryloyloxy dimethyl-γ-butyrolactone (DBA) were synthesized to create thermoresponsive, resorbable copolymers for minimally invasive drug and/or cell delivery to the posterior segment of the eye to combat retinal degenerative diseases. Increasing DBA content was found to decrease both copolymer water content and lower critical solution temperature (LCST). The incorporation of NAS provided an amine-reactive site, which can be exploited for facile conjugation of bioactive agents. ^{1}H NMR analysis revealed the onset of hydrolysis-dependent opening of the DBA lactone ring, which successfully eradicated copolymer phase transition properties and should allow the gelled polymer to re-hydrate, enter systemic circulation and be cleared from the body without the production of degradation by-products. Hydrolytic ring opening occurs slowly, with over 85% copolymer mass remaining after 130 days of incubation in 37^{o}C PBS. These slow-degrading copolymers are hypothesized to be ideal delivery vehicles to provide minimally invasive, sustained, localized release of pharmaceuticals within the posterior segment of the eye to combat retinal degenerative diseases.

Keywords: Ophthalmic materials, N-isopropylacrylamide, resorbable, drug delivery, retina

4.1 INTRODUCTION

Efficient delivery of pharmaceuticals to the back of the eye is one of the most significant unmet needs of visual health care. Numerous pharmaceuticals show promise for the treatment of posterior segment ocular conditions, including vascular endothelial growth factor (VEGF) antagonists capable of minimizing ocular neovascularization, corticosteroids to combat retinal edema and other promising compounds such as antioxidants and anti-hypertensive drugs [1]. However, conventional drug delivery modalities are inefficient for delivering therapeutically relevant doses of pharmaceuticals to affected tissues in the back of the eye. Delivery of drugs to the posterior segment is made difficult by the isolated nature of the eye, which is separated from systemic circulation by blood ocular barriers, including the blood retinal barrier (BRB) and blood aqueous barrier (BAB) [2]. Furthermore, the eye is a segmented structure with numerous barriers to delivery and effective clearance mechanisms efficiently eliminating pharmaceuticals that successfully reach the posterior segment [2]. Topically applied drugs can enter the anterior chamber by crossing the cornea, or through the conjunctiva and sclera [2] or via the systemic circulation, which requires permeation of the BAB. Clearance from the anterior chamber occurs via aqueous turnover, or by re-absorption into systemic circulation [2]. The half-life of a typical drug within the anterior chamber is roughly one hour, however this varies depending on the properties of the pharmaceutical [3]. Drugs can be introduced into the posterior segment, which houses the light-sensitive retina, through systemic circulation by crossing the BRB, through non-corneal permeation into the uvea, or by direct injection into the vitreous [2], with the latter being the most

efficient method of delivering drugs to the posterior eye. Drug clearance from the posterior segment occurs through either the anterior or posterior route; the anterior route involves diffusion across the vitreous and elimination via uveal blood flow and aqueous turnover, whereas elimination via the posterior route requires permeation through the BRB [2].

As a result of the numerous barriers, the effective clearance routes and the segmented nature of the eye, delivery of drugs to the posterior segment is particularly challenging. Topically applied eye drops typically result in less than 5% uptake into the anterior chamber and negligible amounts entering the back of the eye [2]. Furthermore, only an estimated 1 – 2% of a systemically applied dose crosses the restrictive ocular barriers [4]. Therefore, high systemic doses are required to achieve therapeutic concentrations of drug within the posterior segment of the eye [5]. Additionally, many new pharmaceuticals are protein-based and are therefore not suitable for oral delivery as they are rapidly broken down and denatured in the digestive system [6]. Direct injection into the vitreous cavity is a highly efficient technique to introduce therapeutically relevant doses of drug into the vitreous body and retinal tissues while minimizing off-target exposure [5]. However, due to the previously mentioned clearance mechanisms, frequent injections (often every 4 – 6 weeks) are required to maintain therapeutically relevant concentrations [7]. While intravitreal injections are an acceptable means of delivery, in addition to being inconvenient for the physician and patient, frequent injections are associated with increased risk of complications such as endophthalmitis, cataract formation, vitreous haemorrhage, retinal detachment and patient discomfort [5, 8]. Therefore, approaches

that safely utilize the intravitreal route to provide sustained localized delivery of therapeutic concentrations of drug and do not require frequent perforation of the eye wall represent an exciting potential to treat numerous debilitating ocular conditions.

We hypothesized that poly(N-isopropylacrylamide) (PNIPAAm), a thermally sensitive intelligent polymer, which undergoes a rapid, reversible phase transition from liquid to gel when heated above a lower critical solution temperature (LCST) of approximately 32^{o}C, would serve as an ideal delivery scaffold for posterior segment ocular therapy [9]. PNIPAAm's sub-physiologic LCST allows a liquid polymer / drug solution to be injected directly into the vitreal cavity, wherein a thermally-induced phase transition drives the formation of a solid drug depot capable of providing sustained, localized therapy. However, as PNIPAAm is a non-degrading polymer, its introduction into the isolated vitreous would result in its persistence within the eye for the lifetime of the patient, unless surgically removed. Therefore, in attempt to design clinically relevant materials, there has been an emphasis in recent years on developing degradable or resorbable formulations of PNIPAAm that maintain thermal sensitivity but promote the eventual clearance from the body. Neradovic et al. designed NIPAAm-based copolymers containing hydrolysable lactate ester groups [10, 11]. Hydrolysis of hydrophobic side groups results in an increase in copolymer LCST, which, if raised above body temperature, allows the copolymer to undergo a reverse phase transition and revert to a hydrated liquid state, allowing uptake into the systemic circulation and clearance from the body via the kidneys. Ma et al. developed bioabsorbable NIPAAm copolymers possessing strong mechanical properties through copolymerization with methacrylate-

polylactide (MAPLA) and hydroxyethyl methacrylate (HEMA) [12]. Yoshida et al. reported the synthesis of NIPAAm-based copolymers crosslinked with degradable poly(amino acids) [13]. Cui et al. demonstrated that through incorporation of dimethyl-γ-butyrolactone acrylate (DBA), a hydrolysis dependent ring opening of the DBA lactone side group could result in an increase in the LCST above body temperature, allowing the polymer to re-solubilize and be cleared from the body without the formation of degradation by-products [14, 15]. Furthermore, it was found that copolymers of NIPAAm and DBA yielded slow degrading scaffolds with degradation periods of roughly one year required to increase copolymer LCST above body temperature [14]. Based on these results, we propose that copolymers consisting of NIPAAm and DBA would serve as ideal delivery scaffolds for posterior segment therapeutics capable of providing minimally invasive, long-term localized drug release that will increase the time between injections, and upon exhaustion of the drug, hydrolytic degradation will promote clearance from the eye without the need for surgical intervention. However, these polymers lack synthetic flexibility and have limited potential for bioconjugation and cellular adhesion, which may be useful for the subsequent incorporation of cell adhesion peptides for the development of minimally invasive cell carriers capable of delivering cell-based payloads to the subretinal tissues to combat retinal degeneration. Therefore, in this work, we have synthesized a series of synthetically flexible copolymers based on NIPAAm, DBA, acrylic acid (AA) and acrylic acid N-hydroxysuccinimide (NAS). AA was incorporated to balance the hydrophilic and hydrophobic content of the copolymers and control the LCST while the inclusion of NAS was designed to provide a site capable

of facile conjugation with biologically relevant molecules such as drugs or cell adhesive peptides. NAS functionality provides a site for copolymer / drug conjugation, which can theoretically be exploited to obtain controlled release through targeted destruction of a copolymer / drug linkage, although this was not utilized in this work. Copolymer synthesis as well as physical, chemical and biological characterization are described herein.

4.2 MATERIALS AND METHODS

DBA (95%), NAS (≥90%), benzoyl peroxide (BPO, 97%), dexamethasone (98%) and bovine serum albumin (66 kDa) were purchased from Sigma Aldrich (Oakville, ON, Canada), and used as received. N-isopropylacrylamide (NIPAAm) (97%) was purchased from Sigma Aldrich and was purified by recrystallization from a toluene/ hexane mixture. AA (99%) was purchased from Sigma-Aldrich, and was purified by passing the monomer through a packed column containing Sigma-Aldrich inhibitor remover to extract the polymerization inhibitor, 4-methoxyphenol (MEHQ). 1,4- dioxane, toluene, hexane, tetrahydrofuran (THF), dimethylsulfoxide (DMSO) and anhydrous ethyl ether were purchased from Caledon Laboratories (Caledon, ON) and used as received. Sodium hydroxide and hydrochloric acid solutions were purchased as concentrates from Anachemia Chemical (Rouses Point, NY, USA), and were prepared by diluting to 1.0 or 0.1 M with deionized water. Deionized water with a resistivity of 18.2 MΩ cm was prepared using a Milli-pore Barnstead water purification system (Graham, NC, USA). Phosphate buffered saline solution (PBS, pH 7.4) was purchased from McMaster University Health Science facilities and used as received. Human retinal pigment

epithelial (RPE) cells (CRL-2502) were purchased from ATCC (Manasass, VA, USA). Cell culture medium (DMEM-F12) was purchased from McMaster University Health Science facilities. Fetal bovine serum, 1x glutamate, penicillin-streptomycin, Trypan Blue and sodium bicarbonate were purchased from Gibco (Carlsbad, CA, USA). Cellulose dialysis membranes with molecular weight cutoff (MWCO) values from 1 to 12 kg/mol were purchased from Spectrum Laboratories Inc (Rancho Dominguez, CA, USA).

4.2.1 Synthesis of p(NIPAAm-NAS-AA-DBA) Copolymers:

Poly(NIPAAm-NAS-AA-DBA) (pNNAD) copolymers were synthesized via free radical polymerization. NIPAAm (3.84 g, 33.95 mmol), NAS (0.287 g, 1.69 mmol), AA (0.244 g, 3.39 mmol), DBA (0.626 g, 3.39 mmol) and BPO (0.103 g, 0.42 mmol, 1 mol % relative to monomer content) were dissolved in 45 mL 1, 4- dioxane to form a 10 wt % monomer solution (90: 4: 8: 8 molar feed ratio of NIPAAm: NAS: AA: DBA). Dry nitrogen was bubbled through the solution for 15 minutes. The flask was then sealed and subsequently heated to 70ºC for 24 hours in a temperature controlled oil bath with constant stirring to provide uniform mixing. Following the reaction, the polymer solution was cooled to room temperature and isolated by precipitation in anhydrous ethyl ether (1L). The resulting polymer, denoted pNNAD-8, wherein the number represents the copolymer DBA content, was dried overnight in a vacuum oven at 50^{o}C. The copolymer was further purified by repeated precipitation from THF into anhydrous ethyl ether. The purified copolymer was then dried to a constant weight in a vacuum oven at 50°C. pNNAD-8 yield was 90 % (4.5 g)

Copolymerization and purification of similar pNNAD copolymers possessing NIPAAm: NAS: AA: DBA molar feed ratios of 80: 4: 12: 4 (pNNAD-4) and 80: 4: 4: 12 (pNNAD-12) were prepared as described. Copolymer yield of pNNAD-4 and pNNAD-12 was 93 % (4.65 g) and 87 % (4.35 g) respectively. For *in vitro* and *in vivo* testing purposes, pNNAD copolymers were further purified by extensive dialysis in deionized water at 4°C (3.5 kg/mol MWCO), then freeze-dried, and stored frozen at -20°C.

4.2.2 Material Characterization:

The pNNAD copolymer structures were characterized using a Thermo Fisher Nicolet 6700 Fourier Transform Infrared (FT-IR) spectrometer. Copolymer compositions were determined by ^{1}H NMR using a Bruker AV 600 spectrometer with DMSO-*d*6 as a solvent. Copolymer molecular weights were determined by gel permeation chromatography (GPC) using a Waters system consisting of a 515 HPLC pump, 717 plus Autosampler, three Ultrahydrogel columns (0-3, 0-50, 2-300 kDa), and a 2414 refractive index detector. Copolymers were first hydrolyzed via accelerated degradation (as described in section 4.2.5) to remove phase transition properties, thereby allowing analysis via aqueous phase GPC. Samples were eluted with 20 mM PBS buffer, 100 mM $NaNO_3$ at pH 7.2 using a flow rate of 0.8 mL/min, and the system was calibrated with commercially available narrow dispersed molecular weight polyethylene glycol (PEG) standards (Waters, Mississauga, ON).

4.2.3 Lower Critical Solution Temperature Characterization:

Characterization of copolymer LCST was carried out using differential scanning calorimetry (DSC, TA Instruments 2910) and UV / vis spectrophotometry (Cary 300). For DSC analysis, the samples were dissolved in PBS to 20 % and were heated from 0 to 70^{o}C at a rate of 2^{o}C/min in hermetic pans. The thermal transition temperature was considered to be the temperature at which the maximum endothermal peak in the DSC curve was observed. Copolymer cloud points were observed as a change in transmittance using UV spectrophotometry to verify phase transition temperatures obtained via DSC. Copolymers were dissolved in PBS (10 % w/v) and kept at 4^{o}C for 24 hours. The copolymer solutions were then placed in 4 mL UV cuvettes and de-gassed briefly via sonication. The samples were heated from 5 to 45^{o}C with a heating rate of 1^{o}C/min and transmittance was assessed every thirty seconds.

Glass transition temperatures (Tgs) of intact and degraded copolymers (~8 mg) were measured by DSC over a temperature range of -10 to 200°C with a heating rate of 10°C/min.

4.2.4 Water Content:

The water content of the pNNAD copolymers was assessed gravimetrically. Samples were dissolved in deionized water (15 % w/v) and placed in pre-weighed polystyrene dishes. The covered dishes were then placed in a 37^{o}C oven to induce hydrogel scaffold formation. After 6 hours, the supernatant surrounding the hydrogel pellets was aspirated and the gels were carefully blotted dry with tissue paper to remove any surface water. The samples were placed back in their respective dishes and weighed

to obtain the wet mass. The samples were then dried to constant weight in a 65°C oven. Water content was assessed using the following equation:

$$Water\ Content = \frac{(m_w - m_d)}{m_d} * 100\% \qquad \text{(Equation 1)}$$

where m_w is the wet mass of the hydrogel and m_d is the dry mass.

4.2.5 Degradation by Accelerated Hydrolysis:

Accelerated hydrolysis, both partial and complete, of the pNNAD copolymers was performed following ISO 10993 [16]. Briefly, solutions of each polymer were prepared in deionized water (20% w/v) in a 20 ml glass vial. The pH was adjusted to 10.5 (with either 0.1 or 1 M NaOH) and the solution placed in an oven at 70°C. The pH of the polymer solution was adjusted to 10.5 daily. Complete degradation of the copolymers was achieved in 21 days, at which point the pH of the solution remained constant. Fully degraded samples were maintained at pH 10.5 for another three days (24 in total) and collected by dialysis (3.5 kg/mol MWCO) and freeze-dried. During the degradation process, aliquots were collected periodically, dialyzed and freeze-dried to determine the composition of the partially degraded copolymers. Partially degraded pNNAD samples reported in this manuscript were collected from copolymers subjected to 10 days of accelerated degradation conditions.

4.2.6 Copolymer Degradation in Heated PBS:

Copolymers were dissolved in PBS (15 % w/v) in pre-weighed 2 mL plastic eppendorf tubes. The samples were dissolved at 4°C for 24 hours, then placed in a 37°C oven and allowed to gel. After 5, 20, 40, 65 and 130 days of incubation at 37°C, the

supernatant was aspirated and samples were carefully rinsed with pre-warmed Milli-Q water to remove any soluble pNNAD and PBS residue. The rinsed samples were then carefully blotted dry with a tissue paper to remove residual surface water and the resulting polymer wet mass m_{wf} was obtained. The samples were then dried to a constant weight in a 65°C oven, to obtain the final polymer dry mass, m_{df}. Polymer degradation was determined using the following equation:

$$Mass\ Remaining = \frac{(m_{df})}{m_{di}} * 100\% \qquad \text{(Equation 2)}$$

where m_{di} denotes the mass of the initial dry sample.

A Phillips 515 scanning electron microscope (SEM) was used to visualize physical changes in polymer morphology as a function of degradation. Dried polymer samples were collected for each time point of the heated PBS degradation assay and a 10 nm platinum coating was applied to the surface of the degraded copolymer samples to allow surface visualization. Images were captured using Mektech URSA 100 Rev. 1.30 imaging software.

4.2.7 Dexamethasone Release:

Dexamethasone was dissolved in PBS to form a 0.1 mg/ml solution. The pNNAD copolymers were then dissolved to concentrations of 20% w/v (100 mg in 0.5 mL) in the PBS / dexamethasone solution. The samples were cooled to 4°C until the copolymers had fully dissolved. The drug-infused copolymer solutions were then placed in a 37°C oven for two hours to drive scaffold formation and drug entrapment at which point the supernatant was collected and the copolymers were rinsed once with a pre-warmed PBS

solution. The PBS wash was then removed and replaced with 1 mL of fresh, pre-warmed PBS. This was taken as time zero for drug release. Aliquots (100 μl) were removed at regular intervals and replaced with an equivalent volume of fresh, pre-warmed PBS. Samples were analyzed using a Waters high performance liquid chromatography (HPLC) system with a 2707 autosampler, 2489 UV spectrophotometer, 1525 binary HPLC pump, Atlantis dC18 5 μm, 4.6 x 100 mm column and Breeze 2 software (Build 2154). The mobile phase, a 40 % v/v HPLC-grade acetonitrile in water solution, was passed through a 0.45 μm filter and de-gassed via sonication prior to use. A 1.0 ml/min isocratic flow-rate was employed with 10 μl sample injection volumes and a 254 nm detection wavelength. Sample concentrations were assessed relative to a standard calibration curve of dexamethasone prepared in mobile phase.

4.2.8 Cell Culture:

Human RPE cells (CRL-2502) were cultured in a temperature-controlled CO_2 incubator (37^{o}C, 5 % CO_2, 95 % air, 100 % humidity). DMEM-F12 cell culture medium was supplemented with fetal bovine serum (FBS) (6.25 % final concentration), 1 x glutamate (1% final concentration), penicillin-streptomycin (1 % final concentration), and sodium bicarbonate (0.8 % final concentration). Prior to testing, samples were extensively dialyzed in deionized water (3.5 kg/mol MWCO), freeze-dried and then pre-treated with a solution of PBS and penicillin-streptomycin (3:1 v/v). RPE cells were seeded with fresh, supplemented DMEM-F12 culture medium in a 48 well tissue culture polystyrene (TCPS) dish at a density of 50,000 cells per well. After a 2-hour incubation period, which allowed cells to adhere to the bottom of the TCPS dish, the cell supernatant

was removed and replaced with 1 mL of fresh medium containing 10 mg of dissolved copolymer. Test conditions included partially degraded, fully hydrolyzed and intact pNNAD-4, pNNAD-8 and pNNAD-12 copolymers. Fresh culture medium containing no polymer was used as a control. Samples were then returned to the incubator and viability was assessed after 96 hours using a 0.4% Trypan Blue exclusion assay.

4.2.9 Subcutaneous Injections in SKH1-E and C3H Mice:

Following extensive dialysis and freeze-drying, samples were sterilized with ethylene oxide (EO) gas at the McMaster University histopathology laboratory for subsequent *in vivo* testing. Samples were exposed to a 100 % EO atmosphere at 57^{o}C for 2 hours followed by exposure to sterile air for 15 hours to evaporate residual EO. Copolymers pNNAD-4, pNNAD-8 and pNNAD-12 were dissolved in Fischer Brand medical grade saline to concentrations of 15 % w/v in 10 mL aliquots. Polymer samples, syringes and the injection site were pre-cooled with ice to prevent premature polymer gelation during injection. Hairless SKH1-E (strain code 447) or C3H (Charles River, strain code 025) mice were anaesthetized with isoflurane gas and 100 μl polymer suspensions were injected subcutaneously above the left flank of the animal. C3H mice were shaved prior to treatment and the injection site was marked with an indelible pen. C3H mice were sacrificed at day 1, 3, 7 (n = 3) and SKH1-E mice were sacrificed at day 40 (n = 2). The tissue at the injection site was excised, fixed in a 4 % formalin solution for 24 – 72 hours and then embedded within paraffin wax. The fixed tissues were then sliced into 4 mm sections using a Leica RM2255 microtome and stained with Haemotoxilin and Eosin (H&E) or Masson's Trichrome following standard histological

protocols. Images of the stained and processed tissue from the injection site were captured using an Olympus BX51 optical microscope with a QImaging Retiga 2000R camera and Image-Pro Plus (version 7.0) imaging software. Full liver and spleen samples were excised at day 40 and weighed. All animal testing was performed in accordance with the McMaster University Animal Research Ethics Board.

4.2.10 Statistical Analysis:

A one-factor analysis of variance (ANOVA) was used to analyze copolymer water content and RPE viability using an $\alpha = 0.05$. Statistical analysis was performed using PASW Statistics 18 (SPSS, Inc., Il). All error bars represent standard deviation.

4.3 RESULTS AND DISCUSSIONS

4.3.1 Copolymer Characterization:

Copolymers with varying compositions of NIPAAm, NAS, AA and DBA were synthesized via free radical polymerization. The final composition of the various pNNAD copolymers was determined using ^{1}H NMR and the values, which were found to be similar to the co-monomer feed ratios, are reported in Table 4-1.

4.3.2 Physiological and Accelerated pNNAD Degradation Mechanisms:

FT-IR was used to confirm the final structure of the various pNNAD copolymers as well as to examine the changes in copolymer structure as a function of accelerated degradation, Figure 4-1. The pNNAD-4 spectrum in Figure 4-1a shows characteristic NIPAAm peaks of C=O and N-H stretching of the amide groups around 1658 and 1540 cm^{-1} respectively. Additionally, stretching vibration of the N-H amine group appears at

3309 cm^{-1}, and the isopropyl group is present at 1460, 1380, and 1360 cm^{-1} (Figure 4-1a ↲). Characteristic NAS succinimide peaks were observed at 1812, 1781 and 1735 cm^{-1} (Figure 4-1a *). The carbonyl group from AA was observed at 1710 cm-^{1} (Figure 4-1a ↓). The two characteristic DBA peaks, specifically the carbonyl peak in the ring structure and the carbonyl peak connected to the polymer backbone, overlap with the succinimide peaks at 1781 and 1735 cm-^{1} respectively.

During the accelerated degradation process, the pH was adjusted to 10.5 daily with 1M or 0.1M NaOH. Decreases in the pH of roughly 1 unit were observed in the first few days of the process, and were followed by smaller decreases over the next two weeks until equilibrium was achieved after 21 days, indicating complete copolymer degradation had been attained. These degraded samples were maintained at pH 10.5 for 3 more days prior to purification and analysis. Following 10 days of exposure to harsh degradation conditions, partial degradation of the pNNAD copolymers was observed to occur through opening of the DBA lactone ring structure, which rendered a decrease in the DBA ring carbonyl peak and an increase in the carboxylic acid C=O peak around 1652 cm^{-1} (Figure 4-1b, pNNAD-4 shown). Complete degradation of the pNNAD copolymers resulted in the disappearance of the DBA carbonyl peak and the production of a broad carboxylic acid C=O peak around 1652 cm^{-1} (Figure 4-1c), confirming the proposed sequential degradation mechanism.

^{1}H NMR was used to verify the sequential degradation mechanism of the pNNAD copolymers, Figure 4-2. In the pNNAD-4 spectra, Figure 4-2a, two characteristic peaks (CH and CH_2) within the DBA ring can be seen between 5.2 - 5.7 ppm and 3.8 - 4.1 ppm

respectively. Partial degradation following 10 days of accelerated degradation in harsh basic conditions results in a decrease in the magnitude of these characteristic DBA ring peaks and the CH peak shifts to 4.3 – 4.7 ppm, Figure 4-2b. Furthermore, the new CH_2 peak from the former DBA ring appears at 3.0 – 3.5 ppm, confirming successful ring opening while the ester linkage remains intact with the polymer backbone. Complete degradation is confirmed in Figure 4-2c with the disappearance of these two DBA ring proton peaks (CH and CH_2), while the resulting spectra is consistent with a poly(NIPAAm-*co*-AA) signature. As expected, both pNNAD-8 and pNNAD-12 show similar degradation trends (data not shown). The proposed copolymer degradation mechanisms of pNNAD under both physiological and harsh basic conditions are illustrated in Scheme 1.

It was proposed that under physiologic conditions, hydrolytic ring opening of the DBA lactone ring structure would significantly alter copolymer phase transition properties as the hydrophobic lactone ring opens to expose hydrophilic carboxylic acid and hydroxyl groups. The resulting increase in copolymer LCST would initiate a reverse phase transition process, inducing the solid cell or drug scaffold to re-hydrate to a liquid state, allowing the copolymer to be cleared from the eye through the available ocular elimination routes. To prolong the duration of drug release within the hard-to-access vitreous, it is desirable to design copolymers with slow degradation kinetics wherein degradation should occur following exhaustion of the majority of drug reservoir to prevent excessive degradation-induced drug dumping. Slow degradation should decrease the secondary burst associated with scaffold degradation, therefore limiting the amount of

free drug present within the vitreous and minimizing associated complications such as cataract formation and increases in intraocular pressure (IOP), which can lead to secondary open-angle glaucoma [17, 18]. Furthermore, it is desirable to design a copolymer system that does not break down into small molecular weight by-products as these degradation products can be cytotoxic and can induce an inflammatory response [15]. Under physiologic conditions, pNNAD should not produce degradation by-products as resorption should be achieved through a simple hydrolysis-dependent alteration in copolymer critical gelling temperature. However, under harsh basic conditions, such as that of the accelerated degradation process, the copolymer degradation scheme is more rigorous. Harsh degradation conditions result in the hydrolysis of the DBA ester group attached to the copolymer backbone leading to the conversion of the DBA co-monomer to AA. Both physiologic and harsh degradation conditions liberate the hydroxysuccinimide group from NAS, similarly producing AA. However, bioconjugation of the pNNAD copolymers with cell adhesive peptides would produce stable amide bonds that are not susceptible to degradation. In the absence of bioconjugation, capping NAS functional groups would eliminate the hydrolytic release of hydroxysuccinimide *in vivo*. The impact of NAS capping on polymer behavior such as degradation kinetics, LCST, drug release kinetics and final copolymer MW will ultimately need to match the design constraints of the system to preserve the desired copolymer properties.

4.3.3 Water Content:

The water content of the pNNAD copolymers was assessed gravimetrically and, consistent with thermal transition properties, was found to be strongly dependent on AA

and DBA content. As copolymer DBA / AA ratio increased, the hydrophobic nature of the copolymer increased, thereby decreasing the water content and lowering the LCST.

Glass transition temperatures (Table 4-1) of intact and degraded pNNAD copolymers were assessed by DSC and found to be dependent on both AA and DBA content. Intact copolymers with a higher AA / DBA ratio were found to have higher Tg due to increased hydrophilicity. However, after degradation, all copolymers were reduced to similar NIPAAm and AA content as DBA and NAS groups were hydrolyzed to form AA. As a result, Tg for all copolymers following degradation was approximately the same providing further evidence for copolymer composition.

4.3.4 pNNAD Copolymer Phase Transition Properties:

The copolymer phase transition properties were characterized by both DSC and UV spectrophotometry. LCST values obtained via DSC are reported in Table 4-1 and the transmittance curves as a function of increasing temperature are shown in Figure 4-4. pNNAD LCST values were strongly influenced by DBA and AA content; higher ratios of DBA to AA produced more hydrophobic copolymers resulting in lower phase transition temperatures. All copolymers were found to have sub-physiological phase transition temperatures, which is a requirement for *in situ* forming hydrogel scaffolds that utilize body temperature as the stimuli to induce phase transition. The sudden decrease in transmittance as the copolymers are heated above their LCST provides evidence that the copolymers undergo a rapid sol-gel transition, an observation that was verified during *in vivo* testing in which robust polymer gels were formed almost immediately following subcutaneous injection. Rapid gelling kinetics are important for *in situ* forming hydrogels

in order to efficiently entrap the infused therapeutic. Unlike pre-formed drug releasing scaffolds, which are loaded with drug *ex vivo*, the pNNAD copolymers are simply mixed with a drug solution and must gel quickly following injection to form a solid drug depot *in situ* while preventing mass efflux of free drug into the surrounding environment. *In situ* forming hydrogels that gel too slowly do not efficiently entrap the infused drug and are associated with a large initial burst, whereas if gelation occurs too rapidly, it may clog the injection syringe. From our studies, we observed rapid gelation upon injection of 15 - 20 w/v % pNNAD copolymers into pre-heated aqueous solutions and did not suffer syringe clogging when using needles of gauge 18 – 27 with pre-cooled samples.

The sudden decrease in transmittance, as the copolymers transition from a transparent liquid to an opaque white gel, raises one of the main concerns for the pNNAD copolymers; they are not clear. However, this is not anticipated to be an issue as the pNNAD drug depot will reside on the floor of the vitreous, well outside the visual axis, much like similar non-transparent free-floating intravitreal drug delivery scaffolds, Ozurdex (Allergan) and ILUVIEN® (Alimera Sciences).

Following partial and complete degradation via accelerated hydrolysis, there was no observable LCST between 0 - 100^{o}C as assessed by DSC (Figure 4-5b and c respectively). This significant finding demonstrates that the first stages of the sequential pNNAD degradation, which were confirmed by FT-IR and ^{1}H NMR to occur through hydrolytic opening of the DBA ring, are sufficient to eliminate the thermoresponsive nature of the copolymer between 0 - 100^{o}C. Therefore, as the DBA ring opens, the gelled copolymer will revert to a liquid state, allowing its clearance from the eye, uptake into

systemic circulation and ultimate removal from the body via the kidneys, without the liberation of degradation by-products.

4.3.5 Copolymer Molecular Weight:

To determine copolymer molecular weight, organic phase GPC was initially selected because temperature-induced phase transition properties in aqueous conditions prevented the use of aqueous phase GPC. However, organic phase GPC with both THF and DMF solvents yielded highly irregular and inconsistent molecular weight measurements with values exceeding one million Da. Therefore, the copolymers were subjected to accelerated hydrolysis to remove phase transition properties, thereby allowing MW assessment via aqueous phase GPC. Copolymer molecular weights are presented in Table 4-1. As MW measurements were obtained using hydrolyzed pNNAD copolymers, the resulting MW values are slightly lower than fully intact copolymers. However, initial copolymer MW values were quantified using this data by calculating the MW of the hydrolyzed copolymer side groups that were cleaved from the copolymer backbone, Table 4-1. From these calculations, it can be seen that all pNNAD copolymers possess an initial MW below the molecular weight cutoff of the renal system, which has been reported to have an upper limit of approximately 50 kDa [19]. Therefore, intact pNNAD copolymers possessing sufficient quantities of hydrolytically opened lactone ring structures to increase copolymer LCST above body temperature should be readily filtered from the body via the kidneys without the formation of degradation by-products.

4.3.6 Copolymer Degradation Studies:

Copolymer degradation kinetics were studied by dissolving pNNAD copolymers in PBS (15 % w/v). The samples were maintained in a 37^{o}C incubator for 5, 20, 40, 65 and 130 days, at which point, the supernatant was aspirated to remove PBS as well as any pNNAD copolymer that had transitioned back into a soluble state. The samples were then carefully rinsed with pre-heated deionized water to remove residual PBS and hydrolyzed pNNAD. The copolymers were dried to constant weight and the mass remaining was calculated using equation 2, Figure 4-6.

From Figure 4-6, it is apparent that hydrolytic ring opening of the DBA side chain occurs slowly *in vitro* as all scaffolds maintained over 85% of their initial mass following 130 days in heated PBS. As discussed, this slow degradation is highly favorable for ocular drug delivery as it may emulate non-degrading scaffolds and be conducive to providing long-term sustained release of low-levels of drug, minimizing the frequency of intravitreal injections. It is expected that degradation will occur more rapidly in an *in vivo* environment in which harsher conditions can expedite the hydrolytic process. Therefore, future studies will examine copolymer degradation kinetics within the vitreous.

SEM images of the dried pNNAD copolymers were collected at each time point to assess changes in morphology as a function of degradation, Figure 4-7. Though oven drying can introduce artefacts into polymer morphology, these effects would be consistent for all samples and would likely manifest as surface fractures as the polymers dry. Such

fractures as can be observed in the pNNAD-4 day 20 sample should therefore not be interpreted as evidence of degradation.

The SEM micrographs reveal subtle changes in copolymer morphology as a function of time in the heated PBS conditions. Morphological changes in the copolymer surface are most apparent in pNNAD-4, which has the lowest DBA content and highest water content. There is evidence of increased pitting and surface erosion in pNNAD-4, and to some extent pNNAD-8, at day 130. As expected, surface degradation in the pNNAD-12 copolymer, which has the highest DBA content and lowest water content, appears to be less evident than the other two materials. The pNNAD-8 and pNNAD-12 day 40 images were taken of fractures that occurred as a result of sample handling that exposed internal copolymer morphology. The internal copolymer structure does not reveal the same pitting morphology observed on the surface, possibly indicating that erosion occurs primarily on the surface, where there is the greatest amount of water present to expedite the process of lactone ring hydrolysis.

However, none of the copolymers undergo dramatic morphological changes over the course of 130 days in heated PBS, which is consistent with the relatively minor mass loss observed throughout the course of the experiment. As the copolymers continue to hydrolyze, their surfaces will erode and become more porous, increasing the surface area through which drugs can diffuse, which in turn increases the release rate. For long-term sustained release applications, slow degrading materials that do not undergo rapid changes in morphology are desirable to maintain relatively controlled release rates for extended periods of time. Therefore, the minimal surface erosion and slow degradation

kinetics exhibited by the pNNAD copolymers, specifically pNNAD-12, appear to support the hypothesis that these materials would provide desirable vehicles for long-term release of pharmaceuticals in ophthalmic therapeutics.

4.3.7 Dexamethasone Release:

Corticosteroids are thought to combat macular edema through anti-inflammatory and anti-angiogenic properties, the latter of which occurs through suppression of vascular endothelial growth factor (VEGF) expression, which has been shown to play a key role in ocular neovascularization [20]. Corticosteroids are also capable of stabilization of the BRB [20]. As mentioned, free steroid suspensions within the eye can cause a number of complications, such as cataract and glaucoma formation. However, entrapment within a scaffold that slowly releases low levels of drug for sustained periods of time can significantly decrease the amount of free drug present within the vitreous and greatly decrease the associated risk [21]. To examine release kinetics from the pNNAD scaffolds, dexamethasone was selected as the model drug since it is one of the most attractive corticosteroids for the treatment of posterior complications, specifically macular edema [22]. Triamcinolone acetonide (TA) is the most commonly used intravitreal corticosteroid, however, its use is associated with a relatively high rate of cataract formation and glaucoma [22]. Dexamethasone is 5 times more potent than TA and studies suggest it may be associated with a decreased risk of cataract, glaucoma and retinal toxicity [22]. Relative to TA, dexamethasone displayed lower toxicity towards lens epithelial cells [23], trabecular meshwork cells [22, 24] and retinal neurosensory and RPE cells [25, 26] *in vitro*. However, dexamethasone (392.5 Da) suffers from a relatively

short half-life within the eye (3.5 hour), whereas TA (18 days) has been shown to persist for 3 months [27-29]. Therefore, releasing dexamethasone from a slow-releasing pNNAD scaffold (similar to Ozurdex [30]) should help create persistent levels of the potent corticosteroid within the eye, extending its duration of action, minimizing the number of repeat injections required to maintain therapeutic concentrations and lower the incidence of steroid-related complications.

The copolymer drug loading efficiency was calculated by determining the dexamethasone concentration in the collected supernatant from the initial gel formation and from the PBS-rinse prior to commencement of the assay. All three scaffolds demonstrated excellent loading capabilities, with pNNAD-4, pNNAD-8, and pNNAD-12 gels successfully entrapping 93.2, 94.4, and 96.0% of the initially infused dexamethasone. As expected, the pNNAD dexamethasone release curve reveals a small initial burst, which could potentially be helpful in treating the initial hostile environment within the compromised eye by decreasing the elevated VEGF expression and stabilization of the BRB. However, as with all steroids, a large burst would not be desirable and therefore the burst must be controlled. The subsequent stabilization in the release curve that is observed around day 3 to 4, appears to produce the desired slow-releasing scaffold capable of maintaining low levels of drug that are sufficient to sustain a therapeutic concentration within the vitreous for extended periods of time. From day 5 to 24, the release rates were calculated to be 0.18, 0.09, and 0.16 μg/day for pNNAD-4, pNNAD-8, and pNNAD-12 respectively. These release rates are similar to studies performed by Alimera Sciences (Appharetta, GA, USA) examining the release of 0.2 μg/day

fluocinolone acetonide (FA) from the non-degradable intravitreal insert, ILUVIEN® [31]. They found that the low levels of corticosteroid were sufficient to produce a reduction in edema and improvements in visual acuity [31]. Furthermore, it was reported that a similar scaffold releasing slightly higher doses of FA (0.5 μg/day) were associated with mild increases in IOP, whereas the low level insert did not produce any elevation in pressure [31]. Therefore, it is likely that the low levels of corticosteroid released from the pNNAD scaffold following the initial burst are favorable for posterior segment delivery provided that the concentration within the vitreous is sufficient to produce a lasting therapeutic effect while minimizing complications associated with free drug exposure. We envision that the low levels released from the slow-degrading pNNAD copolymers will offer an improvement in release time over currently available degradable systems, and will approach, but likely not match, the sustained release of non-degrading ILUVIEN®. However, such information will need to be elucidated through long-term drug release assays, future animal studies and optimization of polymer / drug conditions. Further *in vitro* investigation will examine the release of different therapeutics, such as anti-VEGF agents and other protein-based drugs that have demonstrated promise in the treatment of ocular diseases. Although less than 20% of the drug had been released after 24 days, this release study had to be terminated prematurely due to improper sample capping, leading to loss of liquid. However, the samples remained intact and long-term release studies are ongoing.

4.3.8 In Vitro Cell Viability:

In vitro testing of the pNNAD copolymers revealed excellent compatibility with RPE cells, as shown in Figure 4-9. Copolymer scaffolds were dissolved in the supernatant of pre-adhered cells and incubated for 96 hours. Viability remained above 90% for all samples tested. Additionally, RPE cells were found to be compatible in culture with the copolymers as they transition through the various stages of hydrolytic degradation from partial to complete hydrolysis (partially degraded pNNAD data not shown). While these preliminary studies were designed to establish a safety profile for subsequent animal testing and demonstrate the compatibility of pNNAD scaffolds with RPE cells in culture, future studies will examine the potential use of cell-adhesive pNNAD formulations that possess the ability to act as temporary cell scaffolds. Subsequent studies have revealed that bioconjugation of pNNAD copolymers with cell adhesive RGDS peptides can easily be achieved through coupling the peptide with the amine-reactive NAS co-monomer (data not shown). Future studies will examine the potential of RGDS-conjugated pNNAD scaffolds to support and maintain a healthy, functional population of RPE cells *in vitro* and within the subretinal space *in vivo*.

4.3.9 Subcutaneous Implantation into Mice:

In accordance with the McMaster University Animal Research Ethics Board, prior to testing pNNAD copolymers in an ophthalmic application, demonstration of initial copolymer safety was required. Therefore, preliminary *in vivo* testing of pNNAD-4, pNNAD-8 and pNNAD-12 was performed via subcutaneous injection above the left flank of either C3H (day 1, 3 and 7) or SKH1-E (day 40) mice. All samples were successfully

injected using a 25-gauge needle and formed a mechanically robust gel beneath the skin. The gel appeared to spread out into an apparent thin film underneath the skin quickly after injection presumably as a result of being compressed between the dermis and underlying adipose tissue. For subretinal cell transplantation, scaffold spreading is favourable as it allows single injections to treat a relatively large area [32]. However, polymer spreading would not be suitable for drug delivery purposes, as a thin film with a large surface area would quickly release infused drug. In the absence of compressive forces however, such as in the drug release and degradation assays, polymer thinning was not observed and the gels maintained their shape throughout the duration of the experiments. The absence of compressive forces within the intravitreal space would therefore be expected to allow injected copolymers to maintain their gelled morphology; this will be examined in future studies.

While material spreading is desirable for subretinal cell therapy, it made identification of the injected copolymer and subsequent histological analysis of the surrounding tissues difficult. Therefore tissue sections were obtained by excising and analyzing tissue from the injection site, which had previously been marked with indelible marker. Histological analysis of tissue at the injection site revealed evidence of a mild inflammatory response to subcutaneous injections characterized primarily by the presence of lymphocytes. Control samples, which received injections of equivalent volumes of saline did not exhibit such inflammation. However, inflammation in the pNNAD-receiving mice appeared to subside by day 7 and was absent in the 40-day post-injection samples. Furthermore, there was very little macrophage accumulation or fibroblastic

proliferation, indicating an acceptable, non-chronic immune response, which was consistent between all three pNNAD materials tested. DBA content did not exert an apparent effect on tissue response to pNNAD copolymers.

While day 1, 3, and 7 samples were collected from the same litter of C3H mice, the 40-day samples were from a nude SKH1-E mouse. The hairless SKH1-E mice were initially used to allow visualization of the skin during injection and to track copolymer location following implantation. However, in subsequent studies, C3H mice were simply shaved to remove hair from the injection site allowing easy visualisation of injection and copolymer tracking, thus eliminating the requirement for a hairless mouse. The distinction in mice type is important when viewing the tissue sections as they yield substantially different dermal histology. SKH1-E mice have large, vacuolated spaces present from aborted hair follicles, which can be misconstrued as pockets of foreign material [33]. Therefore, SKH1-E and C3H histology images have been separated by a space in Figure 4-10 and Figure 4-11. There was no observable fibrous scar reaction, and trichrome staining confirms collagen present appears to be type 1, characterized by regular, thick, wavy bundles. These results show a good *in vivo* tolerance to pNNAD copolymers, and suggest an absence of toxicity or chronic immune activation.

Although analysis of the injection site revealed acceptable histological results, the inability to directly locate non-staining pNNAD copolymers warranted an investigation of distal organs responsible for sequestering and clearing foreign materials. Whole spleen and liver were therefore excised from mice at day 40 and, after visual examination, were weighed. Neither spleen nor liver demonstrated signs of atrophy or inflammation and

masses were consistent between the mice, Table 4-2. Future studies will employ fluorophore-conjugated pNNAD copolymers to allow accurate copolymer identification

4.4 CONCLUSIONS

Several thermoresponsive copolymers based on NIPAAm, NAS and varying compositions of AA and DBA were synthesized for application in posterior segment ophthalmic cell and drug therapeutics. These copolymers were designed to address the serious need to improve upon current ophthalmic drug delivery approaches. All pNNAD copolymers possess sub-physiological phase transition temperatures, allowing minimally invasive delivery of drug-infused polymer suspensions into the back of the eye, followed by a temperature-induced scaffold formation, entrapping the pharmaceutical and creating a solid intravitreal drug depot. The slow degrading pNNAD copolymers were designed to provide a localized, sustained-release scaffold capable of maintaining therapeutically relevant doses of pharmaceutical within the vitreous, thereby minimizing the frequency of intervention and decreasing the associated risks. Degradation of the pNNAD copolymers was observed to occur through a simple hydrolytic opening of the DBA ring, resulting in an LCST increase that initiates scaffold re-hydration and clearance from the body without the need for secondary surgical intervention or the production of low molecular weight degradation products. The copolymers did not appear to elicit an observable adverse response following subcutaneous injection into SKH1-E and C3H mice. Therefore, the preliminary safety profile and promising results warrant further investigation of these copolymers in an ocular environment. Future studies will examine *in vitro* drug release profiles using a number of different pharmaceuticals and protein-based therapeutics. In

addition, we will look at histological analysis of ocular tissues and intravitreal distribution of drug following injection of pNNAD copolymers into the vitreous chamber.

4.5 TABLES

Table 4-1: Polymer feed ratios, final copolymer composition, degraded copolymer molecular weight determined by GPC, intact copolymer molecular weight calculated from degraded samples and phase transition temperatures determined using DSC.

Polymer (feed ratio) NIPAAM-NAS-AA-DBA	Composition[a]	MW (M_n) (kg/mol)[b] (degraded)	MW (M_n) (kg/mol)[c] (intact)	LCST[d] (intact)	LCST[d] (degraded)	Tg (°C) (intact)	Tg (°C) (degraded)
pNNAD-4 (80:4:12:4)	76.0: 4.4: 15.1: 4.5	26563	28166	21.3	NA	94.3	98.6
pNNAD-8 (80:4:8: 8)	74.8: 4.1: 12.9: 8.2	28494	32146	17.0	NA	90.8	97.8
pNNAD-12 (80:4:4:12)	75.2: 3.8: 8.6: 12.4	30776	36034	13.1	NA	87.6	100.9

Copolymer composition in mol % determined by ^1H NMR a), M_n obtained using GPC b), M_n calculated from GPC c), and LCST obtained from DSC d).

Table 4-2: Mass of whole spleen and liver excised from SKH1-E mice after 40 days of sub-cutaneous incubation with pNNAD copolymers.

Sample	Liver		Spleen	
	Mass (g)	Body Weight (%)	Mass (g)	Body Weight (%)
Control	1.48	5.3	59	0.22
pNNAD-4	1.43	5.5	36	0.14
	1.33	5.1	61	0.23
pNNAD-8	1.55	5.3	51	0.17
	1.51	5.1	55	0.19
pNNAD-12	1.49	5.3	29	0.10
	1.41	5.1	39	0.15

4.6 DEGRADATION MECHANISM

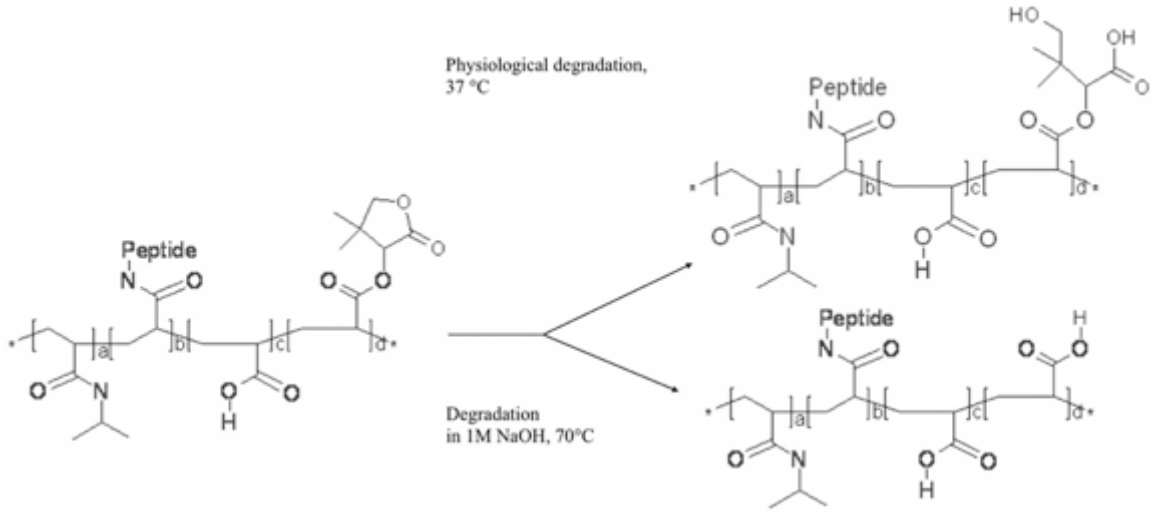

Scheme 4-1: The sequential degradation mechanism of pNNAD copolymers in physiological conditions (top) and under harsh basic conditions employed in the accelerated degradation experiment (bottom). In this schematic, the pNNAD copolymer has been functionalized with a peptide through NAS reactivity. In the absence of conjugation, NAS hydrolyzes to produce AA.

4.7 FIGURES

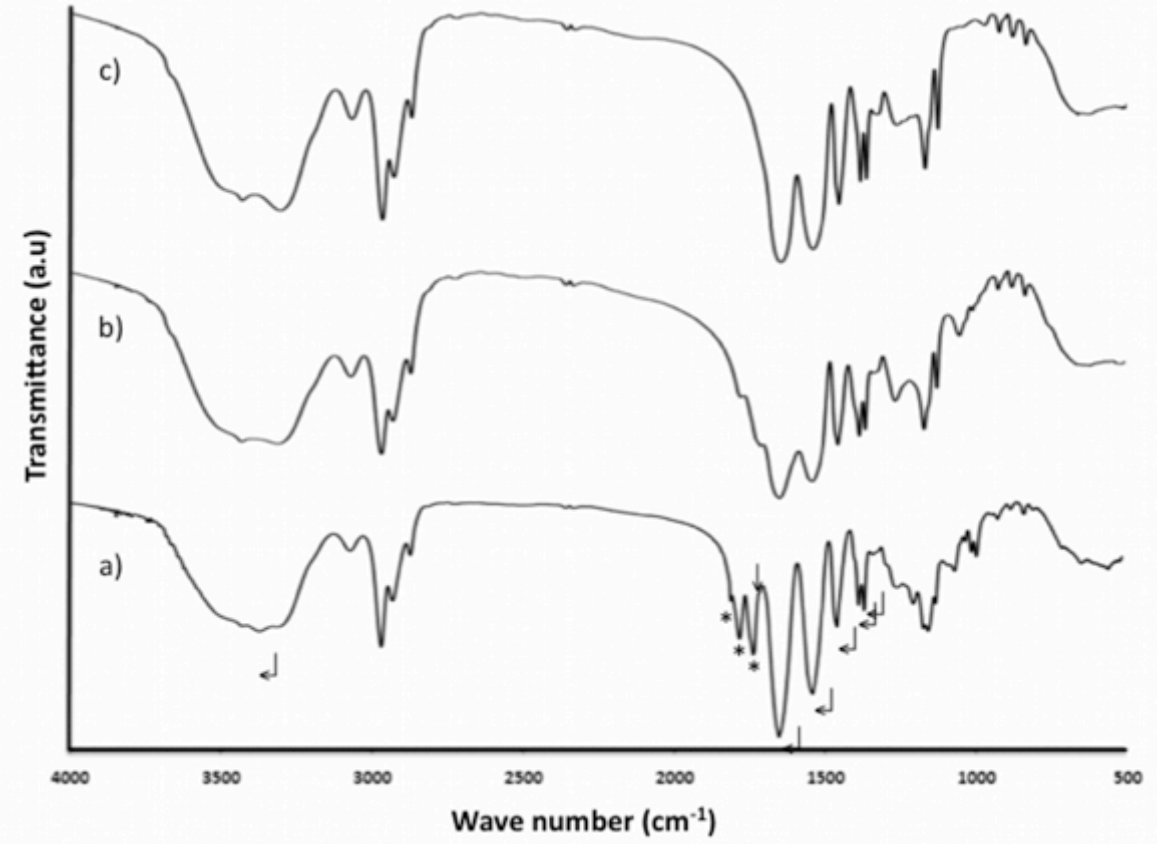

Figure 4-1: FT-IR spectra of pNNAD-4 (a), partially degraded pNNAD-4 (b) and completely hydrolyzed pNNAD-4 (c). Both pNNAD-8 and pNNAD-12 displayed a similar sequential degradation mechanism (not shown).

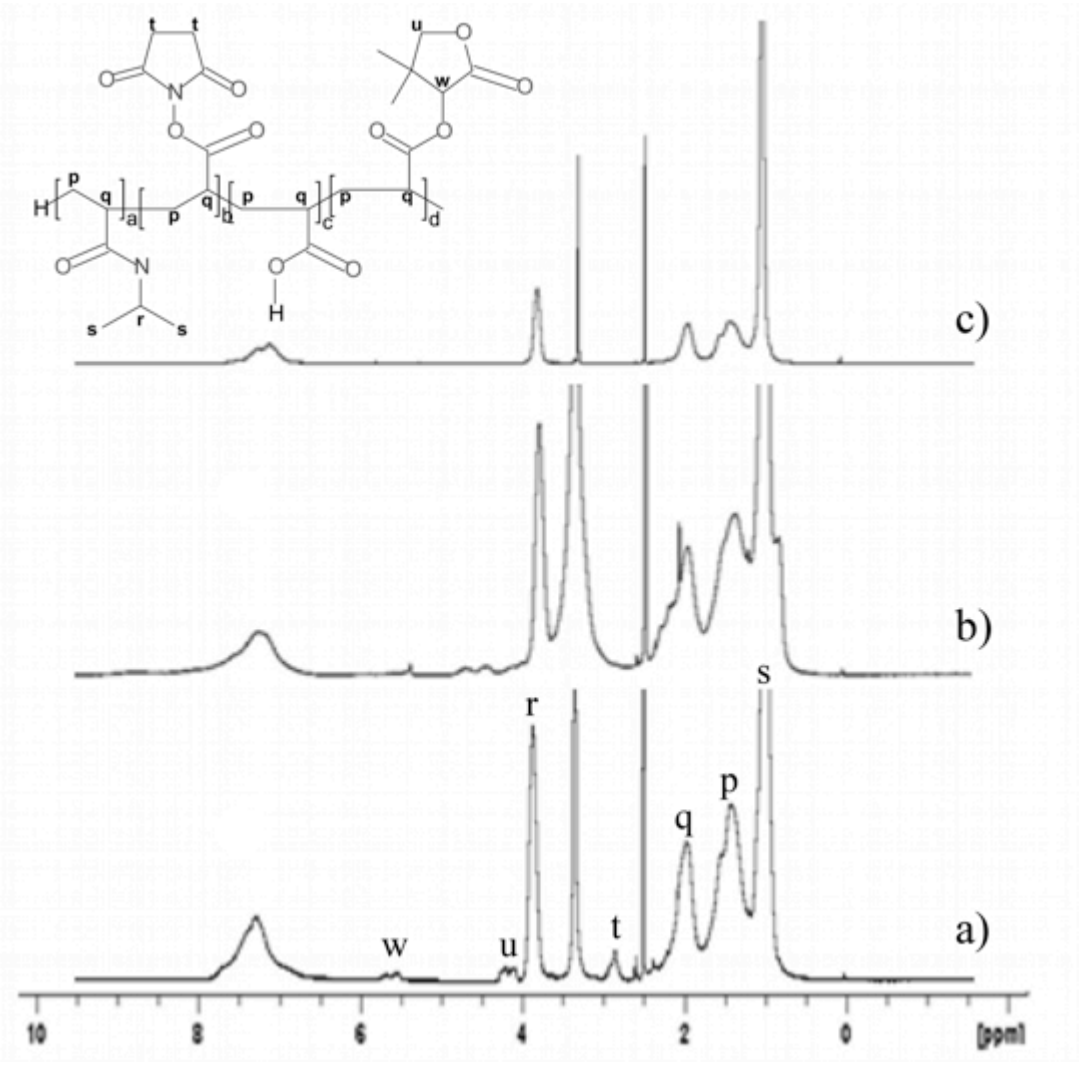

Figure 4-2: Sequential degradation spectra of intact pNNAD-4 (a), partially degraded pNNAD-4 (b) and completely hydrolyzed pNNAD-4 (C) copolymers confirmed by ^{1}H NMR. Both pNNAD-8 and pNNAD-12 displayed a similar sequential degradation mechanism (not shown).

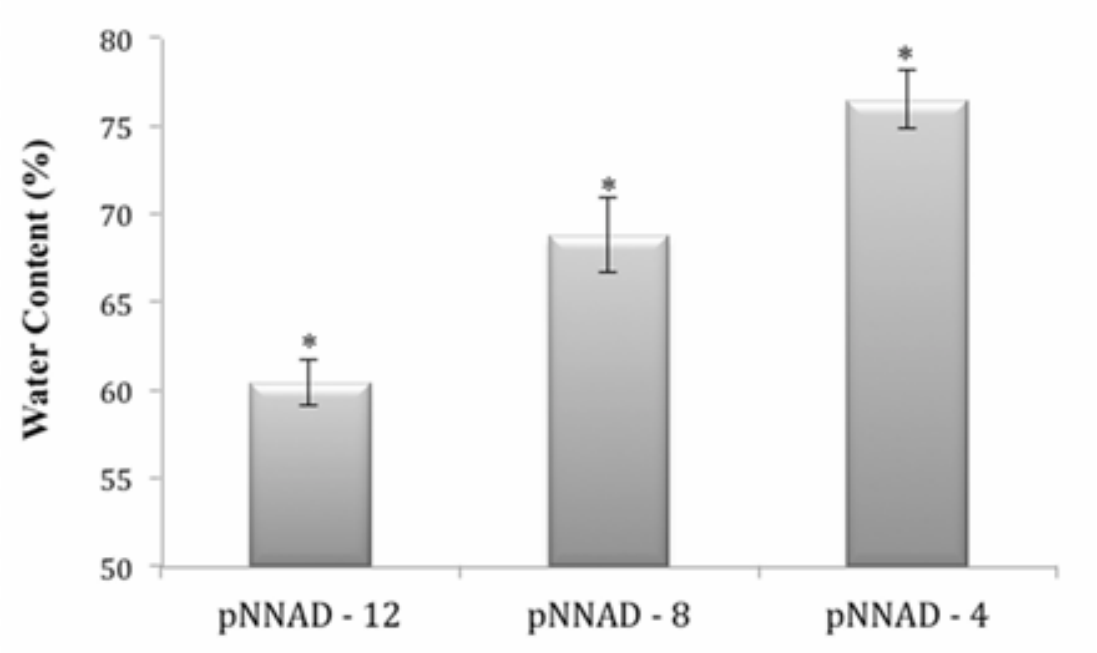

Figure 4-3: Water content of the various pNNAD copolymers was measured gravimetrically and found to be highly dependent on AA and DBA content. The difference among mean water content was statistically significant for all samples ($p \leq 0.01$].

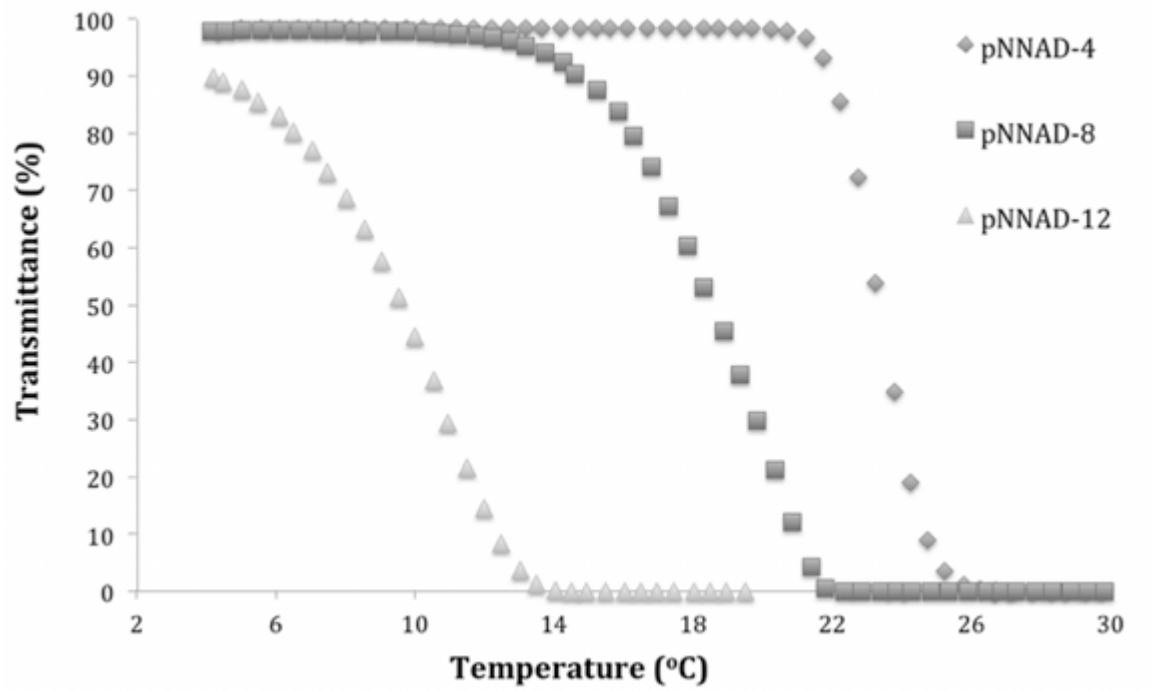

Figure 4-4: Transmittance measurements of the various pNNAD copolymers as a function of increasing temperature demonstrate rapid gel formation at LCST values similar to that observed via DSC.

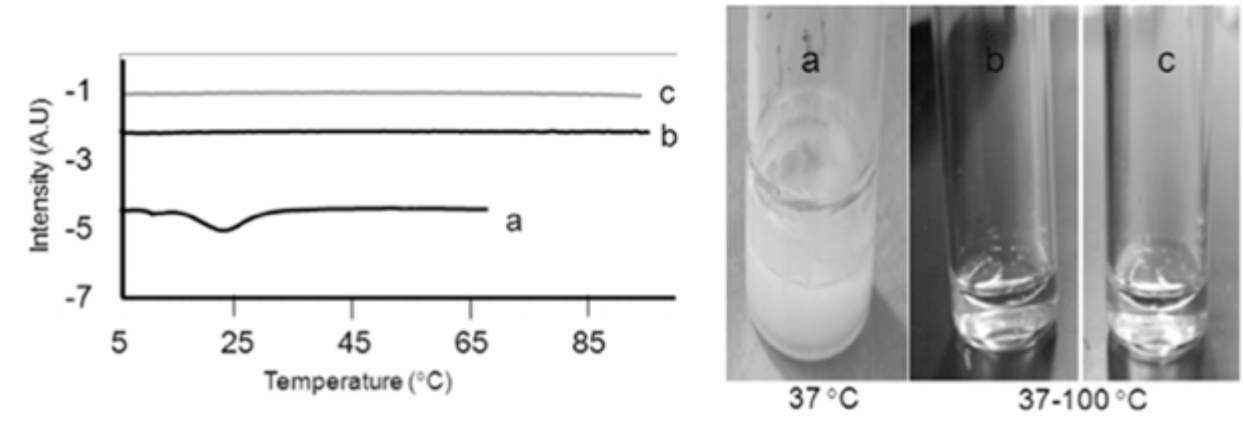

Figure 4-5: DSC analysis (left image) revealed an LCST commencing around 21°C for intact pNNAD-4 (a) and the complete removal of phase transition properties following partial degradation (b) and complete hydrolysis (c) in harsh basic conditions.

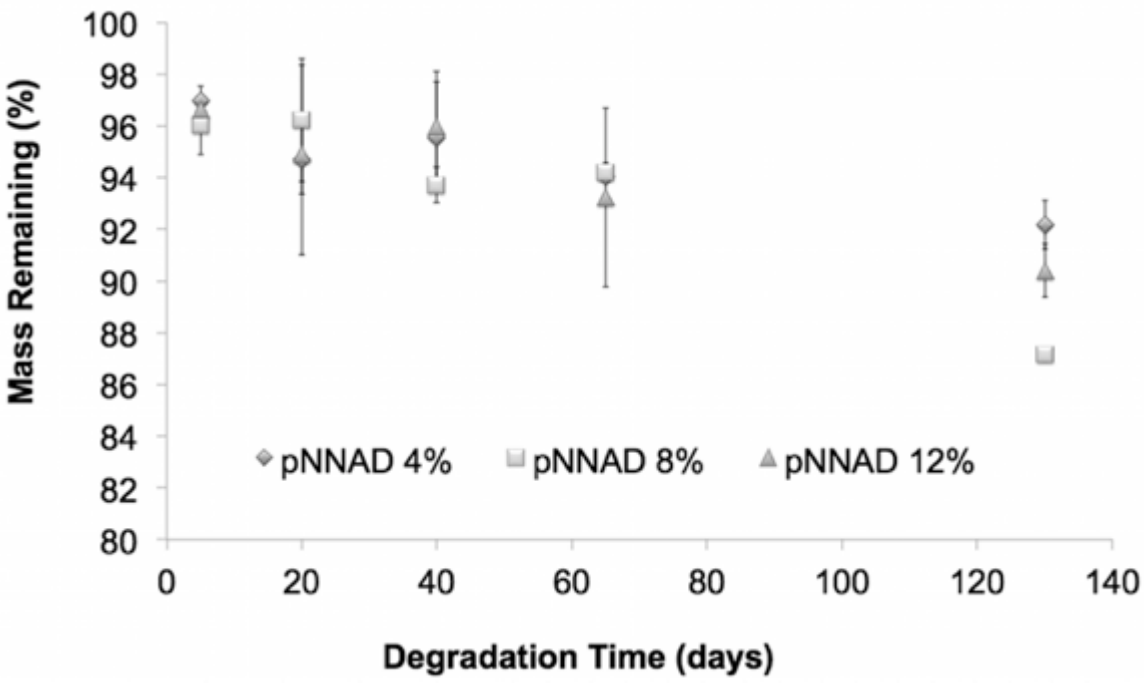

Figure 4-6: Slow pNNAD copolymer degradation kinetics were revealed by assessing mass loss as a function of time in 37°C PBS. Slow degradation may allow for sustained release of low-levels of pharmaceuticals, which ultimately is desired to decrease the frequency of intravitreal injection.

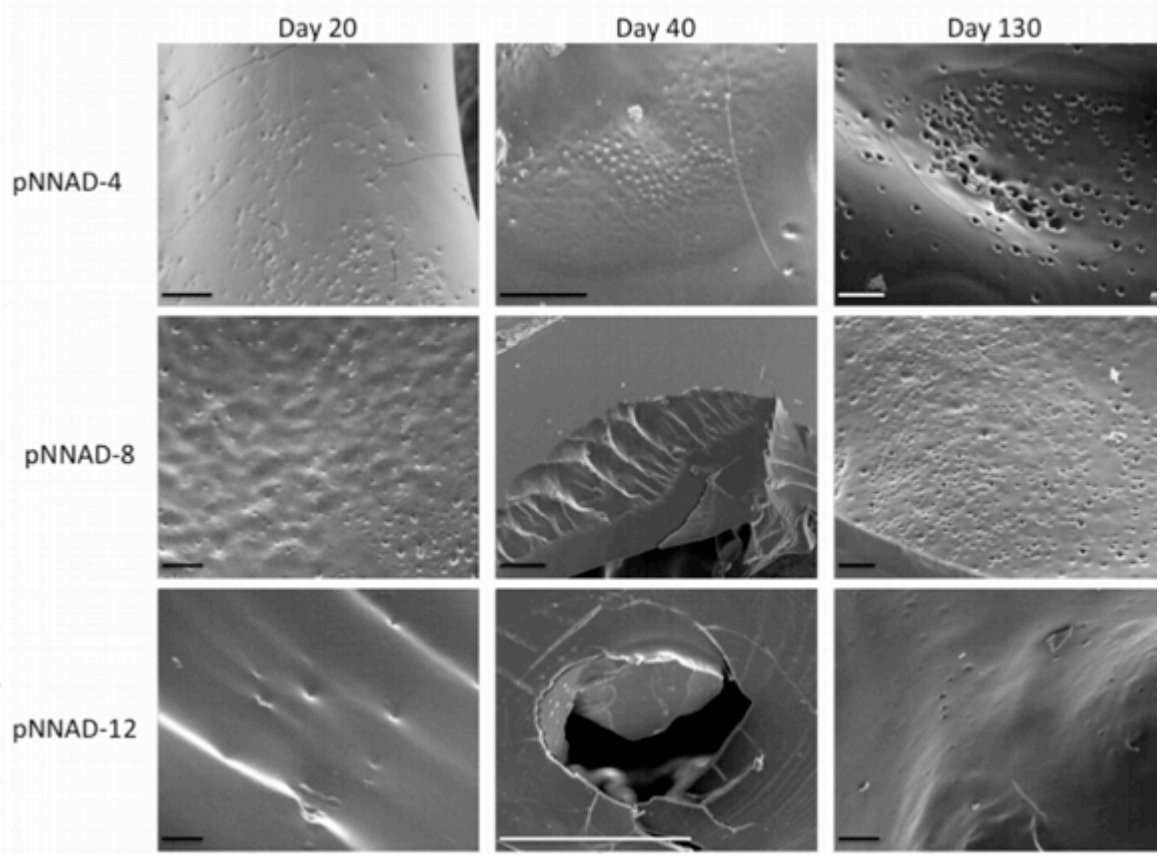

Figure 4-7: SEM micrographs reveal subtle changes in copolymer surface morphology, indicative of the limited degradation that occurred over the 130 days in 37°C PBS. Scale bar: 100 μm.

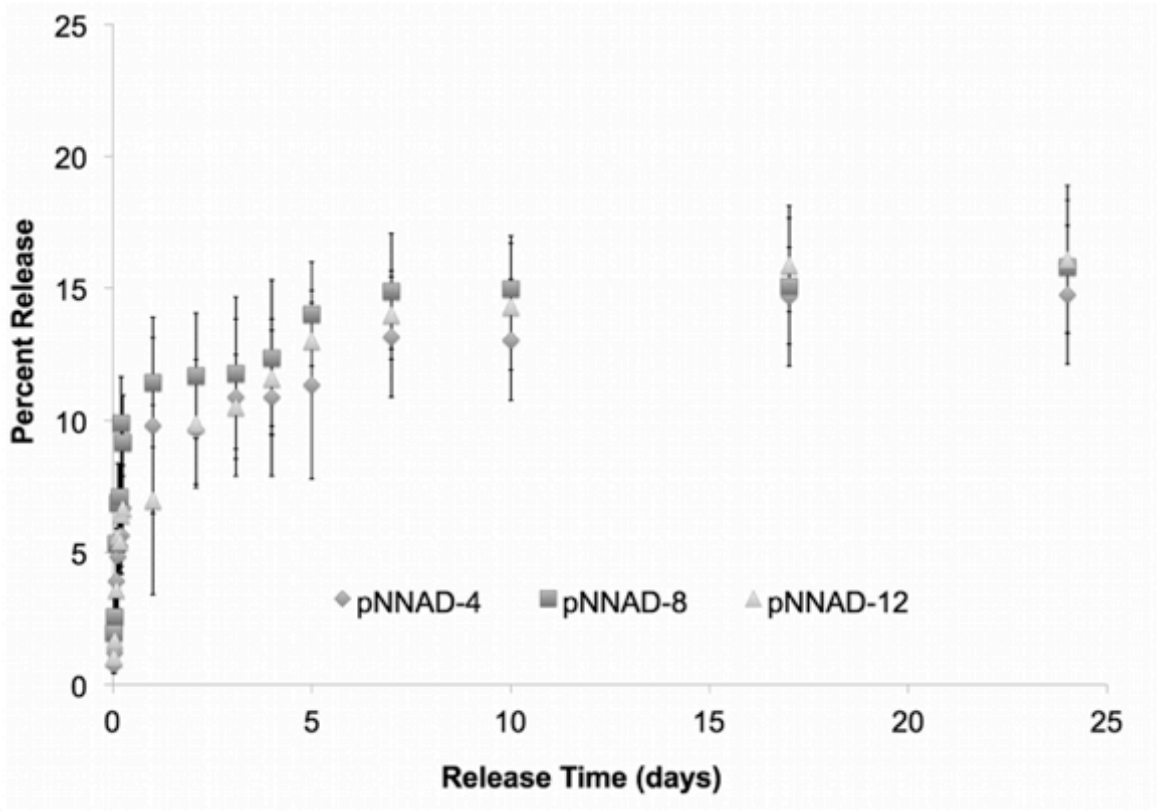

Figure 4-8: Dexamethasone release from the various pNNAD scaffolds. An initial burst phase is observed followed by stabilization, which would ideally be capable of providing low-levels of drug within the vitreous for sustained periods of time.

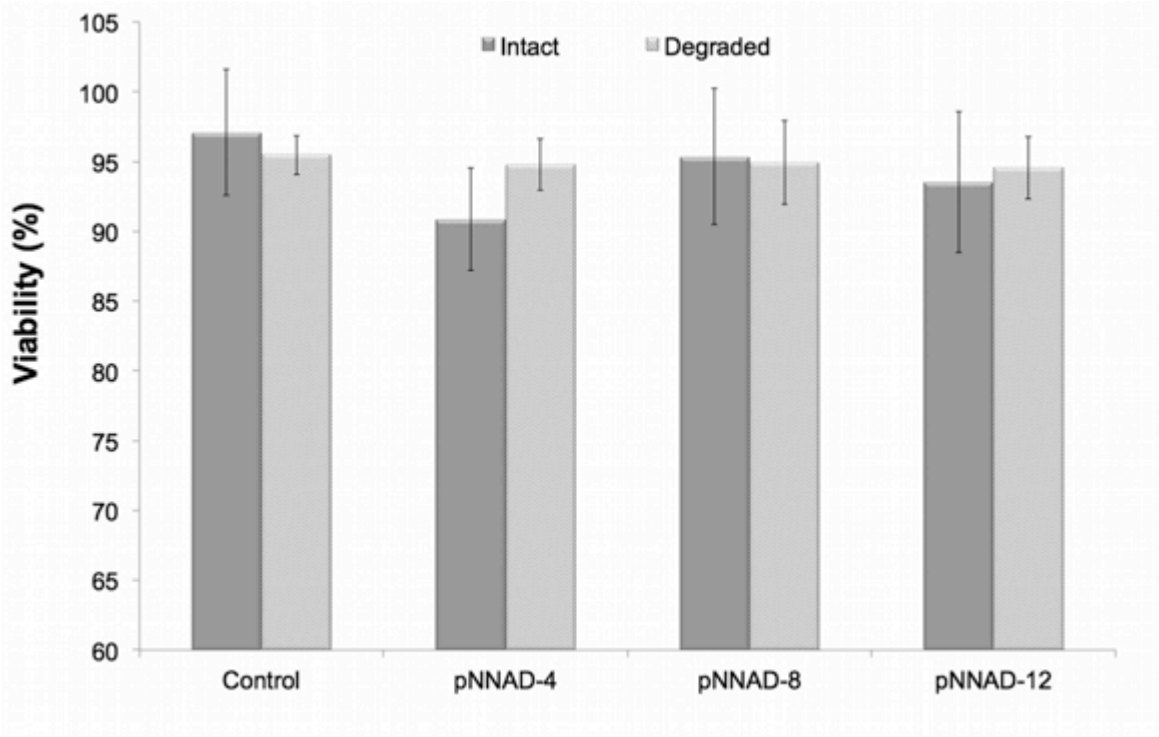

Figure 4-9: Both intact and fully degraded pNNAD copolymers demonstrate excellent compatibility with RPE cells in culture. Partially degraded pNNAD was also found to be highly compatible with RPE cells (data not shown).

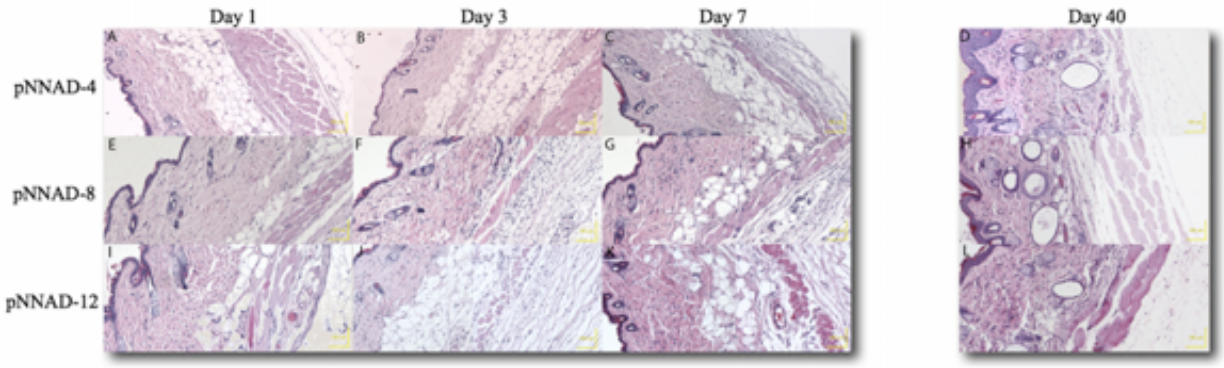

Figure 4-10: Haemotoxilin and Eosin staining of skin taken from the injection site of mice treated with pNNAD-4 (A – D), pNNAD-8 (E – H) and pNNAD-12 (I – L). From left to right, tissues were explanted 1, 3, 7 and 40 days post-implantation. Day 1, 3 and 7 samples were collected from the same litter of C3H mice (n = 3), whereas day 40 samples were from hairless SKH1-E mice (n = 2). Scale bar = 100 μm.

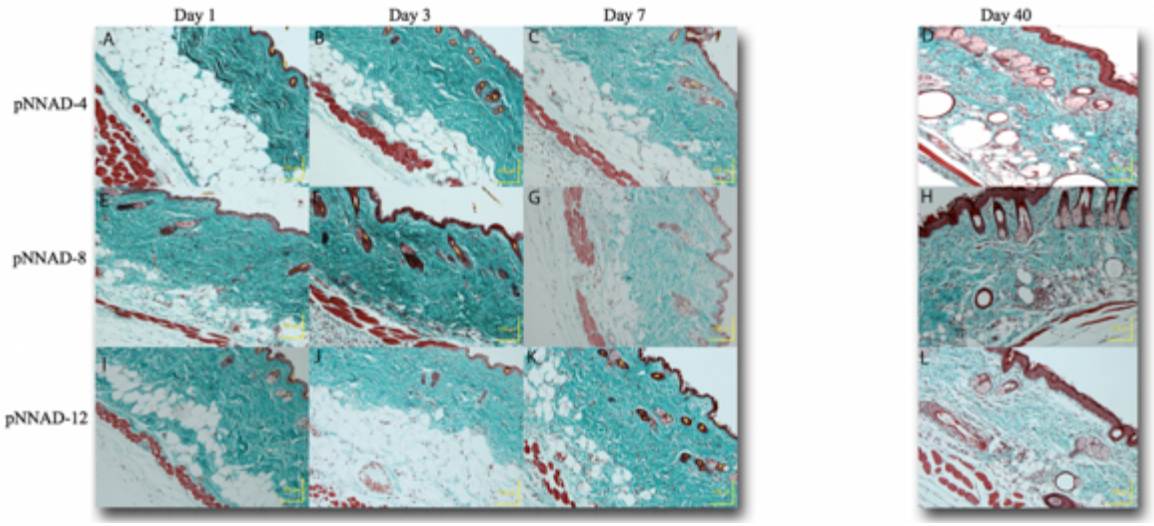

Figure 4-11: Masson's Trichrome staining of skin taken from the injection site of mice treated with pNNAD-4 (A – D), pNNAD-8 (E – H) and pNNAD-12 (I – L). From left to right, tissues were explanted 1, 3, 7 and 40 days post-implantation. Day 1, 3 and 7 samples were collected from the same litter of C3H mice (n = 3), whereas day 40 samples were from hairless SKH1-E mice (n = 2). Scale bar = 100 μm.

4.8 ACKNOWLEDGEMENTS

The authors would like to acknowledge NSERC as well as the NSERC 20/20 Ophthalmic Materials Network for funding.

4.9 DISCLOSURES

Heather Sheardown is the founder of the 20/20 NSERC Ophthalmic Materials Network, which has ties with and receives funding from the following industrial partners: Alimera Sciences, CIBA Vision Corporation, Custom Contact Lenses, Fovea Pharmaceuticals, iCo Therapeutics, Siltech Corporation, Take Control Cosmedix, Vista Optics Limited and Walsh Medical Devices Incorporated.

References

[1] Schwartz SG, Flynn HW, Jr. Pharmacotherapies for diabetic retinopathy: present and future. ExpDiabetes Res 2007;2007:52487.
[2] Del Amo EM, Urtti A. Current and future ophthalmic drug delivery systems. A shift to the posterior segment. Drug DiscovToday 2008;13:135-43.
[3] Urtti A. Challenges and obstacles of ocular pharmacokinetics and drug delivery. Adv Drug Deliv Rev 2006;58:1131-5.
[4] Gaudana R, Jwala J, Boddu SH, Mitra AK. Recent perspectives in ocular drug delivery. PharmRes 2009;26:1197-216.
[5] Choonara YE, Pillay V, Danckwerts MP, Carmichael TR, du Toit LC. A review of implantable intravitreal drug delivery technologies for the treatment of posterior segment eye diseases. JPharmSci 2009.
[6] Morais JM, Papadimitrakopoulos F, Burgess DJ. Biomaterials/Tissue Interactions: Possible Solutions to Overcome Foreign Body Response. Aaps Journal 2010;12:188-96.
[7] Kang Derwent JJ, Mieler WF. Thermoresponsive hydrogels as a new ocular drug delivery platform to the posterior segment of the eye. TransAmOphthalmolSoc 2008;106:206-13.
[8] Jardeleza MS, Miller JW. Review of anti-VEGF therapy in proliferative diabetic retinopathy. SeminOphthalmol 2009;24:87-92.
[9] Fitzpatrick SD, Mazumder MAJ, Lasowski F, Fitzpatrick LE, Sheardown H. PNIPAAm-Grafted-Collagen as an Injectable, In Situ Gelling, Bioactive Cell Delivery Scaffold. Biomacromolecules 2010;11:2261-7.
[10] Neradovic D, Hinrichs WLJ, Kettenes-van den Bosch JJ, Hennink WE. Poly(N-isopropylacrylamide) with hydrolyzable lactic acid ester side groups: a new type of thermosensitive polymer. Macromol Rapid Commun 1999;20:577-81.
[11] Neradovic D, van Steenbergen MJ, Vansteelant L, Meijer YJ, van Nostrum CF, Hennink WE. Degradation mechanism and kinetics of thermosensitive polyacrylamides containing lactic acid side chains. Macromolecules 2003;36:7491-8.
[12] Ma Z, Nelson DM, Hong Y, Wagner WR. Thermally Responsive Injectable Hydrogel Incorporating Methacrylate-Polylactide for Hydrolytic Lability. Biomacromolecules 2010;11:1873-81.
[13] Yoshida T, Aoyagi T, Kokufuta E, Okano T. Newly designed hydrogel with both sensitive thermoresponse and biodegradability. Journal of Polymer Science Part a-Polymer Chemistry 2003;41:779-87.
[14] Cui ZW, Lee BH, Vernon BL. New hydrolysis-dependent thermosensitive polymer for an injectable degradable system. Biomacromolecules 2007;8:1280-6.
[15] Cui Z, Lee BH, Pauken C, Vernon BL. Manipulating degradation time in a N-isopropylacrylamide-based co-polymer with hydrolysis-dependent LCST. J Biomater Sci Polym Ed 2010;21:913-26.
[16] ISO-10993-13. Biological evaluation of medical devices: identification and quantification of degradation products from polymeric medical devices. In: International organization for standardization G, Switzerland, editor.1998.

[17] Quiram PA, Gonzales CR, Schwartz SD. Severe steroid-induced glaucoma following intravitreal injection of triamcinolone acetonide. AmJOphthalmol 2006;141:580-2.
[18] Thompson JT. Cataract formation and other complications of intravitreal triamcinolone for macular edema. AmJOphthalmol 2006;141:629-37.
[19] Ruggiero A, Villa CH, Bander E, Rey DA, Bergkvist M, Batt CA, et al. Paradoxical glomerular filtration of carbon nanotubes. Proceedings of the National Academy of Sciences of the United States of America 2010;107:12369-74.
[20] Shah CA. Diabetic retinopathy: A comprehensive review. Indian JMedSci 2008;62:500-19.
[21] Lee SS, Robinson MR. Novel drug delivery systems for retinal diseases. A review. Ophthalmic Res 2009;41:124-35.
[22] Kuppermann BD. Toxicity Studies on Triamcinolone Acetonide and Dexamethasone. Retina Today 2010:13-4.
[23] Sharma A, Pirouzmanesh A, Patil J, Estrago-Franco MF, Zacharias LC, Pirouzmanesh A, et al. Evaluation of the toxicity of triamcinolone acetonide and dexamethasone sodium phosphate on human lens epithelial cells (HLE B-3). Journal of ocular pharmacology and therapeutics 2011;27:265-71.
[24] Patil AJ, Mansoor A, Sharma A, Kuppermann BD. Effects of dexamethasone on human trabecular meshwork cells in vitro. Association for Research in Vision and Ophthalmology annual meeting. Fort Lauderdale, FL.2009.
[25] Narayanan R, Mungcal JK, Kenney MC, Seigel GM, Kuppermann BD. Toxicity of triamcinolone acetonide on retinal neurosensory and pigment epithelial cells. Investigative Ophthalmology & Visual Science 2006;47:722-8.
[26] Zacharias LC, Luthra S, Dong J, Kuppermann BD. Effect of dexamethasone on mitochondrial func- tion and cell viability in human retinal pigment epithelial and rat neurosensory retinal cells in vitro. Association for Research in Vision and Ophthalmology annual meeting. Fort Lauderdale, FL.2007.
[27] Schwartz SG, Flynn HW, Scott IU. Pharmacotherapy for diabetic retinopathy. Expert Opinion on Pharmacotherapy 2009;10:1123-31.
[28] Beer PM, Bakri SJ, Singh RJ, Liu W, Peters Iii GB, Miller M. Intraocular concentration and pharmacokinetics of triamcinolone acetonide after a single intravitreal injection. Ophthalmology 2003;110:681-6.
[29] Morse LS, Modjtahedi S, Smit-McBride Z. Use of Intravitreal Steroids in the Clinic. Retina Today 2010:6-10.
[30] Haller JA, Kuppermann BD, Blumenkranz MS, Williams GA, Weinberg DV, Chou C, et al. Randomized controlled trial of an intravitreous dexamethasone drug delivery system in patients with diabetic macular edema. Arch Ophthalmol 2010;128:289-96.
[31] Campochiaro PA, Hafiz G, Shah SM, Bloom S, Brown DM, Busquets M, et al. Sustained Ocular Delivery of Fluocinolone Acetonide by an Intravitreal Insert. Ophthalmology 2010;117:1393-U157.
[32] Ballios BG, Cooke MJ, van der Kooy D, Shoichet MS. A hydrogel-based stem cell delivery system to treat retinal degenerative diseases. Biomaterials 2009;31:2555-64.
[33] Sorg H, Krueger C, Vollmar B. Intravital insights in skin wound healing using the mouse dorsal skin fold chamber. Journal of Anatomy 2007;211:810-8.

CHAPTER 5: An Approach to Design Optically Transparent, Resorbable, PNIPAAm-Based Copolymers for Minimally Invasive Posterior Segment Ophthalmic Therapeutics

Authors: Scott D Fitzpatrick*, Mohammad A. Jafar Mazumder*, Benjamin Muirhead and Heather Sheardown.

*These authors contributed equally.

Publication Information: Work in progress. Article not yet submitted.

Objectives: Design of optically transparent, non-shrinking, degradable, thermoresponsive PNIPAAm-based scaffolds for the minimally invasive introduction of pharmaceuticals into the posterior segment of the eye.

Main Scientific Contributions:

- Tailored our previously developed pNNAD copolymers to impart optical transparency into the degradable PNIPAAm-based copolymers.
- In addition to optical transparency, the inclusion of PEG allows copolymers to maintain their aqueous phase following sol-gel transition, creating a non-shrinking gel. This volume-maintaining property may overcome issues of expulsion of the infused therapeutic that sometimes occurs as NIPAAm-based scaffolds expel their aqueous phase during gel formation (ie cell expulsion observed in Chapter 2)
- Copolymers maintained the ability to degrade without the liberation of low molecular weight degradation by-products through copolymerization with DBA.

Author Contributions:

This ongoing work is a collaborative project and contributions are as follows. Scott was responsible for initial copolymer design (with Jafar), polymer synthesis, LCST characterization via UV spectrophotometry, copolymer morphology analysis using SEM, drug release studies and write-up. Jafar was responsible for copolymer design (with Scott), initial polymer synthesis, characterization of copolymer composition via FT-IR and NMR, determination of molecular weight, accelerated degradation studies and DSC. Future work to be performed is as follows. Scott will be responsible for degradation studies, cell culture studies, mechanical testing, drug release studies, and water content analysis. Ben will perform *in vivo* testing, including sub-cutaneous injections and relevant histological analysis and intraocular cell and drug injections.

An Approach to Design Optically Transparent, Resorbable, NIPAAm-Based Copolymers for Minimally Invasive Posterior Segment Ophthalmic Therapeutics

Scott D Fitzpatrick[a]*, *M.A. Jafar Mazumder*[b]*, *Benjamin Muirhead*[a], *Heather Sheardown*[a,b#]

* *These authors contributed equally*

[a]School of Biomedical Engineering and [b]Department of Chemical Engineering

McMaster University
1280 Main Street West
Hamilton ON, Canada
L8S 4L7

#To whom correspondence should be addressed sheardow@mcmaster.ca,
Phone: 1-(905) 525-9140 (24794)
Fax: 1-(905) 521-1350

5.1 INTRODUCTION

One of the major limitations of using N-isopropylacrylamide (NIPAAm)-based copolymers for ocular drug delivery applications is the lack of optical transparency displayed by gelled scaffolds. As the NIPAAm-based copolymers undergo a temperature-dependent phase transition, they lose their optical transparency, changing from a transparent liquid to an opaque white gel. This loss of transparency is not expected to pose significant complications as the gelled scaffold is expected to reside at the injection site on the floor of the vitreal chamber, outside the visual axis. This approach is similar to other free-floating opaque intravitreal drug releasing devices such as ILUVIEN® (Alimeira Sciences) [1] and Osurdex (Allergan) [2], which do not cause significant disturbance of the central vision. However, an optically transparent, thermo-gelling, degradable drug-releasing scaffold would serve as an attractive alternative for sustained release of pharmaceuticals to the posterior segment of the eye and would minimize potential complications associated with scaffold migration. Therefore, as an extension of our previously reported pNNAD materials [3], we attempted to develop optically transparent, thermo-gelling, degradable copolymers.

Hydrophobic and hydrophilic polymers are typically immiscible and tend to phase separate when mixed together. However, if the hydrophobic and hydrophilic polymers are successfully copolymerized, creating an amphiphilic copolymer, the maximal separation length of the two phases is limited, which can lead to microphase separation and the formation of alternating hydrophilic and hydrophobic microdomains [4]. Microphase separated systems with separation lengths around 100 nm or less typically produce

optically transparent materials because the microdomains are significantly smaller than the wavelength of light [4]. The hypothesis is that through the incorporation of relatively large hydrophilic segments into the previously reported pNNAD copolymers, it may be possible to generate copolymers that microphase separate upon thermo-gelation, producing alternating microdomains of hydrophilic and hydrophobic rich environments [5]. In theory, optical transparency can be introduced into the pNNAD scaffolds if copolymerization with a hydrophilic co-monomer yields sufficiently small microphase separation, allowing light to pass through the gelled scaffold without scattering [5]. Thus, it was proposed that through modification of the pNNAD scaffold, by replacing either acrylic acid N-hydroxysuccinimide (NAS) or acrylic acid (AA) with hydrophilic polyethylene glycol (PEG) co-monomers possessing a variety of molecular weights (475, 526 and 1100 Da) and either methyl or hydroxyl pendant groups, it may be possible to obtain such an alternating micro-structure. Therefore, a series of copolymers were synthesized with varying monomers and feed ratios to determine optimal conditions to generate optically transparent, thermo-gelling, degradable scaffolds that are appropriate for minimally invasive posterior segment drug delivery.

5.2 MATERIALS AND METHODS

Acryloyloxy dimethyl-γ-butyrolactone (DBA, 95%), NAS (≥90%), benzoyl peroxide (BPO, 97%), and dexamethasone (98%) were purchased from Sigma Aldrich (Oakville, ON, Canada), and used as received. N-isopropylacrylamide (NIPAAm) (97%) was purchased from Sigma Aldrich and was purified by recrystallization from a toluene/

hexane mixture. AA (99%) and various PEG monomers (475, 526 and 1100 Da) were purchased from Sigma-Aldrich, and purified by passing through a packed column containing Sigma-Aldrich inhibitor remover to extract the polymerization inhibitor, 4-methoxyphenol (MEHQ). 1,4- dioxane, toluene, hexane, tetrahydrofuran (THF), dimethylsulfoxide (DMSO) and anhydrous ethyl ether were purchased from Caledon Laboratories (Caledon, ON) and used as received. Sodium hydroxide and hydrochloric acid solutions were purchased as concentrates from Anachemia Chemical (Rouses Point, NY, USA), and were prepared by diluting to 1.0 or 0.1 M with deionized water. Deionized water with a resistivity of 18.2 MΩ cm was prepared using a Milli-pore Barnstead water purification system (Graham, NC, USA). Phosphate buffered saline solution (PBS, pH 7.4) was purchased from McMaster University Health Sciences facility and used as received. Cellulose dialysis membranes with molecular weight cutoff (MWCO) values from 1 to 12 kg/mol were purchased from Spectrum Laboratories Inc (Rancho Dominguez, CA, USA).

5.2.1 Synthesis of poly(NIPAAm-(NAS / AA)-PEGx-DBAy), p(N(N/A)PxDy)

Several copolymers of poly(NIPAAm-(NAS / AA)-PEG_x-DBA_y were synthesized via free radical polymerization, wherein $_x$ denotes PEG molecular weight (4 = 475, 5 = 526, and 11 = 1100 Da) and $_y$ represents DBA mol content, Scheme 5-1. All copolymers were synthesized with an initial molar feed ratio of 80 : 4 : a : b (NIPAAm : NAS or AA : PEG : DBA). The a : b (PEG : DBA) molar content was either 4 : 12, 8 : 8, or 12 : 4, as indicated by the DBA subscript number in the copolymer nomenclature. Thus, $pNNP_4D_4$ consists of 80 : 4 : 12 : 4 molar ratio of NIPAAm : NAS : PEG : DBA and the PEG

molecular weight is 475 Da. Furthermore, $pNNP_5D_y$ and $pNNP_{11}D_y$ were synthesized with PEG having MW 526 and 1100 Da respectively. Briefly, $pNNP_4D_4$ was prepared by dissolving NIPAAm (2.798 g, 24.73 mmol), NAS (0.209 g, 1.23 mmol), PEG-475 (1.769 g, 3.72 mmol), DBA (0.229 g, 1.24 mmol) and BPO (0.0745 g, 0.307 mmol) in 45 mL 1, 4- dioxane. Dry nitrogen was bubbled through the reaction mixture for 15 minutes. The flask was then sealed and heated to 70^{o}C for 24 hours under continuous stirring in a temperature controlled oil bath. The polymerized product was cooled to room temperature and isolated by precipitation in anhydrous ethyl ether. The precipitate was dried at 50^{o}C in a vacuum oven and then purified by repeated precipitation from THF into anhydrous ethyl ether. The purified copolymer was then dried to constant weight in a vacuum oven and yield was found to be 78%. Similar copolymers were polymerized in this fashion with varying monomer ratios. Co-monomer feed ratios are provided in Table 5-1.

5.2.2 Material Characterization

Copolymer structures were characterized by a Thermo Fischer Nicolet 6700 Fourier Transform Infrared (FT-IR) spectrometer. The compositions were determined using a Bruker AV 600 ^{1}H NMR spectrometer with DMSO-*d6* as a solvent. Aqueous phase gel permeation chromatography (GPC) using a Waters system with a 515 HPLC pump, 717 plus Autosampler, three Ultrahydrogel columns (0 – 3, 0 – 50, 2 – 300 kDa), and a 2414 refractive index detector was used to quantify molecular weights of copolymers subjected to accelerated degradation conditions (which eliminated thermal-sensitivity). Samples were eluted at a flow rate of 0.8 mL/min with 20 mM PBS buffer,

100 mM $NaNO_3$ (pH 7.2) and the system was calibrated with narrow dispersed PEG standards (Waters, Mississauga, ON).

The lower critical solution temperature (LCST) was characterized using both differential scanning calorimetry (DSC, TA Instruments 2910) and UV / visible spectrophotometry (Cary 300). For DSC, samples were dissolved in PBS to form 20% w/v solutions. The solutions were placed in hermetic pans and subjected to a heating rate of 2^oC/min from 0 – 70^oC. The LCST was defined as the temperature at which the maximum endothermal peak was observed. UV spectrophotometry was used to observe the copolymer cloud point temperature and to verify DSC findings. Samples were dissolved in PBS to form 10% w/v solutions. The solutions were placed in 4 mL UV cuvettes and subjected to a heating rate of 1^oC/min from 5 – 45^oC. Transmittance measurements were assessed every thirty seconds.

5.2.3 Accelerated Degradation

$pN(N/A)P_xD_y$ copolymers were subjected to harsh conditions to expedite degradation, allowing analysis of the degradation mechanism and molecular weight characterization using aqueous phase GPC. Samples were dissolved in deionized water to form 20% w/v solutions in 20 mL glass vials. The pH was adjusted to 10.5 using either 0.1 or 1 M NaOH and the solution was placed in a 70^oC oven. The pH was adjusted to 10.5 daily. Complete degradation was achieved after 7 days of exposure to accelerated degradation conditions. Fully degraded copolymer samples were maintained at 70^oC and pH 10.5 for another 3 days and then dialyzed in cellulose tubing with a 3.5 kg/mol

MWCO). The purified product was then freeze-dried. Partially degraded samples were collected and dialyzed periodically throughout the degradation process. These samples were also dialyzed and freeze dried for subsequent ^{1}H NMR and FT-IR analysis. Partially degraded pN(N/A)P_xD_y samples reported in this text were collected after 4 days of accelerated degradation.

5.2.4 Copolymer Morphology

Copolymer microstructure was assessed using a Philips 515 scanning electron microscope. Samples were dissolved in PBS to form 25% w/v solutions. The solutions were then placed in a 37^{o}C oven for 48 hours to drive polymer gelation. At this time, the supernatant (if any) was removed and the gelled copolymers were submersed in liquid nitrogen for 48 hours. The cryopreserved samples were then freeze-dried and a 15 nm gold coating was applied to the sample surface to allow visualization. Images were then captured using Mektech URSA 100 Rev. 1.30 imaging software.

5.2.5 Dexamethasone Release

Dexamethasone was dissolved in PBS to form a 50 μg/ml solution. pN(N/A)P_xD_y copolymers were dissolved in the PBS / dexamethasone solution to form 25% w/v solutions. The samples were placed in a 4^{o}C fridge for 24 hours and then placed in a 37^{o}C oven under gentle agitation for 2 hours to drive scaffold formation and drug entrapment. The supernatant (if any) was then collected and replaced with 1 mL of fresh, pre-warmed PBS, which was defined as time zero for the release assay. Aliquots (0.5 mL) were periodically collected and replaced with an equal volume of fresh, pre-warmed PBS.

Dexamethasone concentration was quantified by HPLC using a Waters high performance liquid chromatography system with a 2707 autosampler, 2489 UV spectrophotometer, 1525 binary HPLC pump, Atlantis dC18 5 μm, 4.6 x 100 mm column and Breeze 2 software (Build 2154). A 40 / 60 acetonitrile in water solution was used as the mobile phase, which was passed through a 0.45 μm filter and de-gassed prior to use. An isocratic flow-rate (1.0 ml/min) was used with 10 μl sample injection volumes. Dexamethasone standards were prepared in the mobile phase and used as a calibration curve.

5.3 RESULTS AND DISCUSSIONS

5.3.1 Copolymer Characterization

Copolymers of varying compositions of NIPAAm, NAS or AA, PEG (475, 526, or 1100 Da), and DBA were synthesized via free radical polymerization using BPO as a free radical initiator. A list of synthesized copolymers, complete with final copolymer composition determined using ^{1}H NMR, LCST values obtained via DSC and observations about the gelled copolymer properties is provided in Table 5-1. While the majority of synthesized copolymers produced opaque gels upon heating above their LCST, several copolymers, specifically those containing 4 mol% PEG-1100 and 12 mol% DBA (pN(N/A)P_{11}D12), were found to remain optically transparent following polymer gelation, as seen in Figure 5-1. While these materials remain transparent at 37^{o}C, turbidity testing (Figure 5-2) reveals that transparency falls off drastically as the temperature is further increased. At relevant physiological temperatures, between 35 – 37^{o}C, both pN(N/A)$P_{11}D_{12}$ copolymers permit an estimated 70 – 85 % transmittance of light (500

nm). From observation, this transmittance does not appear to decrease when the copolymers are preserved in a gelled state at 37^{o}C for prolonged periods of time. Therefore, there appears to be a window between the copolymer LCST (~24, 27^{o}C) and approximately 40^{o}C where the scaffolds form mechanically robust gels and remain optically transparent. However, these copolymers possess limited mechanical integrity, forming highly viscous gels capable of being inverted and maintaining their shape, but are easily deformed by mechanical perturbation. As the temperature is heated beyond 40^{o}C, mechanical integrity is greatly increased as the copolymer transitions to an opaque state. Therefore, it is likely that the transparent window between LCST and 40^{o}C is accompanied by incomplete local self-association of polymer chains within the bulk network, which creates a weak, transparent gel. The copolymer transitions to an opaque, rigid gel upon further heating and global polymer chain aggregation.

FT-IR was used to confirm copolymer structure for the various pN(N/A)P_xD_y copolymers. Figure 5-3 shows representative spectra for the $pNAP_4D_y$ family of copolymers. The spectra shows characteristic C=O and N-H NIPAAm peaks around 1660 and 1540 cm^{-1} respectively. In addition, the N-H stretching vibration appears at 3310 cm^{-1} and isopropyl peaks are observed at 1360, 1380 and 1460 cm^{-1}. The AA carbonyl peak is seen at 1710 cm^{-1} and the CH_2O from PEG appears around 1100 cm^{-1}. Finally, characteristic peaks belonging to the carbonyl peak in the DBA ring structure and the carbonyl peak attached to the DBA backbone appear at 1780 and 1735 cm^{-1} respectively. The DBA ring peaks increase in intensity as the copolymer DBA content increases.

^{1}H-NMR was used to quantify copolymer molar content and to examine the degradation profile of the pN(N/A)P_xD_y copolymers in harsh, alkaline conditions. The intact $pNNP_{11}D_{12}$ spectrum in Figure 5-4 shows a characteristic PEG CH_2 peak around 3.4 ppm, a NAS CH_2 ring peak between 2.8 – 3.0, the NIPAAm CH peak from the isopropyl group between 3.7 – 4.0 and a characteristic DBA ring CH_2 peak between 4.0 – 4.4 ppm. The NAS peak disappears in the partial and completely degraded samples. The DBA CH_2 peak shifts to 3.3 – 3.5 ppm in the partially degraded copolymer spectrum and is absent from the fully degraded sample, thus indicating that, like our previously reported pNNAD copolymers, the material undergoes a hydrolysis-dependent ring opening prior to cleavage of the DBA ester group attached to the polymer backbone. From our previous studies, it is anticipated that simple ring opening should raise the copolymer LCST above physiologic temperature, allowing the copolymer to clear from the body without liberating degradation by-products. Furthermore, from the NMR spectra, it is apparent that PEG remains present within the copolymer following DBA ring opening and subsequent liberation. Thus, if PEG is not cleaved from the copolymer prior to DBA ring-opening, it is anticipated that the copolymer will retain its transparency. However, *in vivo* testing will need to be performed to examine the physiological degradation mechanism and to elucidate the impact of protein fouling and the foreign body reaction on copolymer transparency.

5.3.2 Copolymer Morphology

Scanning electron microscopy was used to shed light on the architectural differences of the copolymer microstructure. Specifically, we were interested in the differences between opaque and optically transparent scaffolds. Careful measures were required in sample preparation to preserve the morphological structure of gelled scaffolds. Gels were formed by heating polymer solutions (25% w/v in PBS) to 37^{o}C for 48 hours and then rapidly immersed in liquid nitrogen to preserve the scaffolds in their gelled morphology. The samples were then lyophilized to produce dried gels possessing morphology similar to their gelled state. A 15 nm gold coating was applied to the copolymer surface to allow visualization of the microstructure. From the SEM micrographs in Figure 5-5, large differences can be seen between the optically transparent and opaque scaffolds. While the pore structure of the transparent materials appears to be significantly larger than the wavelength of light, the scaffolds exhibited a high degree of order and structuring, which is perhaps what permits light to pass through relatively unscathed, producing a gel with good optical properties. Whereas, the opaque gels possess distinct regions with abrupt changes in morphology, which likely contribute to the scattering of incoming light, rendering the scaffolds opaque. Furthermore, it is possible that the cryopreservation technique introduced changes in the copolymer architecture. The swelled scaffolds studied may have been too large to allow rapid freezing, leading to polymer rehydration and structural changes. Therefore, further examination will be performed on swelled scaffolds possessing a thin form factor to allow rapid freezing upon immersion in liquid nitrogen.

5.3.3 Dexamethasone Release

Copolymer drug loading efficiency was calculated by quantifying the dexamethasone concentration of the supernatant removed from the initially formed gels. From this, the total dexamethasone remaining within the scaffolds was determined to be 88.8, 96.1 and 97.0% for $pNNP_5D_4$, $pNNP_5D_8$, and $pNNP_5D_{12}$ respectively. Since the $pN(N/A)P_{11}D_{12}$ samples form a bulk gel, in which no copolymer shrinkage or expulsion of the aqueous phase is observed, no supernatant could be removed from these gels at time zero. Therefore, the loading efficiency was assumed to be 100%. As expected, all scaffolds display a small initial burst release that levels off after the first 24 hours. The release rate of the small hydrophobic drug appears to increase with increasing copolymer hydrophilicity, with $pNNP_5D_4 > pNNP_5D_8 > pNNP_5D_{12}$. While the optically transparent $pN(N/A)P_{11}D_{12}$ copolymers remained transparent following the incorporation of dexamethasone, they also appear to possess relatively fast release rates, which is not ideal for sustained release of pharmaceuticals into the posterior segment, since rapid release would necessitate frequent injections and would not offer a significant advantage over simple free-drug injections. However, this proof of principle study was intended to demonstrate that it is possible to generate optically transparent, degradable NIPAAm-based copolymers that may ultimately be suitable for ophthalmic drug delivery applications. Further tailoring and optimization of copolymer properties is required to produce materials possessing good mechanical properties and slow-release profiles while maintaining optical transparency.

5.4 CONCLUSIONS AND FUTURE WORK

A series of PEG-containing NIPAAm-based copolymers was synthesized in attempts to create optically transparent, thermo-gelling, degradable copolymers. The majority of synthesized copolymers formed opaque white gels when heated above their LCST. However, several copolymers, specifically the $pN(N/A)P_{11}D_{12}$ copolymers, which were comprised of NIPAAm : NAS or AA : PEG (1100 kDa) : DBA in an 80 : 4 : 4 : 12 molar feed ratio, retained optical transparency following the temperature-induced formation of a viscous gel. These copolymers existed as optically transparent, viscous gels when maintained at temperatures between their LCST and approximately 40^{o}C. When heated above 40^{o}C however, the gels increased in rigidity and lost their transparency. Furthermore, it is not known if the viscous gels possess adequate mechanical integrity to act as sustained release drug delivery scaffolds. The simplest approach to improve mechanical integrity is to remove NAS or AA from the copolymer and increase the NIPAAm or DBA content, which will increase the hydrophobic content when heated above the LCST and improve polymer chain self-association. However, the optimal conditions will need to be determined through experimentation as increasing the hydrophobic content will likely decrease the temperature at which the copolymer transitions to a fully opaque state. Therefore, future work will assess the ability of the copolymers to act as sustained release scaffolds in an ocular environment and on the enhancement of copolymer properties. Material development will focus on optimization of monomer feed ratio and the incorporation of additional, or alternative monomers, such as methacrylate-polylactide (MAPLA) and hydroxyethyl methacrylate (HEMA), which

have been demonstrated to improve mechanical properties of NIPAAm-based gels [6]. Additional work required for the completion of this manuscript includes the characterization of copolymer swelling properties, sustained release kinetics of dexamethasone and model proteins, degradation profiles in simulated physiologic conditions, rheological testing, and characterization of material performance *in vitro* and *in vivo*.

Although these drug-releasing copolymer scaffolds are designed to reside outside the visual pathway, we feel that an optically transparent, thermo-gelling, resorbable, sustained-release intravitreal drug depot represents an attractive prospect to combat posterior segment complications.

5.5 SCHEMES

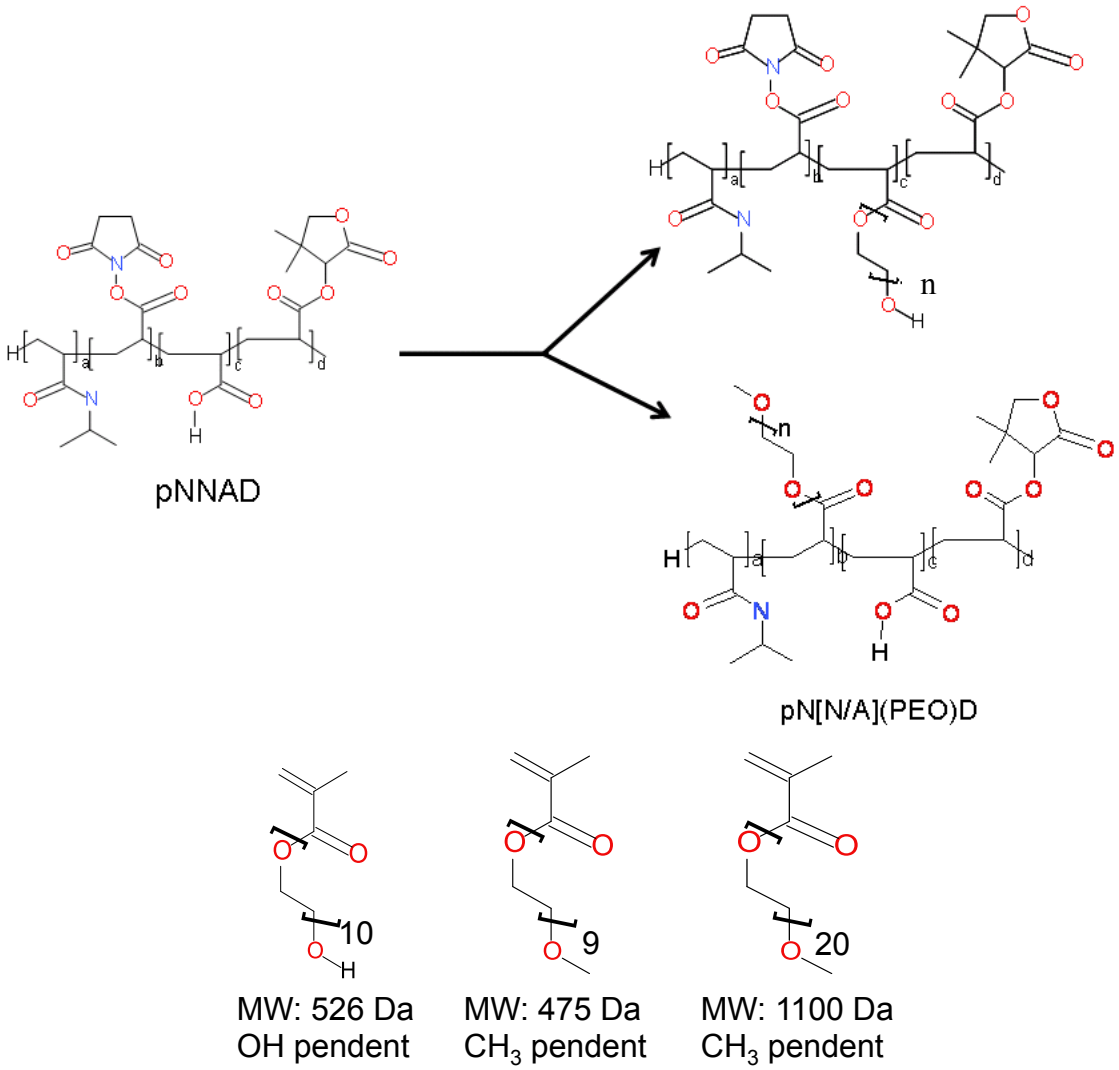

Scheme 5-1: Our previously reported pNNAD copolymers have been modified by replacing either the NAS or AA co-monomers with PEG monomers of varying chain length (475, 526 or 1100 Da) and either a methyl or hydroxyl pendant group.

5.6 TABLES

Table 5-1: Copolymer composition as determined by ^{1}H NMR, LCST values from DSC and observations of polymer gelling properties

Polymer	Composition	LCST	Gel Appearance at 37°C
$pNNP_5D_4$	75.8: 4.9: 14.1: 5.2	35.2	Soft, translucent
$pNNP_5D_8$	76.1: 4.8: 9.3: 9.8	27.7	Stiff, opaque
$pNNP_5D_{12}$	75.7: 4.5: 6.7: 13.1	18.7	Stiff, opaque
$pNAP_5D_4$	75.2: 4.9: 15.2: 4.7	36.9	Soft, translucent
$pNAP_5D_8$	76.1: 5.9: 8.8: 9.2	28.3	Stiff, Opaque
$pNAP_5D_{12}$	75.3: 5.2: 6.2: 13.3	20.8	Stiff, Opaque
$pNNP_4D_4$	75.4: 4.7: 15.4: 4.5	39.1	No gel
$pNNP_4D_8$	75.9: 4.6: 10.2: 9.3	30.9	Stiff, Opaque
$pNNP_4D_{12}$	75.3: 4.4: 7.3: 13.0	20.9	Stiff, Opaque
$pNAP_4D_4$	76.0: 4.8: 13.1: 6.1	41.8	No gel
$pNAP_4D_8$	76.2: 5.0: 9.2: 9.6	32.3	Stiff, Opaque
$pNAP_4D_{12}$	75.9: 5.7: 5.9: 12.5	22.1	Stiff, Opaque
$pNNP_{11}D_4$	76.2: 4.7: 13.1: 6.0	-	No gel
$pNNP_{11}D_8$	76.0: 5.0: 8.3: 10.7	-	No gel
$pNNP_{11}D_{12}$	76.0: 5.3: 5.7: 13.0	23.6	Stiff, transparent
$pNAP_{11}D_4$	75.7: 5.1: 13.9: 5.3	-	No gel
$pNAP_{11}D_8$	75.7: 4.8: 10.3: 9.2	-	No gel
$pNAP_{11}D_{12}$	75.8: 4.8: 6.6: 12.8	26.8	Stiff, transparent

Table 5-2: Number average molecular weight and poly dispersity index for a select few representative copolymers

Sample	Mn	PDI
$pNNP_4D_8$	17626	3.3
$pNNP_5D_4$	19478	2.9
$pNAP_{11}D_{12}$	24551	2.8

5.7 FIGURES

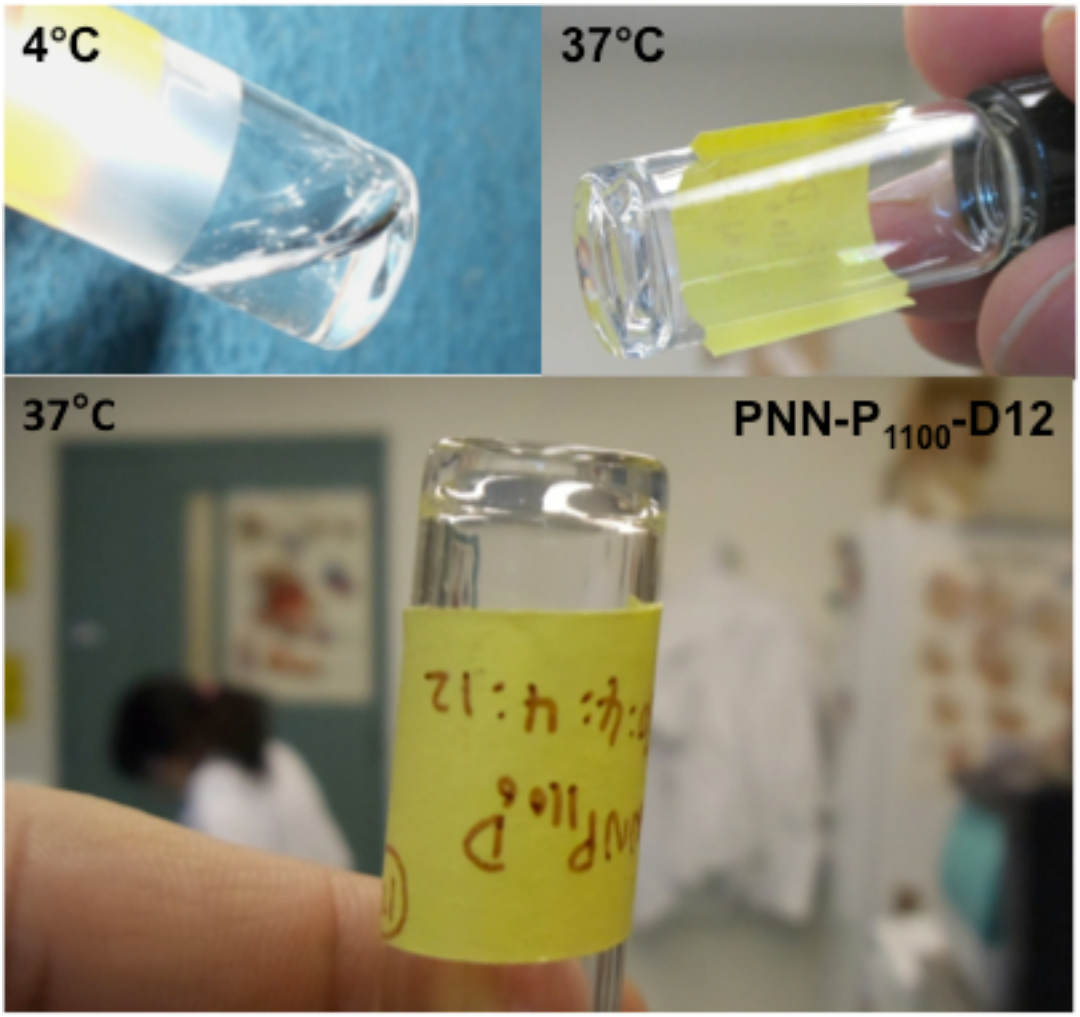

Figure 5-1: Optical transparency was conserved following heating above the LCST in several copolymers, specifically those containing 4 mol% PEG-1100 and 12 mol% DBA.

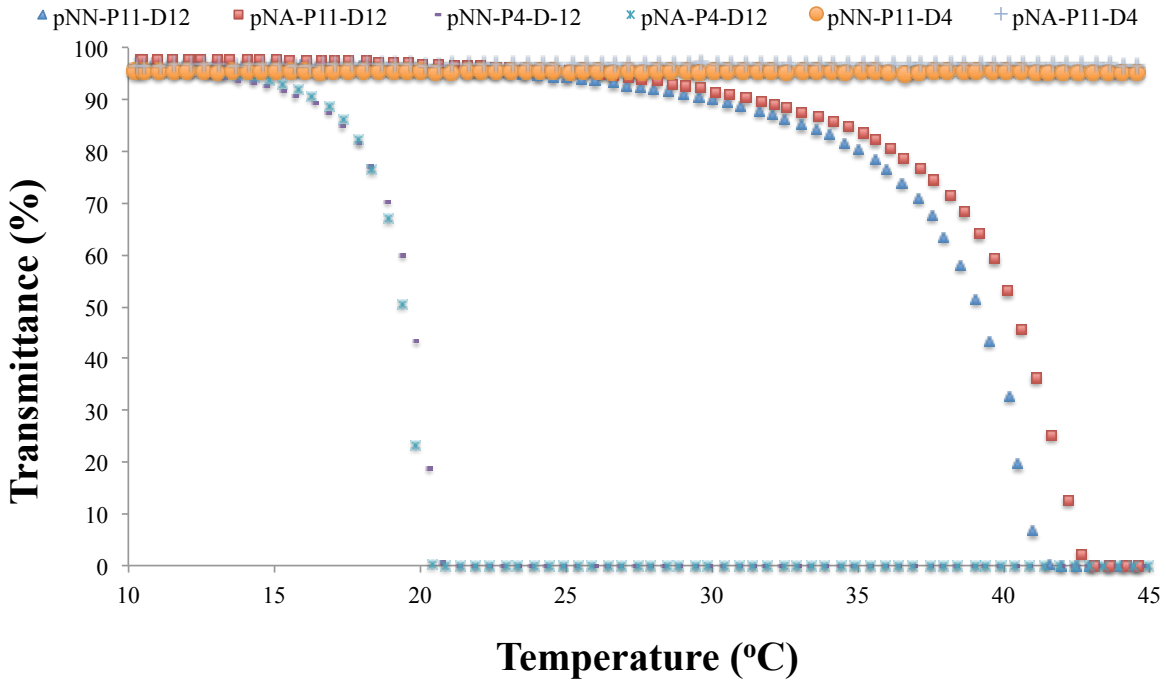

Figure 5-2: Turbidity testing reveals a window between approximately 24 and 40°C in which pN(N/A)$P_{11}D_{12}$ copolymers form optically transparent gels. However, further heating results in the formation of an opaque gel with improved mechanical integrity. The pN(N/A)P_4D_{12} copolymers shown here are representative of the majority of synthesized materials, which formed opaque white gels. Whereas the pN(N/A)$P_{11}D_4$ copolymers that did not lose transparency, also did not form gels.

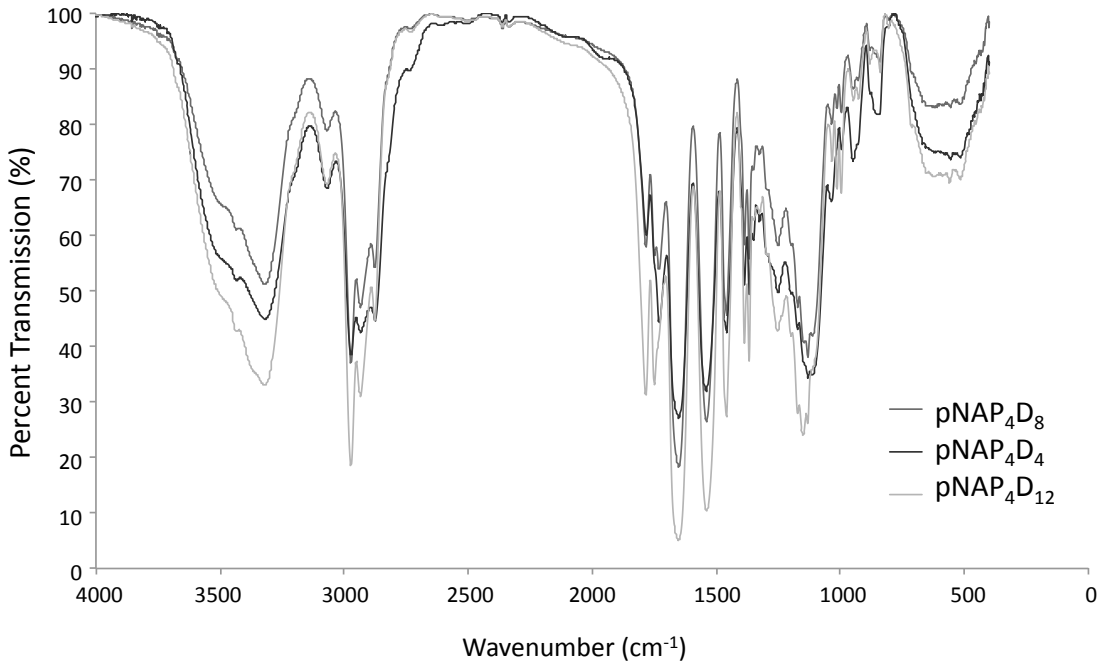

Figure 5-3: FT-IR spectra of the $pNAP_4D_y$ family of copolymers.

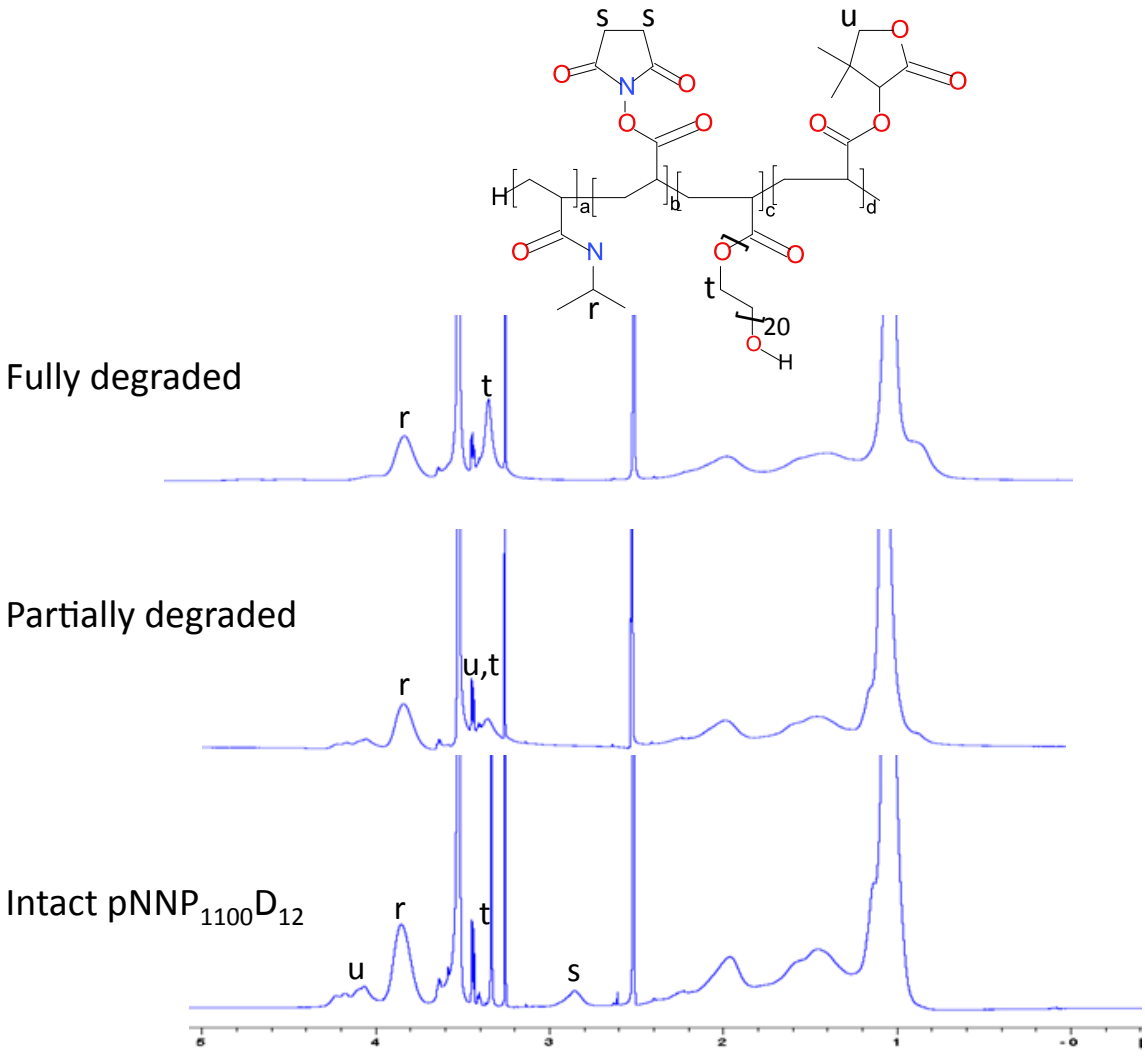

Figure 5-4: ^{1}H-NMR was used to characterize copolymer content and to examine the degradation mechanism in harsh, alkaline conditions.

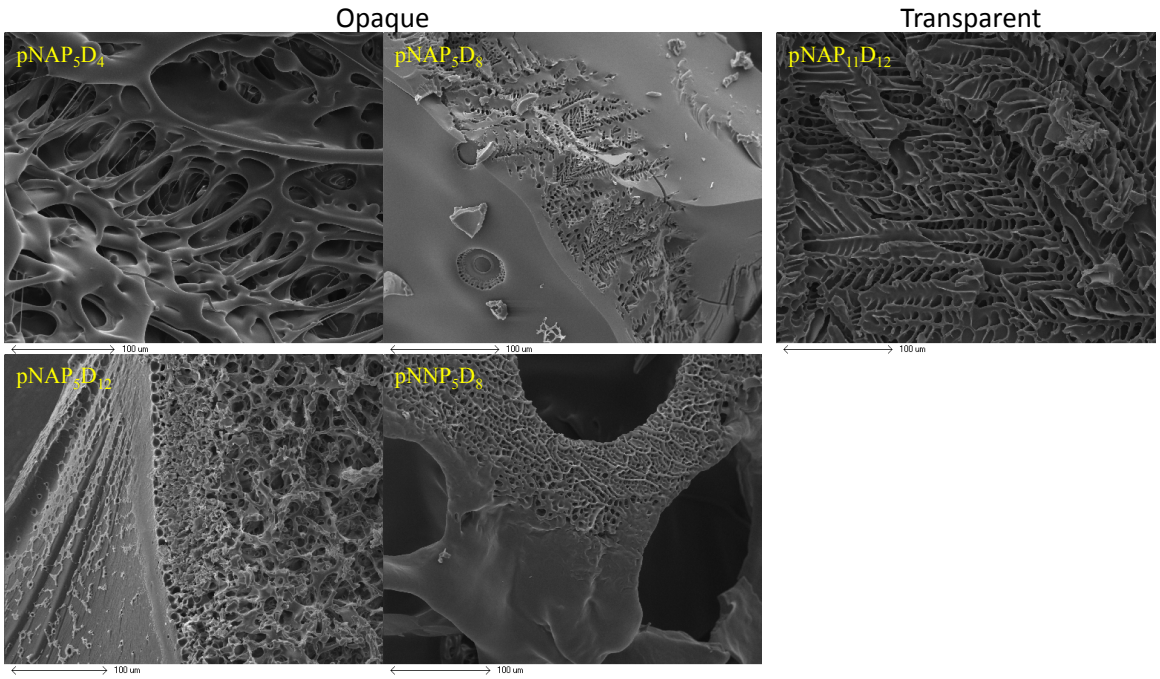

Figure 5-5: SEM micrographs showing the architectural differences in the microstructure of optically transparent and opaque gels. Scale bar = 100 µm.

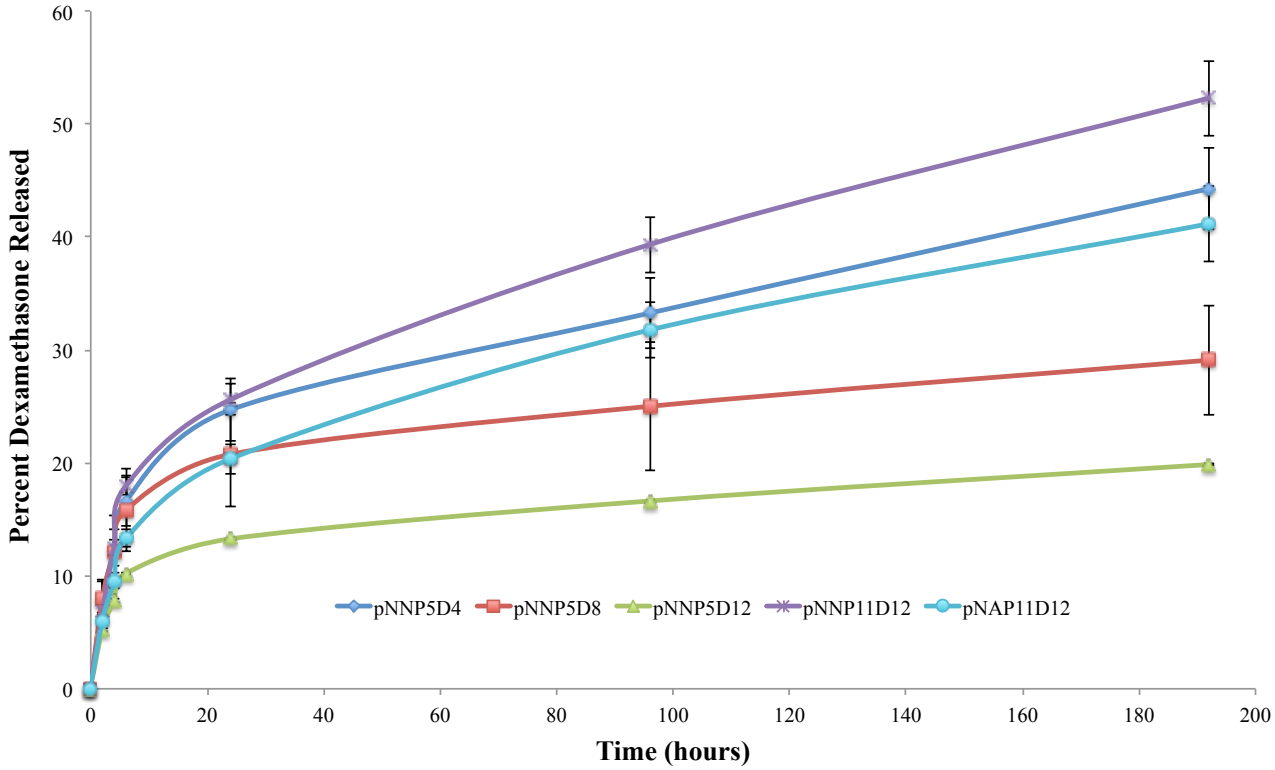

Figure 5-6: Dexamethasone release profile for $pNNP_5D_y$ and $pN(N/A)P_{11}D_{12}$ copolymers. The rate of dexamethasone release increases as copolymer hydrophilicity increases.

References

[1] Kane FE, Burdan J, Cutino A, Green KE. Iluvien (TM): a new sustained delivery technology for posterior eye disease. Expert Opinion on Drug Delivery 2008;5:1039-46.
[2] Saraiya NV, Goldstein DA. Dexamethasone for ocular inflammation. Expert Opin Pharmacother 2011;12:1127-31.
[3] Fitzpatrick SD, Mazumder MAJ, Muirhead B, Sheardown H. Development of Injectable, Resorbable, Drug-Releasing Copolymer Scaffolds for Minimally Invasive Sustained Ophthalmic Therapeutics. Accepted (7/3/2012) for publication in *Acta Biomaterialia* 2012.
[4] Nicolson PC, Vogt J. Soft contact lens polymers: an evolution. Biomaterials 2001;22:3273-83.
[5] Tighe B. Silicone Hydrogels: Structure, properties and behaviour. In: Sweeney D, editor. Silicone Hydrogels: Continuous Wear Contact Lenses: Oxford, Butterworth-Heinemann; 2004. p. 1 - 27.
[6] Ma Z, Nelson DM, Hong Y, Wagner WR. Thermally Responsive Injectable Hydrogel Incorporating Methacrylate-Polylactide for Hydrolytic Lability. Biomacromolecules 2010;11:1873-81.

CHAPTER 6: CONCLUSIONS

Numerous candidate copolymers were synthesized for application as minimally invasive cell or drug carriers for posterior segment therapeutics. The first generation copolymers (PCol and UV PCol) consisted of non-degrading amine-terminated PNIPAAm chains grafted onto a type I collagen backbone, which served to create a bioadhesive, thermoresponsive scaffold that mimics the native basement membrane in the posterior eye, the Bruch's membrane. In the second-generation materials (PNN-HA.RGDS), the bulky collagenous backbone was replaced with small, cell-adhesive RGDS peptides, which have been hypothesized to be the most important binding motif for the support of transplanted RPE cells. Furthermore, hyaluronic acid was incorporated into the scaffold as HA has been shown to improve cellular adhesion, proliferation and migration. In the third-generation materials (pNNAD), degradability was introduced into the thermoresponsive copolymers through the incorporation of acryloyloxy dimethyl-γ-butyrolactone (DBA), which undergoes a hydrolytic ring opening, resulting in a significant increase in copolymer LCST. As the LCST is raised above physiologic temperature, the gelled scaffold reverts to a hydrated state, allowing it to be cleared from the eye and subsequently from the body. Work is currently ongoing for the fourth-generation materials (pN(N/A)P_xD_y), which have introduced optical transparency into the previous pNNAD copolymers through the replacement of either NAS or AA with PEG. While the majority of the (pN(N/A)P_xD_y) copolymers form opaque gels when heated above their LCST, several copolymers, specifically pN(N/A)$P_{11}D_{12}$, appear to possess an apparent window between their LCST and approximately 40^oC, in which the materials

form a viscous, optically transparent, non-shrinking gel. However, when heated above 40^{o}C, the polymer chains appear to collapse out of solution, forming an opaque white scaffold. For ocular applications, it is desirable for the drug scaffold to be optically transparent to minimize potential complications, such as migration of the free-floating scaffold into the visual pathway. However, the inclusion of PEG into the pNNAD copolymers produces a relatively soft scaffold with elevated dexamethasone release rates and likely expedites the degradation process. Additional work is required for the completion of the final manuscript presented in Chapter 5. Specifically, we will examine copolymer swelling properties, degradation profiles in simulated physiologic conditions, polymer mechanical properties, *in vitro* and *in vivo* compatibility assays and long-term release profiles of dexamethasone in addition to several model proteins.

Future work will focus on optimization of copolymer properties and the inclusion of alternative co-monomers, which can increase copolymer mechanical properties, decrease degradation and release rates, while retaining optical transparency and thermoresponsive behaviour. Such scaffolds offer a promising alternative to current posterior segment drug delivery modalities.

CHAPTER 7: APPENDIX

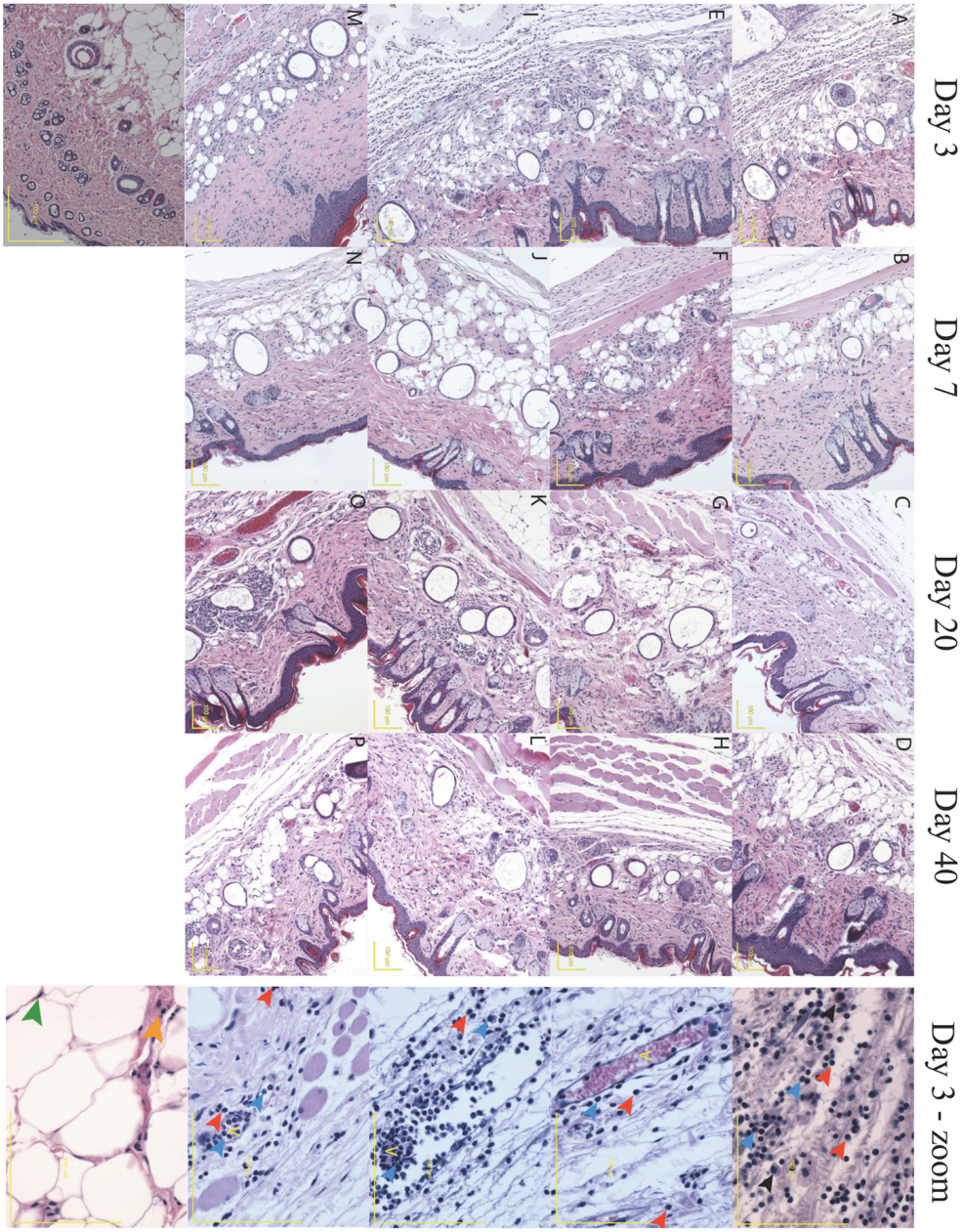

Figure 7-1: High-resolution image of Figure 3-8. Scale bar = 100 μm.